Requirements for CO2 monitoring by Sentinel-5

Final Report of ESA study contract n° 4000103801 - Final version 1.1

NOVELTIS

Universität Bremen

University of Leicester

Koninklijk Nederlands Meteorologisch Instituut
Ministerie van Infrastructuur en Milieu

	Function	Name	Signature	Date
Prepared by	Project Manager / Project Engineers	Julien CHIMOT / Hartmut BÖSCH Heinrich BOVENSMANN Michael BUCHWITZ François-Marie BREON Claude CAMY-PEYRET Cédric BACOUR Michiel VAN WEELE Johan de HAAN Pepijn VEEFKIND	P.P. J. Chimot	30/03/2012
Approved by	Space Department Manager	Pascal PRUNET		30/03/2012
Verified by	Quality Manager	Cindy HORTALA	Hortala	30/03/2012
Authorised by	Production Manager	Frédérique PONCHAUT	Ponchaut	30/03/2012

NOVELTIS

afaq ISO 9001 Qualité AFNOR CERTIFICATION

Parc Technologique du Canal – 2, Avenue de l'Europe – 31520 Ramonville-Saint-Agne – France
Tél. : +33 (0)562 88 11 11 – Fax : +33 (0)562 88 11 12 – E-mail : noveltis@noveltis.fr

ESA STUDY CONTRACT REPORT No ESA Study Contract Report will be accepted unless this sheet is inserted at the beginning of each volume of the Report		
ESA CONTRACT **No 4000103801**	**SUBJECT** **Requirements for CO_2 monitoring by Sentinel-5**	**CONTRACTOR** **NOVELTIS**
*** ESA CR ( ) No**	**No of Volumes:** **This is volume No:**	**CONTRACTOR'S REFERENCE** **NOV-3945-NT-11712** **Ed. 1 – Rev. 1**

ABSTRACT:

This document is the final report related to the ESA contract study 4000103801 titled "Requirements for CO_2 monitoring by Sentinel-5". The main objective of this study is to assess quantitatively the capabilities of the Sentinel-5 mission in a view of CO_2 monitoring.
This study is structured in 3 specific activities: i) specification (on a consensus basis) of quantitative user requirements on the space-based XCO_2 products in order to monitor CO_2 surface fluxes for 3 specific applications focused on specific scales (global to regional scales, megacities and strong local scale), ii) an assessment of the XCO_2 products retrieved from current and improved instrument specifications, achieved through 3 independent algorithms with comparison to the key XCO_2 requirements (*i.e.* spatial scales, random errors and systematic errors), and iii) an Observing System Simulation Experiment-like exercise which allows the link of the Sentinel-5 XCO_2 performances to CO_2 L4 error improvement.
By simulating a wide variety of geophysical conditions, the study has demonstrated the potential of Sentinel-5 (in its baseline configuration) for monitoring CO_2 surface fluxes at global to regional scales. For the expected XCO_2 products derived from Sentinel-5 (in its baseline configuration), with a random error (threshold) of 4 ppm and a systematic error (threshold) of 2 ppm, the associated objectives will be fulfilled at least in parts, particularly through the global coverage and good spatial resolution of the Sentinel-5 mission (pixel size equal or smaller than 10 km).
Actual retrievals have shown a good consistency between the results of the 3 independent algorithms. Performances are better than the thresholds quoted above (random and systematic) in 80% of the cases (after filtering out the "bad "retrievals). The highest XCO_2 systematic error values, which are the most critical parameters when assessing the capabilities of a dedicated CO_2 space-borne mission, are mainly related to major scattering effects (induced by uncertainties in aerosol and cirrus parameters) and are not well enough reduced by the retrieval algorithms.
CO_2 applications related to smaller scales remain out of reach mainly because of the horizontal resolution.
The importance of the spatio-temporal dependence of XCO_2 systematic errors, with respect to the scale of the monitored CO_2 surface fluxes has been underlined through the OSSE-like exercise.
Options for enhancing XCO_2 Sentinel-5 performances, by improving associated instrument specifications above the current baseline, have been examined. The main priorities are: 1) To add a 2 micron spectral channel measuring the strong 2 micron CO_2 absorption band, 2): To improve the spectral resolution in the NIR-2 spectral region (from 0.4 nm, as currently specified, to 0.12 nm).
Finally, 2 additional recommendations are addressed: i) To establish a robust filtering methodology which could be based on ancillary information provided by VII and/or 3MI measurements, ii) To further develop the XCO_2 retrieval algorithms for being able to fully exploit the information of 3 spectral bands (NIR-2, SWIR-1 and SWIR-2) simultaneously.

Names of the authors: Julien CHIMOT – Hartmut BÖSCH – Heinrich BOVENSMANN – Michael BUCHWITZ – François-Marie BREON – Claude CAMY-PEYRET – Cédric BACOUR – Michiel VAN WEELE – Johan de HAAN – Pepijn VEEFKIND

** NAME OF ESA STUDY MANAGER Anne Grete Straume-Lindner DIV: TEC-EE	** ESA BUDGET HEADING

Distribution list

INTERNAL	EXTERNAL	
Name	**Name**	**Company / Organisation**
Documentation NOVELTIS	Anne Grete STRAUME-LINDNER	ESTEC
Richard BRU	François Marie BREON	LSCE
Frédérique PONCHAUT	Philippe PEYLIN	LSCE
Cindy HORTALA	Michael BUCHWITZ	IUP-UB
Pascal PRUNET	Heinrich BOVENSMANN	IUP-UB
Claude CAMY-PEYRET	Pepijn VEEFKIND	KNMI
Cédric BACOUR	Michiel VAN WEELE	KNMI
Julien CHIMOT	Johan de HAAN	KNMI
Carsten Standfuss	Hartmut BÖSCH	ULe

Document status

Requirements for CO2 monitoring by Sentinel-5 Final Report of ESA study contract n° 4000103801 - Final version 1.1			
Issue	**Revision**	**Date**	**Reason for the revision**
0	1	02/12/2011	Draft version 1
1	0	29/02/2012	Final version 1.0
1	1	30/03/2012	Final version 1.1

Modification status				
Issue	Rev	Status *	Modified pages	Reason for the modification
1	1	M	33	Clarification on the work performed under Chapter 2.
1	1	M	75	Clarification on the expected agreement between the results of XCO_2 retrievals obtained by each partner.
1	1	M	163	Clarification on the spatial sampling ensured by the TANSO-FTS instrument on GOSAT.

* *I = Inserted* *D = deleted* *M = Modified*

References

	Reference	Title
[RD1]	Aerosol-cci Models working group: de Leeuw G., Kinne S., Veefkind P., Holzer-Popp T., Stein-Zweers D., Tanré D., Thomas G. and North P.; with contributions from Dubovik O. and Kokhanovsky A., Aerosol-cci, Version 1.0, 02 May 2011.	ESA ECV Project – Proposal for aerosol models.
[RD2]	Bacour C., Peylin P., Chimot J., Bréon F.-M., NOV-3945-MM-11181, 19 April 2011.	Concept of the "Mission CO_2 Simulator" jointly developed by NOVELTIS and LSCE.
[RD3]	Bösch H., Baker D., Connor B., Crisp D. and Miller C., Remote Sens., 3, 270-304; doi:10.3390/rs3020270, ISSN 2072-4292, www.mdpi.com/journal/remotesensing, 2011.	Global Characterization of CO_2 Column Retrievals from Shortwave-Infrared Satellite Observations of the Orbiting Carbon Observatory-2 Mission.
[RD4]	Bréon, F.-M., Proceedings from IWGGMS conference Edinburg Scotland. 15-18 May 2011.	Impact of large point sources on the CO_2 column concentrations.
[RD5]	Buchwitz, M., Chevallier F., Bergamaschi P., Aben I., Bösch H., Hasekamp O., Notholt J., Reuter M., *et al.*, pp. 45, version 1, 3. February 2011, 2011.	User Requirements Document for the GHG-CCI project of ESA's Climate Change Initiative.
[RD6]	Crisp D., JCDSA Seminar, Jet Propulsion Laboratory, California Institute of Technology, OCO-2 Science Lead, 20 April 2011.	Measuring Atmospheric CO_2 from space: The Japanese Greenhouse Gases Observing Satellite (GOSAT) and the NASA Orbiting Carbon Observatory-2 (OCO-2) Mission.
[RD7]	EOP-PIO, IPD-RS-ESA-18, Issue 1, Revision 2, 10.02.2011.	Sentinel-5-UVNS Instrument Phase A/B1 Reference Spectra.
[RD8]	EOP-PIO, IPD-RS-ESA-16, Issue 1, Revision 1, 31.01.2011	Sentinel-5-UVNS Instrument Phase A/B1 System Requirements Document.
[RD9]	EOP-PIO, IPD-RS-ESA-18139, Issue 1, Revision 1, 31.01.2011.	CO_2 observation capability of the Sentinel-5 mission.
[RD10]	Frankenberg C., Butz A., and Toon G.C., Geophys. Res. Lett, 38, L03801, doi:10.1029/2010GL045896, 2011.	Disentangling chlorophyll fluorescence from atmospheric scattering effects in O_2 A-band spectra of reflected sun-light.
[RD11]	IUP-UB, RAL, NOVELTIS, ESA Study Final Presentation, ESTEC Contract 4000101187/10/NL/MP/ef, 16 Marc 2011.	In-Flight Spectral Calibration and Requirements on Reflectance for Sentinel-4.
[RD12]	Joiner J., Yoshida Y., Vasilkov A.P., Yoshida Y., Corp L.A., and Middleton E.M., Biogeosciences, 8, 637-651, 2011.	First observations of global and seasonal terrestrial chlorophyll fluorescence from space.
[RD13]	Krings, T., Gerilowski, K., Buchwitz, M., Reuter, M., Tretner, A., Erzinger, J., Heinze, D., Burrows, J. P., and Bovensmann, H.:, Atmos. Meas. Tech. Discuss., 4, 2207-2271, doi:10.5194/amtd-4-2207-2011, 2011	MAMAP – a new spectrometer system for column-averaged methane and carbon dioxide observations from aircraft: retrieval algorithm and first inversions for point source emission rates
[RD14]	Langen J., Meijer Y., Brinksma E., Veihelman B., Ingmann P., ESA ESTEC, ESA-SMA/1507/JL-dr, 31.01.2011.	GMES Sentinels-4 and -5 Mission Requirements Document.

	Reference	Title
[RD15]	Mclnerney F.A. and Wing S.L., Annual Review of Earth and Planetary Sciences, 39, 489-516, 2011.	The Paleocene-Eocene thermal maximum : a perturbation of the carbon cycle, climate and biosphere with implications for the future.
[RD16]	Oda T., Maksyutov S., Ganshin A., Oshchepkov S., Bril A., Zhuravlev R., Saito M., Andres R.J., Yoshida Y. and Yokota T., Proceedings from IWGGMS conference Edinburg Scotland, 17 May 2011	Data assimilation and model simulations of CO_2 and CH_4 enhancements over large point sources (LPS)
[RD17]	Oda T. and Maksyutov S., Atmos. Chem. Phys., 11, 543–556, www.atmos-chem-phys.net/11/543/2011/, doi:10.5194/acp-11-543-2011, 2011	A very high-resolution (1 km × 1 km) global fossil fuel CO_2 emission inventory derived using a point source database and satellite observations of nighttime lights
[RD18]	O'Dell, C.W., Connor B., Bösch H., O'Brien D., frankenberg C., Castano R., Christi M., Crisp D., Eldering A., Fisher B., Gunson M., McDuffie J., Miller C.E., Natraj V., Oyafuso F., Polonsky I., Smyth M., Taylor T., Toon G.C., Wennberg P.O., and Wunch D., Atmos. Meas. Tech. Discuss., 4, 6097-6158, 27 September 2011.	The ACOS CO_2 retrieval algorithm – Part 1: Description and validation against synthetic observations.
[RD19]	Reuter, M., H. Bovensmann, M. Buchwitz, J. P. Burrows, B. J. Connor, N. M. Deutscher, D. W. T. Griffith, J. Heymann, G. Keppel-Aleks, J. Messerschmidt, J. Notholt, C. Petri, J. Robinson, O. Schneising, V. Sherlock, V. Velazco, T. Warneke, P. O. Wennberg, D. Wunch, J. Geophys. Res., 116, D04301, doi:10.1029/2010JD015047, 2011.	Retrieval of atmospheric CO_2 with enhanced accuracy and precision from SCIAMACHY: Validation with FTS measurements and comparison with model results,
[RD20]	Velazco V.A., Buchwitz M., Bovensmann H., Reuter M., Schneising O., Heymann J., Krings T., Gerilowski K., and Burrows J.P., Atmos.Meas.Tech.Discuss, 4, 5147-5182, 2011.	Towards space-based verification of CO_2 emissions from strong localized sources: fossil fuel power plant emissions as seen by a CarbonSat constellation.
[RD21]	Vermeulen, A. T., Hensen, A., Popa, M. E., van den Bulk, W. C. M., and Jongejan, P. A. C.: Atmos. Meas. Tech., 4, 617-644, doi:10.5194/amt-4-617-2011, 2011	Greenhouse gas observations from Cabauw Tall Tower (1992–2010).
[RD22]	Bacour C., NOV-3737-NT-10512, NOVELTIS, CNES study, technical report.	Simulateur mission CO_2 – phase 3, Description fonctionnelle et documentation du simulateur version 3.
[RD23]	Bovensmann, H., M. Buchwitz, J. P. Burrows, M. Reuter, T. Krings, K. Gerilowski, O. Schneising, J. Heymann, A. Tretner, and J. Erzinger, Atmos. Meas. Tech., 3, 781-811, 2010	A remote sensing technique for global monitoring of power plant CO_2 emissions from space and related applications.
[RD24]	Bovensmann H., Buchwitz M., Burrows J.P., EE8 Mission Overview, 10 June 2010.	Carbon Monitoring Satellite (CarbonSat) as an Earth Explorer Opportunity Mission – Mission Overview.
[RD25]	Butz, A., O.P. Hasekamp, C. Frankenberg, J. Vidot, and I. Aben (2010), J. Geophys. Res., doi:10.1029/2010JD014514, 2010.	CH_4 retrievals from space-based solar backscatter measurements: performance evaluation against simulated aerosol and cirrus loaded scenes

	Reference	Title
[RD26]	Ciais P., Chimot J., Klonecki A., Prunet P., Vinuesa J.-F., Nussli C., Bréon F.-M., AGU 2010.	Modelling atmospheric transport of CO_2 at high resolution to estimate the potentialities of space-borne observation to monitor anthropogenic emissions.
[RD27]	Ciais, P., Dolman, A.J., Dargaville, R., Barrie, L., Bombelli, A., Butler, J., Canadell, P., Moriyama, T. (June 2010).,/FAO, Rome, 48 pp.	GEO Carbon Strategy Geo Secretariat Geneva.
[RD28]	Committee on Methods for Estimating Greenhouse Gas Emissions Board on Atmospheric Sciences and Climate Division on Earth and Life Studies, National Research Council of the National Academy of Science, National Academies Press, ISBN: 0-309-15212-7, 2010.	Verifying greenhouse gas emissions – Methods to support international climate agreements.
[RD29]	GCP 2010, www.globalcarbonproject.org/carbonbudget, released on 21 November 2010.	Global Carbon Project (2010), Carbon budget and trends 2009.
[RD30]	Hungershoefer K., Bréon F.-M., Peylin P., Chevallier F., Rayner P., Klonecki A., and Houweling S., ACP 10, 10503-10520, November 2010.	Evaluation of various observing systems for the global monitoring of CO_2 surface fluxes.
[RD31]	Kaminski, T., Scholze, M. and Houweling, S, Tellus, 62B(5), 784–796, 2010.	Quantifying the benefit of A-SCOPE data for reducing uncertainties in terrestrial carbon fluxes in CCDAS.
[RD32]	National Aeronautics and Space Administration, Jet Propulsion Laboratory (JPL), California Institute of Technology Pasadena, California, Version 1.0 Rev 4, 10 November 2010.	Orbiting Carbon Observatory (OCO)-2, Level 2 Full Physics, Theoretical Basis Document.
[RD33]	NOVELTIS, NOV-3891-SL-10302, CCN 1 of the ESA contract study 21823/08/NL/FF "Support to the Consolidation of Instrument Requirements for Future Earth Observation Missions", Final Presentation, ESTEC, Noordijk, 4 November 2010.	Sentinel-4-UVN pseudo-noise assessment.
[RD34]	O'Dell C.W., Journal of Geophysical Research, Vol. 115, D10206, 15 pp., doi: 10.1029/2009JD012803, 2010.	Acceleration of multiple-scattering, hyperspectral radiative transfer calculations via low-streams interpolation.
[RD35]	Pillai P., Gerbig C., Marshall J., Ahmadov R., Kretschmer R., Koch T., and Karstens U., Atmos. Chem. Phys., 10, 83–94, 2010, www.atmos-chem-phys.net/10/83/2010	High resolution modeling of CO_2 over Europe: implication representation errors of satellite retrievals
[RD36]	Reuter, M., Buchwitz, M., Schneising, O., Heymann, J., Bovensmann, H., and Burrows, J. P., Atmos. Meas. Tech., 3, 209-232, 2010.	A method for improved SCIAMACHY CO_2 retrieval in the presence of optically thin clouds.
[RD37]	Schlüssel P., Philips P., Accadia C. and Munro R., EUMETSAT, EUM/PEPS/REQ/06/0043, v3C, 25 June 2010.	Post-EPS Mission Requirements Document.

	Reference	Title
[RD38]	Benedetti A., Morcrette J.-J., Boucher O., Dethof A., Engelen R.-J., Fisher M., Flentje H., Huneeus N., Jones L., Kaiser J. W., Kinne S., Mangold A., Razinger M., Simmons A. J., and Suttie M.:, J. Geophys. Res., 114, D13 205, doi:10.1029/2008JD011115, 2009.	Aerosol analysis and forecast in the European Centre for Medium-Range Weather Forecasts Integrated Forecast System: 2. Data assimilation.
[RD39]	Bréon F.-M., Ciais P., External geophysics, climate and environment (Climate), C.R. Geoscience 342 (2010) 412-424, December 2009.	Space-borne remote sensing of greenhouse gas concentrations.
[RD40]	Butz, A., Hasekamp, O. P., Frankenberg, C., and Aben, I.: Appl. Optics, 48, 18, 3322–3336, doi:10.1364/AO.48.003322, 2009.	Retrievals of atmospheric CO_2 from simulated space-borne measurements of backscattered near-infrared sunlight: accounting for aerosol effects
[RD41]	GMES Atmosphere Core Service (GACS) 2009, http://www.gmes.info/pages-principales/library/implementation-groups/gmes-atmosphere-core-servicem, April 2009	Global Monitoring for Environment and Security Atmosphere Core Service (GACS), Implementation group – Final Report
[RD42]	Morcrette J.-J., Boucher O., Jones L., Salmond D., Bechtold P., Beljaars A., Benedetti A., Bonet A., Kaiser W., Razinger M., Schulz M., Serrar S., Simmons A. J., Sofiev M., Suttie M., Tompkins A., and Untch, A., J. Geophy. Res., 114, D06 206, doi:10.1029/2008JD011235, 2009.	Aerosol analysis and forecast in the European Centre for Medium-Range Weather Forecasts Integrated Forecast System: Forward modelling.
[RD43]	NOVELTIS consortium, ESA Study 20839/07/NL/HE, Final report, September 2009.	Observation Techniques and mission concepts for Analysis of the Global Carbon Cycle.
[RD44]	Reuter M., Buchwitz M., Schneising O., Heymann J., Bovensmann H., and Burrows J.P., AMT, 2483-2538, October 2009	A method for improved SCIAMACHY CO_2 retrieval in the presence of optically thin clouds.
[RD45]	Veefkind J.P., Levelt P.F., 19 June 2009, ESA contract 21533/07/NL/HE.	CAMELOT Study – GMES Sentinel-4 and 5 Operational Atmospheric Chemistry Monitoring Missions.
[RD46]	Vieitez O., Stammes P., Royal Netherlands Meteorological Institute, Poster 2009.	Development of aerosol altitude retrieval from GOSAT observations of the oxygen A-band.
[RD47]	Winker D., Vaughan M., Omar A., Hu Y., Powell K. A., Liu, Z., Hunt W., and Young S., Journal of Atmospheric and Oceanic Technology, 26, 2310–2323, 2009.	Overview of the CALIPSO Mission and CALIOP Data Processing Algorithms.
[RD48]	Ackerman, K. V. and Sundquist, E. T.: Sci. Technol., 42, 5688–5693, 2008.	Comparisons of two U.S. Power-Plant Carbon Dioxide Emissions Data Sets, Environ.
[RD49]	Connor, B. J., Bösch, H., Toon, G., Sen, B., Miller, C., and Crisp, D.: J. Geophys. Res.-Atmos., 113, D05305, doi: 10.1029/2006JD008336, 2486, 2513, 2514, 2008.	Orbiting carbon observatory: Inverse method and prospective error analysis.
[RD50]	Kleipool Q. L., M. R. Dobber, J. F. de Haan, and P. F. Levelt, J. Geophys. Res. VOL. 113, D18308, doi:10.1029/2008JD010290, 2008	Earth surface reflectance climatology from 3 years of OMI data

	Reference	**Title**
[RD51]	Ingman, P., et al., Nov 2008, ESA Report for Assessment, SP1313/1, 2008.	A-scope - advanced space carbon and climate observation of planet Earth.
[RD52]	Natraj V., Bösch H., Spurr R.J.D., and Yung Y.L., Journal of Geophysical Research, Vol. 113, D11212, doi:10.1029/2007JD009017, 2008.	Retrieval of XCO_2 from simulated Orbiting Carbon Observatory measurements using the fast linearized R-2OS radiative transfer model.
[RD53]	Tolk L.F., Meesters A.G.C.A., Dolman A.J., and Peters W., Atmospheric Chemistry and Physics, 8, 6587-6596, 2008.	Modelling representation errors of atmospheric CO_2 mixing ratios at a regional scale.
[RD54]	Denman K.L., Brasseur G., Chidthaisong A., Ciais P., Cox P.M., Dickinson R.E., Hauglustaine D., Heinze C., Holland E., Jacob D., Lohman U., Ramachandran S., da Silva Dias P.L., Wofsy S.C. and Zhang X., Cliamate Change 2007: The Physical Science Basis, eds. Cambridge University Press, new York, pp. 499-587, 2007.	Couplings between changes in the climate system and biogeochemistry - Contribution of Working Group I to the Fourth Assessment Report of the Intergovernmental Panel on Climate Change.
[RD55]	IPCC2007, Solomon, S., D. Qin, M. Manning, Z. Chen, M. Marquis, K.B. Averyt, M. Tignor and H.L. Miller (eds.), 2007.	Contribution of Working Group I to the Fourth Assessment Report of the Intergovernmental Panel on Climate Change, Cambridge University Press, Cambridge, United Kingdom and New York, NY, USA.
[RD56]	Krijer J.M., van Weele M., Aben I., and Frey R. Atmos. Chem. Phys., 7, 2881-2891, 2007.	Technical Note: The effect of sensor resolution on the number of cloud-free observations from space.
[RD57]	Winker D. M., Hunt W. H., and McGill M. J., Geophys. Res. Lett., 34, L19 803, doi: doi:10.1029/2007GL030135, 2007.	Initial performance assessment of CALIOP.
[RD58]	Aben, I., Hasekamp, O., and Hartmann, W.: J. Quant. Spectrosc. Rad. Transfer, 104, 450–459, 2006.	Uncertainties in the space-based measurements of CO_2 columns due to scattering in the Earth's atmosphere.
[RD59]	Bösch H., Toon G.C., Sen B., Washenfelder R., Wennberg P.O., Buchwitz M., de Beek R., Burrows J.P., Crisp D., Christi M., Connor B., Natraj V., and Yung Y.L., Wisconsin, 111(D23), J. Geophys. Res., 2006	Space-based near-infrared CO_2 retrievals: testing the OCO retrieval algorithm and validation concept using SCIAMACHY measurements over Park Falls
[RD60]	Global Climate Observing System, United nations environment programme, International council for science, GCOS-107, WMO/TD N°.1338, September 2006.	Systematic observation requirements for satellite-based products for climate – Supplement details to the satellite-based component of the "Implement Plan for the Global Observing System for Climate in Support of the UNFCCC".
[RD61]	Hourdin F., Musat I., Bony S., Braconnot P., Codron F., Dufresne J., Fairhead L., Filiberti M., Friedlingstein P., Grandpeix J., Krinner G., LeVan P., Li Z. and Lott F., Clim. Dynam., 27, 787–813, 2006.	The LMDZ4 general circulation model: Climate performance and sensitivity to parameterized physics with emphasis on tropical convection

	Reference	Title
[RD62]	Braum B.A., Yang P., Heymsfield A.J., Platnick S., King M.D., Hu Y.-X., and Bedka S.T., Journald of Applied Meteorology, Volume 44, 1896-1911, 2005	Bulk Scattering Properties for the Remote Sensing of Ice Clouds. Part II: Narrowband Models.
[RD63]	Gurney, K. R., Y.-H. Chen, T. Maki, S. R. Kawa, A. Andrews, and Z. Zhu, J. Geophys. Res., 110, D10308, doi: 10.1029/2004JD005373, 2005.	Sensitivity of atmospheric CO_2 inversions to seasonal and interannual variations in fossil fuel emissions.
[RD64]	Krinner G., Viovy N., de Noblet-Ducoudré N., Ogée J., Polcher J., Friedlingstein P., Ciais P., Sitch S., and Prentice C., Glob. Biogeochem. Cyc., 19, GB1015, doi:10.1029/2003GB002199, 2005.	A dynamic global vegetation model for studies of the coupled atmosphere-biosphere system.
[RD65]	ESA Study, ESA contract No. 17237/03/NL/GS http://www.knmi.nl/capacity/, October 2003 – June 2005	CAPACITY – Composition of the Atmosphere: Progress to Applications in the user CommunITY.
[RD66]	Remer L.A., Kaufman Y.J., Tanré D., Mattoo S., Chu D.A., Martins J.V., Li R.R., Ichoku C., Levy R.C., Kleidman R.G., Eck T.F., Vermote E., Holben B.N., Journal of the Atmospheric Sciences, 62(4), 947-973, 2005.	The MODIS aerosol algorithm, products, and validation.
[RD67]	Crisp D., Atlas R.M., Bréon F.-M., Brown L.R., Burrows J.P., Ciais P., Connor B.J., Doney S.C., Fung I.Y., Jacob D.J., Miller C.E., O'Brien D., Pawson S., Randerson J.T., Rayner P., Salawitch R.J., Sander S.P., Sen B., Stephens G.L., Tans P.P., Toon G.C., Wennberg P.O., Wofsy S.C., Yung Y.L., Kuang Z., Chudasama B., Sprague G., Weiss B., Pollock R., Kenyon D., Schroll S., Advances in Space Research 34 700-709, 2004.	The Orbiting Carbon Observatory (OCO) mission.
[RD68]	Vaughan M., Young S., Winker D., Powell K., Omar, A., Liu Z., Yongxiang H., and Hostetler C., 5575, 16 – 30, doi:10.1117/12.572024, 2004.	Fully automated analysis of space-based lidar data: an overview of the CALIPSO retrieval algorithms and data products, Laser Radar Techniques for Atmospheric Sensing.
[RD69]	Bréon, F.-M. and Peylin, Ph. ESA study 15427/01/NL/MM. Final report. May 2003.	The potential of space-borne remote sensing to contribute to the quantification of anthropogenic emissions in the frame of the Kyoto protocol.
[RD70]	Gurney K.R., Law R.M., Denning A.S., Rayner P.J., Baker D., Bousquet P., Brushwiler L., Chen Y.-H., Ciais P., Fan S., Fung I.Y., Gloor M., Heimann M., Higushi K., John J., Maki T., Maksyutov S., Masarie K., Peylin P., Prather M., Pak B.C., Randerson J., Sarmiento J., Taguchi S., Takahashi T. and Yuen C.-W., Macmilan Magazines Ltd, Nature, Vol 415, 7 February 2002.	Towards robust regional estimates of CO_2 sources and sinks using atmospheric transport models.
[RD71]	Rozanov V.V., Buchwitz M., Eichmann K.U., de Beek R. and Burrows J.P., Advances in Space Research, Volume 29, Issue 11, Pages 1831-1835, June 2002.	SCIATRAN – a new radiative transfer model for geophysical applications in the 240-2400 nm spectral region: the pseudo-spherical version.

	Reference	Title
[RD72]	Kahn, R., P. Banerjee, D. McDonald, and J. Martonchik (2001b), J. Geophys. Res., 106, 11,977– 11,995, 2001.	Aerosol properties derived from aircraft multiangle imaging over Monterey Bay.
[RD73]	Kahn, R., P. Banerjee, and D. McDonald (2001a), J. Geophys. Res., 106, 18,219– 18,238., 2001.	Sensitivity of multiangle imaging to natural mixtures of aerosols over ocean.
[RD74]	Rodgers C.D., Series on Atmospheric, oceanic and Planetary Physics – Vol. 2, World Scientific, 2000.	Inverse Methods for Atmospheric Sounding – Theory and Practice.
[RD75]	Bovensmann H., J.P. Burrows, M. Buchwitz, J. Frerick, S. Noël, V.V. Rozanov, K.V. Chance, A.P.H. Goede, Journal of the Atmospheric Sciences, Vol 56, 2, pp 127-150, 1999.	SCIAMACHY- Mission Objectives and Measurement Modes.
[RD76]	Barnes, W., Pagano, T., and Salomonson, V., Geoscience and Remote Sensing, IEEE Transactions on, 36, 1088 – 1100, doi:10.1109/36.700993, 1998.	Prelaunch characteristics of the Moderate Resolution Imaging Spectroradiometer (MODIS) on EOS-AM1.
[RD77]	Kauss, Jean, Diplomarbeit im Studiengang Physik (Diploma thesis, in German), Universität Bremen, Institut für Umweltphysik (IUP), 17.November 1998.	Aerosol-Parametrisierung für Strahlungstransport-Simulationen im ultravioletten bis nahinfraroten Spektralbereich.
[RD78]	Mishchenko M.I. and Travis L.D., J. Quant. Spectrosc. Radiat. Transfer Vol. 60, No. 3, pp. 309-32, 1998.	Capabilities and limitations of a current fortran implementation of the T-Matrix method for randomly oriented, rotationally symmetric scatterers.
[RD79]	Ciais P., Tans P.P., White J.W.C., Trolier M., Francey R.J., Berry J.A., Randall D.R., Sellers P.J., Collatz and Schimel D.S., Journal of geophysical Research, 100, 5051-5070, 1995.	Partitioning of ocean and land uptake of CO_2 as inferred by $\delta^{13}C$ measurements from the NOAA/CMDL global air sampling network.
[RD80]	Sadourny R. and Laval K., in: New Perspectives in Climate Modeling - edited by: Berger A. L. and Nicolis C., Elsevier Press, Amsterdam, 173–197, 1994.	January and July performance of the LMD general circulation model.
[RD81]	de Rooij W.A., and van der Stap C.C.A.H., Astronomy and Astrophysics, 131, 237-248, 1984.	Expansion of Mie scattering matrices in generalized spherical functions.
[RD82]	National Oceanic and Atmospheric administrations, National Aeronautics and Space administrations, United States Air Force, NOAA—S/T 76-1562, Washington, D.C., October 1976.	U.S. Standard Atmosphere, 1976.

Acronyms

3D	3 Dimensions
3MI	Multi-polarization, Multi-directional, Multi-spectral instrument
ACOS	Atmospheric CO_2 Observations from Space
A-SCOPE	Advanced Space Carbon and Climate Observation of Planet Earth
AIRS	Atmospheric InfraRed Sounder
AOD	Aerosol Optical Depth
AOT	Aerosol Optical Thickness
ATMOS	Atmospheric Trace Molecule Spectroscopy
AUS	AUStralia region
BESD	Bremen optimal Estimation DOAS
BL	Boundary Layer
CAL	Cirrus ALtitude
CALIOP	Cloud-Aerosol LIdar with Orthogonal Polarization
CALIPSO	Cloud-Aerosol Lidar and Infrared Pathfinder Satellite Observations
CAMELOT	Chemistry of the Atmosphere Mission concEpts and sentineL Observations Techniques
CarbonSat	Carbon monitoring-Satellite
CC	Continental Clean (aerosol scenario)
CCI	Climate Change Initiative
CCDAS	Carbon Cycle Data Assimilation
CCI	Climate Change Initiative
CH_4	Methane
CHI	CHIna region
CNES	Centre National d'Etudes Spatiales
CO_2	Carbon dioxide
COD	Cloud Optical Depth
COT	Cloud Optical Thickness
CP	Continental Polluted (aerosol scenario)
DE	DEsert aerosol type scenarios
DISAMAR	Deriving Instrument Specifications and Analysing Methods for Atmospheric Retrievals
DOAS	Differential Optical Absorption Spectroscopy
ECMWF	European Centre for Medium-Range Weather Forecasts
ECV	Essential Climate Variables
ENSO	El Nino Southern Oscillation

ENVISAT	ENVIronmental SATellite
EPS	EUMETSAT Polar System
ESA	European Space Agency
EU ETS	European Union Emission trading System
EUMETSAT	EUropean organisation for the exploitation of METeorological SATellites
EUR	EURope region
FOV	Field OF View
FTS	Fourier Transform Spectroscopy
FWHM	Full Width at Half Maximum
GACS	Global Monitoring for Environment and Security Atmosphere Core Service
GAW	Global Atmosphere Watch
GCOS	Global Climate Observing System
GEMS	Global and regional Earth system Monitoring using Satellite and *in Situ* data
GEO	Group on Earth Observation
GHG	GreenHouse Gases
GLO	GLObal region
GMES	Global Monitoring Environment Security
GOSAT	Greenhouse gases Observing SATellite
GPC	Global Carbon Project
Gt	Giga tonne (10^{12} kg) [t=metric tonne=10^3 kg]
H_2O	Water Vapour
hPa	hecto Pascal
HWHM	Half Width Half Maximum
HITRAN	HIgh-resolution TRANsmission molecular absorption database
HOM	HOMogeneous scene
IASI	Infrared Atmospheric Sounding Interferometer
IFOV	Instantaneous Field Of View (pixel or aggregation of pixels) for a single measurement
ILS	Instrument Line Shape
IPCC	Intergovernmental Panel on Climate Change
IUP-UB	Institute of Environmental Physics - University of Bremen
K	Kelvin
km	kilometre
KNMI	Koninklijk Nederlands Meteorologisch Instituut
L1 / L4 / L2	Level 1 / Level 4 / Level 2
LABOS	Layer Based Orders of Scattering
LEO	Low Earth Orbiting
LIDAR	LIght Diffusion And Ranging

LIDORT	LInearized Discret Ordinate Radiative Transfer
LMDz	Modèle de circulation générale du LMD - Laboratoire de Météorologie Dynamique (Zoom)
LSCE	Laboratoire des Sciences du Climat et de l'Environnement
LUT	Look-Up-Table
MetOp	Meteorological operational
MODIS	Moderate Resolution Imaging Spectoradiometer
MRD	Mission Requirement Document
MRE	Mean Random Error
MSE	Mean Systematic Error
Mt	Mega tonne (10^9 kg)
N_2O	Nitrous Oxide
NAF	North Africa region
NAM	North America region
NASA	National Aeronautics and Space Administration
NCEP	National Centres for Environment Prediction
NIR	Near InfraRed
OEM	Optimal Estimation Method
OCO	Orbiting Carbon Observatory
ODIAC	Open-source Data Inventory of Anthropogenic CO_2 emission
OMI	Ozone Monitoring Instrument
OSSE	Observing System Simulation Experiment
p	pressure
PBL	Planet Boundary Layer
Pg	Peta gramme (1 Pg=1 Gt=10^{15} g)
PP	Power Plant
ppm	part per million (in volume)
POL	low order POLynomials
POLDER	POLarization and Directionality of the Earth'Reflectances
RMS	Root Mean Square
RMSSE	Root Mean Square Systematic Error
RSS	Root Sum Square
RT	Radiative Transfer
RTM	Radiative Transfer Model
S-5	Sentinel-5
SAM	South America region
SAS	Sand/Soil albedo
SCIAMACHY	Scanning Imaging Absorption Spectrometer for Atmosphere Chartography

SG	Second Generation
SIB	SIBeria region
SIC	Snow/Ice albedo
SNR	Signal to Noise Ratio
SRD	System Requirements Document
SRE	Standard deviation Random Error
SRF	Spectral Response Function
SSD	Spatial Sampling Distance
SSE	Standard deviation Systematic Error
StdDev	Standard Deviation
SV	State Vector
SWIR	Short Wave InfraRed
SZA	Solar Zenith Angle
T	Temperature
TANSO	Thermal And Near infrared Sensor for carbon Observation
TCCON	Total Carbon Column Observing Network
TOA	Top Of Atmosphere
TIR	Thermal InfraRed
ULe	University of Leicester
US	United States
USA	United States America
UV	Ultra Violet
UVNS	UV/Visible/Near-Infrared/SWIR
VCF	Vegetation Chlorophyll Fluorescence
VEG	VEGetation albedo
VII	Visible/Infrared Imager
vmr	volume mixing ratio
WMO	World Meteorological Organization
w.r.t	with respect to
XCO_2	Column averaged CO_2 mixing ratio

Definitions

Note that specific details, related to the definitions below, are given in section 2.4.1.

Key parameters for CO_2 L4 requirements

The key parameters to consider are the following:

- **Spatial resolution and sampling** in order to locate the sources and sinks and also to characterise their size. Spatial resolution and sampling are essential when addressing the spatial resolution of the flux products.
- **Temporal resolution:** the purpose is to have a good description of the temporal variability, adapted for each application considered. Temporal resolution is directly linked to the satellite orbit and swath.
- **Accuracy** (defined as the root mean square (RMS) difference between the measurement and truth including both random and systematic (= bias) errors). This refers to the accuracy associated with the detection, quantification and then monitoring of the CO_2 surface fluxes [RD14]. This quantitative value is dependent on the considered spatial scales.

Key parameters for XCO_2 (CO_2 L2) requirements

The XCO_2 requirements are then based on the following parameters:

- **Horizontal resolution:** the required spatial resolution of a single CO_2 column observation is determined by optimization of the observation technique to better constrain the total error budget and not directly by the user requirements on CO_2 emission spatial variability. The main purpose, through the horizontal resolution, is to decrease the probability of cloud contamination in a single observation and to enhance the contrast for localised emission regions (cities, point sources), see 2.5.1.3.2 to better discriminate natural from anthropogenic fluxes. Due to difficulties related to radiative transfer modelling of “cloud holes” (*i.e.* cloud free area surrounded by clouds), a clear pixel or IFOV usable for CO_2 sounding has to be sufficiently cloud free also in the surroundings of a given “cloud hole” [RD5]. Furthermore, the impact of the horizontal heterogeneity of the surface properties should be also considered on the XCO_2 total error budget.
  - Thus, high-resolution temporal sampling reduces the risks for cloud contamination and horizontal inhomogeneity. Cloud contamination is best prevented by small pixel sizes, also reducing horizontal inhomogeneity in the scene. Because 3-D radiative transfer becomes important for the smallest scales a physical minimum of about 1 to 2 km exists for the pixel size in case of atmospheric composition observations (independent pixel approximation).
  - Note that for inverse modelling of regional surface fluxes, the link to horizontal resolution is typically indirect as the size of the target regions for the regional surface flux application is much larger than the satellite footprint size. The real necessity is a high density of sufficiently cloud free data.
- **Vertical resolution:** vertical resolution is mainly limited by the TIR measurement techniques, which can provide only limited independent pieces of information on the vertical profile, derived in the troposphere. The SWIR averaging kernels do not permit to distinguish CO_2 between the troposphere and the stratosphere. It is unclear whether cloud-slicing techniques (combining cloud free and fully overcast pixels) could be made sufficiently accurate to differentiate between CO_2 at higher and lower levels in the troposphere. The synergy of SWIR and TIR observations for deriving CO_2 profiles from satellite instruments is still an open topic.

- **Observing cycle / revisit time for a given location (without screening between clear and cloud pixels)**: the frequency of observation that can be achieved is determined by the orbit, the extent of the swath, and cloud contamination. Moreover, in case of SWIR the CO_2 observations are limited to daylight conditions. Considering clouds, the useful revisit time may be decreased and also depends on location and season (snow/ice covered surface in winter with low reflectivity in the near-infrared, low sun, and more frequent cloud cover).
- **Observation errors:** different type of observation errors exist:
  - **Random errors (or precision):** they represent the quantitative measure of reproducibility or repeatability of the measurement without reference to an absolute international standard. Suitable averaging can improve the random error of the measurement (retrieval) but does not establish the systematic error of the observation.
  - **Systematic errors:** they represent the quantitative measure of the possible systematic offset, or bias between the measured value and the true value that constitutes the SI absolute standard. The required values refer to global long-term statistics (*i.e.* they refer to the ensemble of data products, *i.e.* to a spatio-temporal collection of individual retrievals). Locally in space and time larger values may be acceptable.
  - **Total error:** root sum square of random and systematic errors.
  - **De-biased systematic error:** identical with "Systematic error" but after bias correction.
  - **Stability errors:** they represent the quantitative measure of bias related to the instrumental drift over the years or over the mission lifetime.

Threshold / Breakthrough / Goal requirements (from [RD5]):

The definition of the "threshold" is extracted from the Sentinel-4 and -5 MRD [RD14] whereas the definitions of "breakthrough" and goal are extracted from [RD5]. These definitions are considered in the present document. They are considered for each key parameters mentioned above. More particularly, concerning the XCO_2 requirements, they are considered on random, systematic and stability errors (see chapter 2).

- **Threshold:** The threshold is the **minimum** performance below which the data would have no value in supporting the identified application.
- **Goal:** The goal is an **ideal requirement** above which further improvements are not necessary. The more accurate and precise the satellite XCO_2 data products are, the larger their information content. Therefore, the goal requirement for the uncertainties should be "0.0 ppm" for XCO_2, for example (similar remarks are valid for the other requirements). It may however makes sense to define a value larger than "0.0", *e.g.* if other errors such as model transport errors do not allow to make use of the additional information content data have if they are more accurate than the specified goal requirement.
- **Breakthrough:** The breakthrough is an **intermediate level between "threshold" and "goal"**, which, if achieved, would result in a significant improvement for the targeted application. The breakthrough level may be considered as an optimum, from a cost-benefit point of view when planning or designing observing systems.

Table of tables

Table of figures

Table of contents

1. Introduction

1.1. Context

Under the leadership of the European commission, the Global Monitoring for Environment and Security has been established to fulfil the need amongst European policy-makers, to assess accurate and timely information services to better manage the environment, understand and mitigate the effects of climate change and ensure civil security.

Under the leadership of the European Commission, GMES relies largely on data from satellites observing the Earth. Hence, ESA – in accordance with the European Space Policy – is developing and managing the Space Component for the initiative.

To ensure the operational provision of Earth-observation data, the Space Component includes a series of five space missions called 'Sentinels', which are being developed by ESA specifically for GMES. In addition, data from satellites that are already in orbit, or are planned will also be used for the initiative. The GMES Atmosphere Service [RD41] will provide coherent information on atmospheric variables in support of European policies and for the benefit of European citizens. Services cover: air quality, climate change/ forcing, and stratospheric ozone and solar radiation.

The main functions of the GMES Atmosphere Service are the acquisition and processing of space and in situ observations (Near-Real-Time, historic and ancillary), analysis and forecasting, product generation, dissemination and archiving. In particular, the GMES Atmosphere Service will provide:

- ✓ Standard Global and European data on which downstream services will be based;
- ✓ Information for process assessments;
- ✓ Daily analysis of the atmosphere at various space/time scales;
- ✓ Key information on long range transport of atmospheric pollutants;
- ✓ European overviews and initial and boundary conditions for air quality models;
- ✓ Sustained monitoring of greenhouse gases, aerosols and reactive gases such as tropospheric ozone.

One Task of the GMES operational system is to identify, assess and monitor regional and local sources and sinks of greenhouse gases and pollutants and related tracers in support of emission and sink verification and mitigation policy. CO_2 is often referred to as 'well-mixed'. However, it has large and variable anthropogenic and natural sources and sinks in the Planetary Boundary Layer (PBL). For this reason the concentration distribution of CO_2 has a significant spatial and temporal variability in the lower troposphere, including a strong diurnal cycle in the PBL due to the respiration and photosynthesis of vegetation. Although tropospheric profile information with global coverage will likely be optimal to constrain emissions, tropospheric columns or total column are estimated to contain sufficient information to improve upon emission estimates from surface networks alone and especially help to improve emission estimates on country-by-country basis, as typically required for the protocols [RD14][RD65].

The Sentinel-5 mission is part of the GMES initiative, the overall objective of which is to support Europe goals regarding sustainable development and global governance of the environment by providing timely and quality data, information, services and knowledge. Within the GMES Space Component Programme, Sentinel-5-UVNS covers the needs for continuous monitoring of atmospheric composition, in particular with respect to air quality and climate, with a UV/Visible/Near-Infrared/SWIR (UVNS) sounder to be deployed on the next generation of the European operational polar meteorological satellite series MetOp Second Generation (MetOp-SG) in low Earth orbit (LEO).

The Sentinel-5-UVNS instrument is a high resolution spectrometer system operating with 5 designated bands in the solar reflected spectrum, currently covering the ultraviolet (270-370 nm), visible (370-500 nm), near-infrared (750-775 nm), SWIR-1 (1590-1675 nm) and SWIR-3 (2305-2385 nm) bands.

Within the GMES space component, Sentinel-5-UVNS covers the needs for continuous monitoring of atmospheric composition with a focus on air quality, climate change/forcing, and stratospheric ozone and solar radiation. In the context of global climate change induced by a continuing increase in the average global temperature, the needs for carbon dioxide (CO_2) monitoring are part of the GMES operational system [RD41]. Indeed, the increase of the greenhouse gases (GHG) such as CO_2, but also methane (CH_4) and nitrous oxide (N_2O) are the major contributors on the modification of the global temperature. Despite the clear user need to monitor atmospheric CO_2 [RD27] [RD41] [RD60], the current baseline of the Sentinel-4 and -5 Mission Requirement [RD14] did not explicitly addresses CO_2 with similar priority as atmospheric pollutants and CH_4.

1.2. Objectives of the present document

This document is the Final Report concerning the ESA contract study 4000103801 "Requirements for CO2 monitoring by Sentinel-5".

The main objective of this study is to assess quantitatively the capabilities of the Sentinel-5-mission to provide useful information for monitoring CO_2, with respect to the user needs, and to provide recommendations for improving the mission (if any).

This final report is a self-standing document resulting from a compilation of all the individual reports and results prepared by the consortium during the execution of this project. In addition of this introduction, it contains the following sections:

- Chapter 2 – Review and establishment of user requirements for CO_2 monitoring.
- Chapter 3 - Setup of retrieval software for Sentinel-5 synthetic CO_2 observations.
- Chapter 4 – Capability of the current Sentinel-5 mission for CO_2 monitoring.
- Chapter 5 - Summary of the Sentinel-5 baseline CO_2 performance and recommendation for enhancements.
- Chapter 6 – First analyses of the suggestions for improvements of the current S-5-UVNS instrumental specifications.
- Chapter 7 – First evaluation of the capabilities of the Sentinel-5 mission for monitoring the total CO_2 surface fluxes (natural and anthropogenic) at the global to regional scale.
- Chapter 8 - Conclusions and recommendations.

2. Review and establishment of user requirements for CO_2 monitoring

2.1. Objectives and description of the proposed approach

2.1.1. Objectives of this chapter

One crucial point when assessing the capability of a space-borne mission to monitor CO_2 is the quality of the remote sensing measurements in comparison with the requirements addressed by the users. The user requirements are mostly focused on the estimation of the surface CO_2 fluxes and will depend on their needs and the associated applications.

Thus, the main purpose of this chapter is to provide a synthesis of user requirements for CO_2 monitoring (L2) with respect to flux determination (L4) by the Sentinel-5 mission, based on a review of existing knowledge and literature.

In order to fulfil this main objective, the following elements are detailed in this report:

- General and global objectives related to the monitoring of CO_2 in order to advance the challenges associated with the carbon cycle observation.
- The definition of the CO_2 applications: there are many actors in the CO_2 business. As an illustrative example of the large panel of possible applications, some potential uses of CO_2 flux estimates are listed here:
    - **Reduce uncertainty in the quantification of the CO_2 sink over land,**
    - **Monitor ocean and land fluxes and their response to climate forcing (El Nino, La Nina),**
    - **Measure the dynamic of vegetation through carbon fluxes,**
    - **Measure how vegetation is responding to climate anomalies,**
    - **Monitor the emission at state scale,**
    - **Monitor the emissions at regional scale,**
    - **Monitor the emission at city scale; Monitor the emissions at facility scale (power plants etc.); Verify the emission/sink of a planted forest (for carbon trading),**
    - **Determine the impact of political decision and economic boundary conditions on emissions,**
    - **Measure the respective emissions of airlines such as Air France, Lufthansa etc.;**

However, since the entire user requirements cannot be completely addressed and detailed in this report, a restricted number of user applications (typically a number of 3) has been selected. These applications should address both the inversion of natural fluxes for scientific applications (at global and/or regional scales) and anthropogenic emission monitoring at the local scale.

Related to the 3 selected applications, a literature review was performed in order to identify the corresponding user needs. The review, from which the user requirements shall be derived, were performed from existing material and available documents, and discussed by the expert team of this study.

User needs are transferred into user requirements, specified for the L4 products (*i.e.* CO_2 surface fluxes estimations) and in the XCO_2 space (*i.e.* total column averaged mixing ratio). Thus, the final key parameters to be considered in this study are the L2 requirements on a given observation (*i.e.* one XCO_2 product). For each key parameter, a goal and threshold should be given for each specific application. These key parameters will be justified by the requirements on the Level 4 products (induced by the user needs). A synthesis of the requirements is provided in appropriate tables (see Table 2-3 (L4 requirements), page 53 and Table 2-7 (L2 requirements), page 70). A further translation of the L2 requirements into L1 is not addressed in the present study as it was out-of-scope with respect to the allocated resources. Instead, a set of L1b specifications were translated into L2 with the use of 3 different retrieval algorithms, for then to be compared to the established L2 requirements (Table 2-7). Based on these results, L1b specifications were recommended.

2.1.2. Description of the proposed approach

The proposed approach described in this report (under the present chapter) is summarized in Figure 2-1: for each identified and explained CO_2 application area, user needs are described and detailed, and then translated into terms of precision on the L4 products. Finally, their impacts on various L2 products are provided to ESA as well as documented tables.

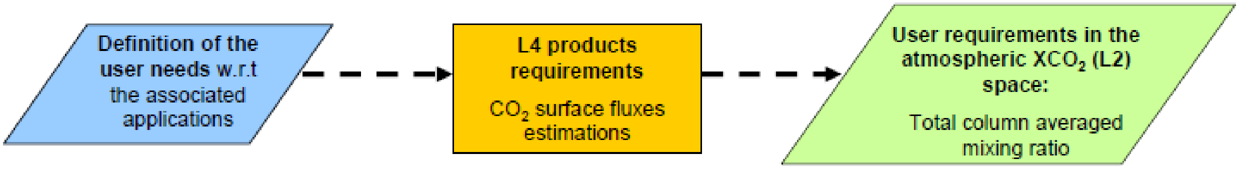

Figure 2-1: Description of the approach proposed under chapter 2

This chapter is divided into the following sections:

- Section 2.2 gives the general and/or global objective related to the GHG context and explains the general challenges associated with the carbon cycle observation;
- Section 2.3 details the 3 particular CO_2 applications selected and the justifications of the choices made by the consortium;
- Section 2.4 describes the end-user needs and transfers them into quantitative requirements for L4 CO_2 remote sensing products;
- Section 2.5 gives explanations of the link between the CO_2 L4 products and the L2 products, based on the atmospheric inverse modelling tools. Then, quantitative requirements for CO_2 L2 products related to each application are given with explanations on the key parameters to be considered.

2.2. Carbon cycle scientific needs

2.2.1. Perturbation of the carbon cycle

The concentrations of CO_2 in the atmosphere are estimated to be at their highest level since the past 56 million years (Myr) [RD15]. The current level of CO_2 has increased by nearly 40% from 280 ppm, in pre-industrial times, to over 386 ppm today [RD43]. The global average mixing ratio of carbon dioxide is still rising at about 2 ppm per year [RD27]. Human activity is the main and dominating contributor to this increase: the primary agent being the enhanced combustion of fossil fuel [RD29]. In addition land-use-change contributes with for about 10% to the total CO_2 emissions. CO_2 emissions induced by land-use change are mainly dominated by tropical deforestations. They can vary over space and time, depending on how the land is used and on the local climate, topography, and soil and vegetation properties. Currently greenhouse gas emissions from land-use change are the highest in tropical areas of South America, South-East Asia, and to a lesser extent, Africa [RD28].

For the period 2000-2008, an average of about 28.5 Gt CO_2 yr^{-1} was released to the atmosphere from the burning of fossil fuels, and it is estimated that an average of 5.6-9.3 Gt CO_2 yr^{-1} was emitted due to deforestation and land-use change during the same interval (*cf.* Figure 2-2). As a result of the very rapid increase of Chinese emissions, the fossil fuel emissions are now more than 30 Gt CO_2 yr^{-1} [RD29] [RD43] (32.2 Gt CO_2 yr^{-1} in 2008 [RD27]), with a more modest increase in most other nations. Almost half of the total anthropogenic CO_2 emission accumulates in the atmosphere. The rest is absorbed by sinks in the ocean and in terrestrial ecosystems. These natural sinks thus provide a discount of around 50% on the potential greenhouse effect caused by increasing CO_2 emission. The ocean takes up some 8.5 Gt CO_2 yr^{-1} and soils and vegetation 11 Gt CO_2 yr^{-1}. For example, extratropical regions in the northern hemisphere have recently represented carbon sinks because of net forest regrowth from earlier harvesting or encroachment on abandoned agricultural land and other processes, such as sequestration of carbon in landfills and water reservoirs and woody encroachment into pastures. These sinks are thought to absorb roughly 5-20% of global CO_2 fossil-fuel emission [RD55].

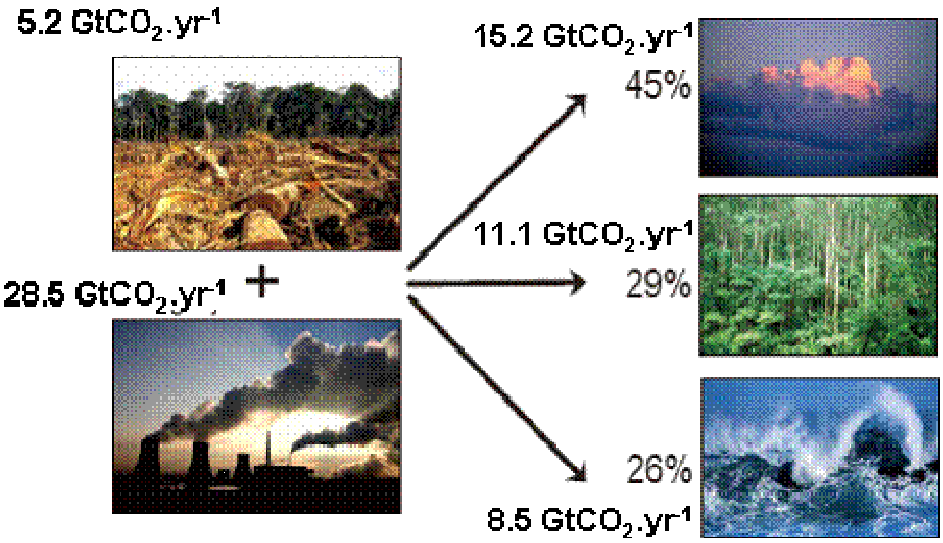

Figure 2-2: The anthropogenic perturbation to the global carbon budget and its fate during the period 2000-2008 [RD27]

The increasing GHG concentrations in the atmosphere will lead to an intensification of the Earth's greenhouse effect. The global climate system will be perturbed in ways that are not well understood, but there is a general consensus that global patterns of temperature and precipitation will change although the magnitude, distribution and timing of these changes are far from being certain [RD55] [RD43].

2.2.2. Global carbon observation challenge

2.2.2.1. Current and evolving carbon cycle observations

The increases in greenhouse gases in the atmosphere, as mentioned previously, are anthropogenically driven but partly compensated by absorption of CO_2 at the Earth's surface and also by chemical reactions in the atmosphere in the case of CH_4. The atmosphere is a rapid but incomplete mixer and integrator of spatially and temporally varying surface fluxes. Atmospheric growth rate of CO_2 exhibits large inter-annual fluctuations of the order of the average yearly long-term trend. The inter-annual variability signal cannot be explained by the variability in fossil fuel use [RD29] [RD43] and is mostly related to biogenic and oceanic cycles.

Improved predictions of future CO_2 levels require better quantification and process-level understanding of the present state of the global carbon cycle, including both natural components and anthropogenic contributions. Limitations in our current understanding also result from the inability to accurately locate key sink or source regions. Independent information on spatial and temporal patterns of CO_2 sources and sinks are necessary for challenging process-based terrestrial cycle models.

Measurements have shown that since 1990, the Kyoto protocol base year for reducing GHG emission, radiative forcing of these long-lived agents had actually increased by 26% in 2008 (about two decades later). Increasing CO_2 alone was responsible for 80% of this increase and has been responsible for over 85% of the increase in radiative forcing during the last decade [RD27]. The goal of this protocol was to reduce the emissions, and only those of some countries. However, it is very clear that, even with a reduction of emissions, the concentration (and therefore the greenhouse effect) will keep increasing.

The ability of nations to implement policies that limit atmospheric GHG emissions, and therefore the rate of increase of the concentrations will depend on their ability to monitor progress in mitigation policies. Uncertainties in existing observations and analyses have to be reduced substantially to support effective national-level policies and international reporting on climate change mitigation. Over the past ten years, the carbon cycle observing system has developed through various programs and projects. The spatial and temporal scale coverage (depicted in Figure 2-3) of the current observation system is essential for monitoring CO_2 emissions and concentrations. **Their extension must be optimised through establishment of new *in situ* monitoring stations and launching space-based remote sensing platforms. Observations have to be integrated across the relevant space and time scales.**

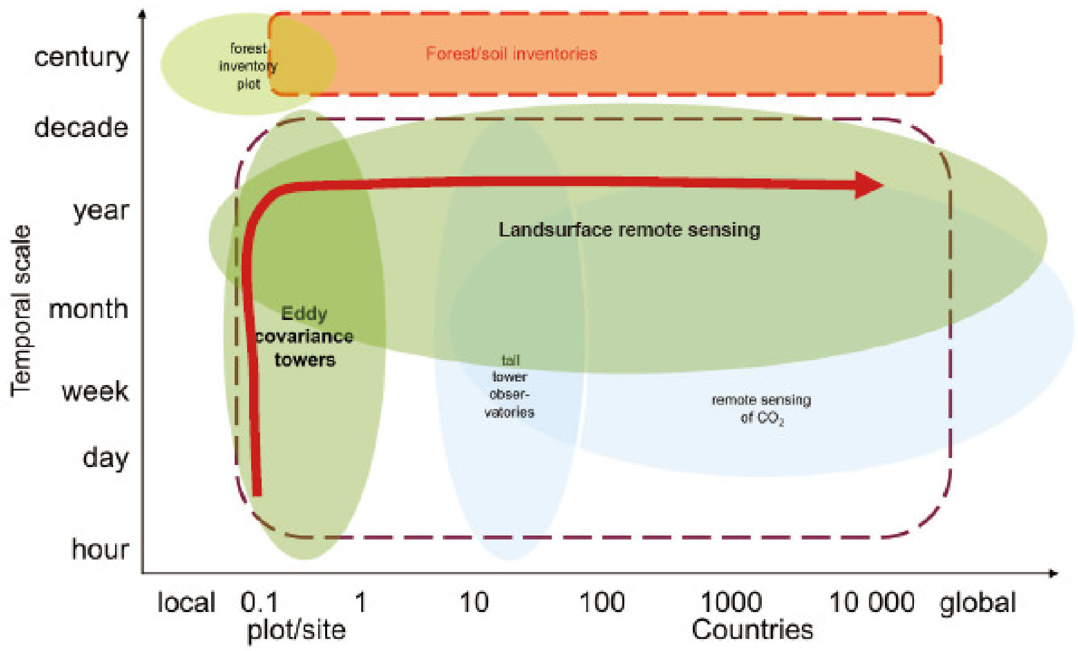

Figure 2-3: Example of the range of observations from a terrestrial fluxes perspective as a function of temporal scale (y-axis) and horizontal scale (x-axis, in km) [RD27].

2.2.2.2. High-level objectives

An integrated global carbon cycle observation and analysis system will have to differentiate the large natural source and sink processes from the smaller anthropogenic exchanges. It should also monitor the short and long-term compliance of specific climate mitigation measures at global and national-level scales. It will need to distinguish fossil fuel and non-fossil-fuel sources and it should be able to track agricultural and forest sinks by detecting relatively small departures from reference levels.

The integrated global carbon cycle observations should provide the following elements [RD27] [RD43] [RD69]:

- Size, location and processes controlling present-day terrestrial and marine carbon sources and sinks by region and/or sector;
- Contributions of deliberate carbon sequestration activities to the global carbon cycle;
- Assessment of the relevance and potential improvements of regional and national GHG management and policy interventions (*i.e.* CO_2 mitigation policies);
- Improvement of the quantification of the natural fluxes, in particular the exchange of vegetation and soil on the continents;
- Detection, quantification and monitoring of temporal variability of the anthropogenic emissions;
- Improvement of the understanding of the behaviour of the carbon sources and sinks at this present, and in the future under higher CO_2 and altered patterns of climate, land vegetation, and ocean circulation (focus on the factors that control the atmospheric level of CO_2);
- Temporal predictions of feedbacks enhancing global warming.

Thus, depending on their final use, the spatial resolution needed for global maps of CO_2 should be improved. As illustrated in Figure 2-4, for global studies with flux inversion, the ultimate target spatial resolution, mentioned by [RD27], is typically 10 km over land and 50 km over the ocean, with temporal resolution of a week or less. The short term objective of monthly fluxes with spatial resolution of 100 km over land and 500 km over the ocean may be possible within the next decade. However, finer spatial resolutions (sub-hectare to 10 km), needed for national-level land-use monitoring, are expected to be available on a time scale of 1-2 decades for demonstrating (by non space measurements) the short term impact of specific reduction/sequestration techniques and the corresponding compliance verification.

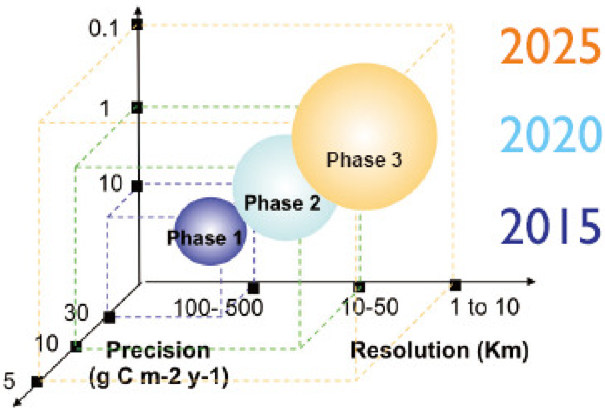

Figure 2-4: Future evolution of requirements toward finer resolution and precision capabilities for producing global maps of CO_2 surface fluxes [RD27]. The vertical axis is the temporal resolution given in days

2.2.3. Focus on the remote sensing of atmospheric CO_2

Despite the continuous expansion of the *in situ* monitoring network, it is clear that it will never have the density required for global monitoring of fluxes at small scales. Furthermore, the *in situ* monitoring network will not be expandable with adequate density over large areas difficult to access (Amazon, Africa, Siberia etc.). Thus, in this context, the use of space-borne observations is appealing. Indeed, space-borne observations complement the *in situ* network by providing high-density of measurements over most of the globe (see Figure 2-5). By densely sampling the observation of the atmosphere, it is expected that satellites will be able to capture CO_2 gradients directly over source/sinks regions.

Time series of CO_2 data from European satellites, with boundary layer sensitivity, started in 2002 with the launch of SCIAMACHY onboard ENVISAT which is measuring at a spatial resolution of 30 km x 60 km (spatial resolution available for measurements in the 1.54 µm CO_2 band). Recently, biases in XCO_2 from SCIAMACHY could be significantly reduced to below 1 ppm [RD19] by applying a so-called "full physics algorithm", which takes into account the scattering characteristics explicitly [RD44].

Presently, the only current mission dedicated to greenhouse gases (GHG) is GOSAT. The NASA OCO-2 mission [RD67] is under construction and will be launched within a few years. Future mission concepts are under study in Europe for improving the precision of XCO_2, as well as the spatio-temporal coverage and spatial resolution. This is needed in order to better quantify natural surface fluxes at regional scale, and to address more challenging objectives (including the possibility to measure strong anthropogenic emission sources). The proposed missions are: CarbonSat (selected as candidate for ESA Earth Explorer 8) [RD23], A-Scope [RD31] [RD51], OCO-2, Microcarb (CNES phase A study). The possibility to optimise Sentinel-5 for CO_2 monitoring is the purpose of this study, and will be addressed in later technical notes.

The objective of these scientific missions is the analysis of natural fluxes at global and regional scales. For achieving this goal in the long run, ESA has launched its Climate Change Initiative (CCI) [RD5] to provide robust CO_2 and CH_4 products from these missions. The Sentinel-5 (S-5) mission is an operational mission within the GMES observational satellite programme. The mission principally serves Europe: *i.e.* the European Union, the individual European countries, regions and their citizens. As part of the atmospheric core service, Sentinel-4 (GEOstationary Orbit) and Sentinel-5 (Low Earth Orbit) will constitute the ESA contribution to GMES for remote sensing of atmospheric composition and parameters. In the case of CO_2, Sentinel-5 may be a good candidate for measurements of this species at the required level of precision. Furthermore the operational aspect of Sentinel-5 is particularly attractive to ensure a sufficiently long time series of measurements. A preliminary analysis of the potential of Sentinel-5 for CO_2 monitoring has been performed in previous ESA definition studies such as CAPACITY [RD65] and CAMELOT [RD45]. These results will be reviewed here.

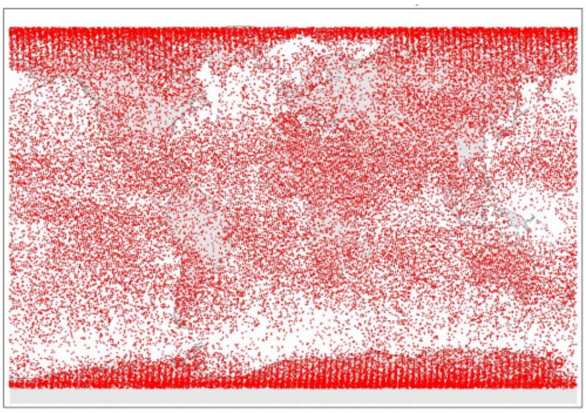

A-SCOPE

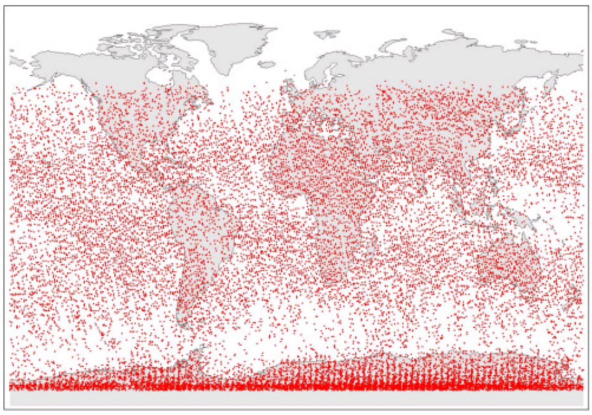

OCO

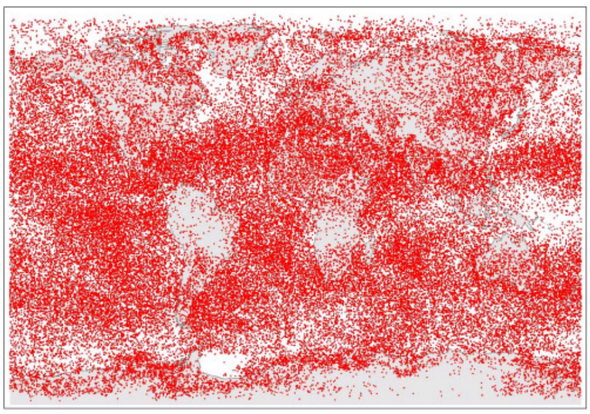

AIRS

Figure 2-5: Simulation of the geographical coverage of different current (AIRS) or proposed (A-SCOPE, OCO) space-borne missions with CO_2 observation capabilities for January 2005 [RD30].

The general climate objective of the Sentinel-4 and -5 satellite missions is ***climate protocol monitoring*** [RD14] [RD45] [RD41].

For the space-borne CO_2 observations by Sentinel-5, the general climate objective can be further divided into two specific mission objectives [RD45] [RD41]:

(i) ***Characterisation and monitoring*** [RD41] of the CO_2 sources and sinks that contribute significantly to climate forcing in terms of their location, strength, and variability;

(ii) Observation-based ***verification*** of emission estimates based on bottom-up inventories of anthropogenic CO_2 sources.

However, two other mission objectives, which have not been explicitly described so far in the context of Sentinel-5, could be envisioned for CO_2 observations by Sentinel-5:

(iii) Provision of observation-based constraints on the carbon ***sequestration*** per country.

Sequestration is defined as the process by which growing trees and plants absorb or remove CO_2 from the atmosphere and turn it into biomass (*i.e.* non-geologic sequestration). Country-wise quantitative estimates of the carbon sequestration would provide policy support on the possible accounting of sequestration in climate protocol negotiations. Country-wise constraints on sequestration are less relevant for small countries whose contribution to global or regional sequestration is limited by their surface area (e.g. Luxemburg)

(iv) Complementarities to ground-based *in situ* observation networks, to support the derivation of global and regional long-term ***trends*** in CO_2 concentrations.

Surface networks are best suited for the determination of global and regional trends in the background CO_2 concentrations because of the low random error on the individual CO_2 observations. The global atmospheric network of CO_2 measurements is composed of many national sampling networks coordinated by WMO GAW. The WMO GAW program (http://www.wmo.int/pages/prog/arep/gaw/gaw_home_en.html) is a unique international framework containing a multitude of national monitoring organisations, and is recognised by the Global Climate Observing System in its implementation plan to the UNFCCC [RD27]. However, until now, the measurements have largely been made under research programs from just a few countries: *e.g.* NOAA/ESRL USA; CSIRO Australia; NIES Japan, LSCE France; MPI Germany. This has prevented a large and uniform geographical coverage of the measurements. More importantly, much of the current surface network remains based on the collection of discrete air samples over ~5 minutes periods on a weekly or less frequent basis, seriously limiting the temporal coverage.

Moreover, not all of the surface stations are properly located to determine background CO_2 concentrations at all times [RD27]:

- Several of European stations are influenced by anthropogenic emissions during certain weather conditions (*i.e.* the spatial extension of the anthropogenic plume is dependent on the wind direction).
- Unlike observations within the marine boundary layer and at mountain observatories above the tree-line, air sampling above vegetation requires a measurement system that can reach or sample (in daytime) the fully developed boundary layer (not just the affected surface layer to avoid undue influence of local vegetation signals and to obtain regionally representative measurements such as $\sim 10^5 - 10^6$ km²).

Therefore, by combining satellite-based measurements with the currently available ground-based observations, additional information on limited temporal trends over rapidly-developing emission areas can be derived, given a mission lifetime of at least 5 years.

In addition to the above mentioned operational applications, space-based CO_2 missions should allow addressing the following science objectives:

(v) Closure of the carbon budget on global, continental, as well as regional scales;

(vi) Quantification of CO_2 land surface exchange processes on different spatial scales;

(vii) Constraining oceanic CO_2 surface exchange fluxes on different spatial scales;

(viii) Assessing the exact contributions of convection, long-range transport and general circulation including Brewer-Dobson circulation and stratosphere-troposphere exchange to the spatio-temporal variability of CO_2 in the atmosphere;

(ix) Determination of the causes of atmospheric CO_2 seasonal and inter-annual variability.

Although these do not necessarily need to be a driver for an operational CO_2 mission, objectives (v)-(ix) could be targeted by a scientific mission such as the ESA EE8 selected candidate-mission CarbonSat.

2.3. Definition of applications and justifications

2.3.1. Selection of 3 applications

User applications for the two primary objectives, ***characterisation/monitoring*** and ***verification*** of sources/sinks, require the generation of monthly and annual quantitative CO_2 emission data sets, and to differentiate these ones as much as possible geographically (cities, regions, countries, and continents) and per source/sink category.

Emission inventories typically contain many (sub-)categories to distinguish between emissions. However, many of these (sub-)categories will be co-located and impossible to differentiate from atmospheric observations. Therefore, it will be necessary to focus on targets having a strong emission pattern that dwarfs that from other flux processes. Examples of such emission patterns are:

- **Biomass burning**;
- ***Aggregated city emissions*** (road traffic, harbours, waste incineration, domestic heating);
- **Emissions from power plants and industrial complexes** (burning, industrial production).

Emissions from the last two categories (cities, power plants and industrial complexes) are localized and fairly continuous. Time-averaged emissions over extended time periods of weeks to months may be sufficient depending on the application considered. Some specific days may be better than other to monitor a local flux as there is a direct inverse relationship between the wind speed and the concentration gradient resulting from a given source. As a consequence, for very weak winds, a local source (sufficiently intense) is generating a strong local gradient than can be detected much more easily than for stronger winds. Because the impact of a given flux on the concentrations is depending on meteorology (wind speed and direction, convection…) any average of the concentrations in space and time must be carefully performed.

Large-scale biomass burning caused by deforestation and wildfires (irrespective of the exact type of ignition, which does not change the corresponding climate forcing) are very much of an intermittent nature and change in their geographical location. Localized time-averaged emissions over weeks to months may be very difficult to construct. Small-scale biomass burning of *e.g.* agricultural waste is of less relevance because of its near-closure of the annual cycle in terms of the CO_2 budget. For policy support on country-wise CO_2 **sequestration,** representative multi-annual averages of the sequestration effect (supported by information on inter-annual variations and long-term trends) are more relevant than monitoring the short-term variations in CO_2.

Maps could be used to visualize the geographical distribution of anthropogenic CO_2 sources in detail. Detailed CO_2 emission maps for the United States (10 x 10 km^2) have been generated e.g. within the Vulcan project (see Figure 2-6; more on http://vulcan.project.asu.edu/) based on extensive compilation of bottom-up activities and inventories. These maps are not constrained by atmospheric CO_2 observations. Similar observation-based compilations in other countries would probably be useful.

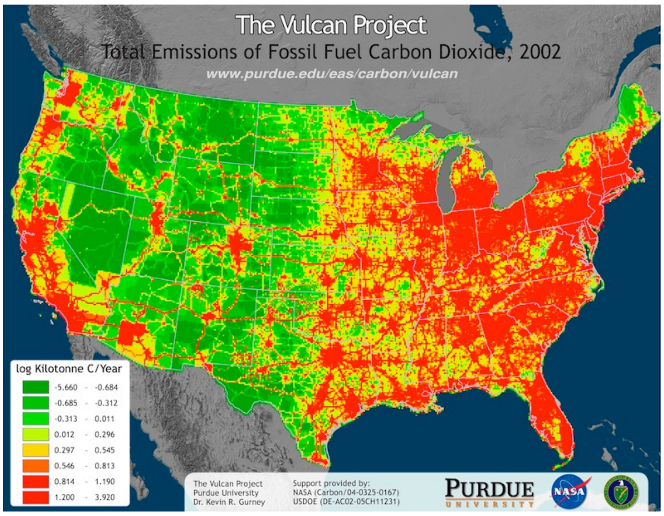

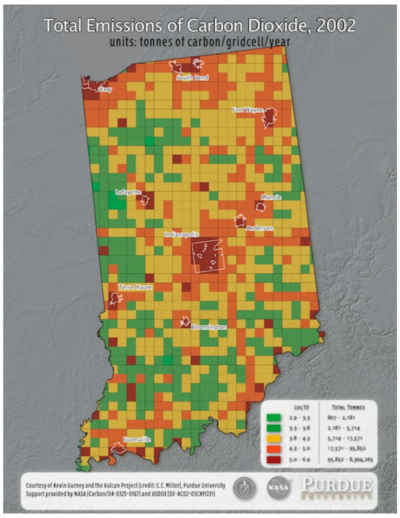

Figure 2-6: Mapping of bottom-up estimates on a 10x10 km² grid for the US (Vulcan project; http://vulcan.project.asu.edu/).

As a consequence, our study will address 3 CO_2 applications in order to specify the user requirements for estimating CO_2 surface fluxes. The consortium has identified 2 "extreme" or rather different applications (*e.g.*, fine scale and a global scale application) among the 3 applications which are selected. All the next 3 applications are focused on land only:

- Application 1: monitoring **total net CO_2 surface fluxes** (natural and anthropogenic) at the **global to regional scale** (~**500-1000 km**);
- Application 2: monitoring **anthropogenic city CO_2** surface emissions at city scale (~**50 km**);
- Application 3: monitoring **large anthropogenic CO_2 point** sources for example power plant CO_2 at **local/point scale** (~**1 km**).

2.3.2. A rationale for the 3 applications

CO_2 surface fluxes cannot be directly measured from space. Rather, remote sensing measurements can be used to quantify the CO_2 concentrations in the atmosphere. The surface emission may then be inferred from the gradient in the observed concentrations by the use of so-called inverse modelling. Inverse modelling makes use of the knowledge of atmospheric transport (wind fields, vertical convection and mixing) and the relationship between an emission at the surface and the resulting increase of concentration along the direction of atmospheric transport/advection. Thus, we assume in this section that the emissions are indeed estimated with such techniques. The principle of inverse modelling (from CO_2 concentrations to the CO_2 surface fluxes) is explained in more details in section 2.5.1.

[RD28] summarizes the current state of the art in CO_2 inversion estimates based on the last studies reported in scientific papers. Understanding of the carbon cycle, including the link between fossil-fuel combustion and increases in CO_2 has been improved through the various measurements of atmospheric CO_2 concentrations and other gases (currently made *in situ* at stations around the world and remotely from satellites). The combined use of CO_2 and oxygen (O_2) atmospheric measurements allows the CO_2 removal from the atmosphere to be partitioned into land and oceanic carbon sinks [RD54]. Other measurements, such as quantifying the less abundant isotopic analogues of CO_2 would significantly aid in verification or refutation of reported national emissions if the pattern of emissions being tested is provided and the measurements are made at sufficiently high spatial resolution and at suitable locations (*e.g.* within or close to the borders of the country whose emissions are being tested).

Although the annual atmospheric increase in CO_2 is known within 7%, **global annual fossil-fuel emissions can be estimated from atmospheric and oceanic data only to within 25%** [RD28] [RD54] [RD70] [RD79]. The reason of the difference is the large inter-annual variation in the size of the sources and sinks of the terrestrial biosphere and oceans, which must be separated from the total atmospheric increase to estimate the contribution from fossil fuel. Uncertainty in the anthropogenic CO_2 emissions from land-use and forestry is greater than 100% because both anthropogenic and natural changes in the terrestrial biosphere have almost identical effects on atmospheric CO_2 and O_2 [RD28].

Therefore, **natural and anthropogenic fluxes are hard to differentiate and usually only total fluxes are obtained.** As a result, the major source of uncertainty to infer CO_2 anthropogenic emissions using the method described above is the natural fluxes. Again, the inversion of CO_2 concentration measurements using an atmospheric transport model does not allow a direct separation of natural and anthropogenic fluxes [RD69]. Nevertheless, if the data have high spatial and temporal resolution and coverage, indirect separation might be feasible in the future by using information on the spatio-temporal behaviour of natural and anthropogenic fluxes.

Furthermore, another major source of uncertainty is the annual cycle. Although some variations are expected along the year, the order of the magnitude of anthropogenic emissions will not change from month to month or from year to year. On the other hand, the natural emissions of CO_2 do show a very large annual cycle together with inter-annual variations. Figure 2-7 and Figure 2-8 compare natural and anthropogenic fluxes of CO_2 on the same scale (expressed in gC m^{-2} d^{-1} or 1.34×10^{-9} Mt CO_2 $m^{-2}.yr^{-1}$) [RD69]. The natural fluxes are computed using a model accounting for meteorology, vegetation type, and phenology. During spring and summer, photosynthesis activity is much larger than the respiration as uptake by vegetation dominates. So, the net flux corresponds to a strong sink. During winter, the respiration of vegetation and soil dominates and the vegetation is a net source of carbon to the atmosphere (although of smaller magnitude than the sink during the growing season). Although the spatial patterns are somewhat different, natural fluxes are of an order of magnitude larger than anthropogenic emissions in most places. At global scales, natural fluxes are more diffuse than anthropogenic fluxes. Thus, it can be considered that atmospheric measurements at low spatial resolution will mostly constrain natural fluxes rather anthropogenic ones. On the other hand, one may expect that observations focused on large anthropogenic sources may be sensitive to these, but their observation does require a high spatial resolution for the measurements

The first application addresses global total net fluxes at the resolution scale of a few hundred kilometres. Thus, to be able to infer anthropogenic fluxes, it is necessary to have information on natural fluxes. As a consequence, looking at natural fluxes is not only an "academic" question but is also important if tackling anthropogenic emissions is required. As a result, **application 1 will provide an order of magnitude of the requirements for total net CO_2 surface fluxes, mostly related to natural fluxes at this spatial scale.**

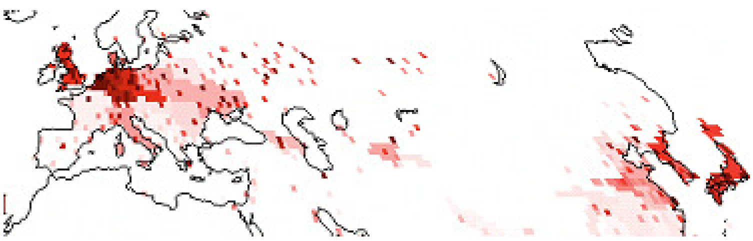

Figure 2-7: Anthropogenic emissions of CO_2 expressed in $gC.m^{-2}.d^{-1}$ or 1.34×10^{-9} Mt $CO_2.m^{-2}.yr^{-1}$ (same scale as figure below) [RD69]

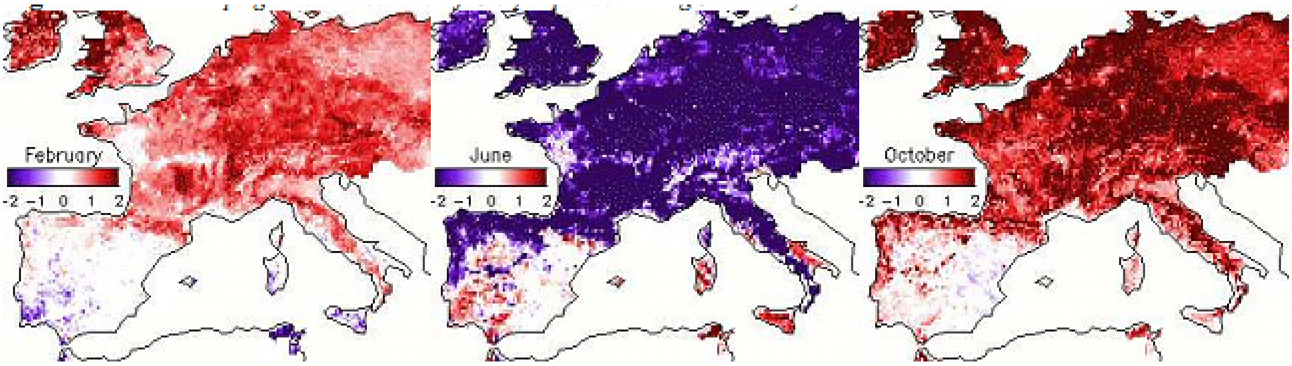

Figure 2-8: Natural fluxes of CO_2 expressed in gC m^{-2} d^{-1} or $1.34x10^{-9}$ Mt CO_2 m^{-2} yr^{-1} [RD69]

Applications 2 and 3 focus on intense anthropogenic emissions monitoring from satellite. The only way to constrain, detect and quantify anthropogenic CO_2 fluxes from remote sensing measurements is to focus on localised sources: *i.e.* cities or power plants for which the flux magnitudes (and thus the atmospheric signature) are stronger and more local than for the biosphere (more diffuse). Depending on the countries, this represents a large part of the anthropogenic CO_2 emissions at country scale. Figure 2-9 illustrates a map of CO_2 anthropogenic emissions over France, at high spatial resolution (2 km). Clearly, over large cities such as Paris, Lyon, Bordeaux and Lille the magnitude of anthropogenic emissions is significantly larger than that of natural fluxes. The remaining emission sources (*e.g.* transport over rural areas ...) are too diffuse to be clearly distinguished from natural fluxes from space based CO_2 measurements. Indeed, planned space-borne measurements have no direct mean to distinguish natural and fossil-fuel fluxes as they lack $^{12}C/^{13}C$ measurements. Furthermore, bottom-up inventories emissions in "open" countries and developed countries present fewer uncertainties at the country scale than at the city and local scales. Thus, there is reasonable hope to monitor intense local sources such as cities and power plants but little hope to measure diffuse anthropogenic fluxes that are mixed up with natural fluxes.

Therefore, **applications 2 and 3 will allow addressing a significant part of anthropogenic emission of a country. However, better monitoring CO_2 emissions at these scales will of course lead to more ambitious requirements** (as well on L4 products as on L2 products) **in comparison with application 1.**

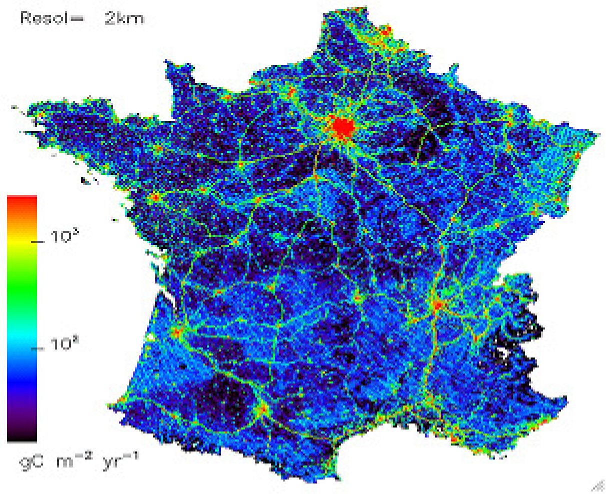

Figure 2-9: CO_2 anthropogenic emissions over France, year 2005, at high spatial resolution (2 km) expressed in gC m^{-2} yr^{-1} or $3.67x10^{-12}$ Mt CO_2 m^{-2} yr^{-1} [RD26]

2.4. User needs associated with the 3 applications

2.4.1. Main assumptions associated with the requirements of CO_2 space-borne products

The requirements given in the following sections for the CO_2 L4 and CO_2 L2 remote sensed products are focused on specific aspects which allow characterising these products in a detailed way. The definitions of these aspects have been provided in a specific section "Definitions", page 15.

There is one crucial element which has to be taken into account concerning the following definitions and requirements on the remote sensed products: a major assumption is made concerning the spatial correlations, when defining the requirements on remote sensed products. If spatial correlations exist between individual observations (from Sentinel-5 or other space-borne missions), it is to be underlined that they are not well characterised today. Characterisation of these correlations is a real scientific topic. This subject seems to be currently at a preliminary stage (as well for OCO, GOSAT, SCIAMACHY etc…) and it is of course out of scope of the present study. However, if in the 5-10 next years, scientists have the necessary tools to quantify these correlations (notably for the Sentinel-5 mission) the requirements (mostly the CO_2 L2 requirements) may be relaxed. This critical and crucial question could be addressed at the end of the study, when linking the S-5-UVNS XCO_2 performances and the current XCO_2 requirements.

2.4.2. Quantitative requirements for fluxes estimations

2.4.2.1. Application 1: Monitoring natural CO_2 surface fluxes at the global scale

2.4.2.1.1 <u>User needs</u>

During the past decades, vegetation has been taking up a significant fraction of anthropogenic carbon dioxide. Actually, it is not yet clear whether this sink globally distributed, lies mainly in the Tropics, North America, Europe or Siberia. Beside, vegetation-climate simulations of the 21st century indicate that vegetation may respond negatively to climate change and become a net source of carbon to the atmosphere after ~2050 [RD55] [RD43]. Thus, it is necessary to locate reliably the vegetation annual sources and sinks, and to promote investigations of the vegetation response to climate change.

Models of the scientific community for vegetation and soil dynamics allow calculating the exchange of carbon with the atmosphere. Their development is very helpful to understand the functioning of ecosystems and to predict their future behaviour including their response to climate change. Measurements of carbon fluxes are very useful to assess and improve these models. Such evaluations are made over specific sites with eddy-correlation measurements. Nonetheless, they are not representative of large-scale areas (probably because of a biased selection of sites over "young" ecosystems that generate net sinks of carbon). There is therefore a need to evaluate the models over areas of larger scale [RD30] [RD43], at least for the short (synoptic) to medium (seasonal) scales. Typical spatial scales needed for this purpose must combine the scale of the synoptic variation of atmospheric variables and the heterogeneity of the land surface cover.

As a consequence, monitoring the natural fluxes at global scale is required to address mainly two questions:

- The feedback **of vegetation induced by the rate of climate change during the 21st century**: this objective is considered as a threshold objective in this case;
- The **modelling of land-vegetation dynamics**: this objective is considered as a **goal** in this case.

Other points could be considered such as to monitor precisely land-use, sequestration on small parcels (since re-forestation and its impact on natural fluxes may play a role to better constrain carbon sequestration). However, these points are more specific and may be too difficult to link to GMES.

2.4.2.1.2 Quantitative requirements for L4 products for application 1

The following L4 requirements are based on [RD30] and on the assumption that monitoring the vegetation feedback to climate change is a threshold, and land-vegetation dynamics modelling is a goal. [RD30] is a scientific paper written by LSCE, where a top-down approach (*i.e.* inversion of CO_2 surface fluxes from the observed spatial and temporal concentration gradients) is performed for comparing the ability of different CO_2 concentration observing systems to constrain surface fluxes (results are partly summarised in section 2.5.5.1).

The L4 requirements presented below are considered as reference requirements for assessing these observing systems. They are defined upon a unique and robust exercise of characterization of the error diagnostic: the TransCom 3 project [RD70]. This project reported estimates of surface atmosphere CO_2 fluxes from an intercomparison of atmospheric CO_2 inversion models, which includes 16 transport models and model variants. The reported estimates of surface atmosphere CO_2 fluxes are provided over various ecosystems regions, at the sub-continental scale, about 2000x2000 km². The maximum number of regions in these inversions and the spatial distributions of fluxes within each region are fixes, precluding sensitivity tests of these inversion components. The key message delivered by the TransCom 3 project [RD70] is an identification of a northern land carbon sink distributed relatively evenly among the continents of the Northern Hemisphere. However, the quantification of this sink is clearly sensitive to the transport differences among models, especially in how they respond to seasonal terrestrial exchange of CO_2. This key message is supported by the following quantitative results [RD70]:

- **Large model uncertainties** (*i.e.* the degree to which transport model differences contribute to the range of flux estimates, as estimated by the standard deviation of the CO_2 flux over the ensemble of models) **are found for northern Africa, tropical America, temperate Asia and boreal Asia** (all greater than 1.9 Gt CO_2 yr^{-1}). For most regions, the between-model uncertainties are of similar magnitude than the within-model uncertainty: *i.e.* the mean of the individual model flux uncertainties. This suggests that the choice of transport model is not the critical determinant of the inferred fluxes. ;
- The ensemble of models identified a temperate North American sink, a small boreal North American source and a large sink for Eurasia with moderate estimated uncertainties associated with each estimated flux (between 1.5 and 2.6 Gt CO_2 yr^{-1});
- **Accurate knowledge on the seasonal biospheric background flux is important** for CO_2 atmospheric transport. Indeed, seasonal exchange with the terrestrial biosphere is responsible for much of the model spread over land regions. Realistic characterization of this aspect of model transport is essential if uncertainties are to be reduced in the future. [RD70] performed the exercise without taking into account the covariance related to this information. In some regions, there are substantial changes to the estimated CO_2 fluxes. An increase of 4.1 Gt CO_2 yr^{-1} in boreal Asia changes it from a moderate sink to a moderate source. Sink strengths increase by 1.3-2 Gt CO_2 yr^{-1} for temperate North America, temperate Asia and northern Africa in order to maintain the required global source. Thus, measurements indicating the strength of the covariance effect in nature are needed to assess this aspect of model transport.
- Current estimates of the net carbon fluxes over various ecosystems vary between 0.7 and 3.7 Gt CO_2 yr^{-1}. Based on these estimations and the associated uncertainties mentioned above, it is found that models provide currently uncertainties values up to 50% for surface CO_2 fluxes. As stated in [RD30], **a realistic objective today is to monitor the CO_2 surface fluxes within 10%**.

Spatial and temporal scales are related to the needs to well monitor and quantify the CO_2 surface fluxes (*i.e.* the so-called L4 CO_2 remote sensing products). Their definitions are given on page 15.

Thus, based on the main results of [RD70] and on the specific assumptions stated above (associated with [RD30]), the L4 requirements deduced for the **application 1** *i.e.* **global scale fluxes** are given below.

- **Spatial resolution / sampling:** Measurements of carbon fluxes are very useful to evaluate and improve vegetation and soil dynamic models over large-scale spatial areas for the short (synoptic) to medium (seasonal) scales. Typical various systems have in the reality a size **between 2000x2000 km²** (threshold) over the Amazonian forest **and 500x500 km²** (goal) for land surface with high heterogeneity (*i.e.* some European ecosystems). Thus, in order to constrain CO_2 surface fluxes estimates by vegetation models, observation spacing between 2000x2000 km² and 500x500 km² is requested. Indeed, these typical spatial scales are needed in order for the models to correctly differentiate the synoptic variation of atmospheric variables and the heterogeneity of the land surface cover. If a larger observation spacing is considered over a heterogeneous region, the probability for producing biased CO_2 surface flux estimates is high [RD70];
- **Temporal scale:** the L4 requirements are based on the need to monitor reliably inter-annual and seasonal variability. As explained above, seasonal exchanges between the atmosphere and terrestrial biosphere are providing crucial information to mitigate the model transport uncertainties. So, as a consensus between the scientific experts of this consortium, **the threshold should be 3 months and the goal is 1 month.**
- **Accuracy:** Current estimates of the net carbon fluxes over various ecosystems at this scale vary between 0.7 and 3.7 Gt CO_2 yr^{-1}. **There is therefore a need to measure the net carbon flux with a precision better than 3.7×10^2 Mt CO_2 yr^{-1} (threshold) or 0.7×10^2 Mt CO_2 yr^{-1} (goal)** (thus, a 10% of error as requested by the scientific community [RD30] [RD70] in order to mitigate the atmospheric transport models uncertainties).

2.4.2.2. Application 2: Monitoring anthropogenic CO_2 surface emissions at city scale

2.4.2.2.1 User needs

A "political" objective for the estimate of CO_2 fluxes is to contribute to the monitoring of the compliance with the Kyoto protocol or its follow-on. The Kyoto protocol only accounts for anthropogenic fluxes at the spatial scale of the countries (typically for European countries 500x500 km²). It requires the countries to decrease their CO_2 emissions by a few percent to the 1990 levels (for a 5-year average). In this context, the verification of a state compliance with a treaty requires a precision of the order of 1% for the net anthropogenic contribution [RD69].

A large fraction of fossil-fuel emissions emanates from large local sources, such as cities or power plants, and thus the effect of national mitigation measures should be obvious in the "domes" of CO_2 that they produce. Cities provide variable types of CO_2 emissions, *e.g.* see Table 2-1. Statistical or systematic sampling of CO_2 emissions from large local sources would provide independent data. That allows comparing trends in emissions reported by the countries in which those sources are located, at least for fossil-fuel emissions. CO_2 anthropogenic emissions from cities are often local and more visible than the CO_2 emissions from sources with larger spatial extent such as highways or have a more disseminated origin as, air traffic etc. [RD17] (see Figure 2-10).

On a methodological point of view, CO_2 fluxes in and out of a given city through transportation of fossil fuel by road/motorway (not to mention pipelines) have to be considered in the final carbon budget of cities (and cannot be achieved by measurements from satellite). The corresponding information would be accessible in "open" countries, but certainly not in countries affected by wars or armed conflicts where the corresponding data is barely accessible.

Sampling in cities, however, requires overcoming technical challenges, including finding ways to effectively construct seasonal averages in the presence of considerable spatial and daily variability and to separate biogenic from fossil-fuel sources. However, intense localized sources may present concentrated fossil-fuel emissions that are large enough to exceed the signal from local natural sources and sinks. For example, the emissions intensity of the greater Los Angeles metropolitan area is ~20 times the annual net sink observed at Harvard Forest (~0.9 kg CO_2 m-² yr^{-1}) [RD28].

Table 2-1: Surface CO_2 emissions for selected cities [RD28]

City (urban area)	Area (km²)	Population (millions)	Total CO_2 anthropogenic emissions (Mt CO_2 yr^{-1})
Los Angeles	3700	17.5	73.2
Chicago	2800	9.5	79.1
Houston	3300	5.5	101.8
Indianapolis	900	2	20.1
Tokyo	1700	29	64
Seoul	600	13	43
Beijing	800	15.6	74
Shanghai	700	18	112
Paris urban area	2730	10	60
Athens	430	4	41.6
Madrid	610	6	41
London	1580	7.4	70.8
New York city	1214	8.2	85.9

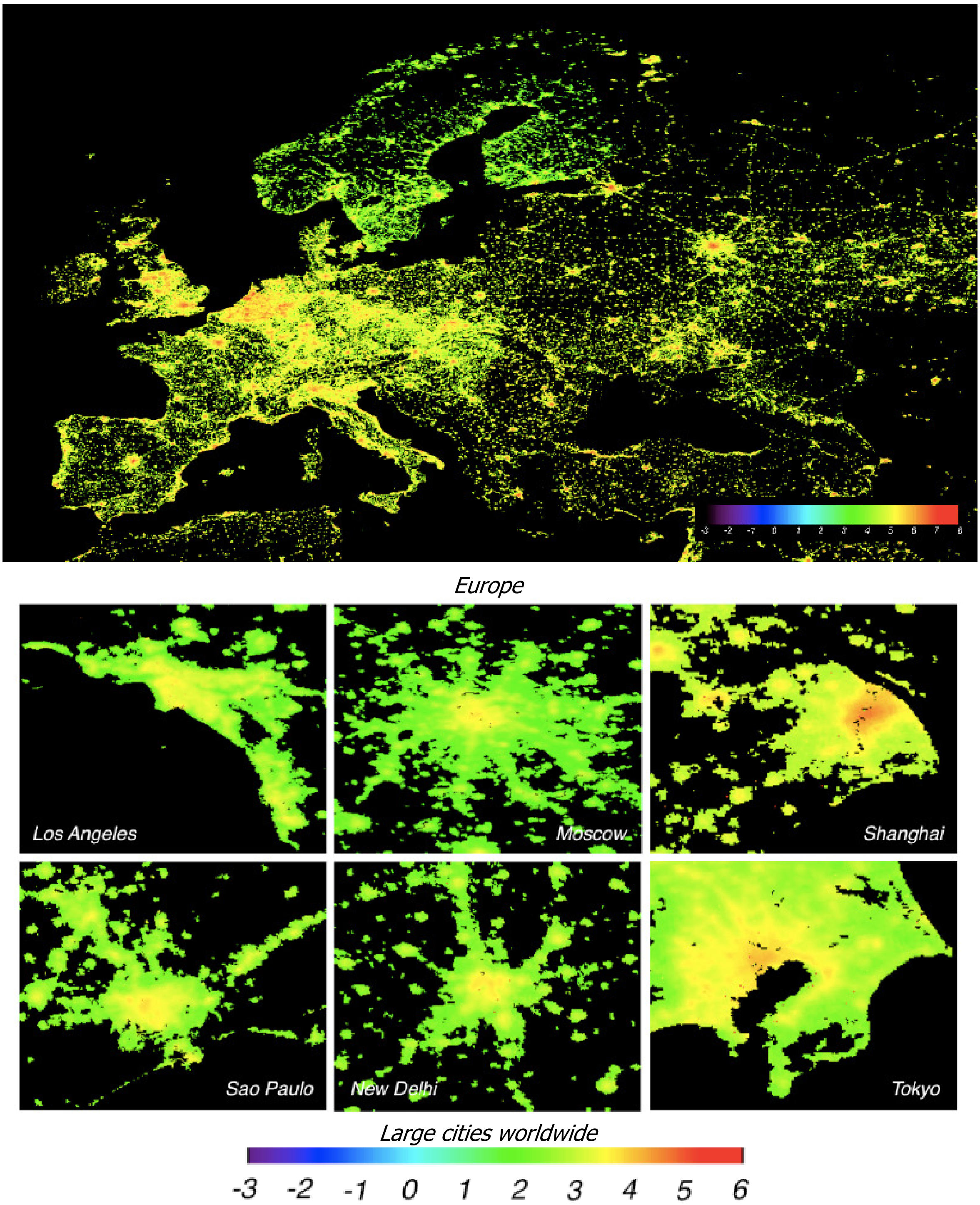

Figure 2-10: ODIAC FFCO$_2$ emission inventory for 2006 (unit = log tonne CO$_2$ per year) [RD17].

2.4.2.2.2 Quantitative requirements for L4 products for application 2

To our knowledge, no explicit document exists in the open literature which addresses clearly and specifically CO_2 L4 requirements for the selected application 2. Thus, **the CO_2 L4 requirements given below have been agreed upon after an intensive scientific discussion between the experts of the present consortium** (mainly during a dedicated working meeting). The main assumptions which are considered for these CO_2 L4 requirements are the following:

- The application 2 considers here the **cities which are in "open" countries**, mainly over European regions and USA. In this respect "open" means countries where free inquiry at the citizen initiative and international scrutiny is effective for generating publicly available and disputable facts, measurements or observations. As an example, countries, such as North Korea, are not considered "open" since their total CO_2 emissions are not accurately known and cannot be really estimated because of an inherent lack of *in situ* measurements and bottom-up inventories available.
- The CO_2 L4 requirements stated below are only valid for the cities with **CO_2 emissions and area size close to the values presented in** Table 2-1. Specific studies where high regional atmospheric transport simulations have been performed show that other types of cities cannot be observed by remote sensing measurement (*i.e.* where the CO_2 plume signal related to their anthropogenic emissions cannot be captured in the CO_2 total column). Figure 2-17 illustrates that only CO_2 emission associated with large cities such as Paris, London, Madrid and other similar cities can be identified by space-borne measurement. Moreover, simulations of atmospheric CO_2 on a 2 km horizontal grid resolution, performed by NOVELTIS and LSCE, have clearly demonstrated that CO_2 emissions of a city like Lyon (area of 48 km², CO_2 less than 8 Mt CO_2 yr^{-1}) cannot be captured by currently existing or proposed remote sensing measurements on this scale (almost no perturbation on the CO_2 total column) [RD4] [RD26].
- Temporal scale is based on the necessity to have **accurate information on the seasonal variation of the CO_2 fossil fuel emissions**. Section 2.4.2.3.2 and [RD63] demonstrates clearly this necessity concerning the local (*i.e.* power plant) emissions in order to estimate the total net CO_2 surface fluxes at the regional scale. The same assumption is made at the city scale, although capturing the seasonal variability at this scale seems less difficult than at the regional scale because less CO_2 diffusion and/or advection has taken place.
- Accuracy values are mainly derived from the requirements expressed by the scientific community in Table 2-2. These requirements are supported by [RD28], where uncertainties associated with current and future US CO_2 emission inventories are given for strong local sources (*e.g.* some power plants, cities) and fossil-fuel combustion. The values of these current uncertainties of CO_2 emissions, by fossil fuel combustion, are between 50% and 100%. By improving future remote sensing programs, one can reasonably expect to reduce these numbers to between **10-20%**, an uncertainty small enough to validate or correct the existing inventories.
- Finally, the spatial scales have been defined based on the size of the corresponding city. The relevant scale is the size of the CO_2 plume associated with the observed city. To be able to compute the CO_2 surface flux, the CO_2 gradient between the plume (where the CO_2 total column values are the highest) and the background (where the CO_2 plume has no more influence) must be estimated. Studies with atmospheric transport models ([RD4], [RD26]) show that CO_2 city plumes may extend up to 20-30 km. Typically, as shown in [RD26], only 24% of the plume is greater than 2 ppm above the background (380 ppm) in a 30 km radius. However, in Table 2-1, Los Angeles is ~1.4 times larger than Paris and the total CO_2 anthropogenic emissions are 1.2 more intense.

Thus, the L4 requirements associated with application 2 *i.e.* CO_2 emissions at city scale are mainly derived from Table 2-2 and finally from the several assumptions stated above and recalled here:

- **Temporal scale:** as a first preliminary assumption, the order of magnitude of the CO_2 anthropogenic emissions is considered not to change strongly from month to month. Thus, a **threshold of 1** year is required. However, over European areas, there is for example more consumption of energy in winter than in summer. Furthermore, as city emissions are less diffuse and more local than biogenic fluxes, time averaged emissions may be washed out because of the variations of synoptic conditions. Thus, **to be able to capture seasonal variability, a goal of 3 months is requested for better monitoring city emissions.**
- **Spatial resolution and sampling:** Table 2-1 shows very variable size for several cities. The most typical sizes are: 50x50 km² (threshold, Los Angeles city like) and 20x20 km² (goal, Paris or London cities like). It has to be noted that – as seen from Figure 2-10 - on city-scale there is a substantial variability down to the km-scale.
- **Accuracy:** Table 2-2 presents the precision requirements of different objectives for monitoring anthropogenic CO_2 surface fluxes, from city to local scales. Regarding the emission associated to large cities (such as Los Angeles, Paris, Madrid etc…), the main need today is the compromise between the quantification of temporal variability and the verification and monitoring of the consistency with existing inventories. Thus, we consider here **10% - 20%** (scientific objective for monitoring inter-annual or seasonal variability) of the surface CO_2 emissions associated with typical cities (such as Los Angeles or Shanghai): **20 Mt CO_2 yr^{-1} (threshold) and 10 Mt CO_2 yr^{-1} (goal) at 50 km to 20 km scale.**

Table 2-2: Precision requirement (in percentage of monthly average) of different objectives for monitoring anthropogenic CO_2 surface fluxes from city to local scales [RD26]

Goal	Precision requirement (in % of monthly average)
Detect the presence of a fossil fuel CO_2 source	<100%
Check consistency of top-down with bottom up inventories	20 to 30%
Quantify seasonal variability	10 to 20%
Quantify inter-annual variability	5 to 10%
Quantify annual trend	1 to 5%

2.4.2.3. Application 3: Monitoring strong anthropogenic local point sources

2.4.2.3.1 <u>User needs</u>

Power plants, most notably coal-fired power plants, are amongst the largest CO_2 emitters. They not only emit CO_2 in large quantities but also a number of other constituents such as aerosols and ozone precursors, which have a significant and adverse influence on air quality and climate. World solid fossil coal reserves are estimated at 930 Gt coal and construction of coal-fired power plants is increasing rapidly, notably in China and India. Thus, it can be expected that CO_2 emissions induced by coal-fired power plants will continue for many decades, and even may further increase [RD20]. The uncertainties of the reported anthropogenic CO_2 emissions are assumed to vary by sector and country, on average by about 3-5% for the USA to 15-20% for China [RD23]. At a single facility level, even in the US, the uncertainty can reach up to 20% [RD48]. **The uncertainty in world's annual fossil fuel emission is 6% to 10% (or 2.2 to ~4 MT CO_2 yr^{-1})** [RD20] [RD23]. This uncertainty is 1.5 to 3.3 times larger than the uncertainty in the atmospheric CO_2 accumulation (± 1.1 to ±1.5 MT CO_2 yr^{-1}) [RD20].

In parallel of China, USA also became the largest national source of CO_2 emissions during 2006. A comparison of the power plant emission data bases has shown that there is an absolute difference (typically about 20%) of the emissions of individual coal-fired power plants in the USA. **Therefore, several independent approaches are needed to reliably estimate how much CO_2 individual power plants are emitting**. The most recent estimates of EU fossil fuel emissions for 2000 are of an order of magnitude larger than the European ecosystem carbon sink. In particular, the CO_2 calculation approach implemented in the EU ETS presents **a bias that can be up to 20% against direct measurements** [RD20].

As a result, those uncertainties in the budget and the distribution of fossil fuel emission sources introduce substantial errors in the overall carbon budget derived from atmospheric inversions, when spatial resolution is increased from continental to regional, national or urban carbon scales [RD23] [RD63]. Indeed, **most common inversion frameworks assume fossil fuel emissions to be well known quantities, only biospheric and oceanic fluxes are corrected via optimization** [RD70]. Nonetheless, this assumption may not be appropriate, particularly as inversions continue to solve for fluxes at improved/better space and timescales [RD20].

[RD63] show results of a study which tries to estimate uncertainties of fossil fuel CO_2 emissions estimates. Three models from the TransCom 3 atmospheric inversion intercomparison project [RD70] run by using two different alterations made to widely used fossil fuel CO_2 emission estimates. The first alteration is the inclusion of a seasonal cycle which depends upon both season and latitude. The second alteration is the inclusion of year-by-year changes in the spatial distribution of fossil fuel CO_2 emissions. These three models span the key components of atmospheric transport and hence can be expected to capture the range of potential bias caused by uncertainties in the assumed fossil fuel CO_2 emissions estimates when interacting with transport processes. Key findings include the lack of seasonal rectification of the seasonally varying fossil fuel CO_2 emissions in the annual mean. This study illustrates that **the lack of seasonality on fossil fuel emissions produced bias of up to 50%** in the seasonal flux estimates during certain times of the year in the USA [RD20].

2.4.2.3.2 Quantitative requirements for L4 products for application 3

Power plants play a big role in the magnitude of fossil fuel emissions. For instance, in 2009, fossil-fuel power plants supplied about 69% of the USA electricity demand and are responsible for 41% of the total anthropogenic CO_2 emissions in the USA [RD20]. Figure 2-11 shows power plant emission statistics for several countries. Power plants emitting more than 5 Mt CO_2 yr^{-1} contribute to 60% of the total power plant emissions of the countries. Thus, if a satellite instrument can achieve a localized flux detection of more than 5 Mt CO_2 yr^{-1}, this would mean that about 60% of the power plant emissions in the USA could be detected.

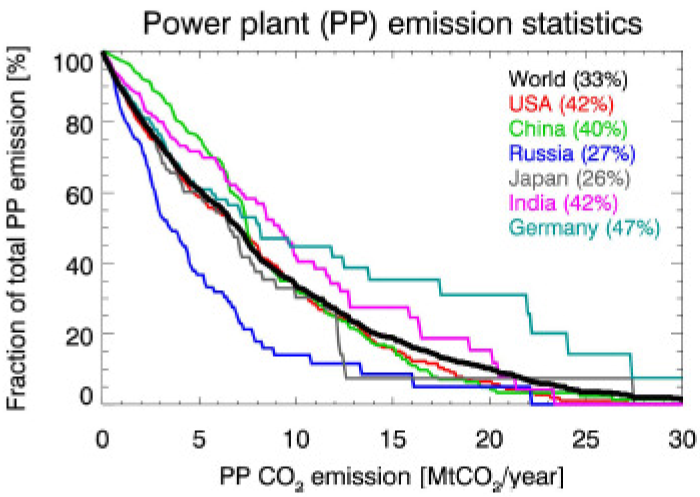

Figure 2-11: Power plant emission statistics for some countries and for the entire world [RD23].

The L4 / L2 requirements associated with **application 3** i.e. **power plant emissions** are mainly derived from [RD23]:

- **Temporal scale: 1 year as threshold** and **1 month as goal** (in order to be able to capture seasonal cycle). The goal value, deduced in a qualitative way by the consortium in this report, is based mainly on the same hypothesis as in section 2.4.2.2.2. The goal is more constraining because of the risk that the CO_2 emission may be substantially diluted by the wind is more important here, since this application is focused on more local CO_2 emissions. Furthermore, the necessity to have accurate information on the seasonal / inter-annual variation associated with the CO_2 fossil fuel emissions is emphasized in [RD63] (i.e. bias of up to 50% on regional total CO_2 surface fluxes if no information is available concerning the seasonality on fossil fuel emissions).
- **Spatial resolution / sampling:** for this application, **the L4 spatial scale is in the order of 1 km (goal)**, as this application concerns the monitoring of "point" source and very local emissions. L2 inversions for quantifying a flux (*i.e.* emission) is achieved over a point with a surrounding of a few km **(threshold 2 km)**;
- **Accuracy: 5 Mt CO_2 yr^{-1} as threshold (at a point)** if we want to monitor more than 60% of the power plants in the world. **2 Mt CO_2 yr^{-1} as a goal (nearly 80% of the power plants in the world).** Moreover, these numbers are supported by the fact that they are one order of magnitude smaller than the actual uncertainties associated with the world's annual fossil fuel CO_2 emissions [RD20] [RD23]. Thus, if CO_2 space-borne observations reach this accuracy, they will allow checking the consistency of bottom-up inventories.

2.4.3. Synthesis of the requirements on L4 products

A synthesis of the L4 requirements expressed in the previous sections (2.4.2.1.2, 2.4.2.2.2 and 2.4.2.3.2) is given in the Table 2-3. The CO_2 L2 requirements will be then derived from this synthesis.

Table 2-3: Synthesis of the user requirements for the CO_2 Level 4 products (CO_2 surface fluxes), derived from remote sensing measurements

Applications	Spatial sampling (km²) Threshold / Goal	Spatial resolution (km²) Threshold / Goal	Temporal scale Threshold / Goal	Accuracy (Mt CO_2 yr^{-1}) Threshold / Goal
1) Monitoring natural CO_2 surface fluxes (global scale ~500-1000 km)	2000x2000 / 500x500	2000x2000 / 500x500	3 months / 1 month	3.7×10^2 / 0.7×10^2 (for a 2000x2000 km² resolution)
2) Monitoring anthropogenic city CO2 surface emissions (city scale ~50 km)	50x50 / 20x20	50x50 / 20x20	1 year / 3 months	20 / 10 (at 50x50 km² to 20x20km² resolution)
3) Monitoring anthropogenic power plant CO2 surface emissions (local/point scale ~1-2 km)	Point up to few km	Point up to 1 km	1 year / 1 month	5 / 2

2.5. Towards CO_2 Level 2 requirements

2.5.1. Atmospheric inverse modelling

2.5.1.1. Introduction

There are conceptually two different approaches to estimate the fluxes of CO_2 over regions. First one can try to measure these fluxes at specific points and then extrapolate to the desired spatial and temporal scales, using known properties of the surface. In the case of industrial emissions, statistical compilations are simply used. The uncertainties associated with these so-called "up-scaling approaches" are usually quite high because of the large heterogeneity in space and time of the surface fluxes.

On the other hand, atmospheric CO_2 concentration measurements can be used through a so-called transport inversion model. These concentrations may be obtained from various instruments distributed around the globe. It is assumed that atmosphere acts as an efficient integrator of spatially and temporally varying fluxes. Despite vigorous mixing, small but persistent concentration gradients in the atmosphere reflect the patterns of surfaces sources and sinks both in space and time (*cf.* Figure 2-12). Atmospheric measurements of the CO_2 concentrations can be considered as a direct signal of the human perturbation of the carbon cycle (combustion of fossil fuel and land-use change) [RD39]. For example, burning of fossil fuel in North America, Europe and Asia would cause CO_2 to be higher in the northern hemisphere by nearly 6 ppm as compared to the southern hemisphere [RD69]. It is thus possible to estimate the spatial distributions of the fluxes that are fitting at best the observed atmospheric concentrations.

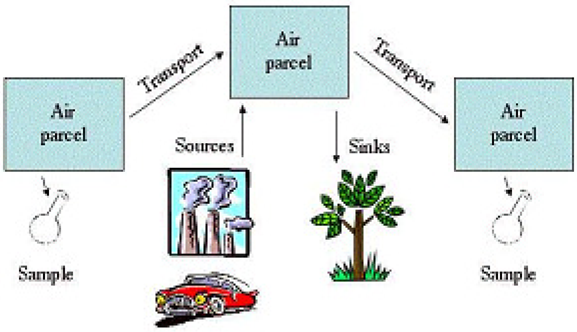

Figure 2-12: Principle of inverse approach: the concentration of an air parcel integrates sources and sinks along transport flow [RD69]

Clearly, the spatial resolution that is accessible with inverse techniques directly depends on the density, in space and time, of the data. Thus, the capability of satellite instruments to quantify surface sources and sinks and reduce uncertainties is strongly dependent on the density of observations, and also on their errors. Despite the different nature of the unknown variables (either fluxes or biosphere parameters) and of the observations (atmospheric concentration measurements), a model is needed to relate the former to the latter. In the case of a flux inversion, this model is an atmospheric transport model [RD43]. Potential improvements may be achieved with appropriate biosphere models, if necessary.

On the other side, the accessible spatial resolution for fluxes is also dependent on the effective resolution of the model, which is also introducing errors. By comparing various inversion studies focused on the terrestrial source-sink distribution, the differences are associated with errors in the simulated atmospheric transport, in the aggregation of the surface fluxes over large areas, in errors due to a poor representation (in the model) of the diurnal and seasonal variations of the surface fluxes with the boundary layer height (*i.e.* "rectification" errors) and errors introduced by the assumption that a point observation represent the average CO_2 mixing ratio (*i.e.* "representation" errors). The representation errors result from our inability to correctly represent point observations with simulated average values of model grid cells. They may be reduced by increasing the resolution of global atmospheric transport models or by employing high resolution regional models [RD53]. However, the lack of knowledge of the small-scale wind field and convection cannot be compensated by an increase of the model resolution due to the lack of observations constraining the model on small scales. Furthermore, correlated observation errors may force observation thinning which again leads to the inability to inverse model sources and sinks at small scales.

2.5.1.2. Implementation of inverse modelling: 3D Inverse formalism

Some distinctions have to be made regarding the implementation of the inverse technique and its aim:

2.5.1.2.1 Global or hemispheric estimates from *in situ* stations

Inverse studies started with the optimisation of hemispheric fluxes for large periods (one up to few years), based on the measurements at only few sites that are supposed to be representative of these very large scales. As a result, the inversion, from simplified chemical transport model, relies mostly on temporal gradients (1D inversion) [RD69]. Parameter inversions offer additional options for combining various sources of data, referred to as Carbon Cycle Data Assimilation (CCDAS). Global inversions are particularly useful in detecting trends and inter-annual variations of the fluxes, which highlight the sensitivity of the terrestrial biosphere to climatic variations, such as El Niño Southern Oscillation (ENSO) [RD43]. Nevertheless, inversion-derived estimates of long-term mean fluxes are much less robust in comparison with temporal variations. The main explanations are the heterogeneous sampling inherent to the sparse surface network and also the systematic errors in the transport models. Alternative approaches exist, based on high frequency measurements from networks of tall towers and Lagrangian, either stand-alone or embedded in an Eulerian atmospheric transport-model operated at a high spatial resolution. However, the robustness of these techniques has still to be established.

2.5.1.2.2 3D estimates from global survey

With the densification of the global atmospheric composition networks and/or the use of CO_2-dedicated satellite instruments, inversion of all surface fluxes (at regional or even finer spatial scale) for a given time step has been performed for CO_2 since the early 90s. However, given the present spatial coverage, the inverse problem is still largely under-constrained for regional estimates and this contributes to an amplification of errors [RD69].

Several techniques are available to circumvent this problem, of which the Bayesian regularisation technique is currently the most widely used. In this approach, a cost function is minimized iteratively, by a sequence of forward and adjoint model calculations, until the solution satisfies a predefined convergence criterion. Each step in the sequence consists of a forward simulation, used to determine the mismatch between the model and measurements, and an adjoint model simulation to determine the multidimensional gradient of the cost function with respect to the parameters, followed by an update of the fluxes using an efficient minimization algorithm [RD43].

Let $\mathbf{x}$ be the state vector corresponding to the spatio-temporal CO_2 fluxes emitted by the surface, $\mathbf{x_b}$ an *a priori* estimation of these fluxes, and $\mathbf{P_b}$ the *a priori* variance covariance matrix of the uncertainty on $\mathbf{x_b}$. Given a set of observations of atmospheric CO_2 concentration $\mathbf{y}$, and their error covariance matrix, $\mathbf{R}$, the optimal state vector of the CO_2 surface fluxes x corresponds to the minimum of the following misfit or cost function, under the assumption of Gaussian error distributions (as described by $\mathbf{R}$ and P_b) [RD2] [RD22] [RD30]:

$$\mathbf{J(x)= (x-x_b)P_b^{-1} (x-x_b)^T + (H(x)-y)R^{-1} (H(x)-y)^T} \qquad \textbf{Equation 2-1}$$

In this equation, $\mathbf{H}$ is the observation operator that quantifies the sensitivity of the atmospheric CO_2 concentrations to the CO_2 surface fluxes. The simulator computes the *a posteriori* error covariance matrix that is associated to the solution CO_2 surface fluxes [RD2] [RD30] [RD22]:

$$\mathbf{P_b' = (H^TR^{-1}H+ P_b^{-1})^{-1}} \qquad \textbf{Equation 2-2}$$

2.5.1.3. Difficulties with satellite data

2.5.1.3.1 Information content of atmospheric concentration measurements

Atmospheric exchanges between the boundary layer and the free troposphere are very slow. Convection and atmospheric transport mix the air higher up over a longer period, typically a few days. The signal from a given source region is then very diluted which makes it difficult to relate a concentration gradient to a localized source. Although theoretically possible, it is more difficult, and more uncertain, to relate concentration gradients in the upper atmosphere to CO_2 surface fluxes. Thus, XCO_2 is required to have a strong sensitivity to the low atmosphere *i.e.* down to the surface.

Clearly, a concentration measurement in the high atmosphere contains no significant information to locate precisely the sources and sinks. However, satellites dedicated to CO_2 monitoring provide users with SWIR measurements. These measurements contain information down to the surface, but are also involving a contribution from the upper troposphere and the less dense atmospheric layers above (see Figure 2-13).

2.5.1.3.2 Assessment and reduction of uncertainties

An important aspect of inverse modelling techniques is the characterization, and then the mitigation of uncertainties. The uncertainties are used to weight the contribution of individual measurements and *a priori* fluxes, accounting for transport model errors. They do not only represent the (analytical) measurement error, but also the so-called representation error which accounts for the mismatch between the time and space that is represented by measured samples and that of corresponding samples of the model. Thus, it is important to take into account model transport errors, particularly the parameterization of the upward transport by convection, and to properly quantify the corresponding error covariance. In all cases, it is necessary to validate model performances in order to determine properly the bias characteristics.

Transport uncertainty causes smaller systematic errors in emission trends than in their absolute magnitude [RD28]. For example, [RD54] compared CO_2 emission estimates from different tracer-transport models and found that the inter-annual emission trends for different regions within the same latitude zone were surprisingly consistent between models, despite of large differences in absolute emission magnitudes.

Moreover, the quantification of the observation error is also a critical parameter to assess the potential impact of an observing system. The observation uncertainty concerns the difference between simulated and observed quantities, and thus contains errors from both atmospheric transport and satellite retrieval. This means observation errors cannot be determined accurately since the true atmospheric state cannot be known. Although robust statistical analyses based on atmospheric transport models are performed, error estimates are combining contributions both from the measurements, retrieval and model uncertainties. The uncertainty is even more difficult to determine before real data become available, and past experience has shown that satellite-based observations do not always have the expected level of precision [RD30]. To assess the errors of the various satellite systems, radiative transfer simulations are usually performed for analysing the impact of both instrument noise associated with the observations (*i.e.* usually random errors) and the quality of the information related to the state of the atmosphere, as input to the forward modelling step and retrieval (*i.e.* usually systematic errors or bias). The associated geophysical parameters may be temperature, surface pressure, u and v wind fields etc…).

[RD5] provides a synthesis of the main results concerning the impact of regional bias error in XCO_2. As an example, regional biases of a few tenths of parts per million in column-averaged CO_2 can impact the inverted yearly CO_2 surface fluxes by a few tenths of Gt C. Thus, the characterisation and mitigation of geophysical biases is crucial e.g. by comparisons with independent well-calibrated observations (*e.g. in situ* observations from TCCON stations sensing FTS observations).

An accurate derivation of CO_2 surface fluxes is clearly dependent on the *a priori* knowledge of meteorological parameters considered in the transport models (*e.g.* local wind conditions, PBL height etc.). Indeed, the following relation illustrates the link between the minimum measurable flux and the minimum detectable change in the CO_2 concentration that can be measured by satellite [RD6].

For a satellite like OCO, designed to measure the column averaged dry air mole fraction XCO_2 (see section 2.5.2), the minimum measurable flux can be approximated as follows:

- Assume the minimum detectable change in XCO_2 is $\mathbf{\Delta XCO_{2min}}$ (*e.g.* 1 ppm);
- If the CO_2 flux, **F**, is constant over an accumulation time interval, **t**, the change in XCO_2 is given by (please note the symbol $\times$ here means "multiply"):

$$\mathbf{\Delta XCO_{2min} = F \times t} \quad \textbf{Equation 2-3}$$

- If we have an average horizontal wind speed, $\mathbf{u(\Phi)}$, in direction, Φ, over time, **t**, and a footprint has a horizontal dimension, $\mathbf{d(\Phi)}$, then the residence time will be:

$$\mathbf{t = d\ /\ u} \qquad \textbf{Equation 2-4}$$

- The minimum increase in the vertical column is therefore related to the minimum detectable flux as follows:

$$\Delta XCO_{2min} = F_{min} \times d / u \qquad \textbf{Equation 2-5}$$

and then,

$$F_{min} = u \times \Delta XCO_{2min} / d \qquad \textbf{Equation 2-6}$$

Thus, for a given XCO_2 sensitivity, the minimum measurable CO_2 flux is directly proportional to wind speed and is inversely proportional to footprint size of the measurement. Table 2-4 and [RD23] illustrate quantitatively the need to have a good knowledge of the wind speed for retrieving CO_2 emissions from power plants and other strong local point sources. The relative error of the inferred emission is thus equal to the relative error of the wind speed. For example, a 10% too high wind speed will impact the derived emission, which will be 10% too high. An error on the wind direction will also affect the results through an erroneous calculation of the concentration gradient $\mathbf{\Delta CO_2/d}$ and an error of 3° may result in an error of the derived emission of about 10%. It has to be noted that imaging XCO_2 over the region of interest of the strong emitter may allow to derive information on wind direction and potentially also on wind speed, if an "image" information of the plume is available.

Table 2-4: Errors of the estimated power plant (PP) CO_2 emission due to errors of the meteorological parameters wind speed (true value = 4 $m.s^{-1}$), wind direction (true value = 60°) and horizontal mixing in the across wind direction [RD23].

PP emission (Mt CO_2 yr^{-1})	Wind speed error (%)	Wind direction error (deg)	Horizontal mixing error (%)	Error or retrieved PP emission (Mt CO_2 yr^{-1})
13.0	+10.0	-	-	+1.3
13.0	-10.0	-	-	-1.3
13.0	-	+3	-	-1.0
13.0	-	-3	-	-1.1
13.0	-	-	+30	+1.3
13.0	-	-	-30	-1.6
26.0	+10.0	-	-	+2.6
26.0	-10.0	-	-	-2.6
26.0	-	+3	-	-2.0
26.0	-	-3	-	-2.2
26.0	-	-	+30	+2.6
26.0	-	-	-30	-3.3

In all cases, the hypothesis of the *a priori* errors on the fluxes must be carefully considered. It is difficult to make realistic assumptions, notably regarding the covariance matrices (diagonal terms and correlations).

Finally, errors related to CO_2 concentrations obtained from remote sensing data must be well characterized. For example, the instrument noise or SNR contribute to the overall uncertainty. Also, the retrieval errors, related to the retrieval methodology, may be dependent on *a priori* information concerning the atmosphere of the instrument calibration. These issues are discussed in the following sections.

2.5.2. Remote sensing techniques for the measurements of CO_2 concentrations

The currently envisioned remote sensing techniques do not allow the retrieval of a vertical distribution of CO_2 concentration (from a spectral measurement) but, rather a mean column concentration which is often referred as "total column XCO_2" [RD39]:

$$XCO_2 = \frac{1}{Psurf} \int_0^{Psurf} Cco_2[p]w[p]dp$$

Where:

- **P** is the atmospheric dry pressure;
- **Cco_2[p]** is the vertical distribution of the CO_2 concentration;
- And **w[p]** is the vertical weighting function expressed as a function of the vertical pressure.

The column averaging kernel vector gives the sensitivity of the retrieved XCO_2 to the true CO_2 mixing ratio profile. In the ideal case, a XCO_2 change introduced by the change of CO_2 at one level is one-to-one [RD44]. Actually, instruments that operate in the thermal infrared have averaging kernels that peaks around ~300 hPa (upper troposphere). On the contrary, instruments operating in the solar infrared are most sensitive in the lowest atmospheric layers (weighting functions extending into the PBL).

Figure 2-13 illustrates theoretical column averaging kernels for several instruments which are used or planned for the monitoring of carbon dioxide from space. Actually, they clearly depend on the data analysis procedure and of the geophysical parameters (temperature profile, atmospheric aerosol, surface albedo…). Passive nadir sounders on a LEO orbit (such as Sentinel-5-UVNS) are more suitable for CO_2 monitoring.

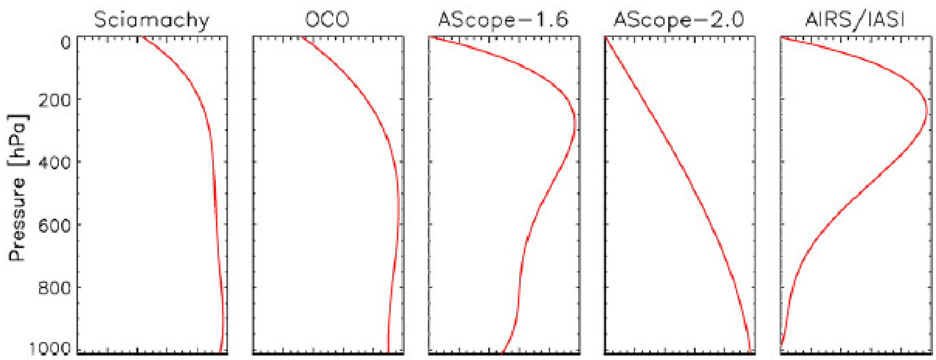

Figure 2-13: Column averaging kernels w[p] for several instruments that are used or planned for the remote sensing of CO_2 from space [RD39].

2.5.3. Theoretical approach for transferring user requirements into CO_2 Level 2 requirements

The translation of user requirements on fluxes into L2 data requirements can be made following the approach outlined in this section. Requirements on CO_2 concentrations or column averaged mixing ratios are based on the assertion of high-quality CO_2 observations which are complemented by a detailed error characterisation per observation. Because the spatio-temporal variability of CO_2 in the atmosphere is relatively small, the requirements w.r.t. the random and systematic CO_2 observation errors are very strict. The L2 data product requirements for CO_2 observations by the Sentinel-5 mission therefore should include:

- requirements for CO_2 data product(s);
- requirements for ancillary data products (needed for the retrieval of XCO_2).

A first practical way to define a limit to the systematic errors (bias) is the requirement that the **single observation total error should not exceed the peak-to-peak amplitude of the targeted CO_2 variations**. However, other upper limits for the total error of individual observations could be considered as well. This statement is of course a too relaxed requirement (although practical as a starting point). More detailed and application-related XCO_2 requirements are considered below.

Once in orbit, the instrument is generating L1 data (spectra) that are converted to L2 products (concentration or mixing ratio) and data assimilation may provide additional information about the total error and biases and even provide means for the validation of different components in the error budget.

2.5.4. Ancillary data products

The theoretical retrieval precision is an important quantity to characterize the performance of the satellite as it essentially determines the detection limit of the sensor. Thus, we have to take into account errors caused by imperfectly accounted for scattering effects and specific synoptic conditions. Thus, ancillary data products are needed for precise characterisation of the error budget. Assimilation of satellite CO_2 observations together with surface and *in situ* observations (*e.g.* from aircraft) in atmospheric transport models, *e.g.* for emission inversions needs such an accurate error characterisation.

The ancillary products needed for the error budget characterisation include:

- aerosol and cloud information (scattering and absorption characteristics affecting the light path – still to be defined more precisely);
- surface characterisation (surface reflectivity or albedo for solar backscatter observations);
- dedicated observations contributing to the characterization of the light path can be useful if they can be translated into parameters determining the light path in the CO_2 absorption band(s) used for the retrieval of XCO_2. Examples of such observations are: the use of information in the O_2-A band or accurate surface pressure provided by (re-)analysis of meteorology data (*e.g.* ECMWF, NCEP).

Moreover, a good description of the instrument and also the treatment of specific instrument aspects must be carefully considered. Indeed, a major reason for bias is spectroscopy and instrument calibration.

2.5.5. Focus on the quantitative XCO_2 requirements for the selected applications

The XCO_2 requirements are given in the following sections for a single CO_2 total column obtained from a space-borne measurement. Specific sections must be taken into account with the following requirements ("Definition" page 15 and section 2.4.1, page 45).

2.5.5.1. Application 1: Monitoring natural CO_2 surface fluxes at the global scale

XCO_2 requirements given in the ESA GHG-CCI study [RD5] have been derived for the GHG-CCI EV data products. The main goal of these specific products is to improve our knowledge of CO_2 sources and sinks located on land, especially in order to better constrain uncertainties of the CO_2 fluxes of the terrestrial biosphere (sources and sinks), at a regional scale. In particular, the threshold requirements are based on specific capabilities which can be reached by the current CO_2 existing instruments (*i.e.* SCIAMACHY and TANSO-FTS on GOSAT).

In the open literature, there is no explicit document today which is deriving XCO_2 requirements for monitoring the vegetation feedback to climate change (threshold) and the land-vegetation carbon flux modelling (goal). Thus, the **XCO_2 requirements given here are derived considering the existing missions (SCIAMACHY, GOSAT) and future planned missions (OCO, CarbonSat) and based on the work performed in** [RD30]. Indeed [RD30] show results of an OSSE study which uses the so-called top-down approach for retrieving surface CO_2 fluxes from the observed spatial and temporal concentration gradients. In this study, various CO_2 concentration observing systems are compared in terms of ability to constrain CO_2 surface fluxes. The various systems are based on realistic scenarios of sampling and precision (that are appropriate to each concept) for satellite and *in situ* measurements. The space-borne instruments OCO, SCIAMACHY and GOSAT are analysed. The assessment of these remote sensing observations is achieved by analysing the error reduction on the L4 products in comparison with the CO_2 L4 requirements given in Table 2-3, which are also defined and explained in [RD30]. Note that [RD30] does not provide requirements for a single XCO_2 measurement. But based on the performances of the space-borne concepts (which reach the L4 performances required) it is possible to deduce what XCO_2 requirements are necessary.

Thus, the XCO_2 requirements given below are based on the results obtained in [RD30]. In this way they are directly linked to the numbers given in Table 2-3. The given values demonstrate that OCO meets most of the goal L4 requirements listed in Table 2-3. GOSAT meets most of the threshold requirements, whereas SCIAMACHY results are mainly depending on the geographical areas and performances are somewhat smaller than those of GOSAT.

The fact that OCO presents capabilities for this specific application despite of 10 km swath width can be explained as follows. The inversion of the surface fluxes from the atmospheric CO_2 columns relies on *a priori* information on the spatial and temporal distribution of these fluxes. One searches a correction to the prior best estimates, and there are some assumptions about the spatial and temporal correlations of these errors (covariances matrices). As a consequence, a measurement can constrain a wide region (both in time and space). In addition, atmospheric transport mixes the signal so that the satellite measurements are sensitive to spatio-temporal averages that can be far (in time and space) to the CO_2 column measurement. This is why OCO can reach the requirements despite its limited swath. Clearly, this holds only if the mentioned hypotheses are true. The retrieval procedure cannot identify fine scale sources and sinks if those are not present in the *a priori* description of the fluxes. If the prior description of the fluxes (together with their uncertainties) is incompatible with the truth, the retrieval procedure will fail.

Thus the CO_2 L2 requirements given below are mainly based on the OCO and GOSAT performances (which will be provided). These requirements are consistent which the ones provided in [RD5] which considers OCO capabilities as goal requirements, and GOSAT/SCIAMACHY capabilities as breakthrough/threshold requirements. However, the requirement on the spatial scale is mainly derived from a specific study analysing the probability of cloud contamination in a pixel observation, depending on the spatial resolution [RD56].

Indeed, the requirements on the spatial resolution are very dependent on the space-borne observation. For this application, it is important to have cloud free accurate measurements. The link between L4 requirements and L2 requirements is very dependent on the density of observations available in the area of interest, as well as on the spatial coverage of the satellite measurements (not only the spatial resolution and sampling, but also the swath width). Figure 2-14, extracted from [RD56], show the fraction of cloud-free observations as a function of the area of the simulated footprint. The first panel is averaged globally between 70° North and South, excluding the polar regions.The second panel shows the same information but now averaged over the MODIS categories coast/desert/land over Europe (latitudes between 35°N and 73°N, longitudes between 10°W and 36°E).

The study in [RD56] is based on the analysis of the MODIS cloud mask at high resolution (*i.e.* 1 km) which gives 4 possible confidence levels: confident clear, probably clear, probably cloudy, and confident cloudy, with a 99%, 95%, 66% and less than 66% confidence clear, respectively. Larger footprints were simulated by combining several adjacent 1 km x 1 km observations depending on the area of the simulated footprint. The different simulated footprints always contain an odd numbers of original 1 km x 1 km observations. The resolutions have been chosen to represent a good sample nof resolutions for future and current missions: 3x3, 5x5, 9x9, 11x11, 21x21, 41x41, 61x61 and 99x99 (km x km). As the presence of clouds in an observation pixel is considered as a crucial problem, 0% threshold is considered as for the CO_2 application. Thus, for an area of 5x5 km², it can be expected to get ~25% cloud-free scenes. If a pixel of 2x2 km² is considered (like OCO), then the probability of cloud-free scenes increases to 30%. Therefore, the spatial resolution requirement derived from current specification of OCO may be relaxed for the present application. Then, it is considered that a goal of spatial resolution of 5x5 km² may be acceptable as the scales associated with this application are large. The gain in terms of probability cloud-free scenes is ~5% between 5x5 km² 2x2 km².

The CO_2 L2 requirements for **application 1** ***i.e.*** **global scale flux inversion** are therefore:

- **Horizontal resolution and sampling: 10x10 km² (threshold, GOSAT)** and **5x5 km² (goal,) (although an even smaller resolution would be better).** This high spatial resolution is essential for the next generation of GHG satellites in order to fulfil the GCOS requirements on the GHG Essential Climate Variables [RD27].
- **Revisit time: 16-day (threshold)** and **3-day repeat-frequency (goal).** This latter value is needed to get good monthly mean GHG fields considering perturbations by clouds [RD27]).
- **Random error: 4 ppm (threshold) and 2 ppm (goal).**
- **Systematic overall error:**
  - **Threshold: 2 ppm (threshold)** systematic error after global bias correction, where bias correction is not limited to the application of a constant offset / scaling factor.
  - **Breakthrough: 0.5 ppm (breakthrough)** systematic error after global bias correction, where bias correction is not limited to the application of a constant offset / scaling factor.
  - **Goal: 0.2 ppm (goal)** systematic error after global bias correction, where only the application of a constant offset / scaling factor independent of time and location is permitted for bias correction.
- **Stability error:** as systematic overall error **but per year.**

As for the systematic overall errors, [RD5] specifies that these values are obtained after application of a bias correction: *i.e.* they can be considered as persistent systematic overall errors values, which are remaining, even though bias are corrected (using aerosol, clouds or other ancillary information, instrumental calibration or regional corrections). Furthermore, for the other 2 applications, we assume that **these errors are not dependent on the considered applications.**

Moreover, because fixing user requirements on XCO_2 systematic error is a very innovative aspect, with many important discussions still in progress in the scientist community, this specific aspect presents requirements containing in addition of threshold and goal values, a breakthrough number.

As the preliminary exercise performed in chapter 7 demonstrates, the constraints on the accuracy with respect to the estimates of surface CO_2 fluxes allowed by a space-borne observing system might be a compromise between the accuracy of the observations and the quantity of available observations. **Therefore, the user requirements on the XCO_2 systematic errors should not be discussed as a single value, but should be defined with clear assumptions on**

- **the capacity to have (or not) a high number of single measurements exploitable in a given area.**
- **the characterization of the patterns associated with the XCO_2 systematic errors.**

Thus, provided that an observing system can deliver very numerous XCO_2 measurements (as Sentinel-5) and XCO_2 biases do not present a so-called "regional structure", as discussed un chapter 7, a threshold of 2 ppm related to a single XCO_2 product may be accepted. However, if the considered observing system would provide a few exploitable measurements over the Earth surface (*i.e.* limited swath width, or high swat width but too many products not exploitable because of strong heterogeneities in the scene for example) and/or regional structures of the biases are characterised, then a XCO_2 bias value of the order of 0.5 ppm (as a maximum) should be necessary.

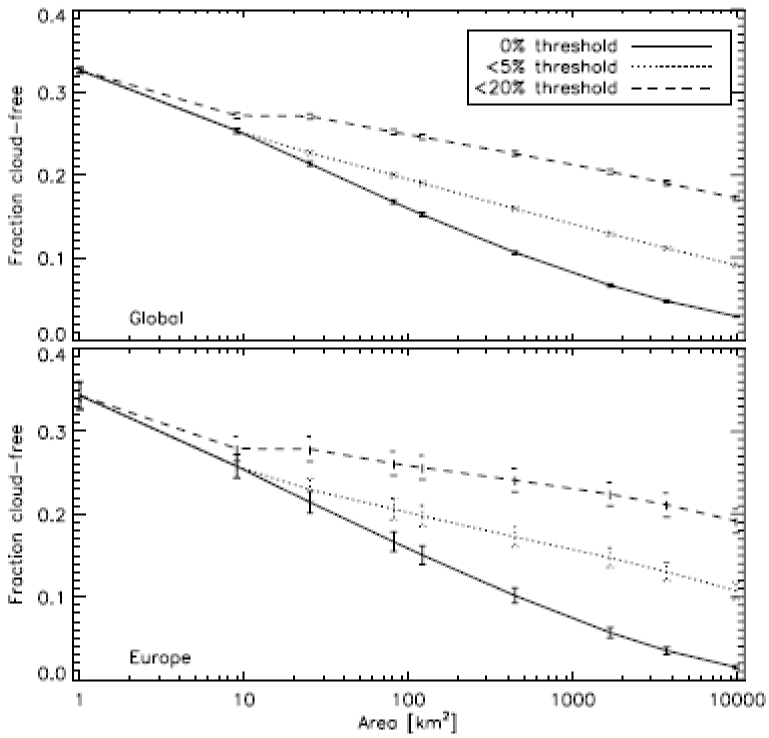

Figure 2-14: The fraction of cloud-free observations as a function of sensor resolution (foot print area), as determined from 1 km x 1 km resolution MODIS TERRA (local overpass time 10:30 UT) cloud mask (MOD35) observations. For each month in 2004 four days (either the 1st or 2nd, the 8th, 15th and 22nd) are analysed and statistics determined. Different line-styles indicate different threshold on cloudiness: 0% indicates that not a single MODIS cloud of 1 km x 1 km was allowed to present in the observed area. The data for the 5% and 20% thresholds includes the areas that were containing clouds up to 5% and 20%, respectively, of the total area observed.
Top panel: globally averaged between latitudes of 70°S and 70°N.
Bottom panel: the same plot but averaged over Europe (latitude range 35°N – 73°N; longitude range 10°W – 36°E) for MODIS categories land, coast, and desert. Coincidently, these cloud-free fractions over Europe are very similar to the global averaged fractions in the upper panel that also include the oceans [RD56].

2.5.5.2. Application 2: Monitoring anthropogenic city CO_2 surface emissions at city scale

A global observation network is developed, covering then large part of the Earth with continuous and event sampling of the CO_2 concentrations (see *e.g.* WMO GAW, http://www.wmo.int/pages/prog/arep/gaw/gaw home en.html; NOAA ESRL, http://www.esrl.noaa.gov/gmd/ccgg/). A first wave of increased attention for the global change issue around 1990 generated an acceleration of research activities, leading to a faster increase of the number of observation sites. A new development at that time was the deployment of tall towers as an observation platform. This is a way to make observations over land that are more representative of a larger region, by minimizing the influence of very local GHG fluxes on the observations.
Observations of CO_2 downwind from an emission area have been performed *e.g.* at the Cabauw tower in central Netherlands. The Cabauw tower was erected in 1972 for meteorological studies of the planetary boundary layer by the KNMI. Today, KNMI still owns and operates this tower, which is used for continuous meteorological and climatological observations and intensive scientific research.

The Cabauw tower is located about 25 km southwest of the city of Utrecht. The direct surroundings of the tower have a relatively low population density, although the area within 100 km of the tower contains a population of more than 7 million people. The main land use of the area around Cabauw is a mixture of intensively and extensively managed grassland [RD21].

The Cabauw tower can be selected as a suitable tower for capturing *in situ* CO_2 concentrations because [RD21]:

- To perform retrieval of CO_2 emissions, it is preferable to use a well established European network of stations for which continuous measurements are available for the synthetic model inversions.
- Based on a Lagrangian model framework using atmospheric transport models, an evaluation of a large number of European stations has been performed focused on a foot print analysis Through this evaluation, Cabauw is characterised as a polluted rural site with one of the largest footprints (about 500 x 700 km²), *i.e.* influence regions, of all the considered stations due to its sampling height and its specific location with relatively large mean wind speeds and large variability of the flow directions, so that air masses are sampled from many different directions [RD21] increasing the extent of the sampled "influence region. Figure 2-15 confirms this evaluation. The 20 m sampling level is much more sensitive to emissions in the near field up to 5° distance latitude and longitude around the tower and shows a more sharp decline of the sensitivity with distance than the 200 m sampling level. The main difference between the 20 m foot print and 200 m footprint is that the 20 m level receives more signals from the North Sea area northwest of Cabauw. Air masses that are transported over ocean or sea do not experience large fluctuations of the PBL height which dilute the concentration signals of fluxes from previous days on the way to the CO_2 sensor. This leads to the effect that during nights with northerly to westerly flow directions, the 200 m sampling level often received air masses that have not been in contact with sea surface emissions, while the 20 m level samples air with relatively high contributions from sea surface emissions. Then, by measuring at several vertical sampling levels, Cabauw tower can receive different weighted combinations of local signals and more remote signals.

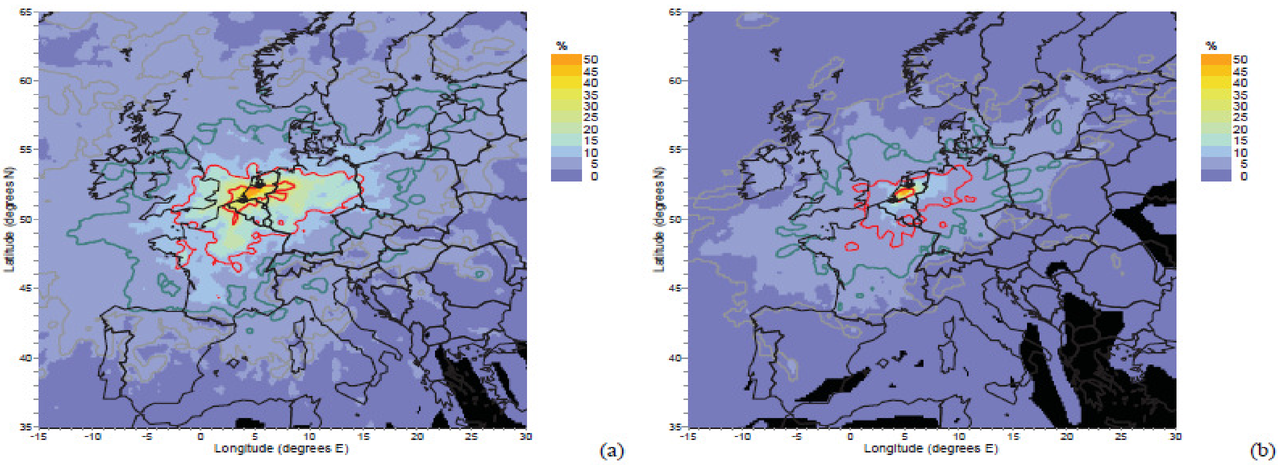

Figure 2-15: (a) Total hourly concentration footprint (2008) for Cabauw 200 m sampling level. First thick red contour contains the area with 25%, next thin red 50%, next thin green 75%, and next thin gray 95% of total potential footprint. Colour scale is percentage of potential footprint per pixel relative to the maximum pixel value; (b) total hourly concentration footprint (2008) for the Cabauw 20 m sampling level, colour scale similar to (a).

Downwind from emission areas boundary layer increases in CO_2 concentrations are observed in Figure 2-16. At an altitude of 200 m, the CO_2 observation at the Cabauw tower in the Netherlands [RD21] shows a peak-to-peak amplitude of about 20 ppm or 5%. At that height, the Cabauw tower receives air masses that have not been in contact with sea surface emissions, while the 20 m level CO_2 sensor samples air with relatively high contributions from sea surface emissions.

Increases at lower altitudes are up to 80 ppm above background levels but probably less representative for the PBL. These lower altitudes are more representative of local sources (or sinks).

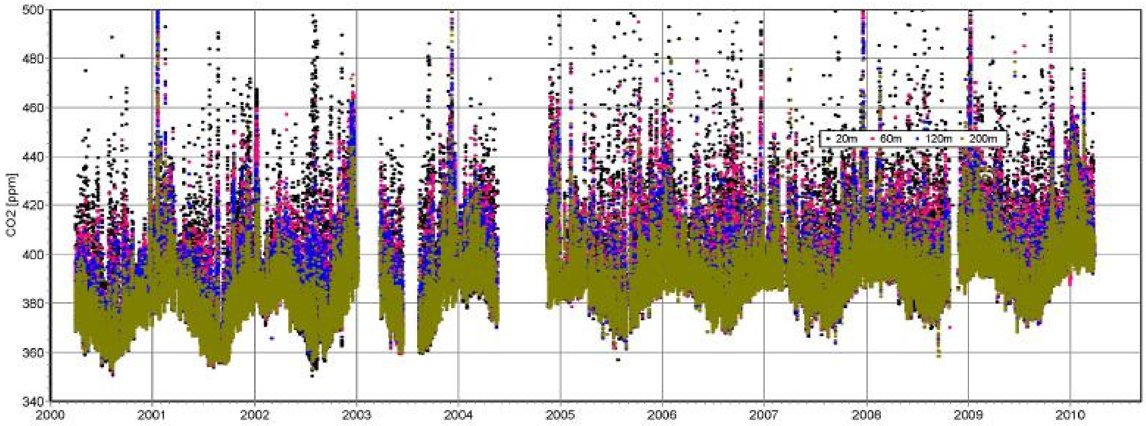

Figure 2-16: Time series of CO_2 at the Cabauw observatory, at 200 m (green), 120 m (blue), 60 m (pink), and 20 m (black) altitude, in the Netherlands [RD21].

The background CO_2 column for a column-averaged mixing ratio of 380 ppm corresponds to ~6000 g/m^2 for the total column and to ~1000 g/m^2 for a ~1.5 km (150 hPa) PBL column. Thus, a 5% increase in the PBL column-averaged CO_2 mixing ratio corresponds to a ~50 g/m^2 (~1%) increase in the CO_2 total column.

City CO_2 emissions per 400 km^2 (20 x 20 km) are estimated up to 10 Mt CO_2.yr^{-1}. For a 5 m.s^{-1} (18 km.hr^{-1}) wind speed the local column will be refreshed within one hour. The column enhancement per hour for 10 Mt CO_2 yr^{-1} emission rate over an area of 400 km^2 will be 2.5 g CO_2 m^{-2}.hr^{-1} (*i.e.* ~0.16 ppm). Lower wind speeds will promote significant (~1%) column increases as well as accumulation on the top of an already enhanced influx.

Table 2-5 explores expected enhancements of the CO_2 mole fraction over metropolitan areas [RD28]. The signal expected to be produced over a single large city relative to its surrounding is comparable to, and in many cases larger than, the average produced by an entire country [RD60]. These signals are derived with a standard assumption of a steady 5 ms^{-1} average wind vector, which would imply that the residence time of air over the metropolitan area would be ~4 hours (excepted for Los Angeles, which is surrounded by mountains on three sides and for which the residence time over this city is much longer). The numbers in the last two columns are typical, but will vary greatly in practice because they are inversely proportional to wind speed. Furthermore, the numbers are based on the assumption that the surface is at sea level for each area.

As illustrated in Table 2-5, a satellite instrument with 1 ppm sensitivity over a ~100 km down-track segment of its orbit might not detect Los Angeles, Chicago, Houston, or Tokyo [RD6].

Looking at the 10 km x 10 km resolution scale it is reported in [RD35] that for example the city plume of London can result in a total column enhancement up to 2-3 ppm (see Figure 2-17) compared to the surrounding areas.

Table 2-5: Expected CO_2 signals for selected metropolitan areas [RD28]

City (urban area)	Area (km^2)	Total CO_2 anthropogenic emissions (Mt CO_2 yr^{-1})	ΔXCO_2 (ppm)	PBL (1 km) (ppm)
Los Angeles	3700	73.2	0.49	4.3
Chicago	2800	79.1	0.60	5.4
Houston	3300	101.8	0.72	6.4
Indianapolis	900	20.1	0.27	2.4
Tokyo	1700	64	0.63	5.6
Seoul	600	43	0.71	6.3
Beijing	800	74	1.10	9.4
Shanghai	700	112	1.80	15.0

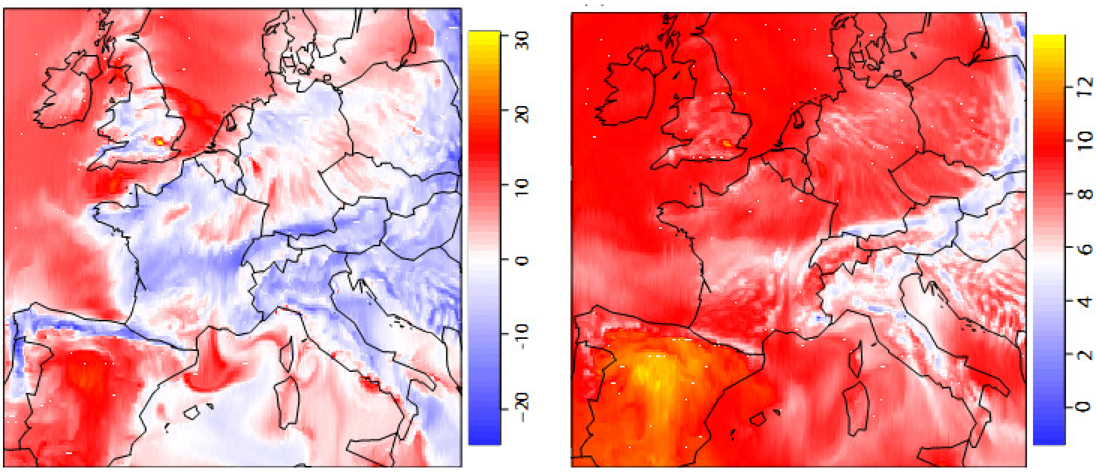

Figure 2-17: WRF-VPRM simulations of CO_2 mixing ratios (on the left) for an altitude of about 150 m above ground (2^{nd} model level), CO_2 surface and (on the right) mass weighted average CO_2 column during 12^{th} July at 14:00 GMT with horizontal resolutions of 10 km for a domain centred over Europe. An offset of 365 ppm is to be added to get total CO_2 in ppm. Note the scale change between near surface and column CO_2 [RD35].

Based on the space-borne instruments specifications of Table 5-1, page 164, and the expected CO_2 signals of Table 2-5, the OCO nominal uncertainty of 1-2 ppm (for a single IFOV) seems consistent for detecting CO_2 city emissions. In contrast, because a GOSAT sample covers a larger area than an OCO sample and presents larger uncertainties for a single CO_2 observation, GOSAT is not suitable for this application. In target mode, OCO could combine up to 7000 measurements at an individual site, under different viewing angles, and could potentially have an uncertainty of 0.1 ppm if systematic biases were characterized and removed [RD28].

OCO would have presented a critical combination of high precision, small footprint, readiness, density of cloud-free measurements, and ability to sense CO_2 near the Earth's surface. However, the OCO mission would have sampled only 7-12% of the land surface with a revisit period of 16 days and a nominal lifetime of only 2 years. Thus, OCO may have presented difficulties for local CO_2 emissions (such as power plants) but many metropolitan areas are large enough to be sampled by the planned orbit. Indeed, when the OCO swath of 10 km is covering a power plant, it will be possible to estimate the emission from it. For small cities, due to the small swath of only 10 km it will be very challenging for OCO to get the CO_2 city plume. Moreover, because of its 2-year mission life, OCO would not have been able to track emission trends. It is understood that OCO-2 will be an exact copy of the OCO satellite that was lost during launch in early 2009, so that the discussion above is indeed a realistic baseline for the future NASA mission.

As there is no explicit document which addresses XCO_2 requirements, for a single observation, for this application to city scale, and based on the previous discussion, an extensive spatial and temporal coverage is critical for monitoring CO_2 city fluxes. Even a single observation with a scale comparable to the target city area is significant.

Therefore, the XCO_2 requirements are mainly qualitative, derived after obtaining consensus between the experts during the working meeting associated with this project. These requirements are focused on the following assumptions:

- According to the scientific experts and as expressed in [RD5], L2 spatial scales should be a reasonable factor smaller than the L4 ones. Furthermore, a same factor applied on random error would allow obtaining the expected signals on CO_2 total columns, at the city scale, described in Table 2-5.
- [RD4] [RD26] have shown that a revisit time as specified for the candidate CarbonSat mission is necessary in order to capture the CO_2 signals (over cities like Paris) in order to eliminate synoptic variations.
- Specific simulations (*i.e.* CO_2 atmospheric transport simulations over the period of June 2005 and over a geographical area including Paris), at high resolution (2 km), associated with the studies [RD4] and [RD17] also provided the following results:
    - In favourable synoptic conditions (weak wind, so weak dispersion), over Paris city, there is an increase on the CO2 total columns between 4 ppm and 6 ppm?
    - In unfavourable synoptic conditions (strong wind, that is efficient dispersion), over Paris city, the increase on the CO2 total columns is limited to 2 ppm?
    - Only 24% of the plume is greater than 2 ppm (higher than the background of 380 ppm) in a 30 km radius around the centre of Paris city. Figure 2-17 does not show greater values in terms of enhancement of the total column.

Based on the above assumptions a threshold requirement of 2 ppm (goal: 1 ppm) is derived for observations that are not stringently selected for the observation conditions. However, the very numerous S-5 observations (compared to *e.g.* OCO-2 and GOSAT) which should be available in the 50x50 km^2 (goal: 20x20 km^2) city areas observed would give the possibility to stringently select observations for only the most favourable conditions (mostly cloud-free and low wind speed). For most cities in the world these conditions occur sufficient regularly during the year to make such stringent selection for quantification of the required annual (threshold; the goal is 3-monthly) city-scale emissions.

The stringent selection of observations would relax the threshold requirement to 4 ppm (goal: 2 ppm) given the expected 4-6 ppm column increases under such conditions (see the assumptions above). For such relaxation the selection should however provide a sufficient number of uncorrelated observations in order to exploit the relatively large number of S-5 observations available.

The possibility to make a stringent selection of individual measurements depends very much on the available ancillary observations to characterise the light path (clouds and aerosols) and surface characteristics (albedo) which is therefore also an important requirement for Application 2.

Sentinel-5 CO_2 observations are likely to be calibrated more easily for the more localized emission sources in application 2 than for the diffuse fluxes in application 1. Regional retrieval biases are relatively less important for application 2 and correlations related to retrieval biases are likely to be smaller over limited city areas than over larger regions.

Thus, the XCO_2 requirements for **application 2**, *i.e.* **city flux inversion** are proposed as follows:

- **Horizontal resolution and sampling: 10x10 km² (threshold)** and **5x5 km² (goal).** This is a factor 4-5 better than the spatial scale on which the anthropogenic emissions are needed: 50x50 km² (threshold); 20x20 km² (goal).
- **Revisit time: 6-day (threshold, typically CarbonSat)** and **3-day repeat-frequency (goal).** The threshold (goal) revisit time provides for most of the larger cities in the world sufficient temporal sampling for quantification of the required annual (3-monthly) emissions using observations selected for the most favourable conditions (*i.e.* cloud-free; low wind speeds).
- **Random error: 2 ppm (threshold)** and **1 ppm (goal).** These requirements are derived for observations that are not yet stringently selected for the observation conditions. Regarding the very numerous S-5 observations which should be available in the targeted emission area there is the possibility to stringently select observations only under the most favourable conditions. In case the remaining selected observations would be sufficiently uncorrelated the threshold requirements could be relaxed to 4 ppm (threshold) and 2 ppm (goal).
- **Systematic overall error: 2 ppm (threshold), 0.5 ppm (breakthrough) and 0.2 ppm (goal).** These are the required relative systematic error after bias correction, where bias correction is not limited to the application of a globally constant offset / scaling factor. Because of the better possibilities to calibrate the Sentinel-5 CO_2 observations at the more localized city-scale sources than at the more diffuse regional flux scale, systematic errors are somewhat less of a concern for application 2 than for application 1.
- **Stability error:** as systematic overall error **but per year.**

2.5.5.3. Application 3: Monitoring anthropogenic power plant CO_2 surface emissions at local/point scale

A coverage ensured by a high spatial resolution (1-2 km to minimize cloud contamination) and a 1-3 day repeat-frequency is needed to effectively monitor emissions from strong local source areas (such as industrialized urban areas or power plants) [RD27]. Table 2-6 shows different results in terms of enhancement of the CO_2 vertical column, at various spatial resolutions, based on a simulation of power plant emission of 13 Mt CO_2 yr^{-1} (a quasi-stationary Gaussian plume model was used) [RD23]. If the ground pixel size is 10 km (*i.e.* similar to GOSAT), the CO_2 column enhancement is about 0.5% (~1.9 ppm) of the background column. High spatial resolution mapping, such as 2x2 km² (CO_2 column enhancement of 2.1%, ~12 ppm) is therefore important for detecting power plant emission. As stronger wind speeds may be met, an upper limit proposed for the random error on a XCO_2 single observation is 2 ppm (threshold) and 1 ppm (goal). Indeed, [RD20] states that plumes from medium-sized power plants (14.8 Mt CO_2 yr^{-1}) elevate XCO_2 levels by ~0.5% (2 ppm) for a few tens km downwind (between 3 and 5 ms^{-1} wind speed). Variations of CO_2 are rarely larger than 1-2% on 100-1000 km scales [RD6].

For typical near-surface fair weather wind speeds in the range 2-6ms^{-1}, [RD23] has demonstrated the theoretical potentiality of a concept such as CarbonSat:

- Statistical uncertainty of the retrieved power plant CO_2 emission due to instrument noise (random error) in the range of 1.6-4.8 Mt CO_2 yr^{-1} for single overpasses (~60% power plant emissions in the world);
- Systematic errors such as wind speed: a 10% wind speed error results in a 10% emission error;
- Systematic error such as neglected enhanced aerosol concentration in the power plant plume may result in errors in the range 0.2-2.5 Mt CO_2 yr^{-1} (~80% power plant emissions in the world), depending on power plant aerosol emission), for a power plant emitting 13 Mt CO_2 yr^{-1} but could be reduced with the CH_4-proxy approach [RD23].

Thus, the XCO_2 requirements for **application 3** *i.e.* **power plant emission** may be summarized as follows [RD23]:

- **Horizontal resolution and sampling: 2x2 km² (threshold)** and **1x1 km² (goal)**.
- **Revisit time: 6-day (threshold**, typically CarbonSat) and **1-day repeat-frequency (goal)**. For example, the satellite swath width has to be sufficiently large to achieve frequent mappings of power plants and their surroundings. Using clear sky statistics, it has been conservatively estimated that typically 20 sufficiently cloud free pixels over a given power plant per year can be expected, given a mission concept such as CarbonSat.
- **Random error: 2 ppm (threshold)** and **1 ppm (goal)**. These requirements are based on [RD23], which shows that a precision better than 1% (~3.8 ppm) is indeed required.
- **Systematic overall error: 2 ppm (threshold)**, **0.5 ppm (breakthrough)** and **0.2 ppm (goal)** required relative systematic error after bias correction, where bias correction is not limited to the application of a globally constant offset / scaling factor.
- **Stability error:** as systematic overall error **but per year**.

Table 2-6: Maximum CO_2 column enhancement (relative to background column (=1.0)) for a power plant emitting 13 Mt CO_2 yr^{-1} for different spatial resolutions of the satellite footprint. The assumed wind speed (at 10 m above the surface) is 1 m s^{-1} [RD23].

Horizontal resolution	Peak of CO_2 column normalized to background
20 m x 20 m	1.126
40 m x 40 m	1.125
1 km x 1 km	1.053
2 km x 2 km	1.031
4 km x 4 km	1.017
10 km x 10 km	1.005

2.5.6. Synthesis of the requirements on L2 products

A synthesis of the CO_2 L2 requirements expressed in the previous sections (2.5.5.1, 2.5.5.2 and 2.5.5.3) is given in the Table 2-7. These requirements must be considered for a single column observation. They can be summarised as follows:

- **Spatial scales (resolution and sampling):** single column observation should present spatial sampling and **resolution between 1 km (local emissions) and 10 km (city scale, typically between 20x20 km² and 50x50 km²).** More specifically, for monitoring CO_2 emissions associated with power plants, the L2 spatial scale must not exceed 2 km.
- **Revisit time:** whatever the application considered, a single point (column observation) must be revisited at least every 6 days for estimating yearly fluxes. This requirement is based on the assumption that CO_2 anthropogenic emissions do not change fr$_o$m month to month. However, it can be interesting to have 3-monthly (cities) or monthly (power plants) fluxes for capturing the cycle related to the seasonal consumption of energy over European areas. Thus, **goals of 1 day (power plants) and 3 days (cities) are required for the CO_2 L2 products.** These differences are explained by the fact that time averaged emissions may be washed out because of the variations of synoptic conditions.
- **Random errors:** for a single column observation, the minimum random errors required are **2 ppm as threshold (max 4 ppm for the application 1) and 1 ppm as goal (max 2 ppm for the a$_p$plication 1).**

- **Systematic overall errors: 2 ppm (threshold), 0.5 ppm (breakthrough) and 0.2 ppm (goal).**
    - It is assumed that these values are obtained after bias correction are applied: i.e. they can be considered as consistent systematic overall values errors values which remain, even though biases are corrected considering aerosol, clouds or other ancillary information, instrumental calibration or regional biases. Large-scale biases can usually be removed by validation and very small scale biases appear almost random. Thus, the spatial scale associated with each application may be considered as the scale of the ensemble used for deriving the accuracy requirement.
    - Threshold value may be accepted if the observing system considered is able to deliver very numerous and exploitable XCO_2 products over a given area and if XCO_2 systematic errors do not present a regional structure. If the considered observing system can provide only few such products and/or if characterisation of the biases show clearly a regional pattern, then the breakthrough value has to be required, and not the threshold.
- **Stability errors:** as systematic overall errors **but per year.**

Large-scale biases can usually easily be removed by validation and very small scale biases appear almost random. Thus, scale associated with each application may be considered as the scale of the ensemble used for deriving the various errors requirements.

As explained in the previous sections, the expected XCO_2 performances derived from:

- GOSAT and OCO instruments have been mainly considered for the **application 1**;
- CarbonSat instrument has been mainly considered for the **application 3**;
- Specific assumptions based on current expertise and past studies (based on atmospheric transport simulations) are considered for the **application 2**.

Table 2-7 would basically state that SCIAMACHY cannot meet the objectives of application 1 (because of the large FOV) or the requirements of revisit time would be quite demanding in comparison of the revisit time related to CarbonSat. Nevertheless, one has to keep in mind that the interpretation of the XCO_2 requirements is clearly a complex problem and requires expert knowledge as the situation is actually not black and white and also, the critical requirements are related (*i.e.* threshold values depend on each other). For example, SCIAMACHY could deliver interesting and relevant information for **application 1** in certain cases despite the large FOV of 60x30 km. The key issue is then the biases or XCO_2 requirement errors as discussed in the next chapters. Nevertheless, SCIAMACHY is not a dedicated GHG mission and thus, the associated XCO_2 performances are not taken into account in the Table 2-7. Finally, these XCO_2 requirements are based on the future objectives stated by the scientific community: *i.e.* the ways to improve the current scientific knowledge on the CO_2 cycle and not the objectives associated with past knowledge (when specifying the SCIAMACHY mission).

Table 2-7: Synthesis of the user requirements for the CO_2 L2 products (CO_2 single total column observation), derived from remote measurements.

Applications	Spatial sampling (km^2) Threshold / Goal	Spatial resolution (km^2) Threshold / Goal	Revisit time (days) Threshold / Goal	Random error ("Precision") (ppm) Threshold / Goal	Systematic overall error (ppm) Threshold / Breakthrough/ Goal	Stability error (ppm yr^{-1}) Threshold / Goal
1) Monitoring natural CO_2 surface fluxes (global scale ~500-1000 km)	10x10 / 5x5	10x10 / 5x5	16 / 3	4 / 2	2* / 0.5* / 0.2#	0.5 / 0.2
2) Monitoring anthropogenic city CO_2 surface emissions (city scale ~50 km)	10x10 / 5x5	10x10 / 5x5	6 / 3	2 / 1	2* / 0.5* / 0.2*	0.5 / 0.2
3) Monitoring anthropogenic power plant CO_2 surface emissions (local/point scale ~1-2km)	2x2 / 1x1	2x2 / 1x1	6 / 1	2 / 1	2* / 0.5* / 0.2*	0.5 / 0.2

 # relative systematic error after global bias correction, where only the application of a constant offset / scaling factor independent of time and location is permitted for bias correction.

** relative systematic error after bias correction, where bias correction is not limited to the application of a globally constant offset / scaling factor*

3. Setup of retrieval software for Sentinel-5 synthetic CO_2 observations

3.1. Definition of the geophysical scenarios

3.1.1. Introduction on the harmonization of the retrievals

The geophysical scenarios proposed in this section are the reference scenarios which are simulated by the expert scientists of the present study, mostly by IUP-UB and ULe which focus on the XCO_2 performances associated with S-5-UVNS. The dataset of simulations can be considered as large enough to provide first guess of statistical results. Simulations of KNMI are based on these scenarios for comparing the algorithms (section 4.4.1) but the approach is different for analysing the synergy of S-5-UVNS with VII and 3MI (see section 4.4.2).

The retrievals of ULe, IUP-UB and KNMI are harmonized by using a harmonized description of the instrument parameters (*cf.* Table 4-1: spectral resolution, noise etc.…) as well as of the geophysical inputs. Specifically, the same atmospheric trace gas, temperature and pressure profiles and surface parameters are used. For aerosols and clouds, the inputs are harmonised to some possible extents with the given existing algorithms. All the retrieval methods are still independent so that this approach still allows verifying the robustness of the results.

3.1.2. Approach

Systematic and random XCO_2 errors - for XCO_2 retrieved from (back)scattered/reflected solar radiation, measured by satellite in the near-infrared/shortwave-infrared (NIR/SWIR) spectral region - have been quantified in a number of publications for instruments such as SCIAMACHY, OCO, GOSAT and CarbonSat (see *e.g.* [RD3] [RD23] [RD36] [RD40] [RD58] and other references given therein). From these studies it can be concluded that errors due to inadequate descriptions of aerosols and (undetected) clouds (esp. thin cirrus clouds) are likely the most important error source for XCO_2 retrievals. Because of this, the quantification of scattering related XCO_2 errors is the focus of the present study.

From these studies it can also be concluded that scattering related errors not only depend on the type and amount of scattering particles (especially thin cirrus clouds and boundary layer aerosol as well as desert dust aerosol) and their vertical distribution but also on other parameters, most notably the Solar Zenith Angle (SZA) and the (spectrally dependent) surface reflectivity. For these parameters a finite set of values has been defined for the radiative transfer (RT) simulations and for the retrievals based on the simulated spectra derived from the RT simulation using an instrument model.

It has also been found that there are a number of other parameters which are less critical. Examples are vertical profiles of pressure, temperature and humidity. The reason is that good *a priori* information is available via meteorological data sets, information on these parameters can be retrieved in addition to the gas of interest (here CO_2). The sensitivity to these parameters is fairly small (compared to the thermal infrared spectral region). For the purpose of this study, only few of these parameters have been varied (see section 4.3.3). Otherwise, constant values have been defined (this is the case in the sections 4.3.2 and 4.4).

Based on these considerations, a number of scenarios have been defined to estimate (random and systematic) XCO_2 retrieval errors.

The set of scenarios needs to be appropriate: *i.e.* large enough and properly selected to permit a first guess of statistical robust conclusions on scattering related XCO_2 retrieval errors.

On the other hand, the number of scenarios has to be small enough in order to minimize the number of very computer time demanding radiative transfer and retrieval simulations. This is required due to the challenging boundary conditions of this study.

To achieve this, key variable (see section 3.1.3) and constant (see section 3.1.3.1) parameters have been identified. For each variable parameter, representative values have been defined covering approximately the range of values encountered in orbit for (nadir) observations over land. For the constant parameters, typical values (primarily vertical profiles) have been defined. Details are given in the following two sub-sections.

3.1.3. Variable key parameters

Scattering related errors depend primarily on Solar Zenith Angle (SZA), surface reflectivity, aerosol amount (*e.g.* characterized by Aerosol Optical Thickness (AOT) at a given wavelength); aerosol type (defining the wavelength dependence of extinction, scattering coefficients (or single scattering albedo) and phase function), Cirrus Optical Thickness (COT) and cirrus altitude.

In order to reliably quantify XCO_2 scattering related errors, a sufficiently large number of appropriate scenarios have to be defined. This number has to be as small as possible because of the demanding computing time needed for the radiative transfer model (RTM) simulations. For each critical parameter, several values have been selected to cover the typical range of values encountered in orbit (focussing on nadir observations over land). The selected values are described in Table 3-1, page 77. The numbers of values per parameter are as follows:

- 3x SZA;
- 3x albedo;
- 4x AOT;
- 3x aerosol type;
- 5x COT;
- 5x cirrus altitude.

If each parameter is combined with each other parameter, this defines a total of 3x3x4x3x5x5 = 2700 different scenarios. This shows that although it may be nice to add more scenarios (*e.g.* more aerosol types), performing the required number of RTM simulations and retrievals is already the upper limit of what can reasonably be done within this study.

Not all parameter combinations are likely to be relevant (and therefore the 3 expert groups are not mandatory to perform simulations for all 2700 scenarios). In order to determine which combinations are relevant and to define an appropriate set of values for each parameter, global data sets based on MODIS (GEMS/MODIS for aerosols and albedo from MODIS: details are given below), population density (for the "Continental polluted" aerosol type) and CALIOP/CALIPSO (for cirrus: details are given below) have been used. Global maps are shown in Figure 3-1, page 76. These maps may need to be refined but they are considered to be a very good starting point for the purpose of scenario definition. The maps indicate that the range of values which are relevant can be covered quite well. The spatial resolution of the maps is 0.5° x 0.5°.

For global information on albedo, (half monthly) MODIS albedo product ("MOD43") obtained from NASA via the internet are used. The "albedo maps" have been generated using MODIS surface albedo at 858 nm and 1640 nm, which are part of the MODIS MOD43 albedo product. The aerosol type maps have been obtained by assigning:

- type "Desert" (DE) to desert surfaces (obtained from the land surface type maps, see Figure 3-1);
- type "Continental polluted" (CP) to land surfaces with high population density (using a population density);
- and type "Continental clean" (CC) to all other areas.

For global information on aerosols, data set generated within the European GEMS project (Global and regional Earth-system Monitoring using Satellite and *in situ* data) [RD38] [RD42] is considered. The data set has been obtained from: http://dataportal.ecmwf.int/data/d/gems_reanalysis/.

This data set covers the years 2004 - 2008 and provides homogeneous and consistent aerosol information in 12 hourly time steps with full global coverage. The GEMS aerosol product is based on the assimilation of MODIS [RD76] aerosol information into a global model [RD38] [RD42].

For the present study, four days of MODIS data have been used and are depicted in Figure 3-1: 15. Jan. 2008 (for "January"), 15 April 2008 (for April), 15 July 2008 (for July) and 15 October 2008 (for October). The MODIS albedo have been used to assign one of three surface types (vegetation (VEG), sand/soil (SAS) and snow/ice (SIC)) to most of the land areas at 0.5° x 0.5° resolution (ocean areas have not been studied here). This has been done using a simple threshold algorithm newly developed for this purpose. The resulting land surface type classification has been "validated" by visual comparisons to available land surface type maps available on the Internet. The purpose of this exercise was to generate a simple but reasonably realistic land surface type classification using only three surface types as appropriate for this study.

Global information on thin clouds derived from CALIOP (Cloud-Aerosol Lidar in Orthogonal Polarisation) on-board CALIPSO (Cloud-Aerosol Lidar and Infrared Pathfinder Satellite Observations) is used in the present study because CALIOP is sensitive to subvisible cirrus clouds (using the operational product derived from 532 and 1064 nm) [RD47] [RD57] [RD68]. Note that it is assumed that cloud contaminated measurements with COT > 0.4 can be identified and removed: *i.e.* the same approach which has been described and used in [RD25] is used in the present project.

CALIPSO is a satellite in the A-Train constellation and was launched in April 2006. The CALIPSO data product (CAL_LID_L2_05kmCLay-Prov-V3-01) provides information on COD, Cloud Top Height (CTH) and Cloud Geometrical Thickness (CGT) with a horizontal resolution of 5 km by 60 m. A one-year data set has been used for this study (2008). The CALIPSO data have been filtered for clouds with COD = 1.0 or less (it is assumed that scenes with thick clouds can be relatively easily identified *a priori* using appropriate pre-processing). Using averaging and interpolation, monthly maps of cloud parameters (COD, CTH and CGT) have been generated with global coverage and a spatial resolution of 0.5°x0.5°. The CALIPSO data set only provides binary information about cloud coverage. Consequently, the relative frequency of cloud occurrence has been computed for every gridbox and is used as CFC data set. Using CALIPSO derived COD and CFC, eCOD (= COD x CFC) has been computed. For this study only cirrus altitude (CTH) and cirrus optical thickness (COD; more precisely eCOD) have been considered.

These data sets have been used (Figure 3-1) to determine some statistics of XCO_2 errors for various regions (*e.g.* USA, Siberia, tropics) and/or to determine, for example, the mean and standard deviation of the XCO_2 error for a given AOT or cirrus altitude.

ULe aimed at analysing all of the 2700 scenarios to quantify aerosol and cloud related XCO_2 errors. IUP-UB focuses on all the 1800 scenarios for the VEG (vegetation albedo) and SAS (sand/soil scenarios) (*i.e.* because of the lack of time available, the analysis of the 900 additional SIC (snow/ice) scenarios could not be performed).

KNMI analyzed a small subset of these scenarios in order to demonstrate that results are obtained that are similar to the retrieval results of the other groups.

Note that no extra "cloud fraction" studies have been performed: only the product of cloud fraction by optical depth matters and is considered in a first order approximation (*i.e.* it is assumed that studying ground pixel fully covered by thin cloud is sufficient). It is proposed to focus on key parameters in priority (SZA, surface reflectivity, aerosols, clouds) since all the parameters cannot be considered (*e.g.* viewing angle dependence, etc…, will not be addressed). On the other hand, aerosol type dependence and cloud type dependence as well as mixed aerosol / cloud scenarios are considered. Finally, a few additional scenarios have been considered by IUP-UB and ULe in order to look into the sensitivity to the aerosol altitude (see section 4.4.2.44.3.3.5) and the surface pressure (see section 4.3.3.2). For these parameters, specific methodology has been used by each organism and is detailed in the corresponding sections.

As described in the next parts of the present report, similar parameters (geophysical parameters for the definition of the scenarios and instrumental specifications for the Sentinel-5-UVNS sounder) are employed in order to be able to have robust results. Perfect agreement is difficult to achieve as this may require code / database changes which were out of scope of this study. Thus, although somewhat different approaches are used by each organism, if this study allows to come to similar conclusions, this fully demonstrates the robustness of the conclusions: *i.e.* the results and the associated analyses do not depend on all the details of the settings. On the contrary, if the deduced results disagree substancially, more investigations would be required anyway to identify the cause. When this happens and if the cause can be traced by to aerosols for example (likely easy to find out by looking at biases for fixed cloud parameters etc…), then, one should look in more details in the aerosol settings. In theory, the different approaches used to deal with aerosols and scattering variability in the different retrieval algorithms would be the main contributors. The modelisations of aerosols and clouds in the radiative transfer codes would likely present smaller impacts.

As a conclusion, robustness of the findings implies that all groups come to the similar conclusions. If the conclusions differ significantly, the cause of the differences has to be identified. The main objective of this study is clearly to make common statements about the capability of the Sentinel-5-UVNS instrument (alone and then combined to VII/3MI) to retrieve XCO_2. This goal has been reached in the next parts of this report. As no equivalent exercise (to our knowledge) has already been done in the past, it is difficult to specify, at this stage of the present study, an accurate criterion in terms of expected agreement between the retrievals of each partner. As the retrieval algorithms and the assumptions considered are very different (because of the input data, the *a priori* state vectors and uncertainties, assumptions considered etc…), individual retrievals cannot be compared. So actually, the overall estimate of XCO_2 systematic errors have to be compared (*i.e.* the so-called "standard deviation systematic error" as mentioned in Table 4-2) with each algorithm. Obviously, if the differences between this estimate are 100% of the requested XCO_2 accuracy (*i.e.* systematic error), the conclusions are not robust. If the agreement is within 5%, the results should be then very robust. Thus, we consider here that an agreement better than 50% (between the overall estimate of systematic XCO_2 errors) should indicate that a good agreement is obtained between the algorithms in the present study. This choice is not scientifically based. It is mainly based on the requirements associated with the XCO_2 systematic errors as specified in Table 2-7. With respect to the threshold, breakthrough and goal values (*i.e.* 2 ppm, 0.5 ppm and 0.2 ppm respectively), it corresponds to 1 ppm, 0.25 ppm and 0.1 ppm respectively. In conclusion, if the assessments made by the different groups using different retrieval algorithms lead to overall accuracy estimates (as defined by the "standard deviation systematic error") which do not differ by more than 50 of the required accuracy, *i.e.* 1 ppm (threshold), 0.25 ppm (brealthrough) and 0.1 ppm (goal), then the conclusions are considered robust.

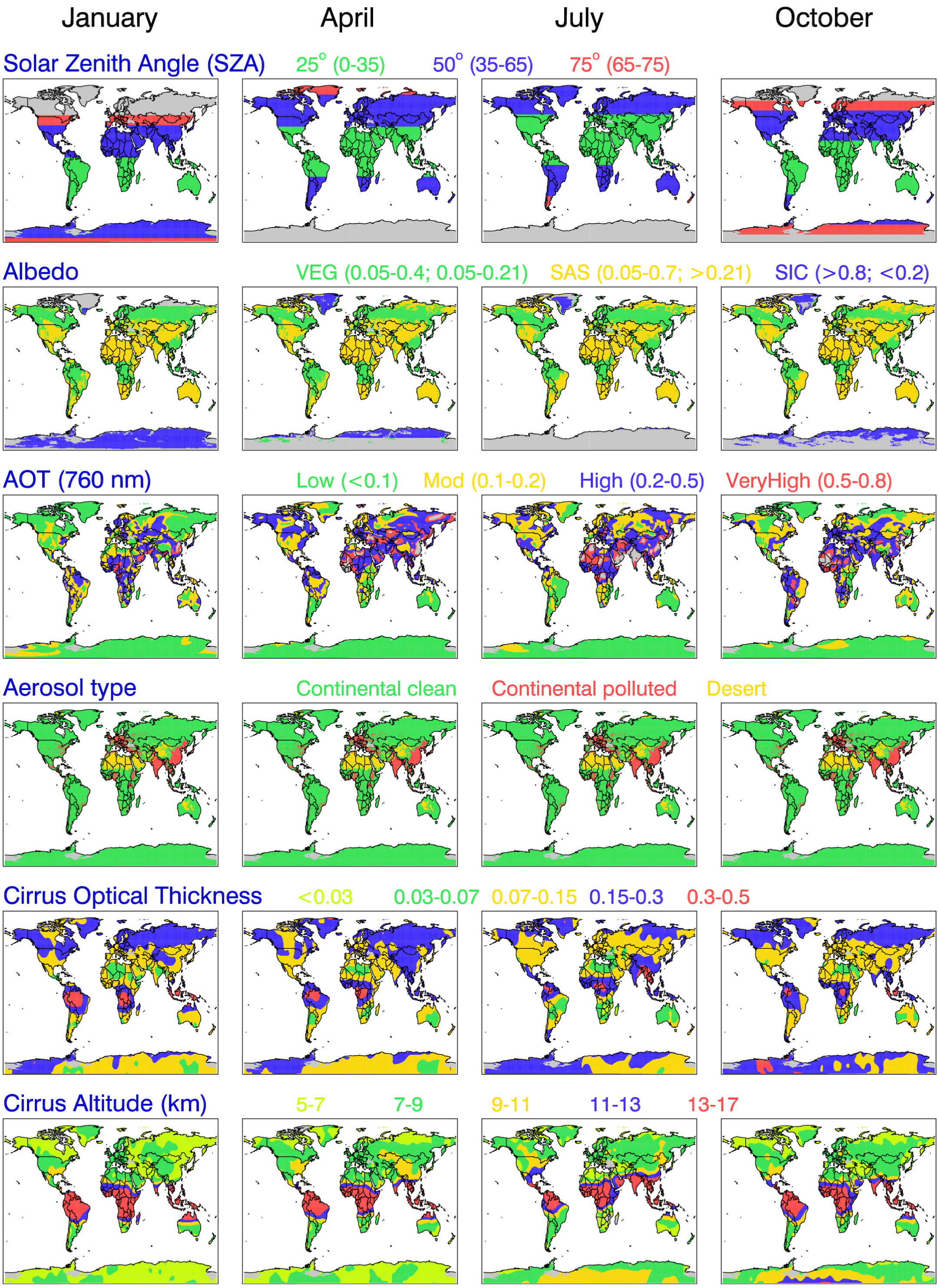

Figure 3-1: Global maps of the variable parameters and their (coarse grid) discrete values for 4 different months. The parameters are (from top to bottom): SZA: 25°, 50°, 75°; albedo: vegetation (VEG), sand/soil (SAS), snow/ice (SIC); AOT (at 760 nm): 0.1, 0.2, 0.3, 0.6; aerosol type: continental clean, continental polluted, desert; COT (NIR): 0.01, 0.05, 0.1, 0.2, 0.4; cirrus altitude: 6, 8, 10, 12, 14 km.

The variable parameters and their selected discrete values are listed in Table 3-1.

Note that, especially for the aerosol and cirrus parameters, the exact values used may depend to some extent on the used RT model and its corresponding data bases (see Table 3-2, Table 3-3 and Table 3-4 for details). For the purpose of this study, exact agreement is not required. Using (somewhat) different aerosol and cirrus modelling schemes by the various groups permits to determine the robustness of the findings with respect to aerosol and cirrus related (random and systematic) XCO_2 retrieval errors.

Table 3-1: Variable parameters and their selected discrete values. #) Albedo from [RD23].

Parameter		Values	Comments
ID	Name		
SZA	Solar Zenith Angle	25°, 50°, 75°	None
ALB	Albedo	VEG, SAS, SIC	VEG: Vegetation (0.76 µm: 0.2; 1.6 µm: 0.1; 2.6 µm: 0.05 #)) SAS: Sand/soil (0.2; 0.3;0.3) #) SIC: Snow/ice (0.8;0.05;0.05)
AOT	Aerosol Optical Thickness (550 nm)	0.1, 0.2, 0.3, 0.6	Valid for approx. 550 nm. Used values may deviate depending on the implementation of the aerosol scheme as used by the RT model. Implementation related details see Table 3-2.
ATY	Aerosol type	CC, CP, DE	CC: Continental clean, CP: Continental polluted, DE: Desert Implementation related details see Table 3-3.
COT	Cirrus Optical Thickness (NIR)	0.01, 0.05, 0.1, 0.2, 0.4	Valid for "NIR" (~ 500 – 1000 nm). Used values may deviate depending on the implementation of the cirrus scheme as used by the RT model. Implementation related details see Table 3-4.
CAL	Cirrus Altitude (km)	6, 8, 10, 12, 14	Implementation related details see Table 3-4.

Table 3-2: Implementation related details for AOT.

Implementation related details: Parameters AOT	
Institute	Comments
IUP-UB	"AOT 0.1" background scenario: Constant boundary layer (BL; 0-2 km) extinction profile of 0.03 km^{-1} (at 550 nm) -> BL AOT = 0.06. Constant (scenario independent) aerosol profile above BL -> Total AOT = 0.1. "AOT 0.2" scenario: As "AOT 0.1" scenario but enhanced BL extinction such that AOT @ 550 nm ~0.2. "AOT 0.3" scenario: As "AOT 0.1" scenario but enhanced BL extinction such that AOT @ 550 nm ~0.3. "AOT 0.6" scenario: As "AOT 0.1" scenario but enhanced BL extinction such that AOT @ 550 nm ~0.6.
ULe	"AOT 0.1" background scenario: Exponential profile with 2 km scale height and 0.06 AOT. Gaussian shaped profile in free troposphere with AOT of 0.04. The reference wavelength for our retrieval is 760 nm and we will transfer the 550 nm AOT to 760 nm via an estimated Angstrom coefficient for the relevant aerosol type. Other aerosol scenarios will be as background scenario but with AOT values adjusted accordingly.

Implementation related details: Parameters AOT	
Institute	**Comments**
KNMI	The wavelength dependence of the aerosol optical thickness is described by the angstrom coefficient which is adjusted to the aerosol models used by IUP-UB. With a few exceptions, the aerosol is located in the boundary layer.

Table 3-3: Implementation related details for aerosol type.

Implementation related details: Parameters Aerosol Type	
Institute	**Comments**
IUP-UB	Aerosol scheme: SCIATRAN aerosol scheme [RD77]: • CC: Composition: 100% water soluble, humidity: 70% (mode radius r_M = 0.0285 µm). • CP: Composition: 46% water soluble (r_M = 0.0285 µm), 54% soot (r_M = 0.0118 µm). • DE: Composition: 87% water soluble (r_M = 0.0285 µm), 11% mineral nucleation mode (r_M = 0.07 µm), 2% mineral accumulation mode (r_M = 0.39 µm).
ULe	Aerosol types are taken from [RD72] [RD73]: • CC: Type 1a: 67% sulphate, 13% sea salt, 10% carbonaceous, 10% accum. dust. • CP: Type 5b 25% sulphate, 12% accum. dust, 54% carbonaceous, 9% black carbon. • DE: Type 4c: 22% sulphate, 51% accum. dust, 16% coarse dust, 11% carbonaceous.
KNMI	The optical properties of aerosol are described in terms of a Henyey-Greenstein phase function with a fixed asymmetry parameter g = 0.70 and a single scattering albedo of 0.95 with an uncertainty of 0.04. The different aerosol models: CC, CP, and DE have different values for the angstrom coefficient, 1.970, 1.862, and 0.245, respectively. These values were calculated from the wavelength dependent aerosol optical thickness used by IUP-UB. There are no additional specifications needed to investigate the possibilities of using S-5-UVNS-VII and S-5-UVNS-3MI for aerosol characterisation.

Table 3-4: Implementation related details for cirrus.

Implementation related details: Parameters COT and Cirrus altitude	
Institute	**Comments**
IUP-UB	SCIATRAN cirrus model using fractal ice crystals of the second generation based on a regular tetrahedron of geometrical dimension 247 x 247 x 100 µm^3: • COT: Specified for 500 nm. Altitude: The specified altitude is the centre altitude of a cirrus layer of geometrical thickness 1 km.
ULe	Optical properties are taken from the cirrus model of [RD62]: • COT is transferred to 760 nm via the Angstrom coefficient. The vertical profile will be a Gaussian shaped profile with a given centre altitude and a width of 1 km.

Implementation related details: Parameters COT and Cirrus altitude	
Institute	**Comments**
KNMI	The phase function for the cirrus cloud is a Henyey-Greenstein phase function with an asymmetry parameter of 0.7. The single scattering albedo is 1.0. The altitude is the centre altitude of the cirrus layer having a geometrical thickness of 1 km.

3.1.3.1. Constant key parameters

The simulations are carried out for direct nadir observations over land using vertical profiles of pressure, temperature, and H_2O and CO_2 mixing ratios.

The vertical profiles are based on the US Standard Atmosphere [RD82], and on an adjusted CO_2 profile (390 ppm). The vertical profiles of p, T, H_2O and CO_2 used are described in Table 3-5.

Table 3-5: Description of the vertical profiles of p, T, H_2O and CO_2 given by the US Standard Atmosphere [RD82].

No.	Altitude (km)	Pressure (hPa)	Temperature (K)	H_2O volume mixing ratio (ppm)	CO_2 volume mixing ratio (ppm)
27	60	0.2196	247.0	4.750	385
26	55	0.4252	260.8	5.100	390
25	50	0.7978	270.6	5.225	390
24	45	1.491	264.2	5.225	390
23	40	2.871	250.4	5.025	390
22	35	5.746	236.5	4.900	390
21	30	11.97	226.5	4.725	390
20	25	25.49	221.6	4.425	390
19	20	55.29	216.6	3.900	390
18	15	121.1	216.6	5.000	390
17	14	141.7	216.6	5.927	390
16	13	165.8	216.6	10.85	390
15	12	194.0	216.6	19.06	390
14	11	227.0	216.8	36.13	390
13	10	265.0	223.3	69.96	390
12	9	308.0	229.7	158.3	390
11	8	356.5	236.2	366.7	390
10	7	411.0	242.7	572.0	390
9	6	472.2	249.2	925.4	390
8	5	540.5	255.7	1397.0	390
7	4	616.6	262.2	2158	390
6	3	701.2	268.7	3182	390

No.	Altitude (km)	Pressure (hPa)	Temperature (K)	H_2O volume mixing ratio (ppm)	CO_2 volume mixing ratio (ppm)
5	2	795.0	275.2	4631	390
4	1.5	846.9	278.45	5351	390
3	1.0	898.8	281.7	6071	390
2	0.5	955.9	284.9	6908	390
1	0.0	1013.0	288.1	7745	390

3.1.3.2. Scenarios for inhomogeneous scenes

The XCO_2 error due to Spectral Response Function (SRF) variations caused by inhomogeneous scenes also needs to be estimated.

A potential key issue for horizontally inhomogeneous scenes is the change of the instrument slit function due to inhomogeneous slit illumination. This is studied here using a few selected worst case scenarios to obtain an upper limit of the resulting retrieval error. This requires that the retrieval teams are provided with slit functions resulting from inhomogeneous illuminations (*e.g.* slit function for "left", "middle", "right" part of slit illuminations).

For this purpose, simulated observations (spectral radiance measurements) were generated using SRF information provided by NOVELTIS (see section 4.3.3.6). An upper limit of the error is determined by performing retrievals based on the perturbed observations (perturbed as the "true" SRF differs from the one assumed for the retrieval). This is an upper limit because the error may be reduced by improving the retrieval algorithm. However, such improvements of the retrieval algorithm are out of scope of this initial study. IUP-UB has estimated this error by performing retrievals for a representative scene (vegetation albedo, SZA 50°) using six perturbed SRFs, each corresponding to a different inhomogeneous scene. The six perturbed SRF contain also quite extreme cases. For all these SRFs, six scenes retrievals have been performed using four different retrieval options (without shift and squeeze correction, with shift and squeeze correction, with shift correction only and with squeeze correction only). A similar study has been carried out by ULe for the same scene and using the same six SRFs. ULe has only investigated the errors for 2 XCO_2 retrieval options (with or without shift and squeeze correction). The description of the six scenarios associated with the perturbed ISRFs is detailed in section 4.3.3.6.1, page 135.

Note that, this specific exercise allows to study the impact of horizontally inhomogeneous scenes due to inhomogeneous illumination of the slit on the XCO_2 error. Impacts of inhomogeneous scenes on the radiative transfer part of the problem, such as an inhomogeneous surface albedo, aerosol / cloud whose optical thickness varies over the pixel, have not been studied. Also, the impact of vertically inhomogeneous scenes is not considered here.

3.2. Summary of the optimal estimation theory

3.2.1. Methodology of the XCO_2 retrieval

All the XCO_2 retrieval, performed by the three experts through their software (see section 3.3) are based on the theory of OEM [RD74] which allows computing the retrieval physical state, as well as the associated error covariance matrix, from the level 1 calibrated radiance measurements. The method requires and is dependent, in general, on the specified *a priori* state as well as on the associated *a priori* error. The forward model used to transport information from the space of physical parameters (*e.g.* gas concentration profiles, temperature profiles, aerosol / cloud parameters as well as surface parameters) to the radiance space is a highly accurate radiative transfer model.

In most cases, the retrieval of CO_2 profile represents an ill-posed inversion problem. This means that at the limits of a measurement error, a measurement y is insensitive with regard to fine structure in the gas concentration. Various methods exist for treating ill-posed problems, whereas the method mostly used in remote sensing is the optimal estimation method. It introduces a minimization of a side constraint in addition to the previous least squares condition. Therefore, the minimization equation can be summarized as follows:

$$\hat{x} = \min_x \left\{ \left\| S_y^{-1/2} (F(x) - y) \right\|^2 + \left\| S_a^{-1/2} (x - x_a) \right\|^2 \right\} \quad \textbf{Equation 3-1}$$

Where:

- $\mathbf{S_a}$ is the (state vector) *a priori* covariance matrix, in the space of physical parameters, associated with the retrieved state vector;
- $\mathbf{S_y}$ is the covariance matrix, in the space of the spectral measurement, including the measurement noise (*i.e.* instrument);
- $\mathbf{x_a}$ is the *a priori* state vector related to the parameter to be retrieved. The definition of $\mathbf{x_a}$, considered by each group of experts is summarized in Table 3-6;
- **F** is the forward model simulating the measurement as function of the state vector.

The optimal estimation method seeks the statistically most likely solution. For this purpose, one assumes that the atmospheric state as observed by a satellite in a particular area and period of time varies in a quasi-statistical manner such that its variation is subject to Gaussian statistics. The optimal estimation method combines *a priori* information on the atmospheric state with statistical information on the state vector, and the measurement in a statistically optimal manner applying Bayes theorem.

The inverse method may use the Levenberg-Marquardt modification of the Gauss-Newton method to find the estimate of the state vector $\hat{x}$ with the maximum *a posteriori* probability, given the measurement **y.** The state vector will typically include a CO_2 profile together with non-CO_2 state vector.

For a linear problem, y=Kx+ε, the "best estimate" state vector $\hat{x}$ is the solution of the corresponding minimization problem. It can be written as follows:

$$\hat{x} - x_a = G(y - y_a) \quad \textbf{Equation 3-2}$$

Where:

- **y** is the measured spectrum. The $\mathbf{y_i}$ in the next sections below are the elements of vector **y**;
- The spectrum computed with $\mathbf{x_a}$ is $\mathbf{y_a}$ = y($\mathbf{x_a}$);
- **G** is the "retrieval gain matrix" defined as follows:

$$G = \hat{S} K^T S^{-1}{}_y \quad \textbf{Equation 3-3}$$

Where:

- **K** is the weighting functions matrix (called also the "Jacobian matrix");
- $\hat{S}$ is the total *a posteriori* retrieval variance/covariance matrix on the retrieved state $\hat{\mathbf{x}}$. It is computed as a simple Bayesian linear error estimate.

After the iterative retrieval process has converged to a solution, the error covariance matrix is:

$$\hat{S} = (K^T S_y^{-1} K + S_a^{-1})^{-1} \quad \textbf{Equation 3-4}$$

- $\mathbf{S_y}$ is the measurement error covariance matrix. $\mathbf{S_y}$ is diagonal and the diagonal elements are the square of the radiance error as computed from the specified SNR (*cf.* Table 4-1);
- $\mathbf{S_a}$ is the *a priori* covariance matrix.

One can also define the "CHI²" parameter (*i.e.* χ^2) which is the average of the quadratic difference between the measure spectra and the simulated spectra, over all the spectral domain used for the retrieval):

$$\chi^2 = \frac{[\delta \mathbf{y}]^T \mathbf{S}_y^{-1} \delta \mathbf{y}}{\mathbf{m}} \quad \textbf{Equation 3-5}$$

Where:

- **m** is the number of spectral channel in the measured and simulated spectra;
- **δy** = is the difference between the measured and simulated spectra ($\delta y = y - y_a$).

Due to the regularization, the retrieved state vector $\hat{\mathbf{x}}$ is a smoothed version of the true state vector **x** and the smoothing can be characterized with the averaging kernel **A**, directly calculated from:

$$A = \partial \hat{x} / \partial x = \hat{S} K^T S_y^{-1} K \quad \textbf{Equation 3-6}$$

Note that the variable $\mathbf{XCO_2}$ is computed from $\hat{\mathbf{x}}$ by computing the ratio of the retrieved CO_2 column (obtained by adding the corresponding elements of $\hat{\mathbf{x}}$) and the retrieved dry-air column (obtained from the element of $\hat{\mathbf{x}}$ which corresponds to surface pressure), *i.e.* the retrieved $\mathbf{XCO_2}$ is as $\mathbf{XCO_2} = f(\hat{\mathbf{x}})$, where $\hat{\mathbf{x}}$ is given by Equation 1. Thus, $\mathbf{XCO_2}$ is inferred by averaging the retrieved CO_2 profile, weighted by the pressure weighting function, **h,** such that:

$$X_{CO2} = \mathbf{h}^T \hat{\mathbf{x}} \quad \textbf{Equation 3-7}$$

The associated column averaging kernel for a level *j* is then given by:

$$(\mathbf{a}_{CO2})_j = \frac{\partial \mathbf{X}_{CO2}}{\partial \mathbf{u}_j} \frac{1}{\mathbf{h}_j} = (\mathbf{h}^T \mathbf{A})_j \frac{1}{\mathbf{h}_j} \quad \textbf{Equation 3-8}$$

and the variance of $\mathbf{XCO_2}$ by:

$$\sigma_{XCO2} = \mathbf{h}^T \hat{\mathbf{S}} \mathbf{h} \quad \textbf{Equation 3-9}$$

The main parameters for the characterization of the XCO_2 retrieval that are calculated by the retrieval algorithm are the *a posteriori* XCO_2 retrieval error given by the square root of the variance (*i.e.* σXCO_2) and the column averaging kernel $\mathbf{aCO_2}$.

IUP-UB and ULe use profile retrieval to determine the CO_2 column. KNMI assumes a fixed shape of the CO_2 profile (which removes the ill-posed nature of the retrieval) and uses *a priori* information to determine the usefulness of information obtained from external sources.

3.2.2. XCO_2 error assessment

If $\hat{\mathbf{x}} = \mathbf{x}$, then the retrieval is perfect (bias free). This however is not the case. Typically, there is a systematic error except if the *a priori* atmosphere (and all other parameters) is exactly identical with the parameters used to generate the simulated measurements.

To characterize the retrieval result, we have computed systematic and random errors for the analyses of the S-5-UVNS stand alone performances. The systematic retrieval error (XCO_2 bias) is directly inferred from the difference between retrieved and true XCO_2:

$$X_{CO2}\,Bias = \hat{X}_{CO2} - X_{CO2}^{truth}$$ **Equation 3-10**

The so-called "random error", associated with the S-5-UVNS stand alone capabilities, is taken from the *a posteriori* error $\hat{S}$ (see Equation 4) calculated directly by the retrieval algorithm.

This error depends on the SNR and the *a priori* error covariance matrix. If the *a priori* errors are very large then inverse of $\mathbf{S_a}$ can be omitted from Eq. (4) (unless they are used for regularization) and the random error is directly related to the SNR of the instrument. On the other hand, when some elements of $\mathbf{S_a}$ are small, representing external information on some of the parameters, then the random error is a complicated mixture of the SNR, the derivatives **K** and the *a priori* error covariance matrix. In some cases the SNR has very little influence on the final random error (see *e.g.* Figure 4-63, page 158). Small values of $\mathbf{S_a}$ are used in section 4.4 to quantify the synergy with VII (and 3MI).

3.3. Description of the retrieval software

Only existing tools can be used in the framework of this study. Existing tools are under development for other satellites (*e.g.* GOSAT, OCO-2, CarbonSat), but they are not yet applicable for S-5-UVNS. **The present study had to be conducted using these tools "as they were" with only minor adjustments which are described in the following sections**. The study results must therefore be considered preliminary rather than final, as retrieval algorithms are not yet optimized for a given S-5 instrument/mission specification, in particular to deal with systematic errors. However, all retrievals use a harmonized description of the instrument parameters (spectral resolution, noise etc.) as well as of the geophysical inputs.

The retrieval analysis tools proposed in this study are the following:

3.3.1. CarbonSat retrieval algorithm BESD (IUP-UB)

3.3.1.1. General description

IUP-UB uses the tools also used for the CarbonSat position paper [RD23], including the following elements:

- SCIATRAN a radiative transfer model (to compute spectral radiances at high spectral resolution for given atmospheric and surface parameters, solar zenith angle, etc.);
- CarbonSat instrument simulator for generating simulated spectra (for a given spectral band, spectral resolution and sampling) and computing their statistical errors (detector noise);
- BESD retrieval algorithm (to relate instrument errors (primarily noise) and errors of geophysical errors (primarily aerosols) to XCO_2 errors).

A major assumption of this study is that existing tools are appropriate for this study as the development of new tools or a significant improvement of existing tools is not compatible with the study schedule. Unfortunately, initial studies conducted at IUP-UB, after the present project starts, showed that the BESD retrieval algorithm as used for [RD23] had to be significantly improved in order to be more appropriate for this study (otherwise errors would be too large, especially thin cirrus related errors, which are not addressed in [RD23]). In order to achieve this, the following major improvements have been implemented:

- Cirrus optical thickness (COT) and cirrus altitude (CTH) has been added as state vector elements;
- In addition, it has been found that an iterative scheme is needed at least for cirrus. A preliminary implementation of this has also been included;
- Terrestrial vegetation chlorophyll fluorescence (VCF) has been added as state vector element as recent studies have shown that this needs to be considered in the O2-A-band spectral region [RD10] [RD12].

A number of important other aspects are also worth mentioning:

- Several tests have been conducted within this study to verify correct implementation of the new features. No obvious problems have been identified. The good agreement with the results of ULe (*cf.* Table 4-5 and section 4.3.1.3) indicates that the improved version of BESD works as specified. Nevertheless, more testing would have been advantageous but was not possible due to the very limited time available for this project.
- The BESD algorithm is under development for CarbonSat using high spectral resolution input data from 3 spectral bands (NIR (around 0.76 µm), SWIR-1 (around 1.6 µm), SWIR-2 (around 2.0 µm)). This algorithm is still in its initial stage of development for CarbonSat and only initial steps towards its application for S-5-UVNS have been undertaken so far. It is therefore at present not clear to what extent the initial results shown here are "optimal". Note that the purpose of this study is to make statements about the capability of S-5-UVNS to provide accurate and precise XCO_2 products. However, conclusions can only be drawn for "an observing system" which is "instrument + retrieval algorithm". This means that errors should not be dominated by shortcomings of the retrieval algorithm but primarily by the instrument. To what extent, the BESD retrieval algorithm in its current

state of development fulfils this requirement is not clear. It is believed that major improvements are possible but unfortunately it is outside the scope of this study to advance BESD as this study requires the application of existing tools with only minor adjustments. Nevertheless, the good agreement with quasi independent results of ULe (see section 4.3.1.3) gives confidence that reliable and robust results for S-5-UVNS have been obtained using BESD.

- BESD is under development for CarbonSat 3-band retrievals (see above). As S-5-UVNS has 2 spectral bands (i.e. NIR-2 and SWIR-1), no 3 bands (i.e. SWIR-2 spectral domain around 2.0 µm is not present), for now at least, this band has been included for the simulations shown here (in order to use BESD "as is") but with zero weight: i.e. the measurement errors have been enlarged such that the band is essentially ignored for the results shown here. This is equivalent to using NIR-2 and SWIR-1 bands only in line with the current specification of S-5-UVNS. This is not expected to be a problem.

3.3.1.2. Set up of the simulations

The BESD algorithm is used to quantify random and systematic XCO_2 retrieval errors associated with S-5-UVNS stand alone. This algorithm is described in detail in [RD23]. Therefore, only a short description is given here. BESD is based on the Optimal Estimation retrieval method (summarised in section 3.2). For each state vector element (*e.g.* CO_2 sub-columns in various layers, temperature profile shift parameter, low order polynomial, etc.), *a priori* values and uncertainties are specified. These parameters are defined using an *a priori* model atmosphere. For the *a priori* model atmosphere, a CO_2 mixing ratio of 390 ppm independent of altitude is assumed. This corresponds to an *a priori* XCO_2 value of 390 ppm. The *a priori* CO_2 (sub-column) uncertainty depends on altitude and is ± 6% (1-sigma) for the lowest layer. The state vector elements are elements of a vector denoted **x**. The state vector elements and *a priori* uncertainties as used for this study are listed in Table 3-6, page 92.

For each type of atmosphere considered in the present study, including the *a priori* atmosphere, and other geophysical parameters related to the surface (*e.g.* surface reflectivity), a high spectral resolution radiance spectrum is computed using the radiative transfer model (RTM) [RD71]. This radiance spectrum is then transformed into a simulated S-5-UVNS radiance spectrum by convolution with the S-5-UVNS ILS (a Gaussian ILS is used by default) and by sampling this spectrum according to the S-5-UVNS wavelength grid (using the specified wavelength range, spectral resolution and spectral sampling ratio). In addition, the (random) error on the radiance is computed using the specified SNR performance (*cf.* Table 4-1).

This "measured" radiance (called $\mathbf{L_i = L(\lambda_i)}$) is then converted into $\mathbf{y_i = \ln(\pi\ L_i\ /\ E_i)}$, where $\mathbf{E_i}$ is the convolved and sampled (= "measured") solar irradiance. The $\mathbf{y_i}$ are the elements of vector **y**. BESD operates on a given spectrum $\mathbf{y} = \mathbf{y}(\mathbf{x})$, computed with unknown **x**,

For each of the scenarios analyzed in Section 4.3.1, a model atmosphere has been defined by varying aerosols and clouds (300 combinations of aerosol and clouds for a given solar zenith angle and surface type). For each scenario, full RTM simulations have been performed (linearization is not used) giving radiances which have been converted to simulated S-5-UVNS radiance spectra (and their random error). Then, these last spectra have been inverted by BESD algorithm to obtain the random and systematic error of XCO_2. For the results shown in Section 4.3.2, other parameters have been varied such as temperature and ILS to obtain the XCO_2 random and systematic errors associated with these specific cases.

Finally, Figure 3-2 shows the BESD Jacobians as used for this study (*cf.* Table 4-1). As can be seen, the spectral resolution in the NIR band (0.4 nm FWHM) is worse compared to the resolution in the SWIR-1 band (0.25 nm FWHM). As a consequence, individual absorption lines are not resolved in the NIR compared to the SWIR-1 band. This results in highly correlated Jacobians for surface pressure, clouds and aerosols. As a consequence, it is unlikely that highly accurate independent information on scattering parameters can be retrieved. One can therefore expect that scattering related XCO_2 errors will be quite large (this is confirmed by the simulations in the following sections). Large errors are also expected because the scattering information from the NIR band cannot reliably be transferred to the SWIR-1 CO_2 band, where they are needed, due to the absence of a 2.0 µm strong CO_2 band.

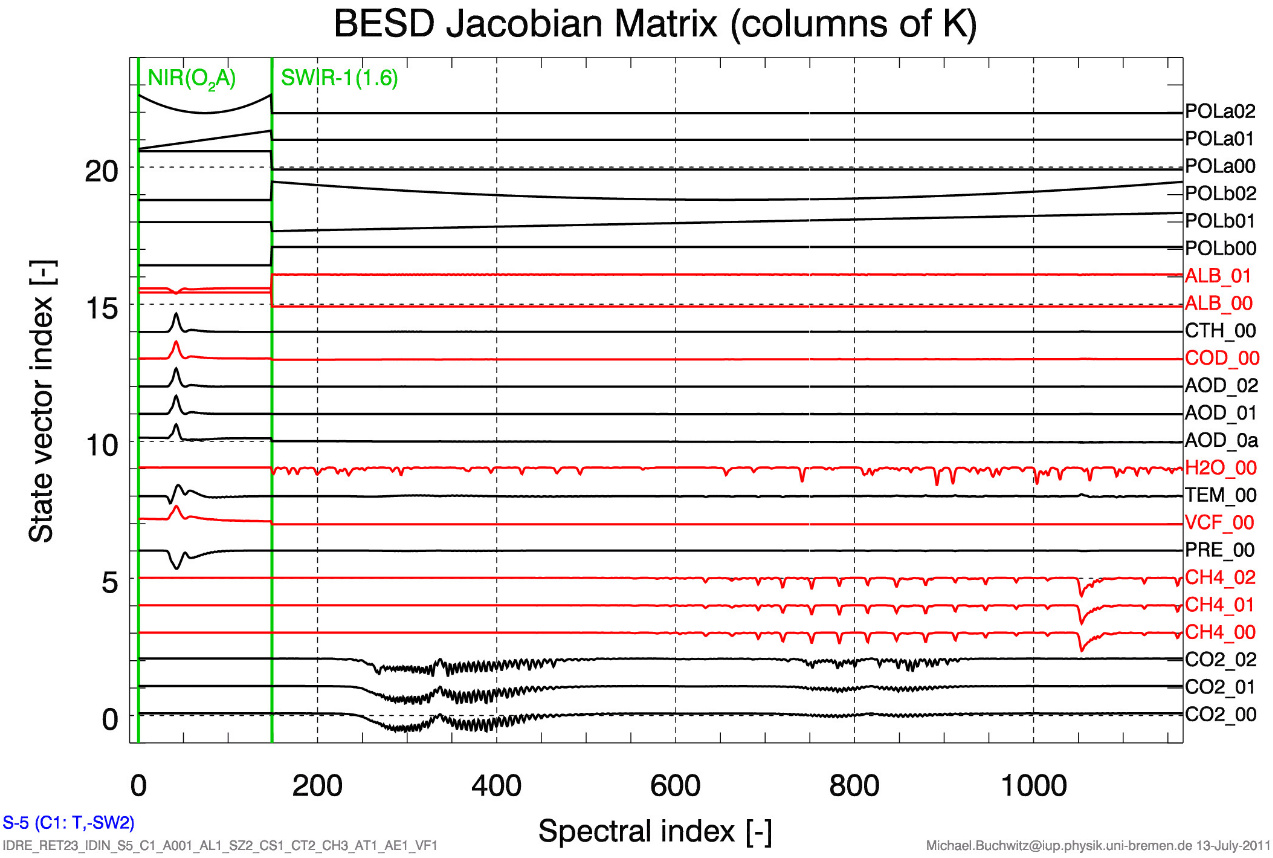

Figure 3-2: Jacobians as used by BESD. The three Jacobians at the bottom are the carbon dioxide ("CO_2") Jacobians for the three atmospheric layers used for the retrieval (the radiative transfer simulations have of course been performed at much higher vertical resolution). Also (from bottom to top) the following Jacobians are shown: methane ("CH_4"), surface pressure ("PRE"), vegetation chlorophyll fluorescence ("VCF"), temperature ("TEM"), water vapour ("H_2O"), aerosol optical depth in three layers ("AOT" or "AOD"), cloud optical thickness ("COT" or "COD"), cloud altitude ("CAL"), surface albedo ("ALB"), and for low order polynomials ("POL"). See Table 3-6, page 92, for a description of the state vector elements.

3.3.2. NASA OCO 'full physics' (ULe)

ULe used the NASA OCO 'full physics' retrieval algorithm and forward model to carry out the analysis [RD3] [RD49] [RD59].

3.3.2.1. General description

The OCO full physics retrieval algorithm was developed to retrieve XCO_2 from a simultaneous fit of the near-infrared O_2 A band spectrum at 0.76 µm and the CO_2 bands at 1.61 and 2.06 µm as measured by the OCO-2 instrument. While the algorithm was developed to retrieve XCO_2 from OCO and OCO-2 observations, it was designed to be adaptable to analyze data from other instruments for algorithm testing and validation. The OCO algorithm has successfully been used to analyze observations from SCIAMACHY, GOSAT, and ground-based Fourier Transform spectrometers (FTS), to simulate Sentinel-5-UVNS measurements (ESA CAMELOT project [RD45]) and spectra for the CNES Minicarb and Microcarb projects. For the simulations and retrievals achived under the present chapter, only the O_2 band and the 1.61 µm CO2 band is used. Including also the 2.06 µm CO_2 band is then investigated in the chapter 6.

The retrieval algorithm uses an iterative retrieval scheme based on Bayesian optimal estimation to estimate a set of atmospheric/surface/instrument parameters, referred to as the state vector **x**, from measured, calibrated spectral radiances.

The forward model describes the physics of the measurement process and relates measured radiances to the state vector **x**. It consists of a radiative transfer model (RTM) coupled to a model of the solar spectrum to calculate the monochromatic spectrum of light that originates from the sun, passes through the atmosphere, reflects from the Earth's surface or scatters back from the atmosphere, exits at the top of the atmosphere and enters the instrument. The top of atmosphere (TOA) radiances are then passed through the instrument model to simulate the measured radiances at the appropriate spectral resolution. The forward model employs the LIDORT radiative transfer model combined with a fast 2-orders-of-scattering vector radiative transfer code [RD52]. In addition, the code uses the low-streams interpolation functionality [RD34] to accelerate the radiative transfer component of the retrieval algorithm.

The monochromatic TOA spectrum calculated by the RTM code is multiplied with a synthetic solar spectrum, which is calculated with an algorithm based on an empirical list of solar line parameters. The solar line list covers the range from 550 to 15,000 cm^{-1} and is derived from FTS solar spectra: Atmospheric Trace Molecule Spectroscopy (ATMOS), MkIV balloon spectra for the range 550–5650 cm^{-1} [41 - 42], and Kitt Peak ground-based spectra for 5000–15,000 cm^{-1} [43 - 44]. The solar model includes both disk centre and disk integrated line lists.

The instrument model convolves the monochromatic radiance spectrum with the instrument lineshape function (ILS). As described in [RD59], the instrument model can also simulate continuum intensity scaling, zero-level offsets and channelling effects.

3.3.2.2. Simulation of spectra

Sentinel-5-UVNS radiance spectra have been simulated by using the forward model of the OCO full physics retrieval algorithm for the geophysical scenarios specified in section 3.1.3 which include 3 SZAs, 3 surface types, 4 AODs, 3 aerosol types, 5 CODs and 5 cirrus heights for a given 27 level atmosphere.

Aerosols are simulated by an exponentially-shaped profile with 2 km scale height plus an additional Gaussian-shaped profile in free troposphere with a width of 3 km and height of 4 km (*i.e.* a Gaussian-shaped profile peaking at a height of 4 km with a Half Width Half Maximum (HWHM) of 3 km). For the "AOT 0.1" background scenario, the exponential profile is given with an AOT value of 0.06 and the Gaussian shaped a value of 0.04 similar to the setup of Bremen. The reference wavelength for our retrieval is 760 nm and we have transferred the 550 nm AOT values to 760 nm using the estimated Angstrom coefficient for the 3 aerosol types used for the simulations. The aerosol optical properties have been calculated for the aerosol types described in [RD72] [RD73]. The optical properties for the spherical components are computed using a polydisperse Mie scattering code [RD81], those for the non-spherical components such as mineral dust, with a T-matrix code [RD78]. For the simulations we have used the so-called types 1a (continental clean), 5b (continental polluted) and 4c (desert dust). The optical properties are taken from the cirrus model of [RD62] for an effective radius of 60 micron. The COT has also been transferred to 760 nm via the Angstrom coefficient. The vertical profile for cirrus has been realized by a Gaussian-shaped profile for the various centre altitudes and a width of 1 km.

The instrument line shape function has been assumed to be Gaussian-shaped with a HFWHM according to the resolution given in Table 4-1 (*i.e.* a Gaussian-shaped profile with a spectral resolution of 0.4 nm in chapter 4 as threshold and 0.06 nm as goal in chapter 6). A tabulated ILS (provided by ESA and NOVELTIS) has been used for specific test called 'inhomogeneous scenes' in section 4.3.3.6. The measurement covariance matrix $\mathbf{S}_\varepsilon$ has been assumed to be diagonal. The diagonal elements are given by the variance of the noise that has been calculated for each spectral element according to Table 4-1.

3.3.2.3. Retrieval of simulated spectra

The simulated spectra have been calculated with the OCO full physics retrieval algorithm using a state vector that includes a CO_2 vmr profile, a scaling factor for the H_2O vmr profile, an offset to the temperature profile, surface pressure, surface albedo and spectral slope per band, an aerosol extinction profile and a cirrus extinction profile. All profiles are given on the same 27 levels that have been used for the retrieval. In the standard retrieval (section 4.3.1), all *a priori* values are as in the simulations except for the aerosol and cirrus parameters.

The aerosol and cirrus *a priori* profiles have been setup so that they are different to all simulations. The aerosol extinction profile is given by a Gaussian-shaped profile, peaking at a height of 2 km with a Half Width Half Maximum (HWHM) of 2 km for an AOD of 0.15. The cirrus cloud extinction profile is given by a Gaussian-shaped profile at 10 km and a HWHM of 3 km. Aerosol and cloud extinction is retrieved as log-value to prevent negative values which would lead to a crash of the retrieval algorithm. The aerosol type used for the retrieval is type '2b' from [RD72] [RD73]and thus differs from the types used for the simulations. The use of type '2b' is arbitrary and the results of the experiment will strongly depend on this assumption. The cirrus type is the same as in the simulations.

To test the effect of the assumed aerosol type on the retrieval, two retrieval experiments have been carried out where the simulated and retrieved spectra do not include cirrus clouds. This results in a total of 108 simulated spectra which have been retrieved using aerosol type '2b' or '3b', respectively. The setup of the aerosol profile is as above.

- The *a priori* covariance matrices for the state vector elements are as follows:
- The CO_2 *a priori* covariance matrix has been calculated to impose only a weak constraint on XCO_2 and to include non-diagonal elements to constrain the profile shape. The matrix has been inferred from a model run of the LMDZ model which has then been scaled to reproduce a root-mean-square (RMS) variability of XCO_2 of 12 ppm.
- The *a priori* covariance matrix for aerosol and cirrus is a diagonal matrix with an *a priori* 1σ uncertainty of a factor of 10 at each level.
- The *a priori* covariance matrix for the temperature and H_2O scaling is 3.16 K and 0.316, respectively.
- For surface pressure a 1-sigma uncertainty of 4 hPa is used.
- Surface albedo and its slope are essentially unconstrained.

In section 4.3.2, potential retrieval errors when the *a priori* for the atmospheric profiles differs from truth are also investigated. Here, the setup aerosol and cirrus is in the same way for the simulations and the retrievals. Only atmospheric parameters i.e. temperature, H_2O, surface pressure or CO_2 have been perturbed. For these retrievals, we have simulated a subset of spectra (SZA = 50°, albedo = vegetation) using aerosol type '2b' as in the retrievals. The setup of the aerosol profile and the cirrus setup are as for the simulations described above.

All the information concerning the *a priori* (state vectors and uncertainties) are summarised in Table 3-6**.**

Section 4.3.2 also includes a study on the effect of the *a priori* aerosol profile shape. To this end, the height or the width of the *a priori* aerosol profile used in the standard retrieval have been modified. The simulations are as for the standard simulations except that aerosol type '2b' is used in the simulations and the retrievals.

3.3.2.4. Linear analysis

Linear error analysis is used to estimate errors due to instrument calibration uncertainty (section 4.3.3.7). Here, the inverse model is applied once to a set of simulated spectra calculated assuming that the state vector is the truth, *i.e.*, we assume that the iterative retrieval scheme has already converged. We treat instrument calibration as a forward model parameter error **b** and the XCO_2 uncertainty is then given by:

$$\sigma^{b}_{XCO2} = \boldsymbol{h}^{T} \boldsymbol{G}_y \boldsymbol{K}_b \boldsymbol{S}_b \boldsymbol{K}_b \boldsymbol{G}_y \boldsymbol{h}$$

Where:

- $\mathbf{G_y}$ is the gain matrix, that represents the mapping of the measurement variations into the retrieved state vector variations;
- $\mathbf{K_b}$ are weighting functions (called also "Jacobians") for the parameter **b**;
- $\mathbf{S_b}$ is the error covariance matrix for **b** where the diagonal elements give the variance of the assumed uncertainty;
- and **h** is the pressure weighting function.

Error estimates obtained with linear error analysis will be realistic as long as errors do not become large and are within a linear regime: *i.e.* if the relation between XCO_2 error and $\mathbf{S_b}$ is not linear, the error estimates are not valid anymore. Note that a linear approximation is always valid over small (error) intervals. As the error becomes larger, the linearity between $\mathbf{S_b}$ and XCO_2 error might no longer be granted and the error estimates become inaccurate (might be too strong). This means that small errors should be more accurate than large errors. However, when the error is large, then it does not matter too much if the estimate is not very accurate.

3.3.3. DISAMAR (KNMI)

3.3.3.1. General presentation

KNMI will use the DISAMAR tool in the optimal estimation mode. DISAMAR stands for Determining Instrument Specifications and Analyzing Methods for Atmospheric Retrieval. The wavelength range considered is 270 – 2400 nm (UV-VIS-NIR-SWIR). Initially, it has been developed to derive level 1b requirements given specific level 2 requirements. The ESA CAMELOT project [RD45] has been used to calculate Level 1b requirements for the Sentinel-5 mission. Recent improvements and extensions are:

(i) checking and cross-checking of input parameter values using keywords and a parser;

(ii) much faster retrievals for relatively smooth absorbing spectra (not for line absorption spectra);

(iii) an output format that is readily transformed into HDF data format;

(iv) interfacing with python which makes series of retrievals possible;

(v) the ability to read external files with reflectance data that can be used to process measured spectra, *e.g.* OMI measurements;

(vi) enforcing hydrostatic equilibrium in the atmosphere and options to fit temperature profiles, *e.g.* for the O_2-A band near 760 nm;

(vii) option to use polarized light in the forward model calculations;

(vii) option to use more advanced aerosol / cloud models based on Mie scattering.

DISAMAR contains a radiative transfer module to calculate the simulated measured reflectance and the so-called forward model used in the retrieval. Three types of retrieval are available, namely Optimal Estimation Method described in section 3.2, DISMAS (an efficient version of Optimal Estimation based on a DOAS-like approach), and DOAS. For line absorbing molecules (H_2O, O_2 A band, CO_2, and CH_4), only Optimal Estimation can be used. The radiative transfer is based on the adding/doubling method and includes a more efficient variant, called Layer Based Orders of Scattering (LABOS). The derivatives (weighting functions) that are needed for the retrieval are calculated very efficiently using semi-analytical expressions. Observations in different spectral bands (or fit intervals) can be combined.

The cloud and aerosol models were initially very simple as they are either a Lambertian surface (cloud) or a scattering layer with a Henyey-Greenstein phase function. The optical thickness of the cloud / aerosol layer can vary with wavelength according to the Angstrom law. In an improved version, the coefficients for the expansion in generalized spherical functions that describe the scattering matrix are computed. This makes it possible to use more advanced scattering properties for cloud and aerosol. The surface below the atmosphere is a Lambertian reflector with an albedo that can vary with wavelength. The wavelength dependence of the surface is modelled as a low-degree polynomial. It is assumed that the surface albedo does not vary within pixel, except in section 6.3.4 where an inhomogeneous surface is considered.

3.3.3.2. Aerosol model included in DISAMAR

The atmosphere is divided into so-called intervals defined by pressure levels, *e.g.* 1013, 800, 600, 400, 0.05 hPa. In each interval aerosol and/or cloud particles can be added.
The volume extinction coefficient and the single scattering albedo for the aerosol and cloud particles are independent of the altitude or pressure within the interval. So the scenario listed in Table 3-2 can be copied in DISAMAR.

The radiative transfer properties of the aerosol for a specific wavelength are described in terms of the volume extinction coefficient, the single scattering albedo, and the coefficients for the expansion of the phase function in Legendre functions (polarization can be ignored here). For this project, Henyey-Greenstein phase functions have been chosen with a fixed value of the asymmetry parameter g = 0.70 and a wavelength dependent optical thickness that is given by the angstrom coefficient. This made it possible to use aerosol models that have the same wavelength dependence of the aerosol optical thickness as the models used by IUP-UB.

The HITRAN 2008 database is considered for the absorption cross sections of CO_2, H_2O, and O_2.

In DISAMAR, the ground surface is a Lambertian surface and there are no bidirectional effects. The surface albedo as function of the wavelength is specified for each spectral band separately and can be a low-order polynomial in the wavelength. It is assumed that the models VEG, SAS, and SIC are also Lambertian surfaces or can be made Lambertian surfaces. In this project, wavelength dependence is ignored within the spectral fit windows around 760, 1600, and 2050 nm.

In DISAMAR the altitude grid is calculated from the temperature profile given as function of the pressure. The altitude grid is calculated assuming hydrostatic equilibrium. The US standard atmosphere is assumed to be consistent with hydrostatic equilibrium.

3.4. Solar spectrum

An appropriate high resolution solar spectrum [RD32] (the OCO team "Toon spectrum") is used by all retrieval teams. This spectrum is made available by ULe. This synthetic solar spectrum was calculated by the OCO-2 Forward model. The solar model consists of two parts: the solar absorption model and the solar continuum model. This solar model offers several advantages over a measured solar spectrum:

- The solar spectrum can be computed on the exact spectral grid that is needed, avoiding the complication of re-sampling the measured spectrum which can result in under-sampling structures;
- A measured solar spectrum is already convolved with the ILS of the spectrometer that measured it. Using such a measured solar spectrum may cause spectral artefacts.

The solar absorption model calculates the solar lines based on empirical solar line list that has been optimized for either a disk-centre or a disk-averaged observation. This solar absorption model has been used extensively for the analysis of ground-based FTS spectra, both in the infrared and the NIR. Solar absorption is assumed invariant in the time. This is considered as a good assumption in the infrared and near-infrared spectral domains.

The solar line list covers the range from 550 to 15,000 cm^{-1} and is derived from FTS solar spectra: Atmospheric Trace Molecule Spectroscopy (ATMOS), MkIV balloon spectra for the range 550-5650 cm^{-1} [41,42] and Kitt Peak ground-based spectra for 5,000-15,000 cm-1 [43-44]. The solar model includes both disk centre and disk integrated line lists [RD3].

- Several combinations of L1B products and retrieval methods are employed (*cf.* section 3.3):
- DOAS method where the L1B product is *ln*(radiance spectrum) – *ln*(irradiance spectrum);
- Fit of the reflectance spectrum;
- Or direct fit of the radiance spectrum (with a complete forward modelling of both the solar and atmospheric components).

In all cases, it is understood that the irradiance spectrum (in fact the out of the atmosphere solar spectrum illuminating the diffuser) is used for radiometric calibration (hence potentially contributing the systematic errors).

3.5. Overall summary of the geophysical state vectors taken into account in the 3 retrieval software

The Table 3-6, page 92, summarises the geophysical state vectors which are taken into account by the 3 groups of experts, with the retrievals algorithms described in the previous sections (*cf.* 3.3.1, 3.3.2 and 3.3.3). The Optimal Estimation Method requires, as already explained in section 3.2, *a priori* uncertainties to be assigned to each parameter and the corresponding values, which are to be interpreted as 1-sigma uncertainties.

The values chosen for the *a priori* uncertainties can influence to some extend the value for the retrieved XCO_2 and its errors estimates as presented in the next sections. The approach chosen here is to use *a priori* uncertainties such that they only impose loose constraints on the state vector, except when external information is used such as in section 4.4. Then, XCO_2 retrievals will be mainly dominated by the spectral measurements. It can be expected that minor modifications to the *a priori* covariance matrices will have a negligible effect on the inferred retrieval errors. The effect of substantial modification to the *a priori* covariance matrices, in particular when choosing much more constraining matrices/uncertainties, will need to be studied elsewhere. The nine polynomial parameters of IUP-UB are the coefficients of the quadratic polynomials in the 3 spectral bands. They are the standard DOAS polynomial which accounts for albedo effects (for the corresponding spectrally smooth broadband effects) but also for many other things. Actually, DOAS polynomial accounts mainly for all the spectral smoothly varying multiplicative radiance errors (instrument and modelling). However, for surface albedo, there are additional parameters which, in addition, account for high spectral resolution albedo effects on the spectral radiance.

It has to be noticed that the results in the following chapters (especially the results in section 4.3.1.3, page 112) show that robust conclusions can be drawn despite the differences geophysical inputs considered in each algorithm. This indicates that differences in the geophysical scenario inputs are not critical in terms of impact in the XCO_2 retrievals.

Table 3-6: Description of the *a priori* state vectors considered for the XCO_2 retrieval during the present study.

		ULe	BREMEN	KNMI
CO_2	SV element	CO_2 profile described in Table 3-5	CO_2 profile described in Table 3-5	CO_2 column with the profile shape based on Table 3-5
	Uncertainty	Covariance matrix derived from LMDZ model with non-diagonal elements scaled to root of 12 ppm (StdDev for XCO_2)	CO_2 partial column upper layer : 0.005 (relative) CO_2 partial column middle layer: 0.03 (relative) CO_2 partial column lower layer: 0.06 (relative)	10% for the column.
H_2O	SV element	Profile scaling *a priori* profile see Table 3-5	Profile scaling (from the *a priori* profile see Table 3-5)	H_2O column with the profile shape based on Table 3-5
	Uncertainty	StdDev of 0.31	2.0 (relative)	100% for the column.
T	SV element	Temperature shift *a priori* profile see Table 3-5	Temperature shift (from the *a priori* profile see Table 3-5	Temperature is not fitted.
	Uncertainty	StdDev of 3.16 K	0.1 (relative)	

		ULe	BREMEN	KNMI
CH_4	SV element			CH_4 is ignored in the model atmosphere
	Uncertainty	StdDev	CH_4 partial column upper layer : 0.01 (relative) CH_4 partial column middle layer: 0.06 (relative) CH_4 partial column lower layer: 0.12 (relative)	
Surface Pressure	SV element	Surface pressure Table 3-5	Surface pressure Table 3-5	Surface pressure from Table 3-5
	Uncertainty	StdDev of 4 hPa	0.001 (relative)	StdDev of 5 hPa
Surface albedo	SV element	Mean value and spectral slope for each band *a priori* values: Same as for observations	Mean value for each band *a priori* values: Same as for observations (this was required to analyze the large number of scenarios using a fast look-up-table scheme; some test have been done using SCIATRAN coupled to BESD giving essentially the same results if albedo is retrieved rather than prescribed.	Mean value for each band
	Uncertainty	StdDev of 1 for mean albedo; slope unconstraint	0.05 (relative) for each band	StdDev of 1 for mean albedo
Aerosol	SV element	Extinction profile (as log)	Aerosol optical depth *a priori* values: CC aerosol scenario with AOD = 0.3 @ 550 nm.	Aerosol optical thickness at 550 nm
	a priori	Gaussian shaped with 2 km height and 2 km width	Altitude dependent but scene independent profile	Depends on the case considered (see Table 2). Often the *a priori* is the same as the value used for the simulation.
	Uncertainty	Diagonal covariance matrix with StdDev of factor of 10 per level	Upper layer: 0.001 (relative) Middle layer: 0.001 (relative) Lower layer: 1.0 (relative)	Variable as it is used as constraint. Typical values are 1.0, 0.10, 0.05, and 0.01.
	Opt. properties	Type '2b' (different to simulations): *i.e.* 29% sulphate; 12% sea salt; 39%accum. Dust; 19%corase dust	*a priori*: CC Simulations: CC, CP, DE	Angstrom coefficient varies depending on the aerosol model CC, CP or DE. Asymmetry parameter is fixed to 0.7. Single scattering albedo is 0.95 with a StdDev of 0.04.
Cirrus	SV element	Extinction profile (as log)	CTH: Cirrus altitude COD: Cirrus optical depth	CAL: Cirrus altitude COT: Cirrus Optical thickness
	a priori	Gaussian shaped with 10 km height and 1 km width	10 km height 1 km width	Variable often 8 or 10 km as specified.

		ULe	BREMEN	KNMI
	Covariance	Diagonal matrix with StdDev of factor of 10 per level	CTH: 1.0 (relative) COD: 1.0 (relative) CAL: 1.0 (relative)	CAL: 4 km COT: 1.0
	Opt. properties	Same as in simulations	Same as in simulations	Same as in simulations. Single scattering albedo is 1.0 and the asymmetry parameter is 0.7.
Polynom parameter	SV element	Not used	-	Not used.
	Uncertainty		SWIR-1 (quadratic): 1000 (relative) SWIR-1 (linear): 1000 (relative) SWIR-1 (constant): 1000 (relative) NIR (quadratic): 1000 (relative) NIR (linear): 1000 (relative) NIR (constant): 1000 (relative)	
Vegetation Chlorophyll Fluorescence	SV element	Not used		Not used.
	Uncertainty		3.0 (relative)	

4. Capability of the current Sentinel-5 mission for CO_2 monitoring

4.1. Objectives and description of the proposed approach

4.1.1. Objectives

The goal of the exercise presented here is to assess quantitatively the errors associated with a total column CO_2 derived from a single-sounding observation of the Sentinel-5-UVNS sounder, only based on the current instrumental specifications of S-5. Later, chapter 7 focuses on enhancing the performance by examining modifications/optimisations to S-5-UVNS, based on the results and recommendations of this present report.

This chapter focuses on instrument specifications as given in the S-4/5 MRD [RD14] (NIR and SWIR-1 spectral domains, SNR, spectral resolution and sampling, ILS knowledge, instrument systematic errors, error budget). The current specifications includes also the use of other instruments (main the VII imager, and qualitatively 3MI during the study), where applicable. Making use of other instruments on the platform may make the mission more efficient.

The main performance parameters which are considered in this study are the XCO_2 errors associated with a single XCO_2 product retrieved from the S-5-UVNS sounder. When analysing the S-5-UVNS sounder stand alone, XCO_2 random and systematic errors will be differenced and analysed carefully.

Random errors analysed are related to the instrument features and assess how the signal to noise ratio of the spectra maps to XCO_2 uncertainties. Systematic errors are calculated using end-to-end retrievals (see section 3.2.2). The significations and analyses of the systematic errors are detailed in section 5.4.2. Their interpretations may be various as different sources are associated with them (*cf.* section 5.1).

The impact of the synergy of S-5-UVNS with VII or 3MI for XCO_2 retrieval derived from an individual S-5-UVNS measurement will be estimated, in terms of XCO_2 errors, without distinction between random/systematic errors. Indeed, the methodology employed on this specific aspect is different. Thus, total XCO_2 errors will be discussed.

All these XCO_2 errors are computed and analysed in order to understand how the (small or large) magnitude of each specific (geophysical or instrumental) parameter impacts a single retrieved total column CO_2, derived from current instrumental specifications of the S-5-UVNS. Then, the results are discussed with respect to the user requirements expressed in Table 2-7.

4.1.2. Description of the proposed approach

A statistically representative set of geophysical scenarios and simulations are defined (*cf.* section 3.1.3). XCO_2 retrieval analyses are performed from these scenarios, after ESA gave its approval for the definition of the scenarios. The number and nature of these scenarios and simulations are clearly stated in section 3.1.3, and justified with respect to complete analyses which are performed in the sections 4.3 and 4.4. It is pointed out that conclusions **on the global, statistically representative, performances (at least for systematic error) cannot be drawn from this set of simulations (although the number of simulations performed is higher than the numbers stated in the proposal document),** but they should be treated as 'case studies', which are well chosen to give **the best possible first guess of the S-5-UVNS CO_2 performances**.

In the present report TN2, both expert partners, IUP-UB and ULe, study random and systematic errors on Sentinel-5-UVNS sounder stand alone in order to double check and to improve/assess the robustness of the findings (important as existing tools, initially developed for other space-borne XCO_2 measurements will be used for the first time for S-5-UVNS during the study). The third expert partner, KNMI, assessed quantitatively the expected total XCO_2 errors derived from Sentinel-5-UVNS sounder combined with VII in priority. Based on these results and the expertise on 3MI, the expected XCO_2 performances derived from the combination Sentinel-5-UVNS-3MI are addressed qualitatively.

IUP-UB, ULe and KNMI algorithms are based on their "in house" existing tools. Their tool have been set up to the homogenised input instrument, methodology of simulations and scenario parameters Comparisons of the results, from the three teams, allow to characterise the agreement between the 3 algorithms. Limited number of representative full retrieval allowed the assessments of XCO_2 errors related to the uncertainties of various geophysical parameters (*e.g.* aerosol, cirrus, albedo, SZA, etc…), as done in A-Scope study (A-SCOPE, 2008) [RD43]. Finally, the quantitative results are interpreted with respect to the user needs specified in section 2.5.6.

The proposed approach described in the present chapter is summarised in Figure 4-1.

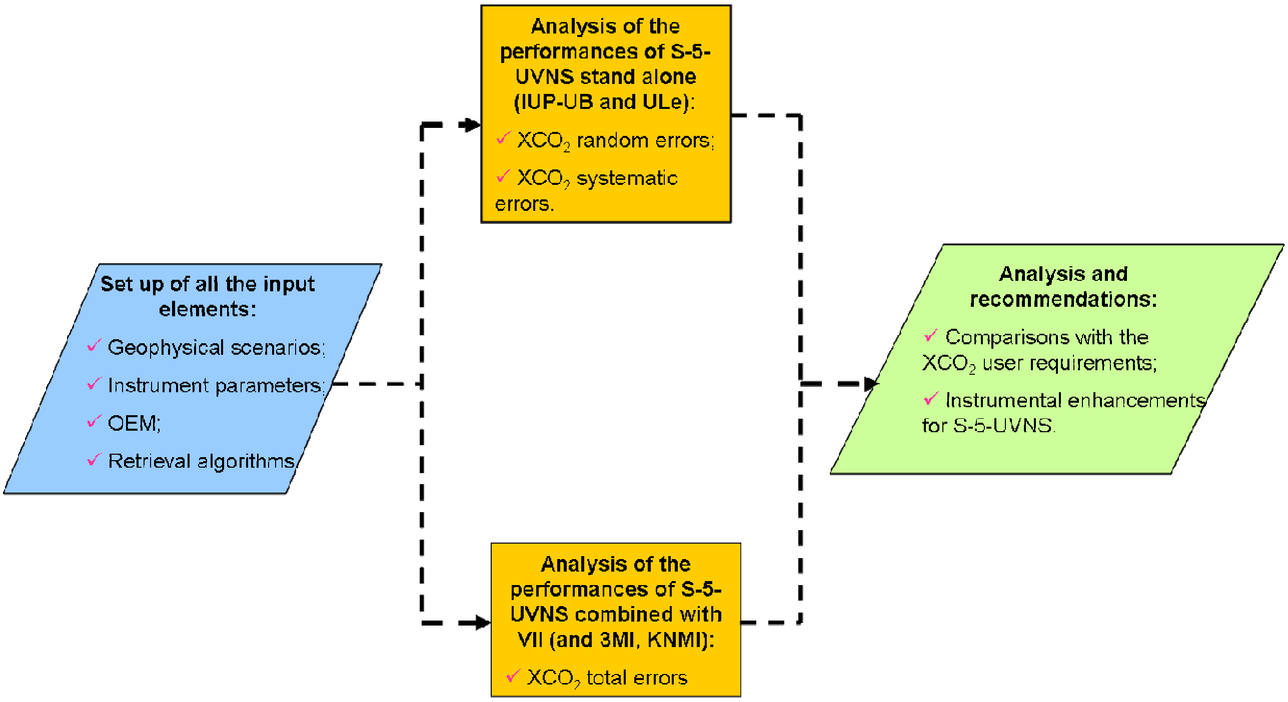

Figure 4-1: Description of the proposed approach under the chapter 4

The chapter 4 is divided into the following sections:

- Section 4.2 described the instrument parameters as input for the simulations of L1B Sentinel-5-UVNS observations.
- Section 4.3 provides the results of the quantitative error analyses associated with the Sentinel-UVNS sounder stand alone. Random and systematic budget are discussed as function of the different sources of the XCO_2 errors (*i.e.* sources of scattering related XCO_2 errors in section 4.3.2 and also some less critical sources in section 4.3.3, such as meteorological or instrumental parameters).
- Section 4.4 gives qualitative and quantitative explanations of the potentials to combine the S-5-UVNS sounder with the VII imager or the 3MI polarimeter for improving (or not) the XCO_2 errors associated with individual XCO_2 products, obtained during the retrievals, through the capacities of these instruments to detect and obtain clouds and aerosols information combined with the S-5-UVNS pixels.

4.2. Setup for Sentinel-5 synthetic CO_2 observations

4.2.1. Towards the characterisation of the S-5-UVNS L2 CO_2 uncertainties

The SWIR Sentinel-5-UVNS measurements rely on absorption spectroscopy using the Sun as the light source. The photons are absorbed in the Earth atmosphere by CO_2 (and other gases molecules). After reflection at the surface and upward transmission in the atmosphere, the photons are measured by the sounder. Depending on the spectral resolution associated with the instrument, it may be possible to measure the depth of individual absorption lines. The depth of the CO_2 lines is directly related to the number of CO_2 molecules along the line of path. They are also affected by temperature and pressure profiles. Moreover, atmospheric scattering due to molecules, aerosols and clouds impact the spectra. Thus, the retrieval process (described in sections 3.2 and 3.3) uses background information on atmospheric profiles and uses both the CO_2 absorption lines and the O_2 lines to separate the effect of CO_2 absorption and atmospheric scattering.

The CO_2 total column retrieval errors caused by several unaccounted effects, under various atmospheric and observational conditions, are computed using a radiative transfer code. This code allows simulating the L1B measurement (*i.e.* the spectra associated with the instrument considered) from a description of geophysical features in the atmosphere. These simulations are based on specific instrument parameters (see section 4.2.2.1) and are achieved for the scenarios described in section 0.

When retrieving a single sounding XCO_2, it is important to simulate correctly the mean light path corresponding to the observed scene. Thus, it is expected that elements of "correction" for the light path will be a critical point for obtaining an accurate XCO_2 product (as explained in detail in section 3.1.2). **Under the present chapter, the baseline approach for this correction is to exploit the O_2 A band and weak CO_2 (1.6 µm) SWIR-1 spectral band (as specified under [RD14]) through simultaneous retrievals, for which currently available full-physics algorithms have made significant progress during the last years.**

Moreover, additional information can be provided by the VII imager, and the 3MI missions. Both of these instruments can add value as they will be flown on the same MetOp-SG platform as the Sentinel-5-UVNS sounder. Potential added value through these synergies can be addressed by the 2 following ways:

- External information on clouds and aerosol can be considered as auxiliary information to improve (if possible) the accuracy of XCO_2 retrievals. Cloud and aerosol scenarios provide XCO_2 uncertainty sensitivity as a function of the cirrus optical thickness, aerosol optical thickness, their altitude and type. These sensitivities are combined with expected performances for these parameters of VII and 3MI, based on MODIS and POLDER experience. Using these external information can help for assessing to what extent:
    - VII (and 3MI) help to filter out significantly aerosol and cloud contaminated scenes;
    - XCO_2 retrieval errors are reduced if VII (and 3MI) aerosol and cloud standard products and their error characteristics are used as *a priori* information.
- Simulations based on the broadband backscatter information through the VII imager L1 measurements are performed in order to obtain a good scattering correction of the Sentinel-5 XCO_2. For that purpose, VII spectral bands are included in the spectra simulations and for some aerosol scenarios, retrieval simulations exploiting S-5-UVNS and VII measurements in synergy are performed and analysed.

4.2.2. Simulations of the L1B S-5-UVNS products

4.2.2.1. Instrument parameters

The instrument parameters considered under the present chapter 4 are derived from the reviews of:

- [RD14] and [RD8] for the main parameters related to the Sentinel-5-UVNS sounder;
- [RD7] for additional information on the SNR in the NIR-2 and SWIR-1 spectral domains;

- and from [RD37] for the VII imager and 3MI polarimeter.

All the simulations in the sections 4.3 and 4.4 are based on these instrument parameters and the radiative transfer models presented in section 3.3.

The instrument parameters related to S-5-UVNS and assumed here are listed in Table 4-1. It is assumed the focus of this chapter will be on threshold (T) values rather than on goal (G) values.

Table 4-1: Sentinel-5-UVNS instrument parameters used as input for this study. The SSR is the number of spectral resolution elements (detector pixel) per spectral resolution Full Width at Half Maximum (FWHM). The SNR is the SNR per detector pixel (not per FWHM).

S-5-UVNS	Band	
Parameter	**NIR-2**	**SWIR-1**
Spectral range [nm]	750-775	1590-1675
Spectral resolution FWHM [nm]	0.4 (T) 0.06 (G) => under chapter 6	0.25
Spectral sampling ratio (SSR) [-]	3	3
Signal-to-noise ratio (SNR) [-]	500@755nm and see [RD7] Radiance dependence: square root	See [RD7] Radiance dependence: square root

4.3. Analysis of the XCO_2 single-sounding retrieval error: Sentinel-5-UVNS stand alone

4.3.1. General results

4.3.1.1. IUP-UB results

In order to obtain statistically meaningful results, several regions have been defined as shown in Figure 4-2**.** For each region a weight has been assigned for each of the 1800 scenarios analyzed by IUP-UB using the maps shown in Figure 3-1. The 1800 scenarios are all combinations of the "Variable key parameters" presented in Section 3.1.3., except for "Snow/Ice" albedo scenes (SIC). The SIC scenarios have been omitted as they are not relevant for nearly all scenarios analyzed but also in order to reduce processing time.

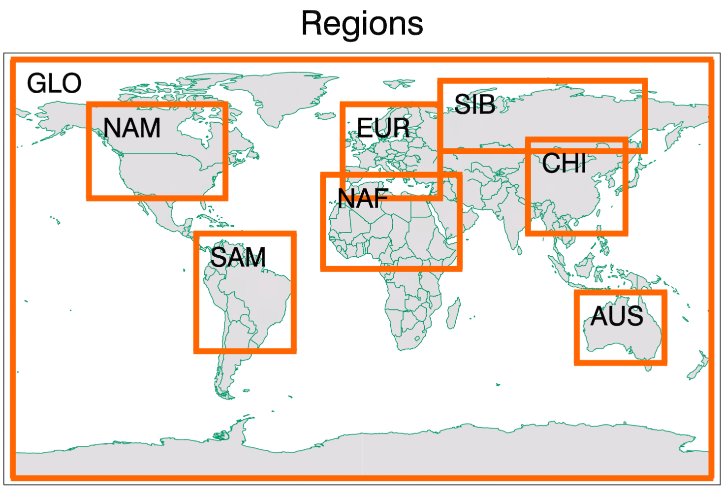

Figure 4-2: **Regions defined for this study. GLO = Global, NAM = North America, SAM = South America, EUR = Europe, NAF = North Africa, SIB = Siberia, CHI = China, AUS = Australia.**

For information, the AOTs of the aerosol scenarios used by IUP-UB are shown in Figure 4-3. As shown in Figure 4-4, the XCO_2 biases are typically large for the desert aerosol type scenarios (DE). Figure 4-3 shows that the AOTs are particularly high for DE at all relevant wavelength although the AOTs are identical for all three scenarios at 550 nm. As can be seen, the AOTs are much higher for DE compared to CC and CP at all relevant wavelength (although the AOTs are identical at 550 nm). From this, one may expect larger XCO_2 errors for the DE scenarios compared to the other two aerosol type scenarios and this is essentially confirmed by the results shown below.

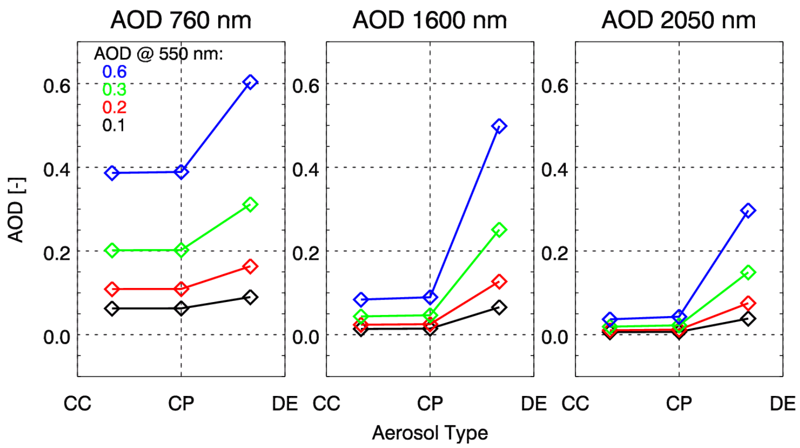

Figure 4-3: **Aerosol optical depth (AOD) of the three aerosol types Continental Clean (CC), Continental Polluted (CP) and Desert (DE) as used by IUP-UB. Each panel shows four curves corresponding to four specified AODs at 550 nm (see annotation).**

An overview about the systematic and random errors for all 1800 scenarios is given in Figure 4-4. As can be seen, **the XCO_2 random error varies only little and is in the range 1-3 ppm. In contrast, the XCO_2 biases show large variability.** Most important is the red curve which shows the systematic error after the data have been filtered. Accepted as "good" are only those observations which meet the following criteria:

- Retrieved AOT(NIR) + retrieved COT < 0.3;
- Deviation of retrieved surface pressure from *a priori* (meteorological) surface pressure < 10 hPa.

As can be seen, this removes many of the outliers but not all. Errors are particularly high at high COT, large SZA but also for desert aerosols (DE) as can be seen in more detail in Figure 4-5 and Figure 4-6, page 103.

Detailed results for the 3 selected regions are shown in Figure 4-7**,** Figure 4-8**,** Figure 4-9. They show that the XCO_2 systematic errors can be quite high and that the bias is particularly large at high COT, high AOT, especially for the desert aerosol scenario, and at high SZA.

More details on the various sensitivities are given in the following sub-sections but a summary of the IUP-UB analysis of scattering related errors is already given in Table 4-2:

- XCO_2 random error presents an average value of 1.6 ppm (over the complete 1800 scenarios). All the values do not exceed 3.4 ppm (which is the maximum value deduced over all the simulations).
- The dependence of the XCO_2 systematic error is pretty complex and is described in the next sections. However, it can be already noticed that 95% of the scenarios simulated have a XCO_2 systematic value lower than 2 ppm. But, only 47% of these scenarios present values lower than 0.2 ppm (which is the goal requirement expressed in the Table 2-7).

Table 4-2: Overall summary of the estimate of Sentinel-5's scattering related XCO_2 errors as obtained by IUP-UB using the BESD retrieval algorithm. The results for the systematic error are based on the GLO scenario shown in Figure 4-7. The results for the random error are based on the GLO scenario.

X [ppm]	Systematic Error Fraction of scenarios with systematic error < X ppm (after quality filtering)	Random error (in ppm, 1-sigma)
0.2	48%	Mean: 1.6
0.5	79%	Range: 0.7 – 3.4
1.0	82%	
2.0	95%	
4.0	100%	
8.0	100%	
	Number of scenarios analyzed: 1800 Number of scenarios accepted after quality filtering: 616 (34%)	

Figure 4-4 illustrates systematic and random errors of XCO_2 obtained by applying the IUP-UB BESD algorithm to S-5-UVNS simulations for all 1800 scenarios (uniquely numbered from 1-1800). After filtering, accepting only retrievals retrieved AOT+COT < 0.3 and surface pressure within +/-10 hPa of the *a priori* pressure, which still flags 34.2% of the 1800 scenarios as "good", are shown in red. As can be seen, systematic errors are large, especially for large COT and large SZAs. More details (zooms) are shown in Figure 4-5 and Figure 4-6. In contrast, XCO_2 random errors (blue line) are pretty constant (within ~1-3 ppm).

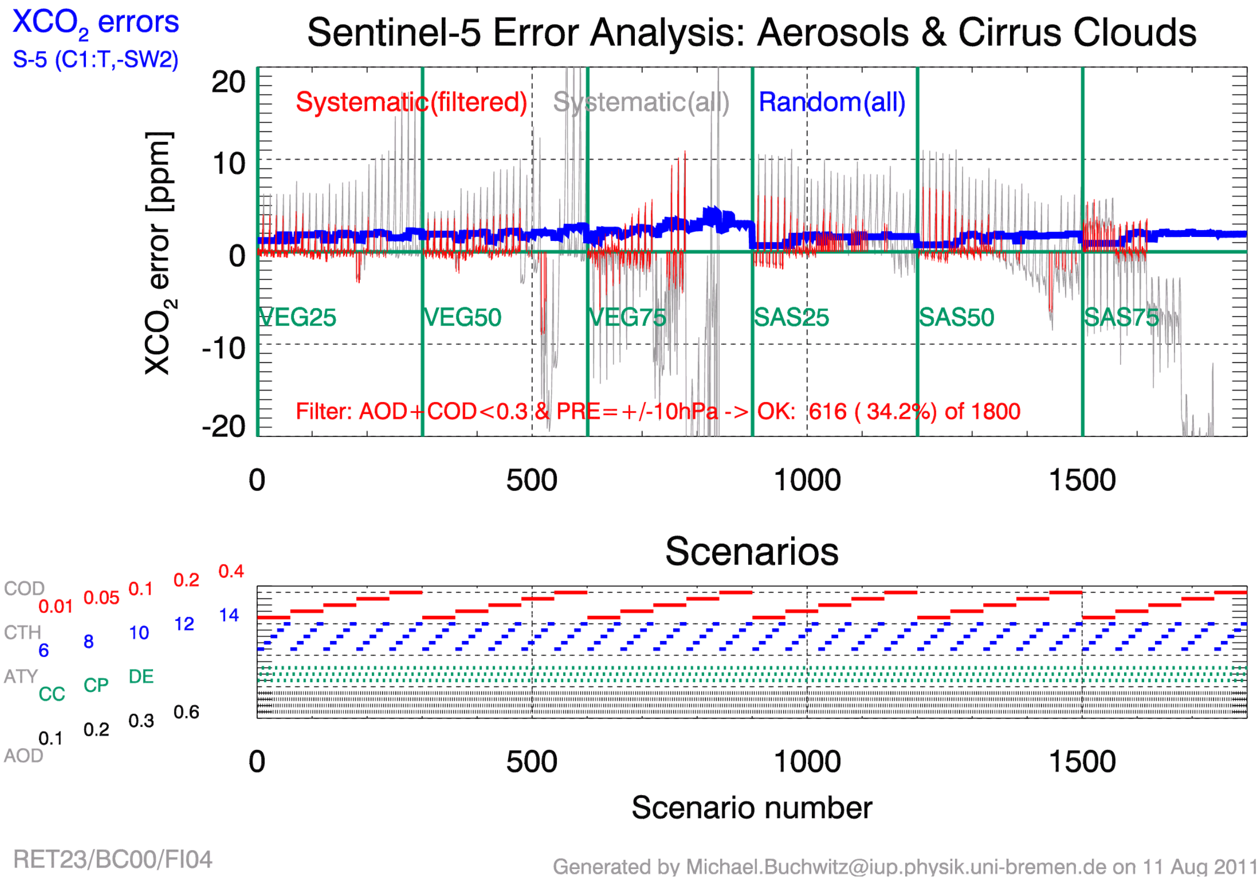

Figure 4-4: **Systematic and random errors of XCO_2 obtained by applying the IUP-UB BESD algorithm to S-5 simulations for all 1800 scenarios (uniquely numbered from 1-1800) corresponding to the VEG (vegetation) and SAS (sand/soil) surface albedo scenes. The bottom panel shows the corresponding AOD, aerosol type (ATY), cirrus altitude (CTH) and optical depth (COD). Surface albedo and solar zenith angle are indicated by the green text items (VEG25, VEG50, …) and the green vertical lines in the top panel. The top panel shows the systematic errors for all 1800 scenarios in grey.**

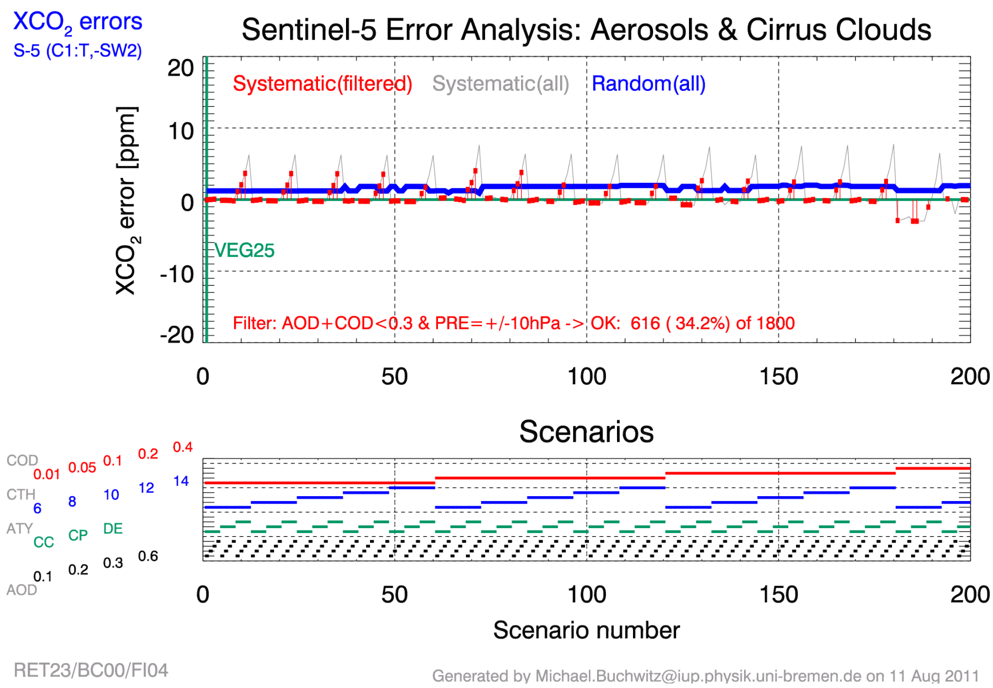

Figure 4-5: **As Figure 4-4 but zooming into the scenario number 1-200 region. As can be seen, the systematic errors are high for the desert aerosol type scenario with errors increasing with AOD.**

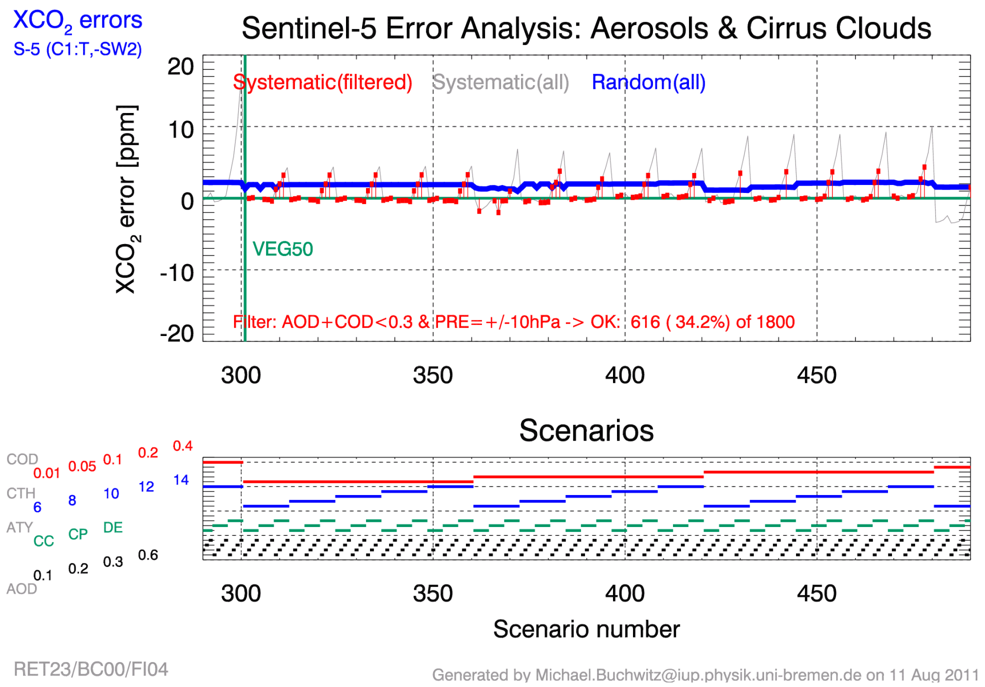

Figure 4-6: **As Figure 4-4 but zooming into the scenario number 290-490 region. As can be seen, the systematic errors are high for the desert aerosol type scenario with errors increasing with AOD.**

As illustrated in Figure 4-7, XCO_2 systematic errors are particularly high (average between 1 and 2 ppm) for high COT (0.1 – 0.2). XCO_2 bias present also values up to 8 ppm (in absolute) for large SZAs (75°)). There also seems to be a (relative) high bias (variations up to 5 ppm) at large AOT (0.2-0.3) and a high bias for the desert aerosol (DE). However, it should be noticed that XCO_2 bias for SZA = 75° are not representative here as these scenarios were automatically removed when the filter has been applied.

Overall, the scatter of the biases is quite high and the dependencies are complex (as all parameters depend on each other). Also listed are various statistical parameters such as peak-to-peak (p2p) bias for the four months analyzed, the fraction of scenarios with bias less than several pre-defined values (*e.g.* 79% of the scenarios have a bias of less than 0.5 ppm), as well as the overall bias (-0.3 ppm), the root-mean-square-error (RMSE), which is 0.99 ppm, and the standard deviation of the bias which is 0.95 ppm.

Figure 4-8 and Figure 4-9 are similar illustrations to the Figure 4-7 but zoomed on specific regions: Europe and South America.

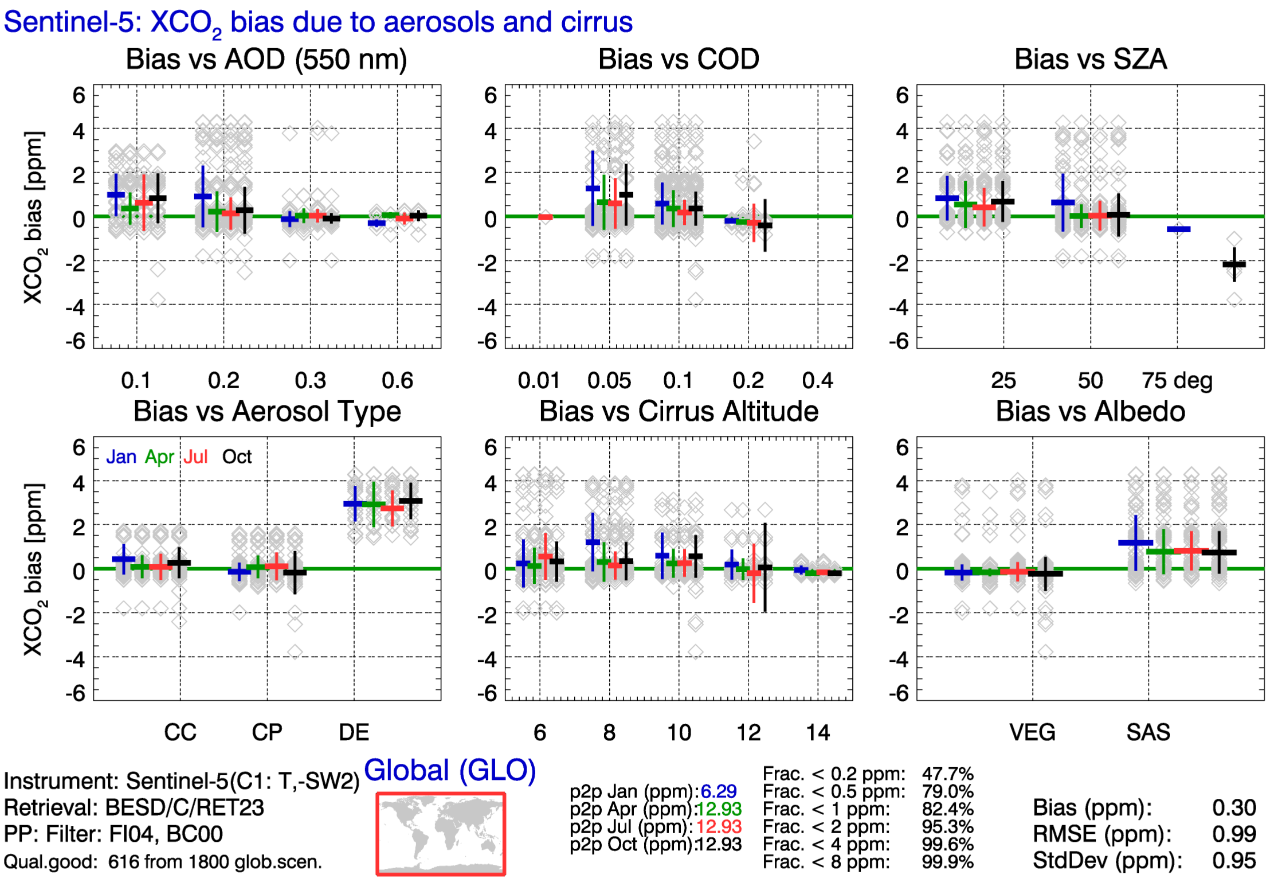

Figure 4-7: Dependence of the XCO_2 bias (already filtered) on various parameters for the region GLO (see map in Figure 4-2). The peak-to-peak bias is given for 4 months analysed (January, April, July and October) with the overall bias, RMSE and the standard deviation (StdDev).

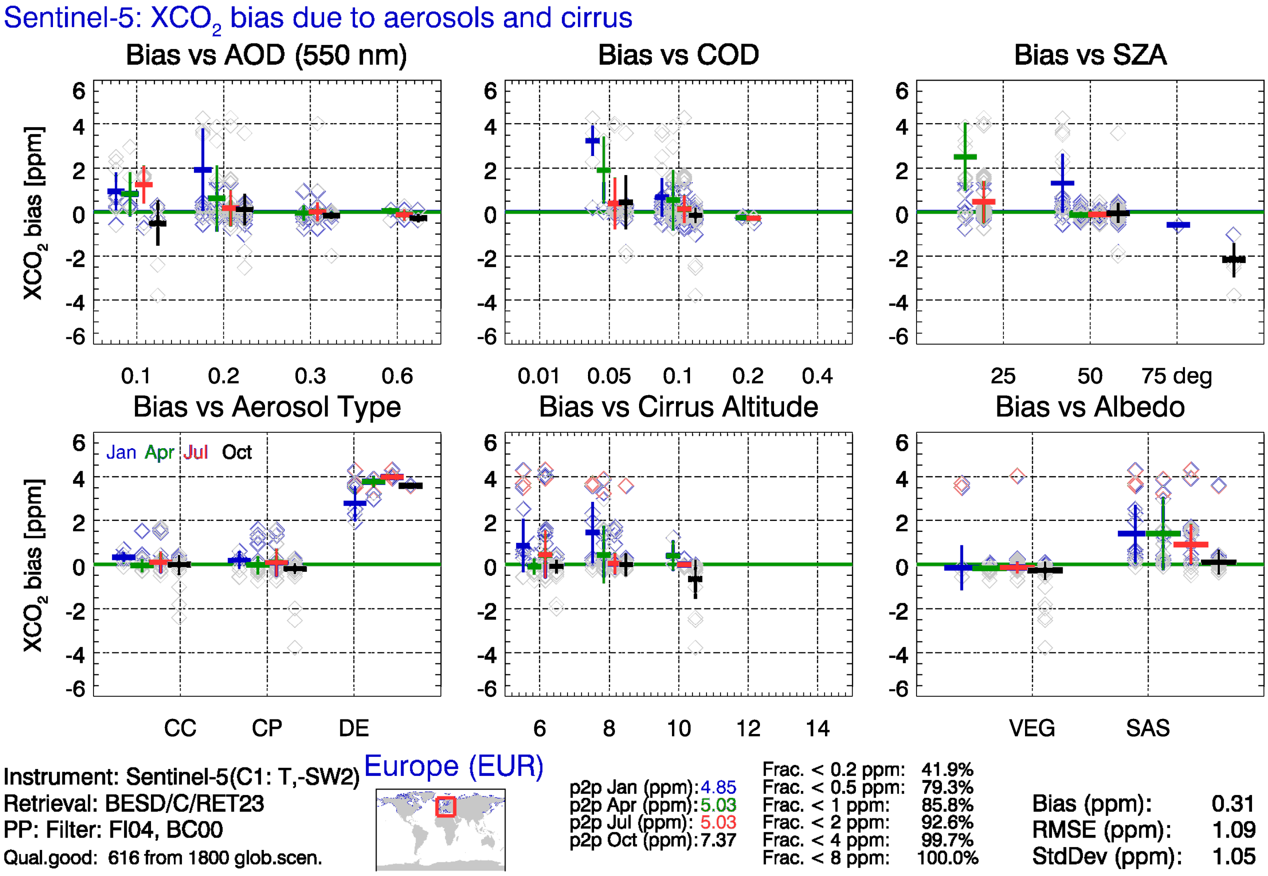

Figure 4-8: **As Figure 4-7 but for the region Europe (EUR).**

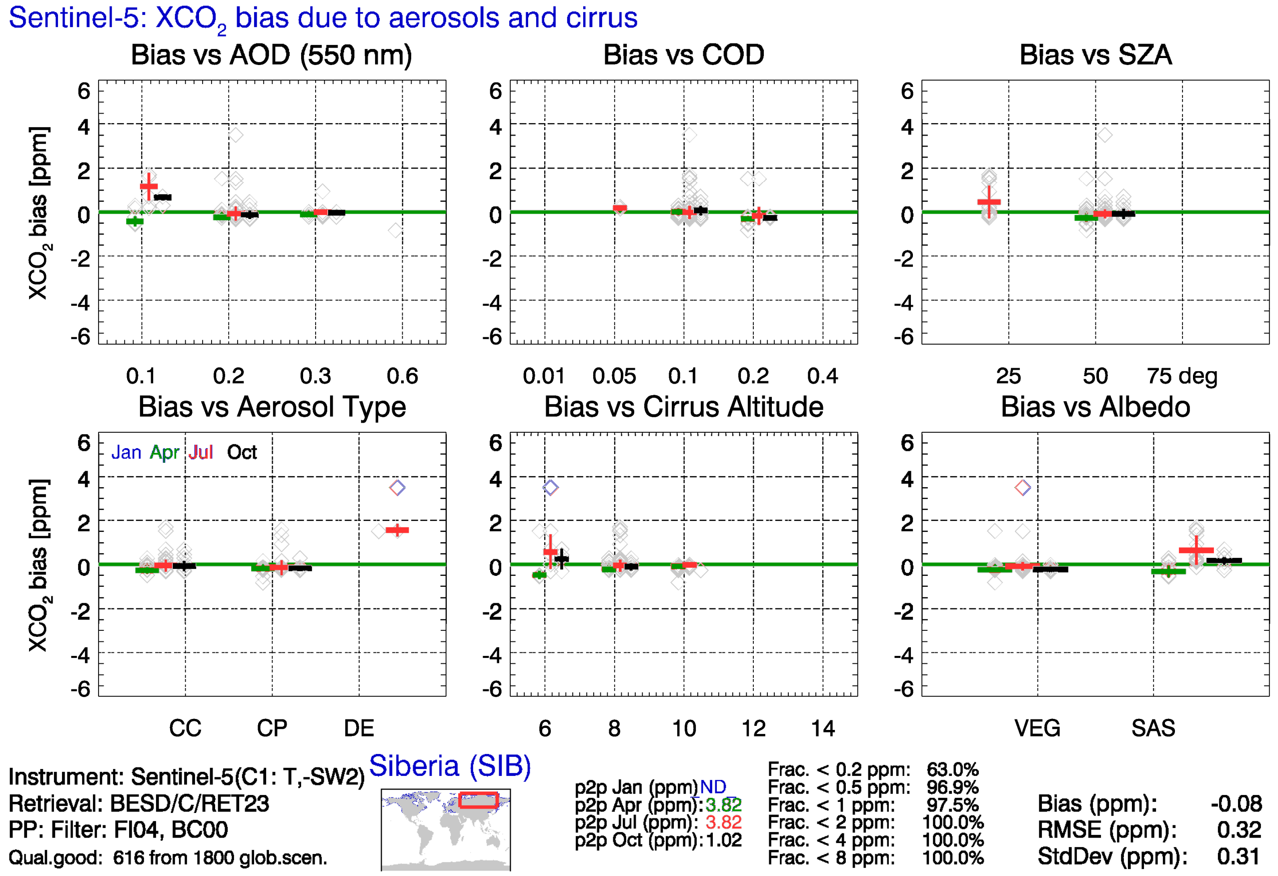

Figure 4-9: **As Figure 4-7 but for the region South America (SAM).**

4.3.1.2. ULe results

To investigate XCO_2 biases introduced by aerosols and clouds, retrievals from simulated spectra have been carried out where the retrieval setup for aerosols and clouds differs from the simulations whereas the atmospheric and surface parameters are the same in simulations and the *a priori* for the retrievals. Details of the setup of simulations and the retrievals can be found in sections 3.2 and 3.3.2 . The differences between retrieved and true XCO_2 result from the differences between aerosols and clouds and can be directly used to quantify related retrieval biases. In total, 2700 spectra are simulated and retrieved. However, a larger number of these spectra are inversed under conditions where an accurate retrieval is usually not expected (large SZA, low albedo and/or high aerosol+cirrus load). A post-processing quality filter will be necessary to filter out poor retrievals. In addition, it is expected that a number of retrievals will not converge to a solution, *i.e.* the number of iterations exceeds the limit of 10 or the number of diverging steps exceeds 5.

A quality filter is applied to converged retrievals. This quality filter is based on the following criteria:

- Abs (surface pressure-1013 hPa) < 10 hPa ;
- Retrieved AOT+COT < 0.3;
- CHI^2 < 1 (in each spectral band);
- Number of diverging steps < 4;
- *a posteriori* XCO_2 error < 1.2 ppm.

The first two components are as in the filter applied by Bremen. The filter for CHI^2 and number of diverging steps is necessary to exclude cases that have converged to a local minimum; both have little effect on the results (see Figure 4-14). The filter for the *a posteriori* error has been included as the biases tend to increase with a *posteriori* XCO_2 error (or poor SNR). Without such a filter (or a filter with a similar effect such as a filter for SZA, or surface albedo or degrees of freedom) the results tend to be poor. Such filter has a large effect on the result and there might be possible to modify the criteria in order to obtain similar results but a larger fraction of the retrievals would be saved.

The effect of the quality filter is shown in more detail in Figure 4-12 and Figure 4-13, page 110.

The summary of the retrieval results are given in Table 4-3. Only approximately 60% of the retrieval converges to a solution. The failed cases are primarily related to large COTs, high cirrus altitude and large AOTs (amplified by large SZA) which all differ substantially from the *a priori* (and first guess) setup and thus the retrieval is not able to converge to a solution due to the high non-linearity of the retrieval problem. Choosing *a priori* values for the aerosol and cirrus profile more appropriate for these situations, *e.g.* based on information from a different instrument), should lead to an increase in converged retrievals for such situations. However, the retrieved XCO_2 might still be substantially biased.

The mean XCO_2 bias of the converged scenes is around 1% with a standard deviation larger than 2% and the mean random error exceeds 2 ppm with a very large spread of values. It may be assumed that a mean bias can be successfully removed by validation (*i.e.* comparison with more precise data, such as *in situ* observations). The spatially and temporally variable component of the bias as described by the standard deviation is the most relevant parameter to be compared with the level 2 requirements described in technical note 1. However, it should be considered that standard deviation of the XCO_2 systematic errors of all soundings is only a crude proxy for regionally biases.

Applying a quality filter as defined above largely improves the results. Nevertheless, it reduces the number of data points to 13% of the original 2700 soundings. The mean bias is reduced to 0.3 ppm with a standard deviation of 1.9 ppm. The mean precision is reduced to 1 ppm with a standard deviation of 0.12 ppm.

A more detailed analysis of the results is given in Figure 4-10 to Figure 4-13 and in the following sections.

To investigate the impact of the *a priori* setup for aerosol and cirrus on the retrieval results statistics, two additional retrieval experiments are carried out for a small subset of the simulations. The aerosol subset uses only simulations for SZA = 50°, vegetation surface and cirrus height of 10 km. The simulated spectra are retrieved with the standard setup and with an additional setup where the aerosol type 3b (35% sulphate, 10 sea salt, 47% carbonaceous, 8 black carbon) is used instead of 2b. In this case, the mean bias and the standard deviation of the bias are significantly increased whereas the precision and number of scenes is very similar. The second subset is a cirrus subset which uses all simulations for SZA = 50°, vegetation surface and AOT of 0.1. In this case, the standard retrieval setup and then a retrieval setup are considered with an *a priori* cirrus profile with a centre height of 12 km instead of 10 km. The effect on the mean statistics is very small, however with the second setup. An increased number of XCO_2 retrievals for a cirrus profile height of 14 and 12 km and a smaller number of XCO_2 retrievals for low cirrus heights are obtained.

Table 4-3: Summary of XCO_2 retrieval results for the standard retrieval (aerosol + cirrus) and the 2 additional experiments that include only aerosols in the simulations and the retrievals.

Complete Aerosol + Cirrus Set	
Num of total scenes	**2700**
Converged SCENES	
Num of scenes	**1614**
Mean XCO_2 bias (ppm)	**2.99**
StdDev XCO_2 bias (ppm)	**7.37**
Mean XCO_2 random Error (ppm)	**2.28**
StdDev XCO_2 random Error (ppm)	**1.74**
Filtered Scenes	
Num of scenes	**346**
Mean XCO_2bBias (ppm)	**0.31**
StdDev XCO_2 bias (ppm)	**1.86**
Mean XCO_2 random Error (ppm)	**1.00**
StdDev XCO_2 random Error (ppm)	**0.12**

Table 4-4: Summary of XCO_2 retrieval results for an aerosol subset (only SZA = 50 deg, vegetation surface and cirrus height of 10 km) and a cirrus subset (only SZA = 50 deg, vegetation surface and AOD of 0.1). The retrieval has been carried out with the standard retrieval setup and when using aerosol type 3b instead of type 2b in the retrieval or when using a cirrus *a priori* profile with a centre height of 12 km instead of 10km.

	Aerosol Subset Standard	*Aerosol Subset Aerosol Type 3b*	*Cirrus Subset Standard*	*Cirrus Subset Cirrus Height of 12 km*
Num of total scenes	**60**	**60**	**75**	**75**
Converged SCENES				
Num of scenes	**49**	**44**	**51**	**51**
Mean XCO_2 bias (ppm)	**0.67**	**1.80**	**-0.61**	**-0.77**
StdDev XCO_2 bias (ppm)	**1.49**	**2.05**	**1.54**	**1.46**
Mean XCO_2 random Error (ppm)	**1.36**	**1.11**	**1.11**	**1.06**
StdDev XCO_2 random Error (ppm)	**0.49**	**0.21**	**0.32**	**0.21**
Filtered Scenes				
Num of scenes	**24**	**28**	**37**	**38**
Mean XCO_2 bias (ppm)	**0.24**	**1.91**	**0.01**	**-0.19**
StdDev XCO_2 bias (ppm)	**0.76**	**1.84**	**0.68**	**0.63**
Mean XCO_2 random Error (ppm)	**1.00**	**0.99**	**0.96**	**0.96**
StdDev XCO_2 random Error (ppm)	**0.09**	**0.05**	**0.09**	**0.08**

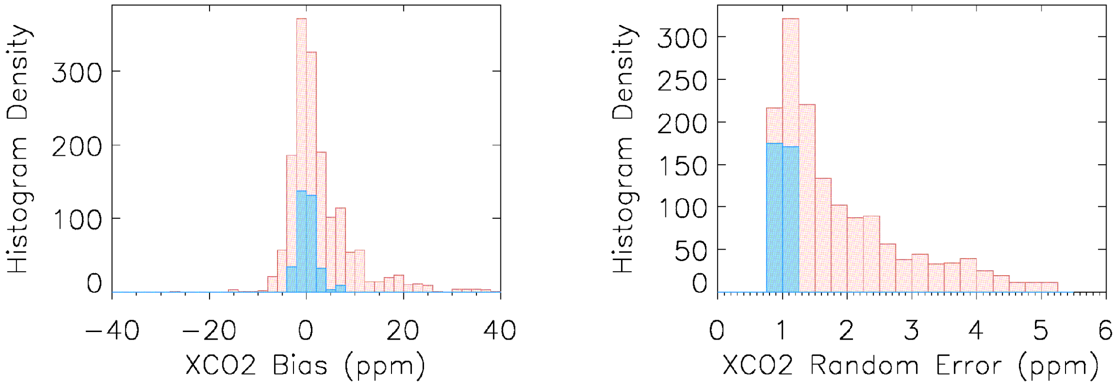

Figure 4-10: XCO_2 bias (left) and XCO_2 *a posteriori* error (right) for the aerosol+cirrus simulations. Red bars show the results for all scenes and blue bars are the filtered results.

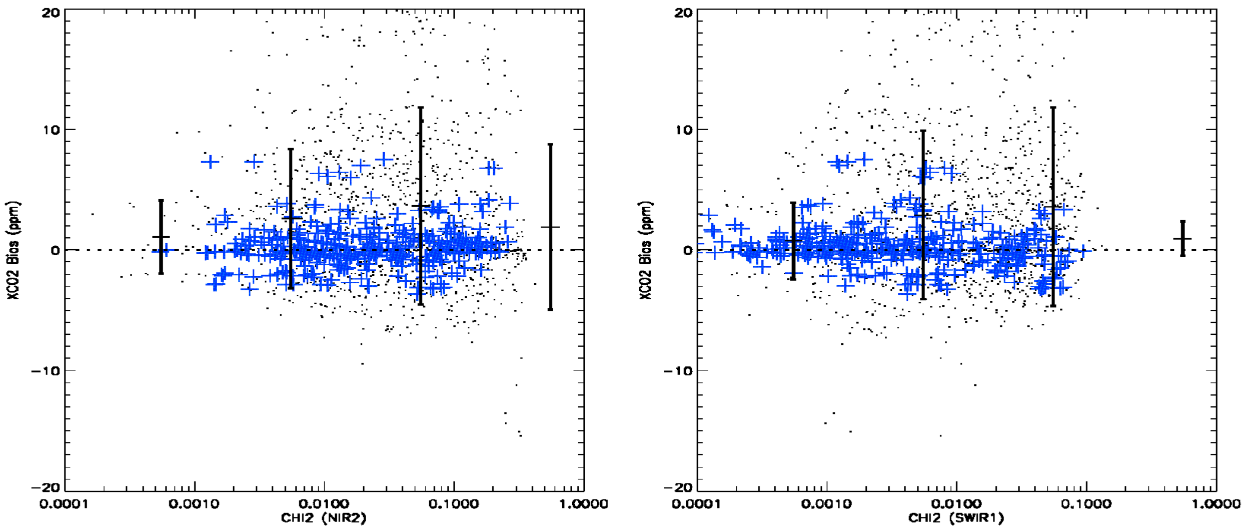

Figure 4-11: XCO_2 bias as a function of CHI_2 (left: band 1; right: band 2) for the aerosol+cirrus simulations. Black symbols give the results for all scenes and blue symbols for the filtered scenes. Also given is the mean value and StdDev for all scenes for a number of bins.

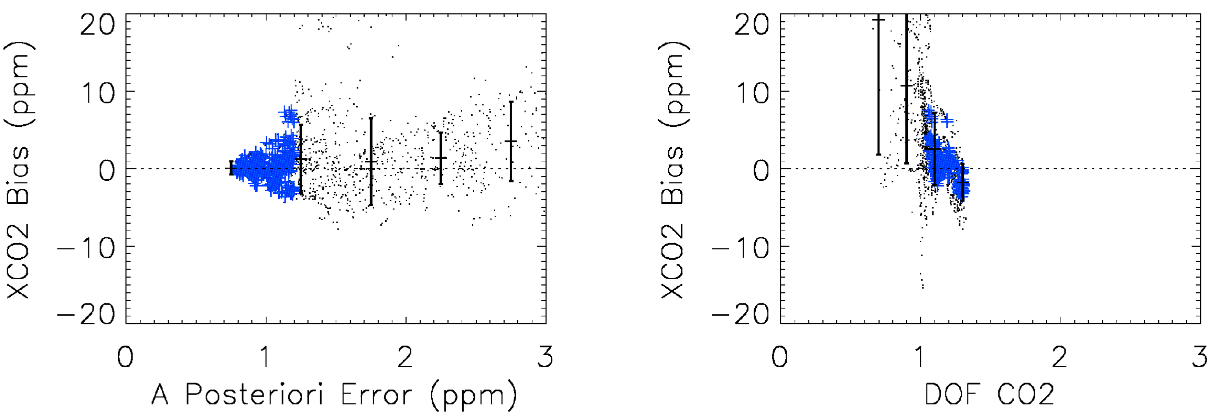

Figure 4-12: XCO_2 bias as a function of *a posteriori* error (left) and degrees of freedom for CO_2 (right) for the aerosol+cirrus simulations. Black symbols give the results for all scenes and blue symbols for the filtered scenes. Also given is the mean value and StdDev for all scenes for a number of bins.

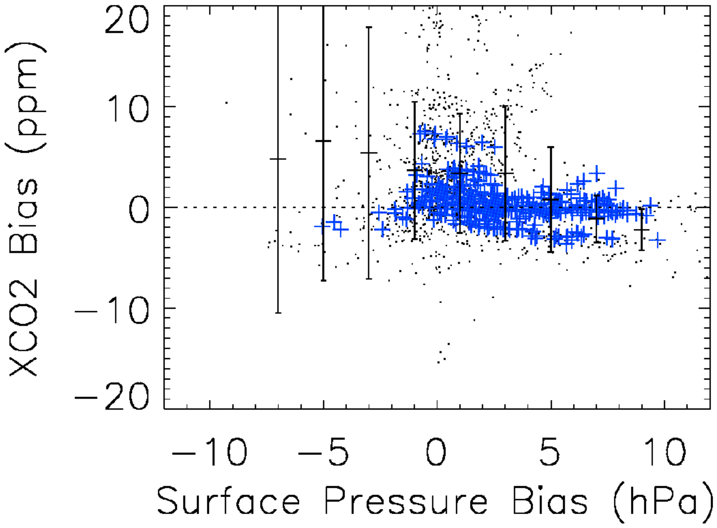

Figure 4-13: XCO_2 bias as a function of surface pressure bias for the aerosol+cirrus simulations. Black symbols give the results for all scenes and blue symbols for the filtered scenes. Also given is the mean value and StdDev for all scenes for a number of bins.

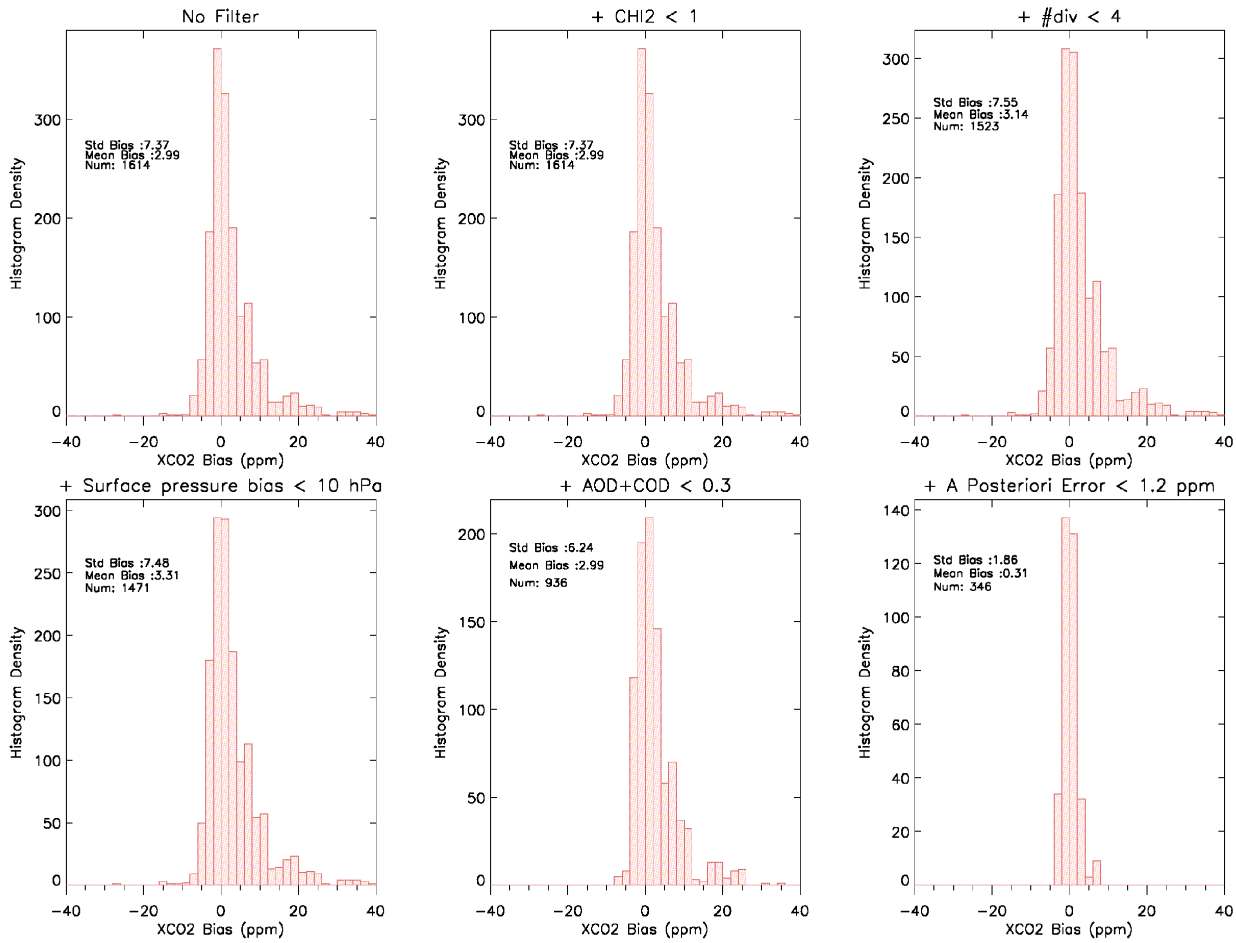

Figure 4-14: Distribution of XCO_2 bias for different parameters of the applied filter. The filter is applied cumulative and the top left panel shows no filter and the bottom right panel the final filter.

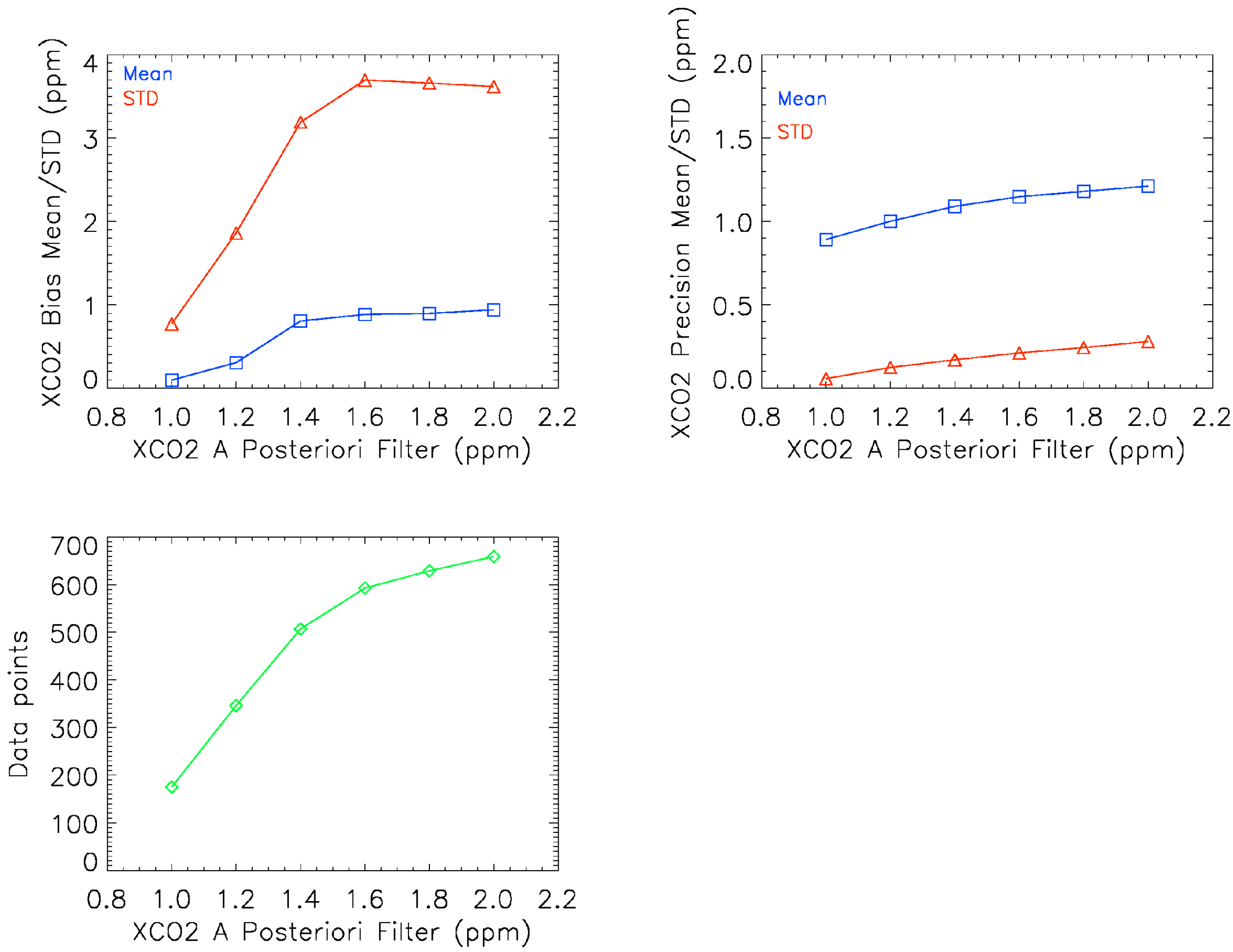

Figure 4-15: Final statistics of the filtered ensemble for different values of the *a posteriori* filter threshold. Top left panel gives the mean and standard deviation of the bias, top right panel the mean and standard deviation of the random error and the bottom panel gives the number of data points.

4.3.1.3. Comparison of results between IUP-UB and ULe

Table 4-5 summarises the major results of IUP-UB and ULe quantifying the XCO_2 capabilities, in terms of random errors (precision) and systematic errors (accuracy) for all the scenarios and also depending on specific cases (such as scattering effects, temperature or inhomogeneous scenes).

This summary is given through several statistical variables:

- Mean Random Error (MRE): this the average of the statistical error over the scenes for the corresponding type. The statistical error is the sqrt[diag($\mathbf{S_x}$)] in the OEM formalism *i.e.* the square root of the *a posteriori* variance, a quantity related to the variance/covariance of the measurement noise $\mathbf{S_y}$ and of the *a priori* of the state vector Sa (also involving the Jacobians) (*cf.* section 3.2).
- Standard deviation Random Error (SRE): standard deviation of the statistical error over the scenes for the corresponding type.
- Mean Systematic Error (MSE): which may be called also "bias" is the quantity (retrieved – truth, *cf.* section 3.2) averaged over the scenes for the corresponding type.

$$MSE = \left(\sum_{i}^{NumberofScenes} XCO_2 retrieved(i) - XCO_2 truth(i) \right) / NumberofScenes$$ **Equation 4-1**

This quantity can be positive or negative. It is a systematic bias of the observing system with respect to the "truth" (in simulations).

- Standard deviation Systematic Error (SSE): standard deviation of the quantity (retrieved – truth) over the scenes for the corresponding type. Thus,

$$SSE = \sqrt{\sum_{i}^{NumberofScenes} (XCO_2 retrieved(i) - bias) - XCO_2 truth(i))^2 / NumberofScenes} \quad \textbf{Equation 4-2}$$

So, the standard deviation is given with respect to the mean. This is the bias corrected to systematic error. The quantity retrieved(i)-bias is the unbiased measurement.

- Root Mean Square Systematic Error (RMSSE): is defined by

$$RMSSE = \sqrt{\sum_{i}^{NumberofScenes} (XCO_2 retrieved(i) - XCO_2 truth(i))^2 / NumberofScenes} \quad \textbf{Equation 4-3}$$

One should have: $RMSSE^2 = SSE^2 + MSE^2$ (in theory, SSE is smaller than RMSSE)

- Overall error or Root Sum Square (RSS) is defined by:

$$RSS = \sqrt{(a^2 + b^2 + c^2)} \quad \textbf{Equation 4-4}$$

Where: a = SSE values related to the scattering scenes;

b = SSE values related to the temperature scenes;

c = SSE values related to the inhomogeneous scenes

Note: It is NOT divided by the number of scenes.

Results presented in Table 4-5 are related to the filtered scenarios. Indeed, results associated with the not filtered CO_2 total column retrievals should not be considered as they represent spectra observed for conditions where no accurate retrieval is expected (too large SZA, too low albedo and/or high aerosol+cirrus load). So, the results are obtained by filtering out poor retrievals (see sections 4.3.2.1.1 and 4.3.2.1.2).

More details, corresponding to the different nature of the sources of XCO_2 errors are analysed in the next sub-sections. However, general comments can be given as follows:

- Clearly, as expected, the XCO_2 random errors computed by both of the expert groups present a significant dependence with respect to the SZA values and the type of surface (*i.e.* albedo). Indeed, when SZA values increase from 25° to 75°, MSE values go up (from 0.92 ppm to 1.14 ppm for ULe, and from 1.50 ppm to 1.99 ppm for IUP-UB).
- Some differences are observed between the values of XCO_2 random errors between IUP-UB and ULe. However, the results allow to state that they are smaller than the XCO_2 requirements (see section 2.5.5.1, page 59, and Table 2-7, page 70): average values vary between 1 ppm (ULe) and 1.68 ppm (IUP-UB) with StdDev between 0.12 ppm and 0.57 ppm for all the scattering scenarios. Differences may be explained by the different state vector elements and the different *a priori* elements (*e.g.* IUP-UB elements are all considered to be un-correlated, including the 3 CO_2 parameters).
- There are some differences on the number of scenes which remain after the filtering. These differences have various explanations: the initial number of simulations performed by IUP-UB and ULe are not identical (2700 for Ule and 1800 for IUP-UB; IUP-UB has not performed the 900 additional snow/ice scenarios to better focus on other more relevant scenarios (initial results - which have been confirmed by ULe - showed that the performance is poor for snow/ice covered surfaces due to low reflectivity in the SWIR bands)), the methodologies of XCO_2 retrievals are not exactly similar and the criteria of filtering present some (small) differences. The post-processing filter has an

important impact on the number of analysed cases which are saved. This result is one of the arguments on the necessity to have robust ways for filtering scenes (in order to detect bad quality retrievals, see section 6.3.4, page 199). Note that one of the ULe criteria is to save the XCO_2 retrievals presenting a posteriori XCO2 error value less than 1.2 ppm. As a result, one should expect to have the mean XCO2 random error less than this requirement (this is confirmed by an average value of 1 ppm, after filtering).

- The scattering effects are clearly the main contributors of the high values obtained for the XCO_2 systematic errors (SSE of ~1.98 ppm for IUP-UB for all aerosol and cirrus scenario). This is confirmed by the ULe results with SSE = 1.86 ppm.
- Impact of meteorological parameters (such as temperature) and horizontally inhomogeneous scenes is small (SSE of 0.1 ppm temperature effects and 0.2 ppm for inhomogeneous scenes – IUP-UB and ULe). IUP-UB analysis has shown that the temperature related error is approx. 0.1 ppm per 10 K temperature error (assuming a temperature profile shift error in the troposphere, primarily in the boundary layer). This indicates that temperature profile related errors is much less important than most of the other error sources investigated in this study. Surface pressure errors are more critical as surface pressure is strongly constrained in the IUP-UB BESD retrieval algorithms, in the present study (assumed 1-sigma *a priori* uncertainty: ± 1 hPa). More studies are needed in order to determine if this strong constraint can be relaxed in the future. As discussed in [RD18], the typical accuracy of ECMWF data is about 2-3 hPa but likely higher at high latitudes and for complex topography. Therefore, [RD18] is using ± 4 hPa for GOSAT XCO_2 retrieval using the NASA/ACOS algorithm.
- By comparing the StdDev values of the XCO_2 systematic errors related to all the scattering scenarios, very good agreement are obtained between the expert groups (remark: StdDev values are more representative than average value, for the XCO_2 systematic errors as they represent absolute variations): 1.98 ppm (IUP-UB) and 1.86 ppm (ULe). This is a very good result, although some differences can be observed when looking in detail at specific scenarios. Thus, as XCO_2 systematic errors are the most critical variable for driving strong recommendations dedicated to S-5-UVNS CO_2 measurements, strong and well justified enhancements can be provided by analysing all these results (in the next sub-sections) and by confronting them with the XCO_2 "accuracy" user requirements (see section 2.5.5).
- Table 4-5 indicates also the number of XCO_2 retrievals which are successfull (i.e. they meet the criteria defined by each organism) and the percentage of these successful retrievals, with respect to the number of simulations containg the value of each geophysical parameter indicated in the columns of the table. As the software and the methodlogies of XCO_2 retrievals (*i.e.* input *a priori* variables, number of total simulations achieved) are rather different, these number can be compared between each partner only which great care. Moreover, although each expert has considered a filter for selecting and analysing only the success retrievals, the methodologies of filtering are not identical. But, these differences do not avoid to have consistent results which are already mentined above and which are described in detail in the following sections and in the chapter 5.

In summary, the results obtained by IUP-UB and ULe are consistent. Overall, the statistical results obtained from averaging over many scenes are in good agreement. For individual scenes however the results may be different as expected as both groups use different retrieval algorithms with different assumptions w.r.t. *a priori* information. The latter is however not considered to be relevant for this study.

Geophysical parameter considered (error source)	Values / Type	Number of scenes considered (*i.e.* successful XCO_2 retrievals)	Percentage of successful XCO_2 retrievals, compared to total number of scenes available for each geophysical parameter considered (%)	Partners results	Mean Random error ("Precision") (ppm)	Standard Deviation Random error ("Precision") (ppm)	Mean Systematic error ("Accuracy") (ppm)	Standard Deviation Systematic error ("Accuracy") (ppm)	Root Mean Square Systematic error ("ppm")
Overall summary	Scattering: All aerosol + Cirrus	616	34.2	IUP-UB	1.68	0.57	0.60	1.98	2.07
		346	12.8	ULe	1.00	0.12	0.31	1.86	-
	Root-Sum-Square	-	-	IUP-UB	-	-	-	2.0	-
		-	-	ULe	-	-	-	1.87	-
Aerosol-only	Continental clean (CC)	66	55	IUP-UB	1.41	0.57	0.10	1.11	1.11
		65	36.1	ULe	1.01	0.13	0.43	2.32	2.35
	Continental polluted (CP)	74	61.7	IUP-UB	1.43	0.58	-0.20	0.94	0.96
		64	35.6	ULe	1.02	0.14	0.97	0.96	1.37
	Desert (DE)	68	56.7	IUP-UB	1.37	0.58	2.35	2.42	3.36
		66	36.7	ULe	0.99	0.13	0.21	2.19	2.19
	AOT(550 nm): 0.1	42	46.7	IUP-UB	1.75	0.44	0.33	0.70	0.77
		90	66.7	ULe	1.01	0.13	0.14	1.58	1.57
	AOT(550 nm): 0.2	57	63.3	IUP-UB	1.56	0.55	1.04	1.52	1.83
		56	41.5	ULe	1.01	0.15	0.77	2.56	2.65
	AOT(550 nm): 0.3	83	92.2	IUP-UB	1.24	0.56	0.94	2.66	2.81
		42	31.1	ULe	0.98	0.13	0.75	1.34	1.52
	AOT(550 nm):	26	28.9	IUP-UB	1.02	0.46	0.02	1.35	1.33

Geophysical parameter considered (error source)	Values / Type	Number of scenes considered (*i.e.* successful XCO_2 retrievals)	Percentage of successful XCO_2 retrievals, compared to total number of scenes available for each geophysical parameter considered (%)	Partners results	Mean Random error ("Precision") (ppm)	Standard Deviation Random error ("Precision") (ppm)	Mean Systematic error ("Accuracy") (ppm)	Standard Deviation Systematic error ("Accuracy") (ppm)	Root Mean Square Systematic error ("ppm")
	0.6	7	5.2	ULe	1.03	0.10	2.37	2.62	3.39
Cirrus-only	COT: 0.01	28	93.3	IUP-UB	1.23	0.55	-0.04	1.30	1.23
		90	66.7	ULe	1.01	0.13	0.14	1.58	1.57
	COT: 0.05	29	96.7	IUP-UB	1.74	0.49	0.03	0.15	0.15
		52	38.5	ULe	0.99	0.11	-0.34	1.48	1.50
	COT: 0.1	12	40	IUP-UB	1.98	0.70	0.02	0.06	0.06
		14	10.4	ULe	1.01	0.10	-0.20	1.04	1.02
	COT: 0.2	0	0	IUP-UB	-	-	-	-	-
		0	0	ULe	-	-	-	-	-
	COT: 0.4	0	0	IUP-UB	-	-	-	-	-
		0	0	ULe	-	-	-	-	-
	CAT: 6 km	13	43.3	IUP-UB	1.10	0.39	0.17	0.96	0.94
		30	22.2	ULe	1.01	0.12	-0.37	1.26	1.29
	CAT: 8 km	14	46.7	IUP-UB	1.35	0.45	0.02	1.06	1.02
		25	18.5	ULe	1.01	0.13	-0.13	1.34	1.32
	CAT: 10 km	14	46.7	IUP-UB	1.64	0.54	0.09	1.04	1.00
		30	22.2	ULe	1.00	0.12	0.08	1.28	1.26
	CAT: 12 km	14	46.7	IUP-UB	1.90	0.69	-0.13	0.44	0.44

Geophysical parameter considered (error source)	Values / Type	Number of scenes considered (*i.e.* successful XCO_2 retrievals)	Percentage of successful XCO_2 retrievals, compared to total number of scenes available for each geophysical parameter considered (%)	Partners results	Mean Random error ("Precision") (ppm)	Standard Deviation Random error ("Precision") (ppm)	Mean Systematic error ("Accuracy") (ppm)	Standard Deviation Systematic error ("Accuracy") (ppm)	Root Mean Square Systematic error ("ppm")
		41	30.4	ULe	1.02	0.12	0.29	1.65	1.66
	CAT: 14 km	14	46.7	IUP-UB	1.86	0.66	-0.14	0.48	0.48
		30	22.2	ULe	0.98	0.12	-0.24	1.85	1.83
Solar Zenith Angle	25°	233	38.8	IUP-UB	1.50	0.42	0.76	1.55	1.73
		134	14.9	ULe	0.92	0.12	-0.45	1.19	1.27
	50°	217	36.2	IUP-UB	1.63	0.47	0.43	1.97	2.01
		134	14.9	ULe	1.00	0.09	-0.12	1.31	1.32
	75°	166	27.7	IUP-UB	1.99	0.72	0.61	2.46	2.53
		78	8.7	ULe	1.14	0.04	2.34	2.14	3.16
Albedo	Vegetation (VEG)	360	40	IUP-UB	1.92	0.50	0.33	1.98	2.01
		243	27	ULe	0.95	0.11	-0.56	1.70	1.83
	Sand/soil (SAS)	256	28.4	IUP-UB	1.35	0.49	0.9	1.92	2.15
		103	11.4	ULe	1.12	0.05	0.68	1.93	2.01
	Snow/ice (SIC)	-	-	IUP-UB	-	-		-	
		-	-	ULe	-	-		-	
Temperature profile	BL + FT	7	100	IUP-UB	-	-	-	0.10	-
	BL + FT	10	100	ULe	-	-		0.07	

Geophysical parameter considered (error source)	Values / Type	Number of scenes considered (*i.e.* successful XCO_2 retrievals)	Percentage of successful XCO_2 retrievals, compared to total number of scenes available for each geophysical parameter considered (%)	Partners results	Mean Random error ("Precision") (ppm)	Standard Deviation Random error ("Precision") (ppm)	Mean Systematic error ("Accuracy") (ppm)	Standard Deviation Systematic error ("Accuracy") (ppm)	Root Mean Square Systematic error ("ppm")
ILS pseudo-noise induced by horizontally heterogeneous scenes	ILS	5	100	IUP-UB	-	-	-	0.27 *)	-
	ILS	-	-	ULe	-	-		0.19 *)	

Table 4-5: Synthesize of the major results obtained by IUP-UB and ULe, related to the XCO_2 performances derived from the S-5-UVNS measurements (stand alone), as specified currently in [RD14]and [RD8]– These results are related to the scenarios saved after applying the filter of each expert – "-" means that no value is available.

*) Here the worst case assumption has been used that this error is entirely systematic. A more realistic assumption is probably that this error is mainly random. In this case it would only very slightly enhance the random error and would not contribute to the systematic error.

4.3.2. Specific analyses focused on the sources of scattering related XCO_2 systematic errors

Results analysed in the next sub-sections are focused on the different sources which impact the XCO_2 systematic errors.

4.3.2.1. Sensitivity to solar zenith angle

4.3.2.1.1 IUP-UB results

The IUP-UB analysis (see Figure 4-16) shows that the systematic XCO_2 retrieval error as a function of the SZA. SZA dependent bias can be observed only for specific regions: GLO and EUR. Depending on the geographical regions and SZA values, XCO_2 bias can vary between ~0 ppm up to 4 ppm (in Europe). Over the GLO region (but also over the regions, *e.g.* EUR), the XCO_2 bias values decrease (from 2 ppm to ~3 ppm) when SZAs values increase for SZAs below 75°. This is most likely due to a larger sensitivity to scattering related errors at larger observed air masses (the sensitivity to light path variations due to scattering increases with the length of the light path).

Often, however, there are less representative results for SZA 75° present as the data have been "automatically" removed using the BESD filtering scheme (233 scenarios saved for SZA = 25° and 166 for scenarios SZA = 75°). This aspect indicates that for extreme values for extreme values of SZA, it is not expected to have accurate XCO_2 products (derived from S-5-UVNS as well as for any other space-borne instrument). This last point is confirmed by the SSE values (from 1.55 ppm at SZA = 25° to 2.46 ppm at SZA = 75°) and RMSSE values (from 1.73 ppm at SZA = 25° to 2.53 ppm at SZA = 75°) (*cf.* Table 4-5). All the RMSE and SSE values exceed 1.7 ppm.

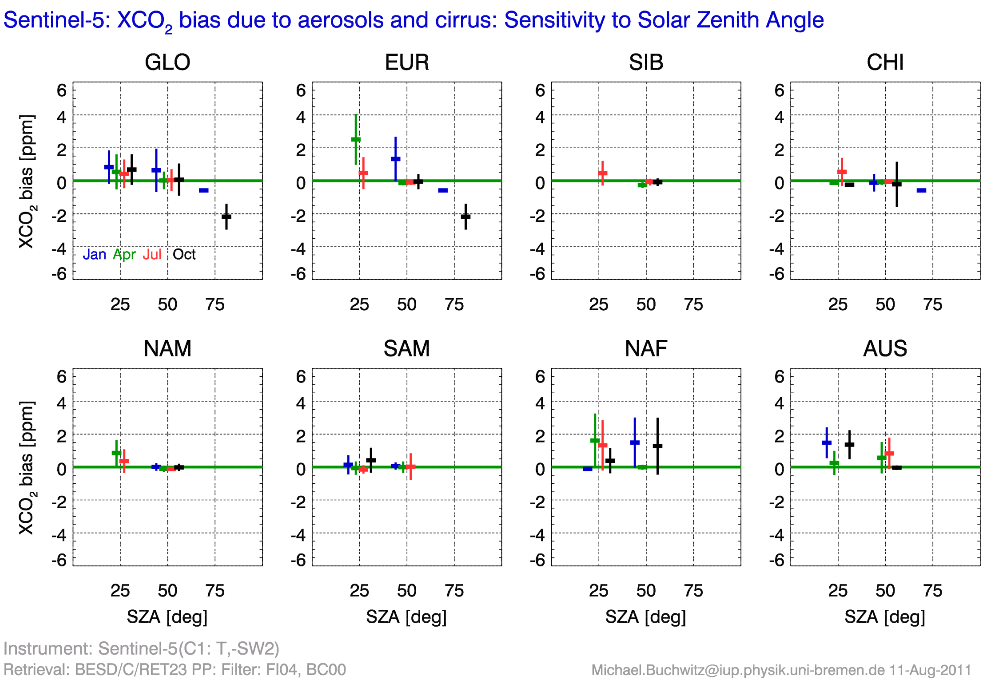

Figure 4-16: Dependence of the XCO_2 bias as obtained using IUP-UB's BESD algorithm as a function of the solar zenith angle (SZA) – Filtered scenarios - The peak-to-peak bias is given for 4 months analysed (January, April, July and October) with the overall bias, RMSE and the standard deviation (StdDev).

4.3.2.1.2 ULe results

The XCO_2 bias as a function of the solar zenith angle is shown in Figure 4-17 for all converged retrievals and for the filtered retrievals. A clear increase is observed in median bias and spread for SZA of 75° for the unfiltered and filtered results

Concerning the filtered results, SSE values increase from 1.19 ppm (SZA = 25°) to 2.14 ppm (SZA = 75°). The increase of SSE values, when SZA increasing as well, is also observed with IUP-UB results.

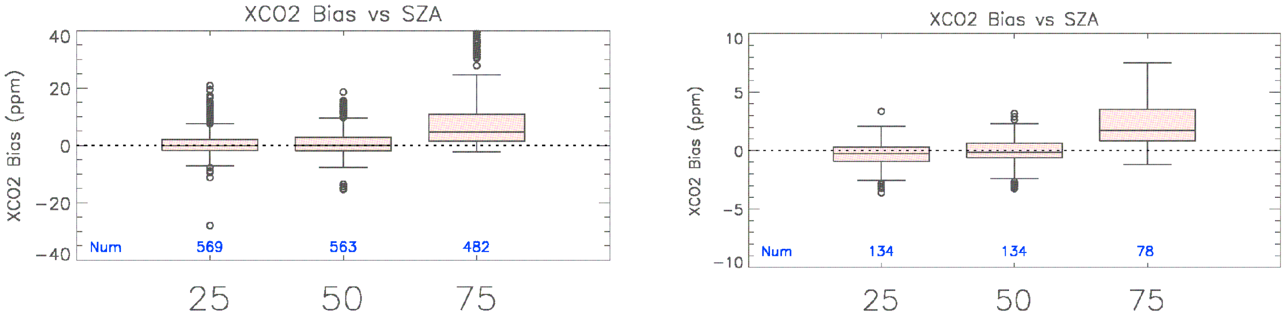

Figure 4-17: XCO_2 bias for different SZAs for the aerosol+cirrus simulations for all scenes (left) and the filtered scenes (right). The box encloses the interquartile range given by the difference between the third and first quartiles. The whiskers extend out to the maximum or minimum value of the data, or to the 1.5 times either the third and first quartiles. Outliers are identified with small circles. The centre line in the box gives the media value. The numbers at the bottom denote the number of data points for each SZA value.

4.3.2.2. Sensitivity to albedo

4.3.2.2.1 IUP-UB results

Figure 4-18 shows the systematic XCO_2 retrieval error as a function of surface albedo as obtained from the IUP-UB analysis. As can be seen, the mean bias as well as the scatter varies significantly depending on region. It appears that overall the errors are somewhat larger (average values between ~0.2 ppm and ~1.8 ppm). Whatever albedo scenario studied (SAS or VEG), SSE values (1.98 ppm for VEG and 1.92 ppm for SAS) and RMSSE values (2 ppm for VEG and 2.15 ppm for SAS) are high (close to 2 ppm) (*cf.* Table 4-5).

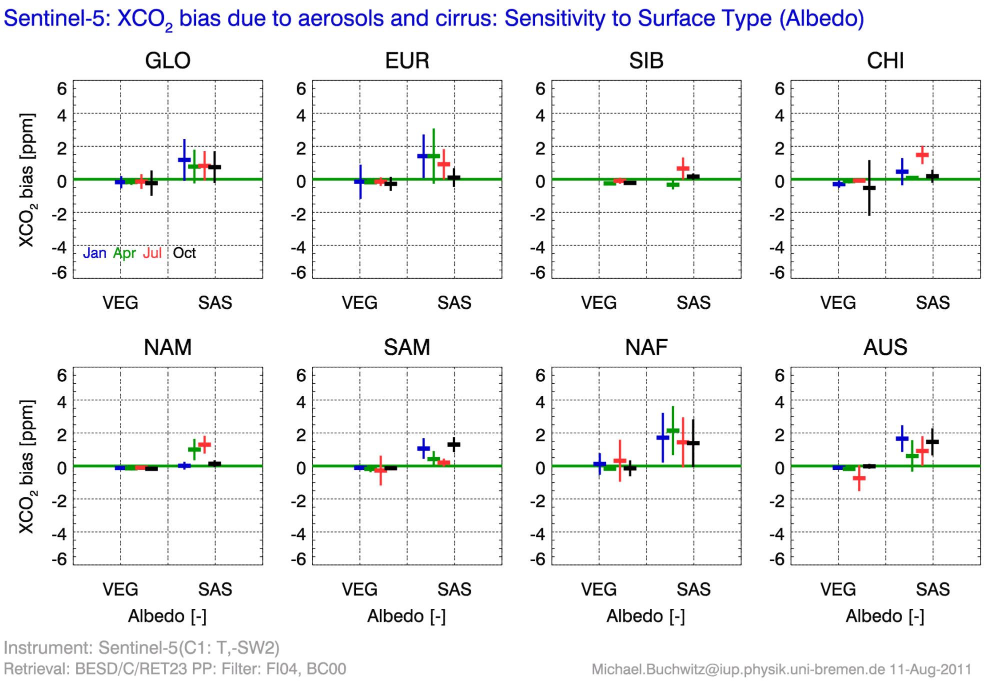

Figure 4-18: Dependence of the XCO_2 bias as obtained using IUP-UB's BESD algorithm as a function of the surface albedo for two types of surfaces: vegetation (VEG) and sand/soil (SAS) – Filtered scenarios - The peak-to-peak bias is given for 4 months analysed (January, April, July and October) with the overall bias, RMSE and the standard deviation (StdDev).

4.3.2.2.2 ULe results

The XCO_2 bias as a function of the surface type is shown in Figure 4-19 for all converged retrievals and for the filtered retrievals. For the unfiltered results, a clear increase in median bias and a spread are observed for the ice surfaces. The filter subsequently removes all the XCO_2 retrievals over ice which presented XCO_2 random errors whith high values. The individual retrievals as a function of retrieved albedo are shown in Figure 4-20.

Filtered retrievals show similar results than IUP-UB: SSE values vary between 1.94 ppm (SAS) and 1.70 ppm (VEG).

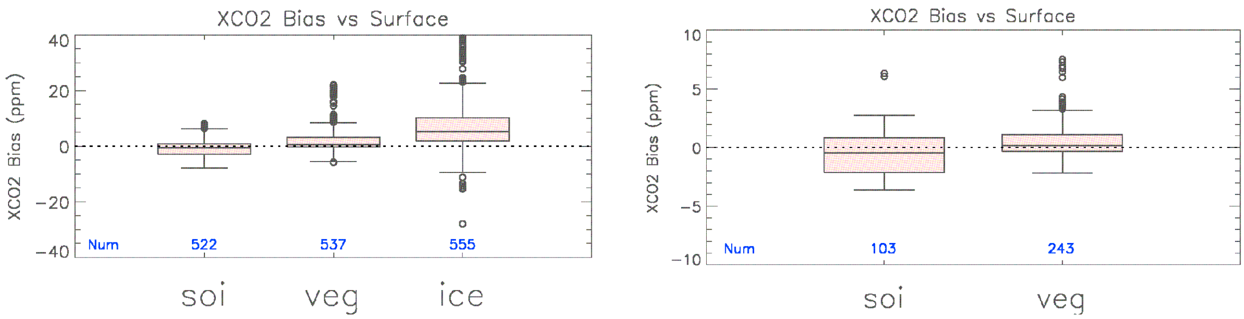

Figure 4-19: XCO_2 bias for different surface types (soil, vegetation and ice) for the aerosol+cirrus simulations for all scenes (left) and the filtered scenes (right). For details on the Box-Whisker plot see.

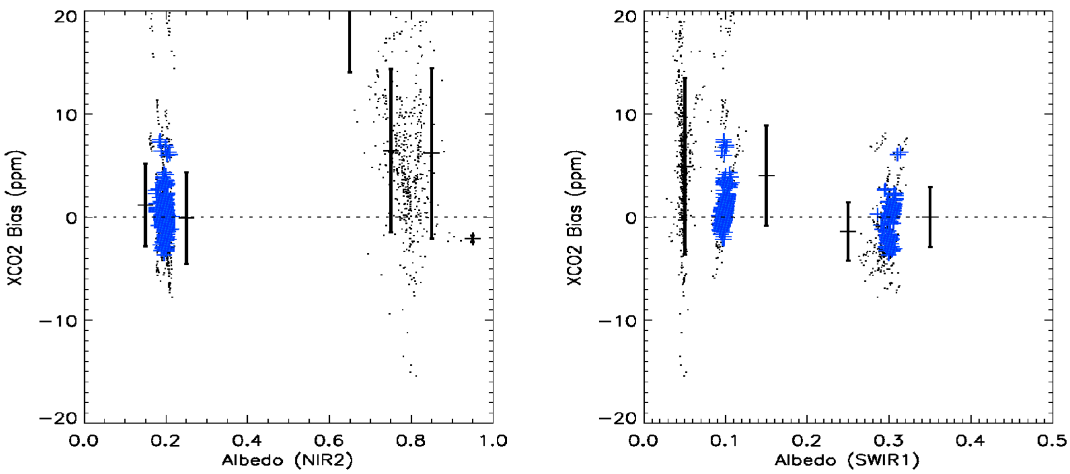

Figure 4-20: **XCO_2 bias as a function of surface albedo (albedo band 1: left; albedo band 2: right) for the aerosol+cirrus simulations. Black symbols give the results for all scenes and blue symbols for the filtered scenes. Also given is the mean value and StdDev for all scenes for a number of bins.**

4.3.2.3. Sensitivity to aerosol optical thickness

4.3.2.3.1 IUP-UB results

Figure 4-21 shows the systematic XCO_2 retrieval error as a function of AOT as obtained from the IUP-UB analysis for all regions. As can be seen, the dependency is rather complex. Whatever the geographical region considered, there is not a clear link between XCO_2 bias and AOT values.

However, SSE values and RMSE values are higher for AOT = 0.3 (SSE = 2.66 ppm and RMSE = 2.81 ppm) and lower for AOT = 0.1 (SSE = 0.70 ppm and RMSE = 0.77 ppm) (*cf.* Table 4-5). All the SSE and RMSE values exceed 0.7 ppm.

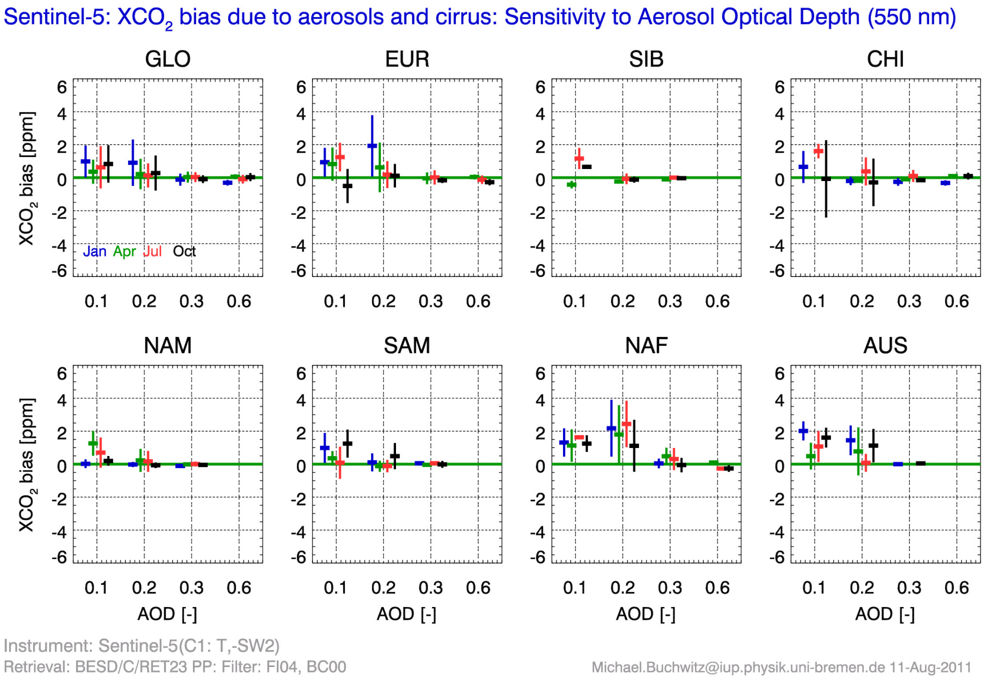

Figure 4-21: **Dependence of the XCO_2 bias as obtained using IUP-UB's BESD algorithm as a function of the AOD – Filtered scenarios - The peak-to-peak bias is given for 4 months analysed (January, April, July and October) with the overall bias, RMSE and the standard deviation (StdDev).**

4.3.2.3.2 ULe results

The XCO_2 bias as a function of the AOT is shown in Figure 4-22 for all converged retrievals and for the filtered retrievals. The increase in median bias and in spread with respect to AOT values is clearly visible for the unfiltered and filtered results. The filtered results shows significant variability between the different AOT values which the poorest results being found for AOT of 0.6. The individual retrievals as function of retrieved and true AOT values are shown in Figure 4-23.

For the filtered results, minimum SSE values (between 1.3 and 1.6 ppm) are obtained for AOT = 0.1 and AOT = 0.3 Maximum SSE values do not exceed 2.6 ppm. Note that Table 4-5 gives SSE values for different AOT values only by considering COT (Cirrus Optical Thickness) = 0.01. Then, these numbers are directly related to aerosols, and are not "biased" by the presence of cirrus.

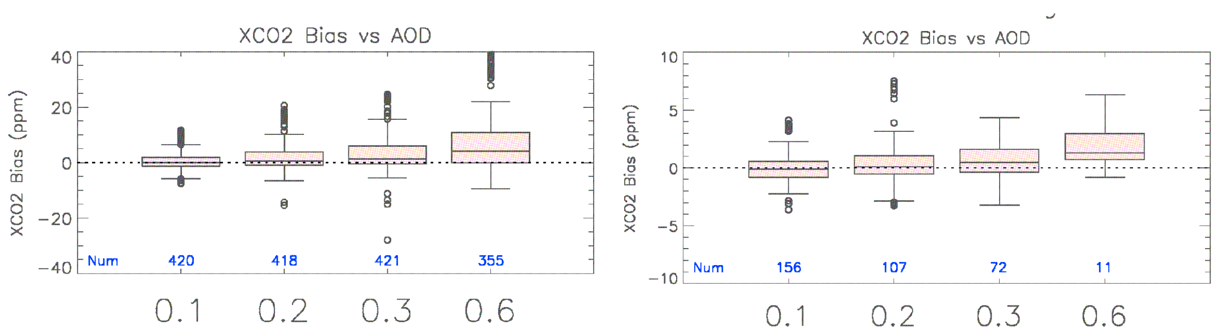

Figure 4-22: XCO_2 bias for different AODs for the aerosol+cirrus simulations for all scenes (left) and the filtered scenes (right).

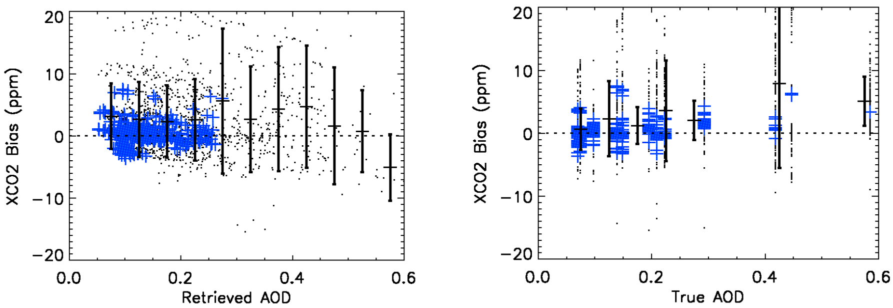

Figure 4-23: XCO_2 bias as a function of retrieved AOD (left) and true AOD (right) for the aerosol+cirrus simulations. Note that the true AOD corresponds to the AOD at 760 nm derived from the 550 nm values using the Angstrom coefficients for the 3 different aerosol types used in the simulations. Black symbols give the results for all scenes and blue symbols for the filtered scenes. Also the mean value and StdDev are given for all scenes for a number of bins.

4.3.2.4. Sensitivity to aerosol type

4.3.2.4.1 IUP-UB results

Figure 4-24 shows the systematic XCO_2 retrieval error as a function of aerosol type as obtained from the IUP-UB analysis for all regions. As can be seen, the dependency is rather complex but there is typically a high XCO_2 bias for the desert aerosol type (DE): values are very often between 2 and 4 ppm, while for the other aerosol types, values rarely exceed 2 ppm. This is confirmed by the SSE and RMSE values (SSE = 2.42 ppm and RMSE = 3.36 ppm) (*cf.* Table 4-5). Smaller values are obtained for the CP type (SSE = 0.94 ppm and RMSE = 0.96 ppm).

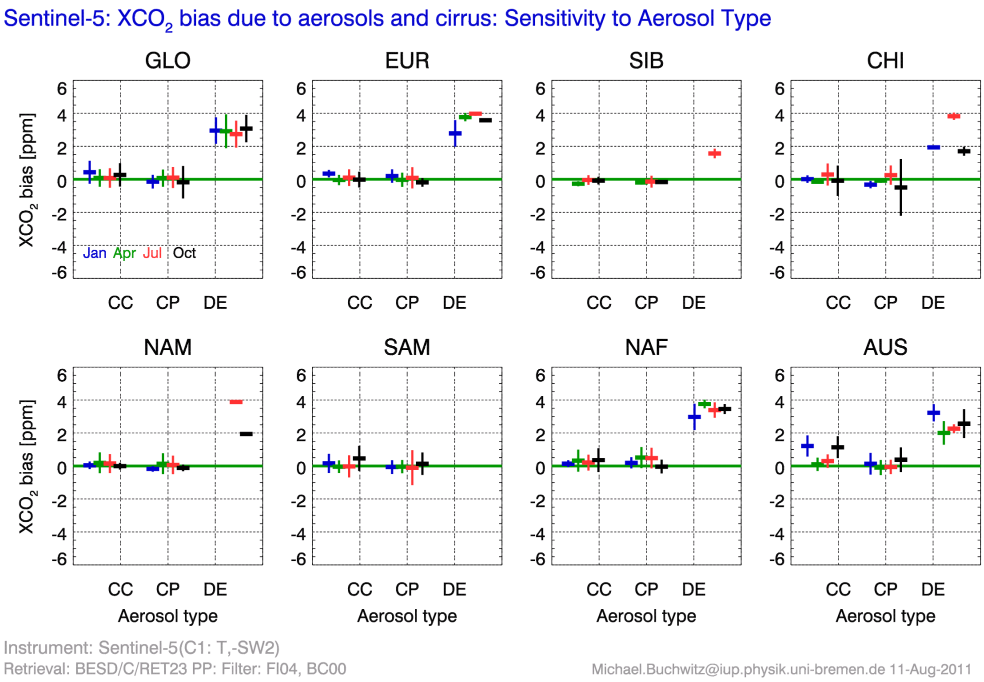

Figure 4-24: Dependence of the XCO_2 bias as obtained using IUP-UB's BESD algorithm as a function of the aerosol type – Filtered scenarios - The peak-to-peak bias is given for 4 months analysed (January, April, July and October) with the overall bias, RMSE and the standard deviation (StdDev).

4.3.2.4.2 ULe results

The XCO_2 bias as a function of the aerosol type is shown in Figure 4-25 for all converged retrievals and for the filtered retrievals. As for IUP-UB, the smallest spread is found for type 4c (*i.e.* CP aerosols) in the unfiltered results and filtered (SSE = 1.37 ppm). Maximum values are obtained for CC aerosols (SSE = 2.33 ppm).

The filtered results show a reduced sensitivity on type. However, note that if the results are also filtered for low COT (see tabulated results) then aerosol type 4c (CP) gives a much standard deviation as for the other two aerosol types.

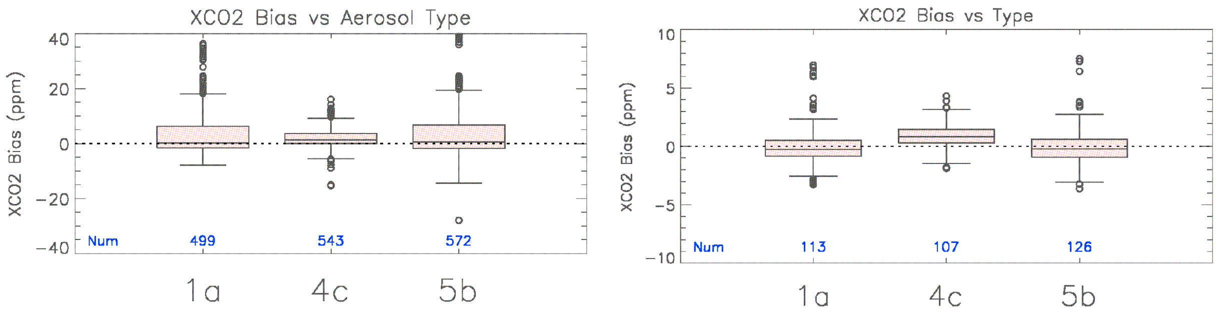

Figure 4-25: XCO_2 bias for different aerosol types for the aerosol+cirrus simulations for all scenes (left) and the filtered scenes (right) – 1a = CC aerosols, 4c = CP aerosols and 5b = Desert aerosols.

4.3.2.5. Sensitivity to cirrus optical thickness

4.3.2.5.1 IUP-UB results

Figure 4-26 shows the systematic XCO_2 retrieval error as a function of cirrus optical thickness (COT) as obtained from the IUP-UB analysis for all regions. As can be seen, the dependency is rather complex. Thus, whatever the geographical region considered, there is not a clear link between XCO_2 bias and COT values.

However, one can notice that after filtering out, no scenario with COT more than 0.2 is saved. This is due to the fact that XCO_2 retrievals did not meet the requirement of the filter. Higher SSE and RMSE values are obtained for COT = 0.01 (SSE = 1.3 ppm and RMSE = 1.27 ppm) (*cf.* Table 4-5). Minimal values are close to 0.06 ppm. If those measurements can be used only where cirrus COT value is below 0.2, this raises the question about the probability to meet COT below 0.2 in a given observation scene. This question cannot be answered without a detailed study using, *e.g.* CALIPSO data but Figure 3-1 suggests that cirrus with COT value larger than 0.2 frequently occurs, especially in the tropics and at high latitudes.

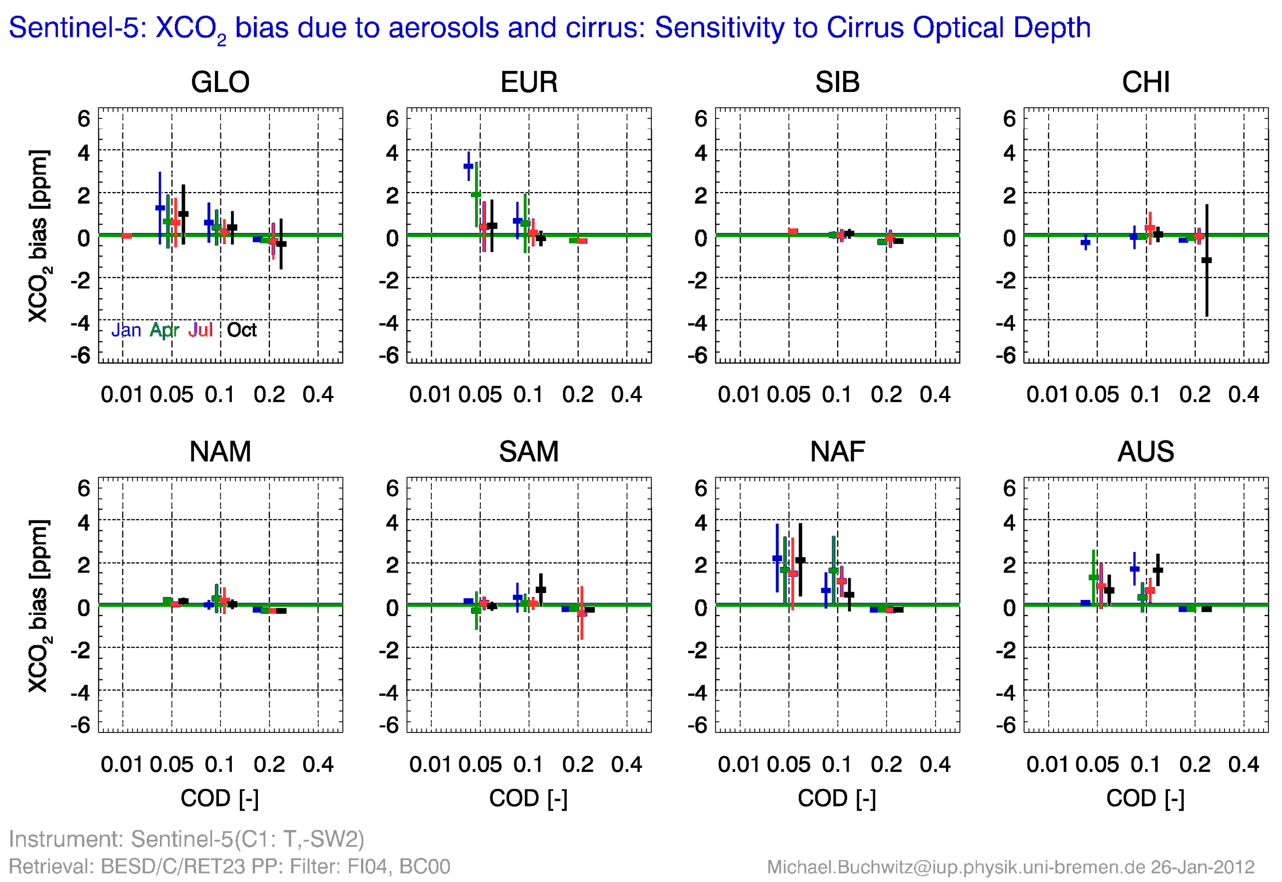

Figure 4-26: **Dependence of the XCO_2 bias as obtained using IUP-UB's BESD algorithm as a function of the cirrus optical depth – Filtered scenarios - The peak-to-peak bias is given for 4 months analysed (January, April, July and October) with the overall bias, RMSE and the standard deviation (StdDev).**

4.3.2.5.2 ULe results

The XCO_2 bias as a function of cirrus optical thickness is shown in Figure 4-27 for all converged retrievals and for the filtered retrievals. The unfiltered results for COT of 0.2 and 0.4 tend to deviate from those obtained for smaller COTs. However, at the same time, the number of data points is substantially decreased which might be the main cause for the observed differences. In the filtered case, there is a tendency for smaller spread with increased COT. Note that no retrieval with COT larger 0.2 passes the filter. The individual retrievals as a function of retrieved COT are shown in Figure 4-28.

Concerning the filtered retrievals, maximums SSE values (*i.e.* 1.58 ppm) are obtained for COT = 0.01 (as IUP-UB results). Minimum SSE values are close to 1 ppm.

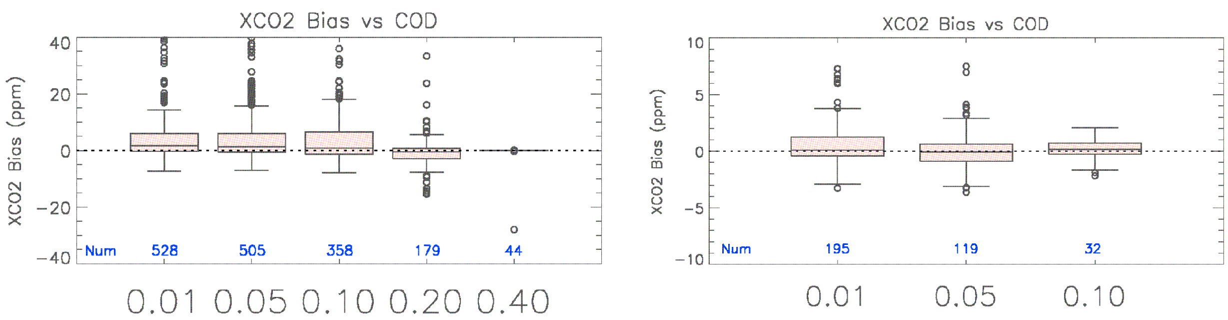

Figure 4-27: **XCO_2 bias for different COTs for the aerosol+cirrus simulations for all scenes (left) and the filtered scenes (right).**

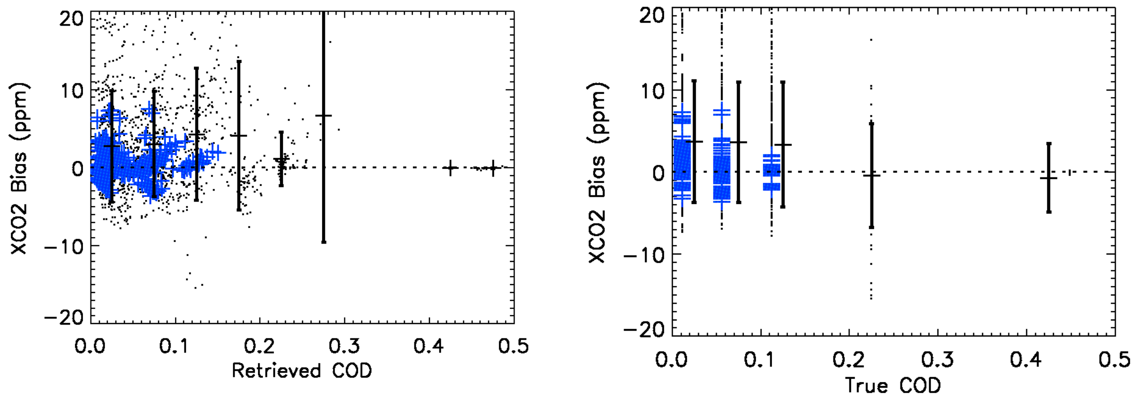

Figure 4-28: **XCO_2 bias as a function of retrieved COT (=COD, left) and true COT (=COD, right) for the aerosol+cirrus simulations. Black symbols give the results for all scenes and blue symbols for the filtered scenes. Also given is the mean value and StdDev for all scenes for a number of bins.**

4.3.2.6. Sensitivity to cirrus altitude

4.3.2.6.1 <u>IUP-UB results</u>

Figure 4-29 shows the systematic XCO_2 retrieval error as a function of cirrus altitude as obtained from the IUP-UB analysis for all regions. As can be seen, the dependency is rather complex. Thus, whatever the geographical region considered, there is not a clear link between XCO_2 bias and AOT values.

Higher SSE and RMSE values are obtained for a cirrus altitude of 6 km (SSE = 1.06 ppm and RMSE = 1.02 ppm). Minimal values are close to 0.94 ppm (*cf.* Table 4-5).

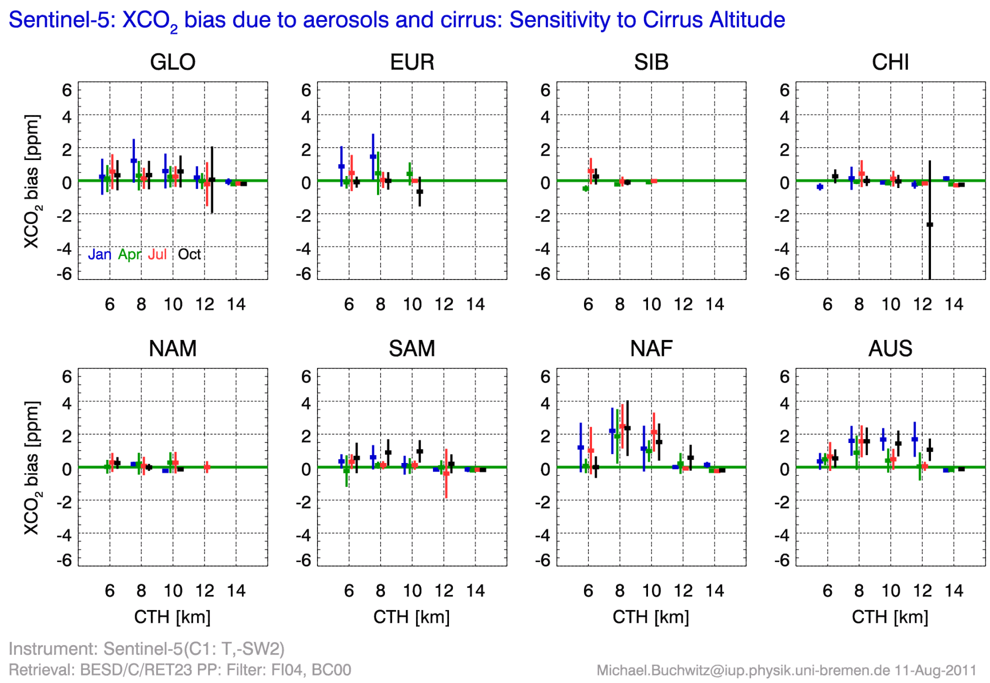

Figure 4-29: **Dependence of the XCO_2 bias as obtained using IUP-UB's BESD algorithm as a function of the cirrus altitude (CAL or CTH)– Filtered scenarios - The peak-to-peak bias is given for 4 months analysed (January, April, July and October) with the overall bias, RMSE and the standard deviation (StdDev).**

4.3.2.6.2 ULe results

The XCO_2 bias as a function of cirrus centre height is shown in Figure 4-30 for all converged retrievals and for the filtered retrievals. The unfiltered results show a clear tendency towards increased median biases and increased spread with increased height. The filtered results show much less dependency on the cirrus height with the exception of the results for 14 km which show much higher SSE value (1.85 ppm). Minimal SSE values are obtained for CAL=6 km (*i.e.* SSE = 1.26 ppm).

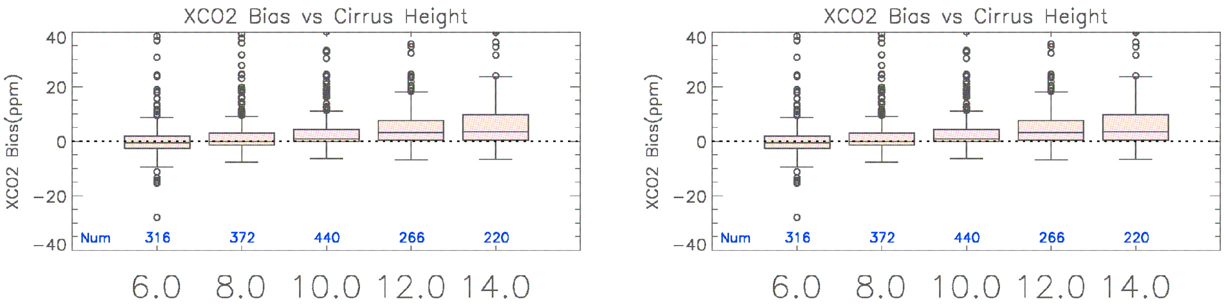

Figure 4-30: **XCO_2 bias for different cirrus heights for the aerosol+cirrus simulations for all scenes (left) and the filtered scenes (right).**

4.3.3. Specific analyses focused on the other sources of scattering related XCO_2 systematic errors

4.3.3.1. Sensitivity to temperature profile

4.3.3.1.1 IUP-UB results

The XCO_2 error due to a temperature profile error has been estimated by applying the BESD retrieval algorithm to simulated Sentinel-5-UVNS spectral measurements generated using different scenarios for temperature vertical profiles. BESD considers temperature variability by including a single state vector element for temperature profile variations. It has however not been attempted to obtain vertically resolved temperature information (to what extent this is possible has not yet been studied). Therefore, a temperature profile error typically results in an error of the retrieved XCO_2. This error has been estimated by perturbing the temperature profile in the boundary layer and in the free troposphere (here the error is assumed to be half of the boundary layer error).The results are shown in Figure 4-31. As can be seen**, the error is about 0.01 ppm per Kelvin (~0.002%/K), *i.e.* 0.1 ppm per 10 K boundary layer temperature error. Then, the XCO_2 systematic error associated with the temperature variations is not considered as important, with comparison to scattering effects.**

As XCO_2 is the driver for the present study, the question of the quality of the pressure surface retrieved from an incorrect T profile is of indirect importance (*i.e.* not relevant here). This question cannot be investigated as the algorithm is only optimized for "good" XCO_2 retrieval. An accurate surface pressure retrieval probably needs a somewhat different algorithm.

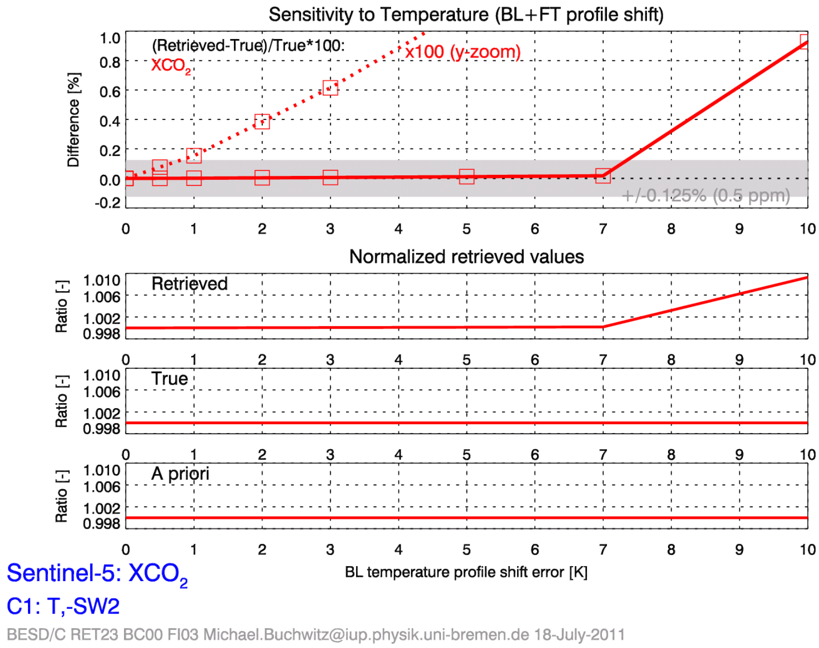

Figure 4-31: **Top panel: XCO_2 error due to a temperature vertical profile error in the Boundary Layer (BL, 0-2 km). A temperature error in the free troposphere (2-10 km) of half the BL error is also assumed. As can be seen, the error is about 0.002% (~0.01 ppm) per Kelvin temperature error if the temperature error is less than about 7 K. For larger temperature errors, there is a jump in the XCO_2 error due to the relatively coarse look-up-table (LUT) grid used for retrieval in this study. Three bottom panels: Corresponding retrieved, true and *a priori* XCO_2 (normalized to the corresponding value at zero temperature error).**

4.3.3.1.2 ULe results

The sensitivity to the temperature profile has been investigated by applying a perturbation to the *a priori* temperature profile used for the retrieval. Otherwise, all *a priori* values (including aerosol and cirrus) are identical to truth. The *a priori* profile between 0 and 2 km altitude has been offset by a temperature shift between 1 and 10 K and the *a priori* profile between 2 km and the tropopause has been offset by half of the applied offset. The temperature in the stratosphere has been left unchanged.

The characteristics of the bias seem to depend primarily on the total amount of cirrus and larger biases are found when the cirrus amount is small. **For small COT values, the biases are up to 0.2 ppm for a 10K shift which will make a noticeable contribution to the error budget** (*cf.* Figure 4-32). Note that the uncertainty in the *a priori* temperature profile taken from meteorological analysis should be mostly random on larger scales and thus this will mostly contribute to the random error budget, but some small regional systematic effects are well possible.

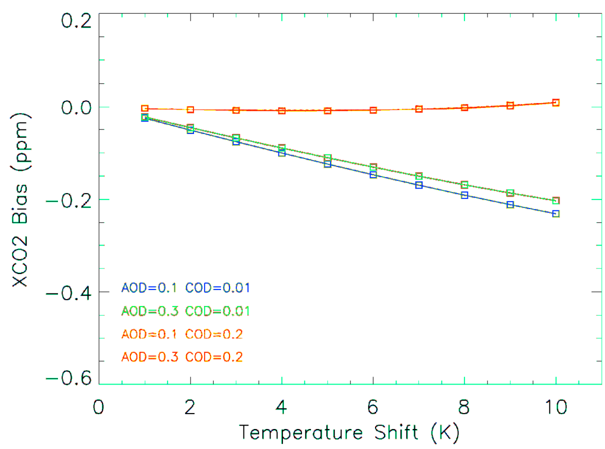

Figure 4-32: XCO_2 bias as a function of temperature offset for 4 geophysical scenarios.

For filtered retrievals, IUP-UB and ULe obtain similar SSE values (*i.e.* 0.1 ppm for IUP-UB and 0.07 ppm for ULe).

4.3.3.2. Sensitivity to surface pressure

4.3.3.2.1 IUP-UB results

The error due to a surface pressure variation has been estimated by applying the BESD retrieval algorithm to simulated Sentinel-5-UVNS spectral measurements generated using different scenarios for pressure vertical profiles. The results are shown in Figure 4-33.

As can be seen, the XCO_2 error depends strongly on the assumed *a priori* uncertainty of the retrieved surface pressure. **The XCO_2 error depends nearly linearly on the surface pressure error** (similar as the retrieved CO_2 column, not shown) and reaches for the default retrieval **1 ppm for a surface pressure error of 2 hPa**. In relative (percentage) terms, the XCO_2 error equals the CO_2 column error (not shown), whereas the error of the retrieved surface pressure is much smaller (for the default retrieval). This is because the surface pressure is strongly constrained for the default retrieval: the assumed *a priori* uncertainty is ±0.1% (1-sigma). This high sensitivity of the BESD retrieved XCO_2 on surface pressure errors need to be studied in more detail. As has been shown in this study, the sensitivity can be significantly reduced by relaxing the *a priori* constraint on surface pressure but it has not been investigated to what extent this adversely affects the errors caused by aerosols and clouds. As discussed [RD18], the typical accuracy of ECMWF data is about 2-3 hPa but likely higher at high latitudes and for complex topography. Therefore, [RD18] is using ± 4 hPa for GOSAT XCO_2 retrieval using the NASA/ACOS algorithm. It has to be investigated if a relaxed surface pressure constraint can also be used in BESD in the future.

It is however likely that this error can be significantly reduced by optimizing the retrieval algorithm as indicated by the results of the 2nd retrieval shown in Figure 4-33: the uncertainty has been relaxed to ±0.7%. As can be seen, the XCO_2 error is much smaller in this case and even changes its slope (pretty **close to 0.1 ppm for a surface pressure error of 1 hPa**).

It has to be noticed that IUP and ULe do nearly the same thing, namely assuming for the retrieval that CC in primarily in the boundary layer.

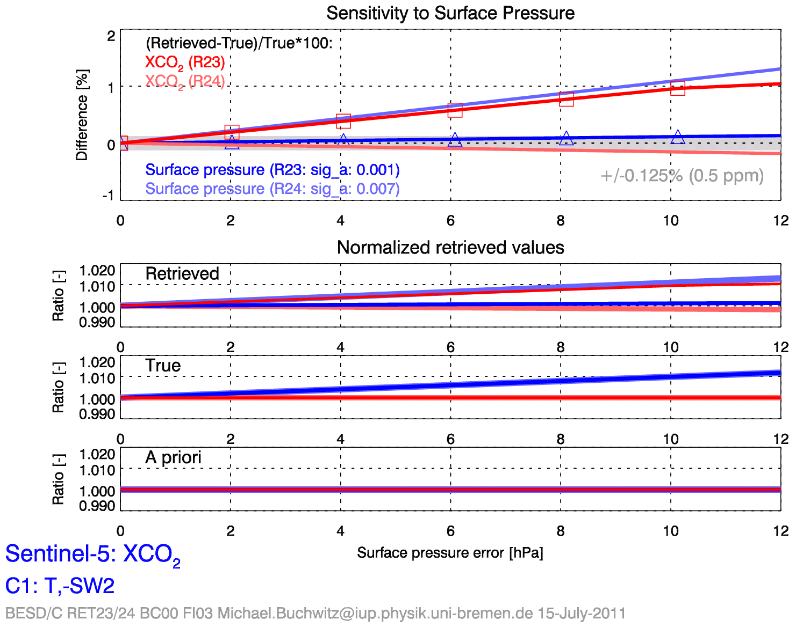

Figure 4-33: Top panel: XCO_2 error due to surface pressure error (red: default retrieval, light red: 2nd retrieval performed for sensitivity purposes). Also shown is the retrieved surface pressure (blue: default retrieval; light blue: 2nd retrieval). The retrieved XCO_2 is essentially the ratio of CO_2 vertical column and surface pressure. The 2nd retrieval is illustrated by light blue and light red. The three bottom panels show separately the curves for the retrieved, true and *a priori* quantities (using the same colour as has been used for the top panel).

4.3.3.2.2 ULe results

The sensitivity to the surface pressure has been investigated by applying perturbation *a priori* surface pressure used for the retrieval a large range of values ranging from 1 and 10 hPa. The retrieval of ULe uses a a priori uncertainty of 4hPa whereas the results of IUP-UB (see section 4.3.3.2.1) use 0.1% and 0.7%. The results presented here are quantitatively a little different but the same key messages are delivered. It has to be reminded that ULe algorithm assumes 0-2 km CC aerosol in all their retrievals, which then introduces biases if the type is different.

XCO_2 biases related to the surface pressure a priori value are only significant for relatively large shifts of the surface pressure a priori value (*cf.* Figure 4-34). **XCO_2 biases are very small (XCO_2 biases smaller than 0.1 ppm) for surface pressure biases within the expected accuracy of 2-3 hPa of ECMWF data.** For small values of COT, the inferred XCO_2 biases remain small even for larger surface pressure shifts. In contrast, it is found that for COT of 0.2 the XCO_2 biases can be significant with values exceeding 0.5 ppm for large values of the applied surface pressure shift.

The discontinuity in the XCO_2 bias for surface pressure shifts of 6 and 7hPa correlates with similar discontinuity in the retrieved surface pressure bias. In this case (with a large difference between *a priori* and true surface pressure), a very different solution can better minimize the cost-function of the iterative retrieval. As for temperature, it is expected that the surface pressure errors from meteorology analysis on small scales will be mostly random but there will be some regional effects due to the militated accuracy of NWP models. Since surface pressure is a retrieved parameter (*cf.* Figure 4-35), the surface pressure interference error (i.e. the effect of the smoothing error in surface pressure on the XCO_2 error) is automatically included in the *a posteriori* XCO_2 error assuming a random distribution of surface pressure uncertainties according to the *a priori* covariance matrix.

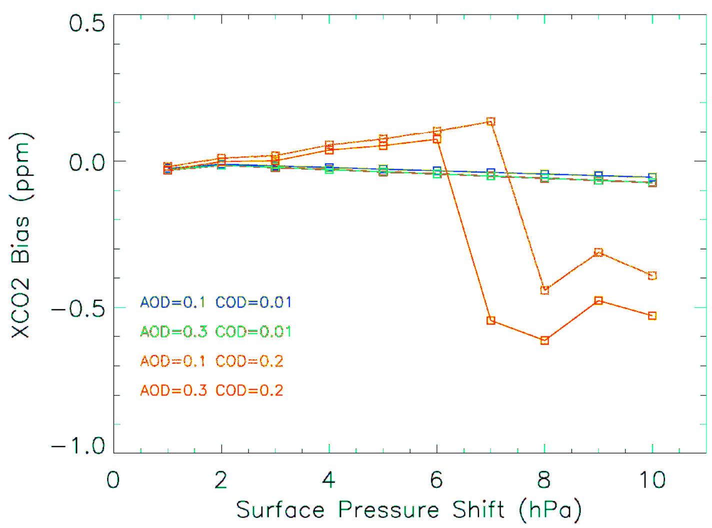

Figure 4-34: XCO_2 bias as a function of surface pressure offset for 4 geophysical scenarios.

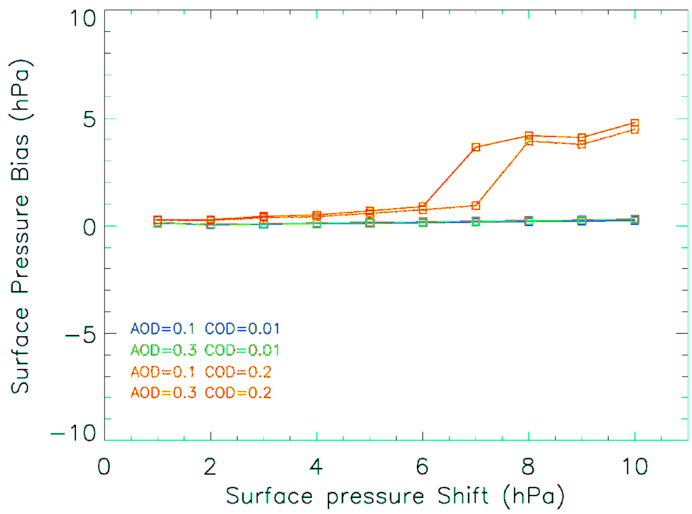

Figure 4-35: Surface pressure bias as a function of surface pressure offset for 4 geophysical scenarios.

4.3.3.3. Sensitivity to H_2O profile (ULe results)

The sensitivity to the H_2O profile has been investigated by ULe only, by applying a perturbation to the *a priori* H_2O profile used for the retrieval. Otherwise, all *a priori* values (including aerosol and cirrus) are identical to truth. The *a priori* profile between 0 and 2 km altitude has been increased by a factor between 10 and 100% and the *a priori* profile between 2 km and the tropopause has been increased by half of the applied factor. The H_2O profile in the stratosphere has been left unchanged. **Overall, the observed values for the XCO_2 bias are small (less than 0.04 ppm, *cf.* Figure 4-36) and they will not make a significant contribution to the overall error budget.**

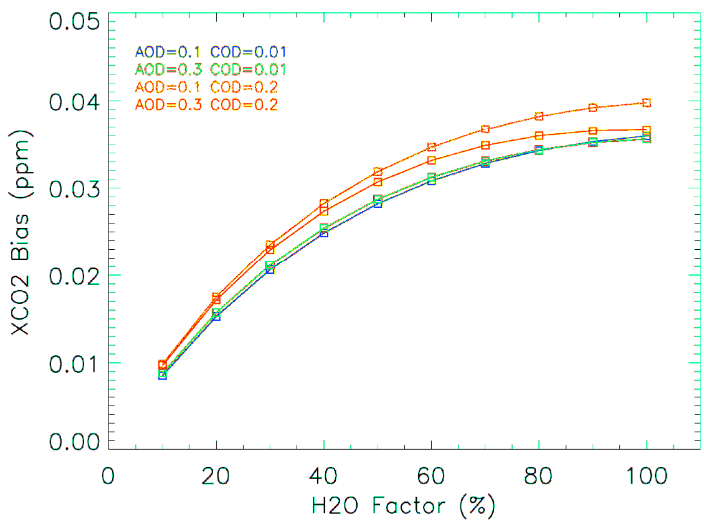

Figure 4-36: XCO_2 bias as a function of the H_2O factor applied to the *a priori* profile for 4 geophysical scenarios

4.3.3.4. Sensitivity to CO_2 profile (ULe results)

The sensitivity to the CO_2 profile has been investigated by applying a perturbation to the *a priori* CO_2 profile used for the retrieval. Otherwise, all *a priori* values (including aerosol and cirrus) are identical to the truth. The *a priori* profile between 0 and 2 km altitude has been offset by a CO_2 shift between 1 and 10 ppm and the *a priori* profile between 2 km and the tropopause has been offset by half of the applied offset. The CO_2 profile in the stratosphere has been left unchanged.

Figure 4-37 shows that values can reach 0.2 ppm and a relatively weak dependence on the aerosol and cirrus load. Since the CO_2 profile is retrieved, the smoothing error is automatically included in the *a posteriori* XCO_2 error assuming a random distribution of CO_2 uncertainties according to the *a priori* covariance matrix.

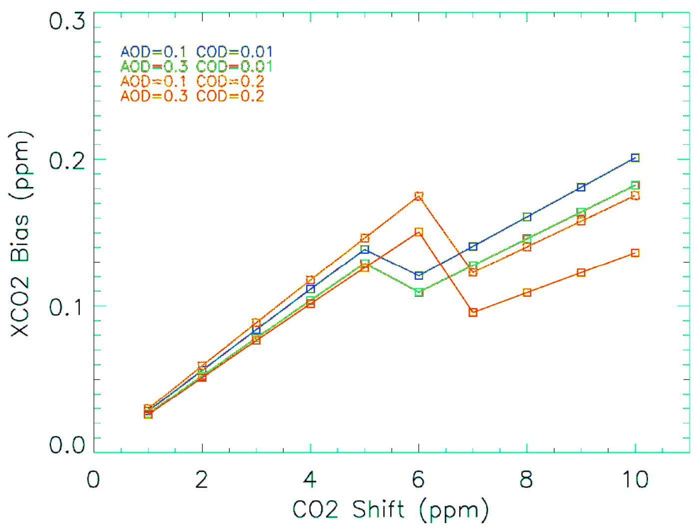

Figure 4-37: XCO_2 bias as a function of the CO_2 shift for 4 geophysical scenarios

4.3.3.5. Sensitivity to aerosol altitude

4.3.3.5.1 <u>IUP-UB results</u>

The systematic error due to aerosol altitude and layer thickness has been estimated by applying the BESD retrieval algorithm to simulated Sentinel-5-UVNS spectral measurements generated using different scenarios. The aerosol has been stretched and shifted in altitude but the total AOD (at 550 nm) has been kept constant (0.3).

Figure 4-38 shows the corresponding results for the aerosol type Continental Clean (CC). As can be seen, **the XCO_2 error may be as large as 0.5 ppm**. To what extent this error can be reduced by improving the retrieval algorithm cannot be estimated without further study.

Figure 4-39 and Figure 4-40 show the corresponding results for the Continental Polluted (CP) and Desert (DE) aerosol types. Also for these aerosol types, the error can reach 0.5 ppm.

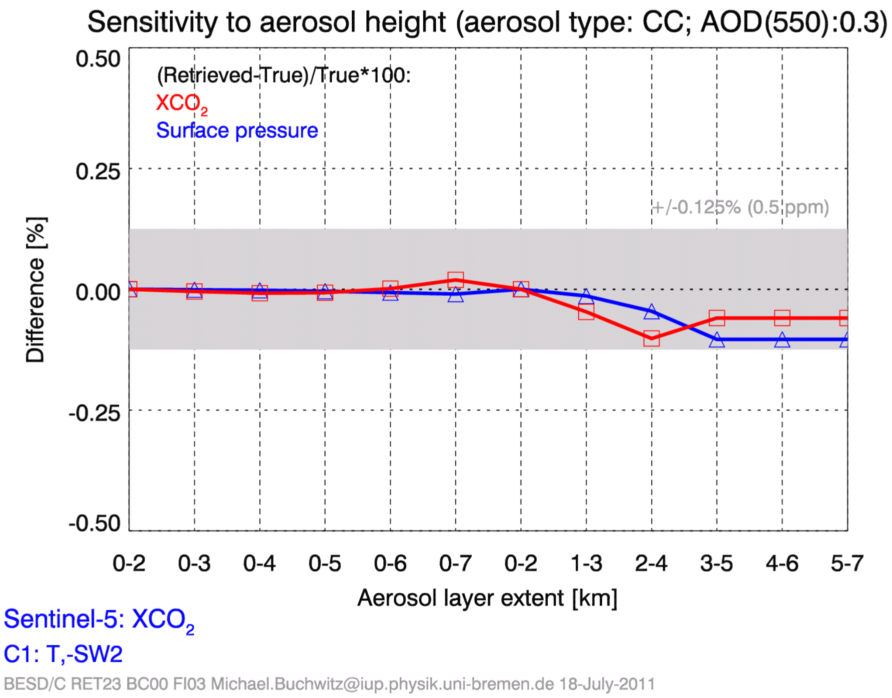

Figure 4-38: XCO_2 **error for different aerosol layer vertical extents. Note that the error is zero for the height range 0-2 km (left) as this is the height range assumed by the retrieval algorithm.**

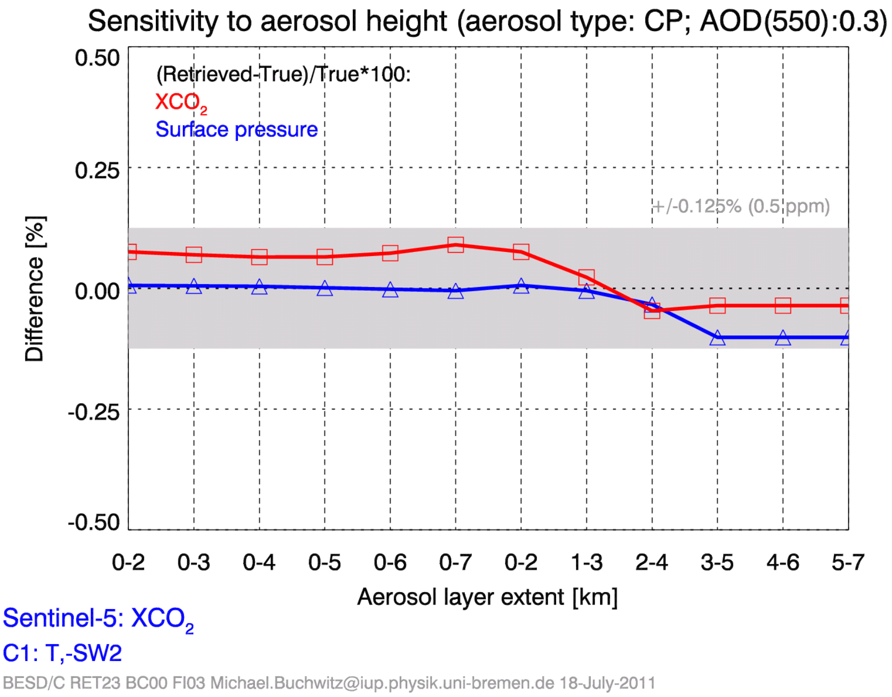

Figure 4-39: **As Figure 4-38 but for the aerosol type CP.**

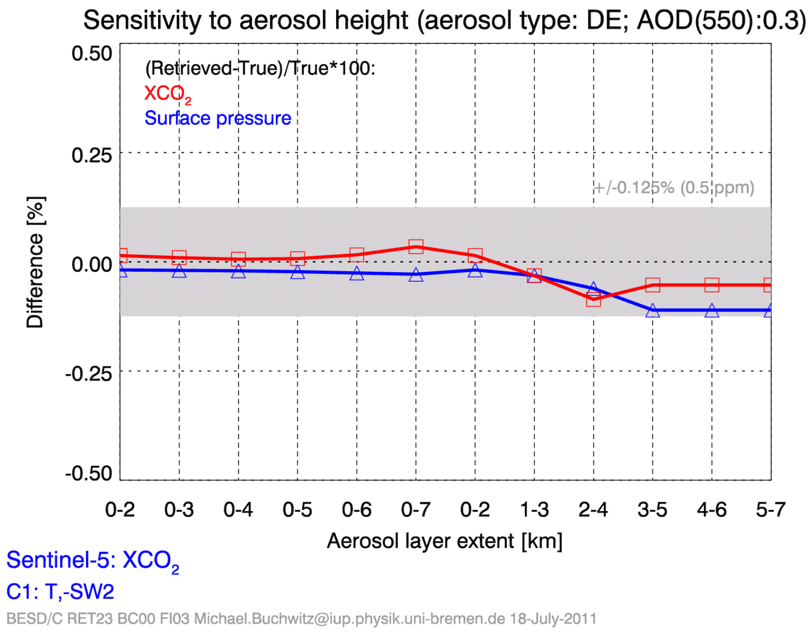

Figure 4-40: **As Figure 4-38 but for the aerosol type DE.**

4.3.3.5.2 ULe results

The sensitivity to the profile shape of the aerosol *a priori* profile has been investigated by changes to the aerosol layer HWHM (Half Width Half Maximum) or aerosol profile centre height. The simulations include the same aerosol profile as in the standard setup with a boundary layer and a free tropospheric contribution. The simulations also include cirrus clouds of varying COD with the same setup as the standard simulations. The aerosol type in the simulations and the retrievals is the same (2b). The standard retrieval uses a Gaussian-shaped profile with a centre height at 2 km and a HWHM (Half Width Half Maximum) of 2 km for an AOT of 0.15 which is perturbed to represent a centre height between 1 and 5 km. For a centre height of X, the HWHM (Half Width Half Maximum) has been varied between 1 and 5 km. The retrieval also includes a cirrus cloud according to the standard retrieval setup (which is different to the simulations). The XCO_2 bias is now given relative to the standard setup with a height and width of 2 km.

In Figure 4-41, the XCO_2 biases show a **clear dependence on the assumed layer centre height for conditions with low cirrus COT and can be as large as 1 ppm. For large COTs the XCO_2 biases show little dependence on the height of the aerosol profile** due to the reduced impact of aerosol itself on the spectrum. XCO_2 **biases introduced by the HWHM of the *a priori* aerosol (*cf.* Figure 4-42) profile show a significant dependence on the layer thickness (between 0.5 ppm for a height of 1 km and almost 1 ppm for a height of 5 km)** for all 4 geophysical scenarios.

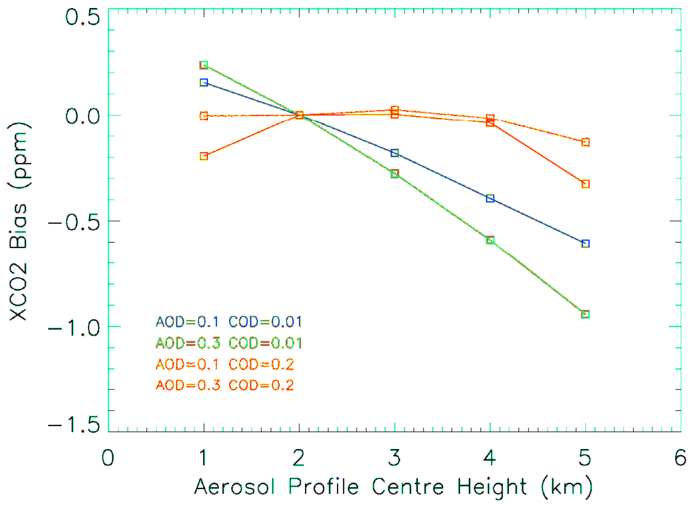

Figure 4-41: XCO_2 bias (relative to a 2 km centre height) as a function of the *a priori* aerosol profile centre height for 4 geophysical scenarios and cirrus COD

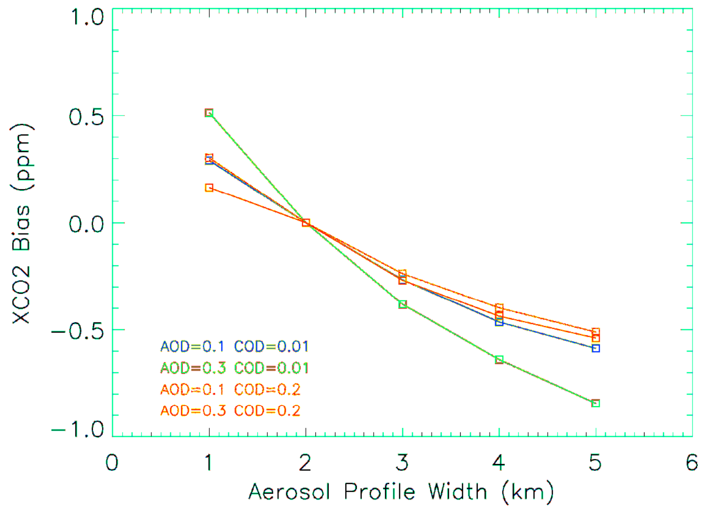

Figure 4-42: XCO_2 bias (relative to a 2 km HWHM) as a function of the *a priori* aerosol profile HWHM for 4 geophysical scenarios and cirrus COD

4.3.3.6. Sensitivity to ILS pseudo-noise induced by horizontally heterogeneous scenes

4.3.3.6.1 Generation of the IRSF by NOVELTIS

NOVELTIS has set up a Spectral Response Function (SRF) Model during previous activity in parallel to late phase B1 of Sentinel-4, reused later on within the Sentinel-4 science study (final presentation in March 2011 [RD11]).

Further reuse of this model was possible to generate Spectral Response Functions for sub-sample across the slit, which allows simulating the impact of across-slit scene heterogeneity. Iterations with ESA have been performed for validating assumptions, some instrumental parameters in Table 4-1 and some input elements related to the Point Spread Function (PSF): notably, the spectral oversampling factor are 3.0 for the NIR-2 channels and 2.5 for the SWIR channels.

Sub-samples in object space are defined along-track samples of width 500 m (at nadir) averaged over the across-track dimension. They are numbered consecutively from 1 to 50 centred on the nominal along-track centre of the FOV, Sub-samples 1 and 50 are centred 12.25 km behind/in front of the centre.

Due to the assumption of Gaussian PSF shape, the total SRF is symmetric with respect to its barycentre (*cf.* Figure 4-45 and Figure 4-46.).

Notes:

1) The sub-sample SRF are normalised to the integrated energy in each sub-sample, see Figure 4-47.
2) Motion smear is much larger than the slit width, in particular in NIR-2. The SRF is therefore identical for a considerable number of central sub-samples (samples 21-30 in NIR-2, samples 23-28 in SWIR-1/2).
3) According to the input assumptions, the SRFs are strictly identical in SWIR-1 and SWIR-2, except for a scaling factor 2 of the spectral axis. SWIR-2 simulations are not analyzed in this TN.
4) In case of a future modification of the SWIR-1 spectral resolution (*e.g.* from 0.25 nm (goal) to 0.35 nm (threshold)), it is convenient to apply the corresponding scaling factor to the computed SRFs, recomputation of the SRFs is not required as long as the PSF and slit size hypotheses do not change.

The five reference scenes, named W1-W5 (see Figure 4-44) for the study of the impact of scene heterogeneity were selected from a data set of 400 MODIS scenes which have been analyzed (by NOVELTIS) in the Sentinel-4-UVN pseudo-noise assessment as a part of the study: Support to the Consolidation of Instrument Requirements for Future Earth Observation Missions (ESA CONTRACT No 21823/08/NL/FF) [RD33]. The selection was meant to cover a variety of realistic cases. For the parameterization of the cases, two quantities as defined in that study were used as a proxy: barycentre shift of the resulting ISRF and scene contrast (reflectance gradient). In addition, one "extreme case" has been considered. All the selected scenes, used in the present study, are identical for both of the SWIR channels, SWIR-1 and SWIR-3, although the relative weight differs [RD33]. They are characterized as follows:

- Inhomogeneous Scene 1 (IH1, using weights W1): minimal barycentre shift, high contrast;
- Inhomogeneous Scene 2 (IH2 using W2): minimal barycentre shift, low contrast;
- Inhomogeneous Scene 3 (IH3 using W3): moderate barycentre shift, high contrast;
- Inhomogeneous Scene 4 (IH4 using W4): moderate barycentre shift, low contrast;
- Inhomogeneous Scene 5 (IH5, using W5): extreme barycentre shift, high contrast;
- "Extreme case" EX1 has been defined using a step-function scene weight as also shown in Figure 4-44.

4.3.3.6.2 IUP-UB results

IUP-UB has estimated the XCO_2 retrieval error by applying the BESD retrieval algorithm to simulated Sentinel-5-UVNS spectra generated using Instrument Line Shape Functions (ILS) generated for a homogeneous scene, on one hand, and for six inhomogeneous scenes, on the other hand. For the retrieval, the ILS related to a homogeneous scene is always used whereas for the simulated spectra the specific ILS for inhomogeneous scenes are used. The systematic ILS error results in a systematic XCO_2 error which has been quantified.

The various ILS have been generated using the input data provided by NOVELTIS. They are illustrated in Figure 4-43, Figure 4-44, Figure 4-45 and Figure 4-46.The resulting ILS are shown in Figure 4-48 and Figure 4-49.

The XCO_2 error for the six inhomogeneous scenes is shown in Figure 4-50. The results shown are valid for the VEG50 scenario (vegetation albedo, SZA = 50°, no errors due to clouds and aerosols). As can be seen, **the XCO_2 error typically can reach 0.3 ppm (or even 0.8 ppm for the extreme case EX1) if no correction algorithm is used**. Switching on the spectral "shift & squeeze" algorithm or only the "shift" algorithm implemented in BESD reduces the error to some extent As shown in Figure 4-50, the standard deviation of the XCO_2 error for the five (less extreme) inhomogeneous scenarios IH1-IH5 is 0.27 ppm. It is therefore concluded that the error caused by ILS variations due to inhomogeneous slit illumination is typically 0.3 ppm. The results also indicate that (although the ILS errors are not symmetric), a spectral shift algorithm helps to reduce the error considerably. Indeed, as shown in Figure 4-50, the error is typically 0. 75 ppm and is reduced to 0.27 ppm if the correction algorithms are considered.

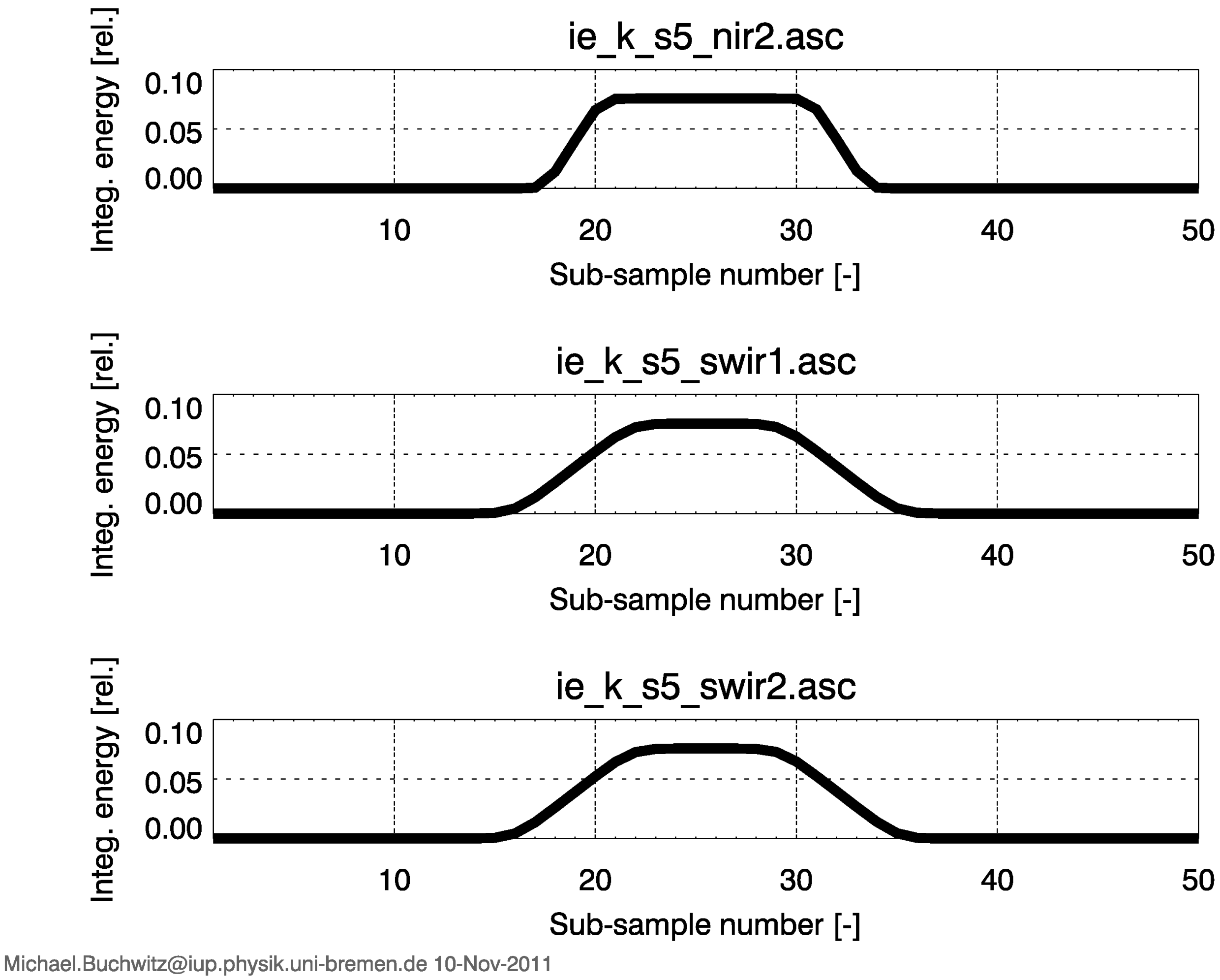

Figure 4-43: Assumed Sentinel-5 integrated energies for 50 (along track) spatial sub-samples – defining along track weights for obtaining the ILS - for the three spectral bands NIR2 (top), SWIR-1 (middle) and SWIR-2 (bottom). Note that SWIR-2 has not been used for the results shown in this section.

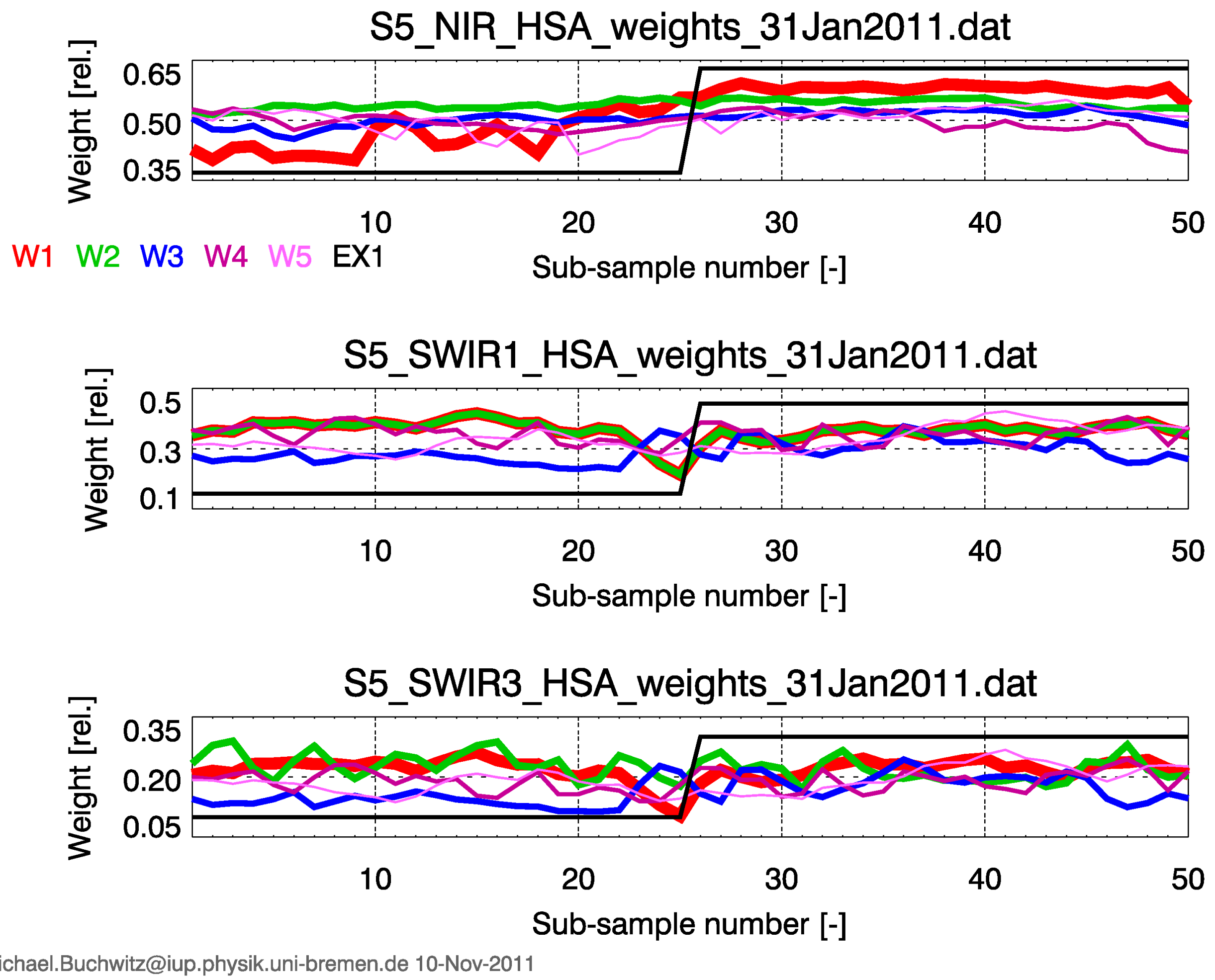

Figure 4-44: Sub-sample along track scene weights (obtained from high resolution MODIS data by KNMI) for six different inhomogeneous scenes (W1-W5) (different colours) plus the "extreme case" EX1 (black). IUP-UB has used, in this study, there scene weights to generate perturbed ILS for one VEG50 scenario only (=surface type vegetation, SZA = 50°, no error due to clouds and aerosol, *i.e.* for one of the 300 VEG50 scenarios) analyzed in this study. Note that only NIR (top) and SWIR-1 (middle) has been used for this study.

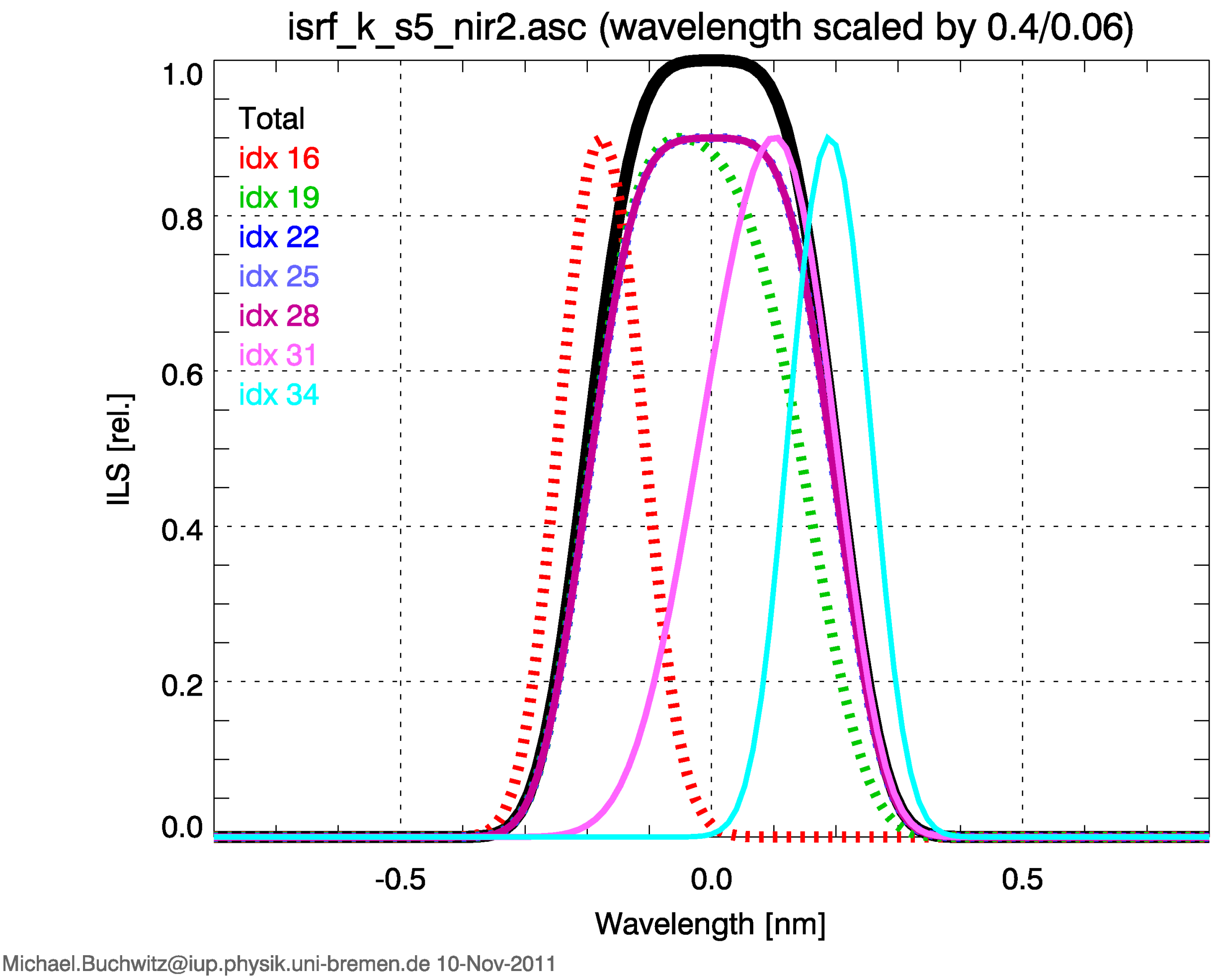

Figure 4-45: Normalized ILS (total and selected sub-samples) for band NIR-2 for different (along track) sub-samples.

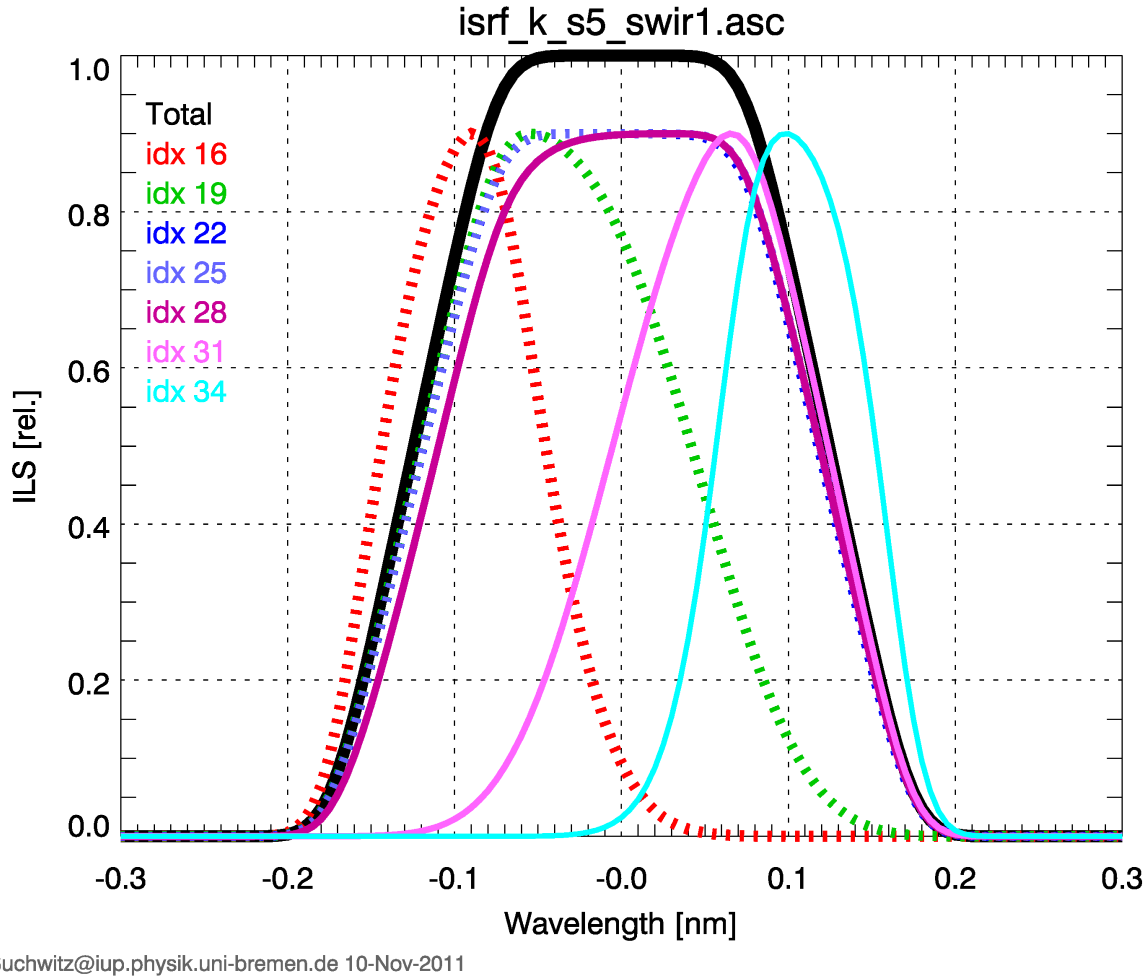

Figure 4-46: Normalized ILS (total and selected sub-samples) for band SWIR-1 for different (along track) sub-samples.

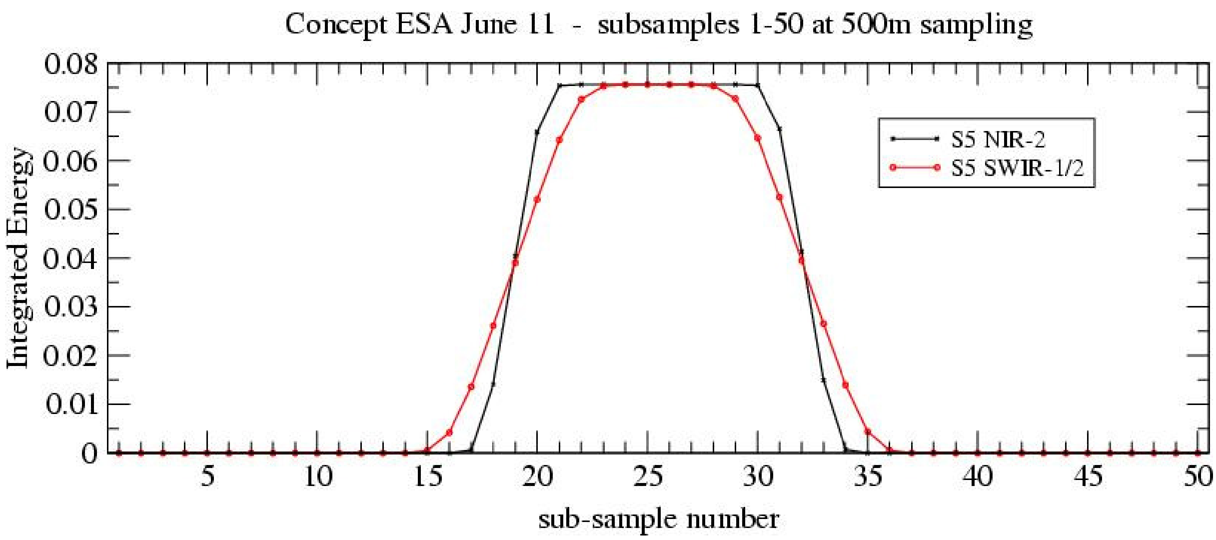

Figure 4-47: Along-track PSF (expressed as integrated energy, *i.e.* normalised to 1) as function of sub-sample number for NIR-2 and SWIR-1/2.

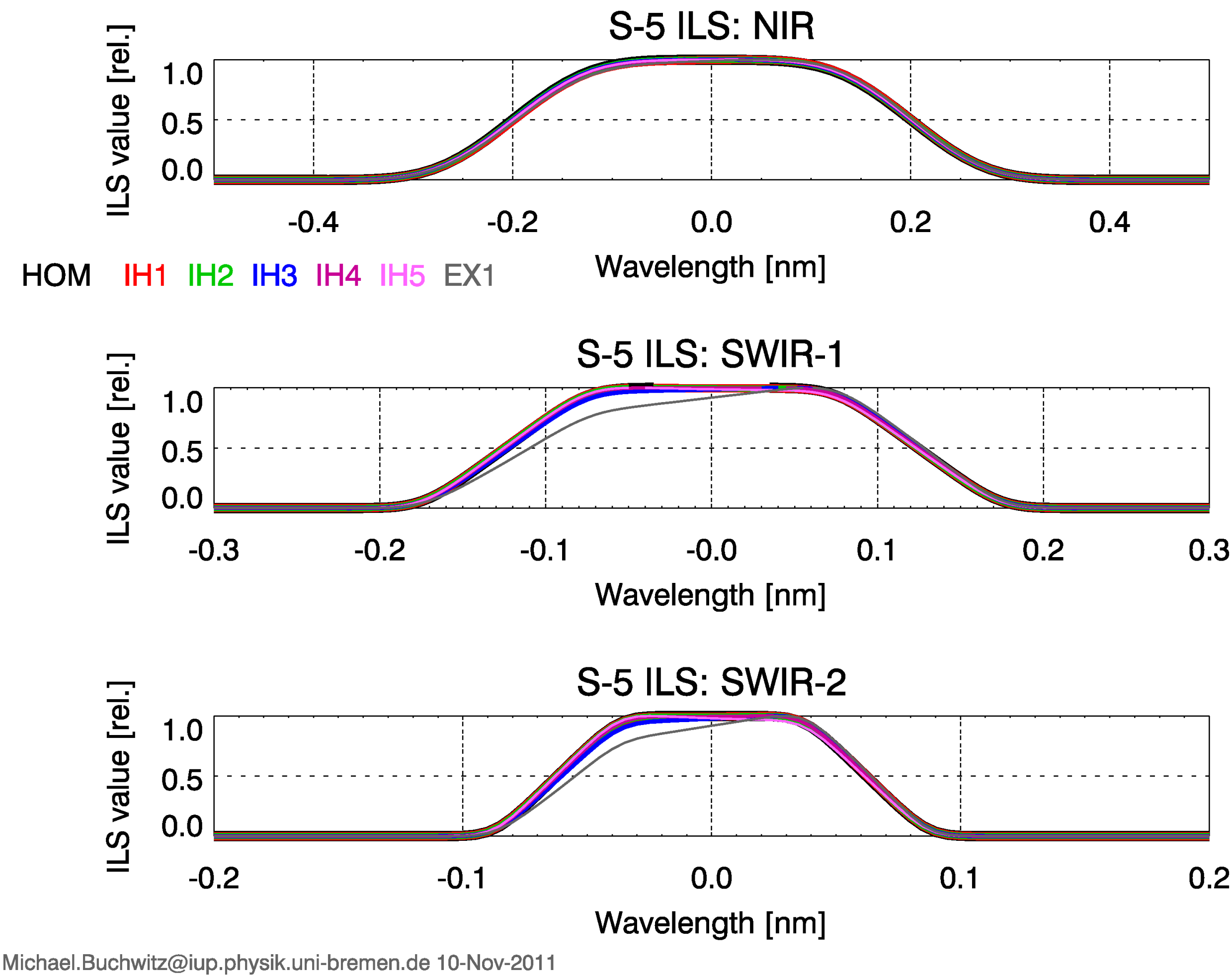

Figure 4-48: ILS for a homogeneous scene ("HOM") and various inhomogeneous scenes (IH1, IH2, ..., IH5 corresponding to scene weights W1-W5 shown in Figure 4-44). The results of the "extreme case" EX1 are also illustrated.

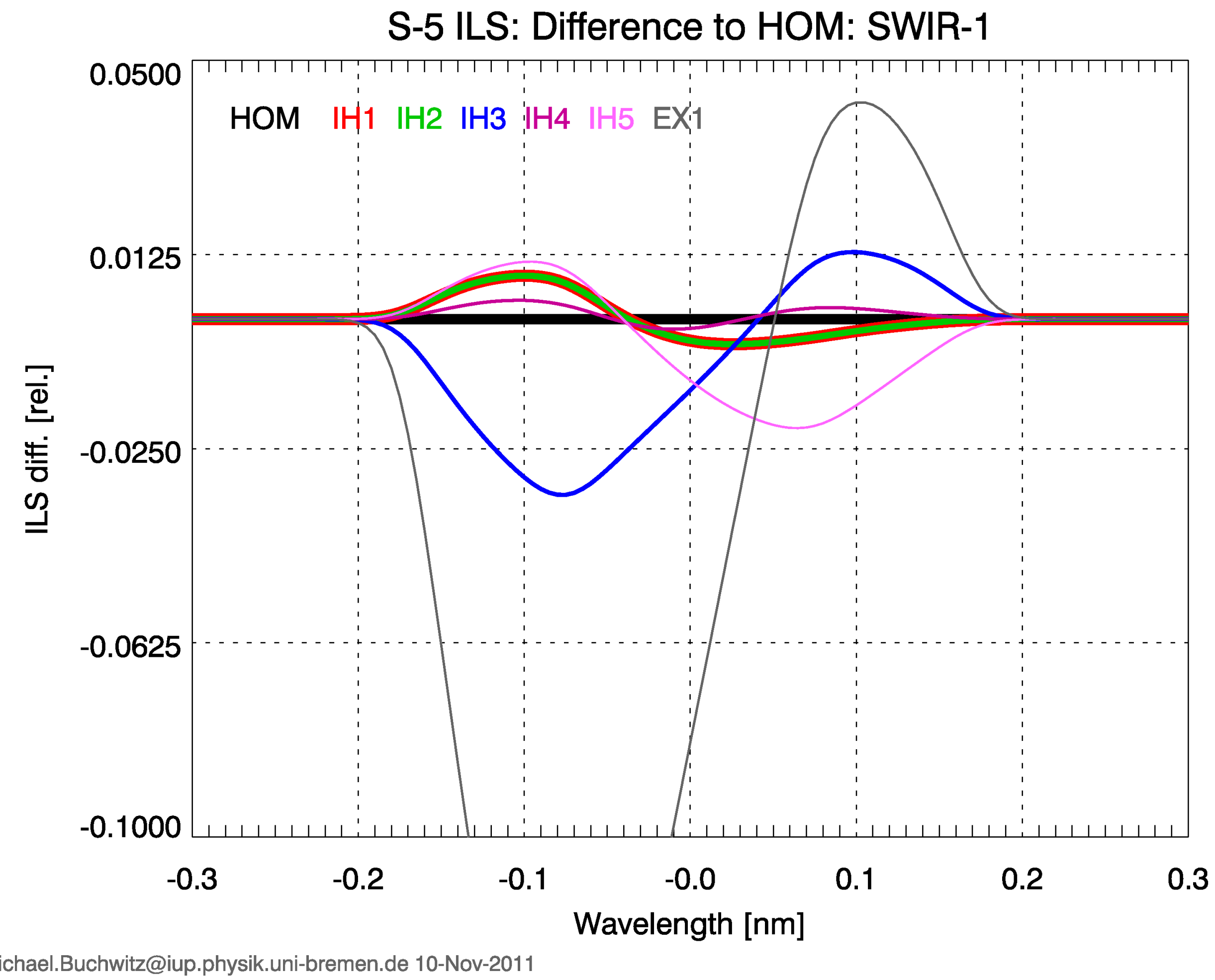

Figure 4-49: As Figure 4-48 but for the difference w.r.t. the HOM ILS, *i.e.* the ILS for the homogeneous scene (where the retrieval error is zero as this is also the assumed ILS for the retrieval).

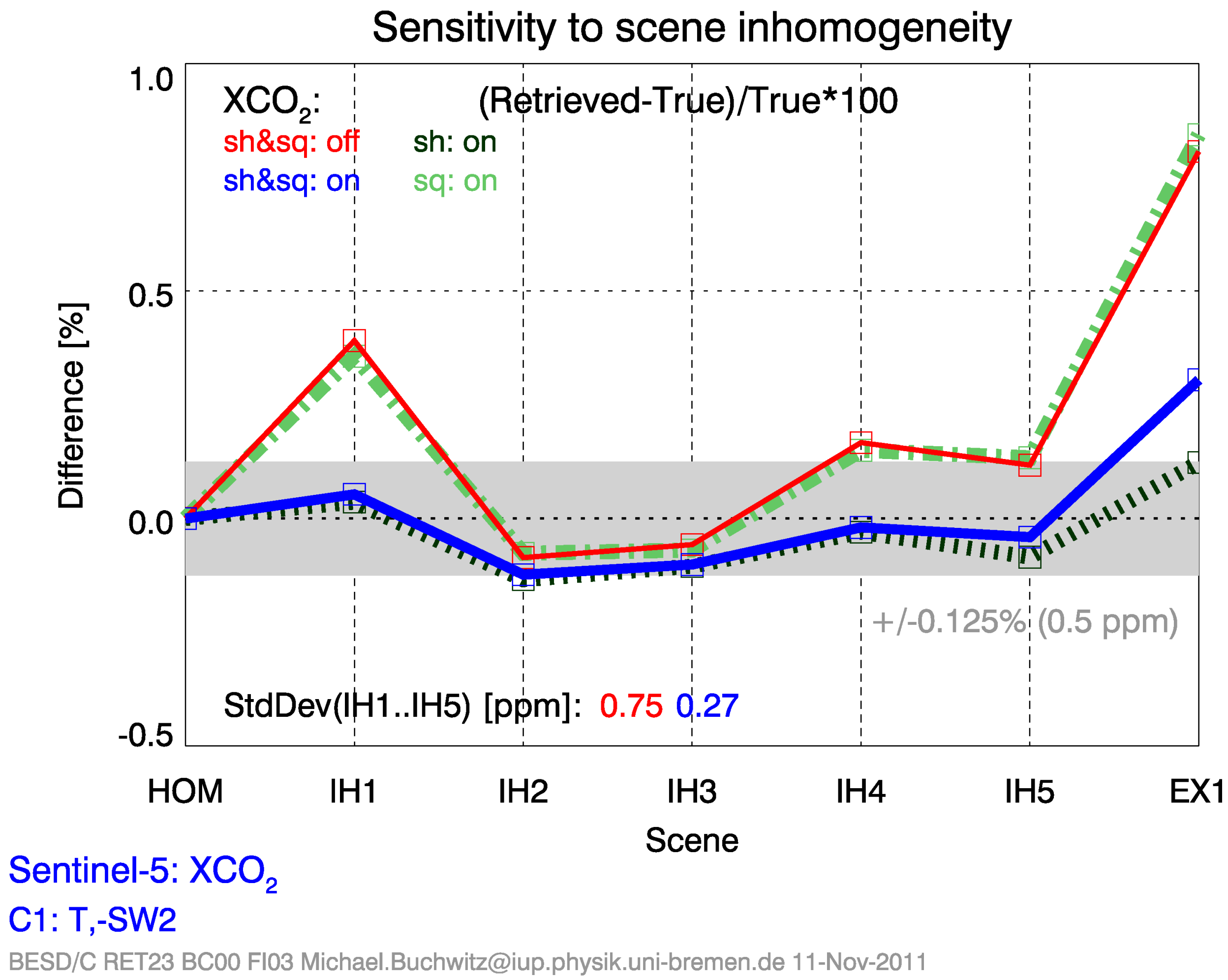

Figure 4-50: Estimate of systematic XCO_2 retrieval errors for the six spatially inhomogeneous scenes (IH1-IH5 plus EX1 corresponding to scene weights W1-W5 and EX1) and for a homogeneous scene (HOM). XCO_2 retrieval errors are shown for four retrieval configurations: without spectral shift & squeeze correction (red) and with shift & squeeze correction (blue), with shift correction only (dark green) and with squeeze correction only (light green). As can be seen, shift & squeeze as well as shift correction partially corrects for ILS variations due to inhomogeneous slit illumination. The results indicated that the shift correction is the most relevant correction method.

4.3.3.6.3 ULe results

To investigate the effect of variations in the instrument line shape function due to inhomogeneous scenes, spectra have been simulated for vegetation surfaces and SZA of 50° using the instrument line shape function for a homogenous scene which has then been retrieved with the instrument line shape function for 5 different inhomogeneous scenes. The instrument line shape function for the homogenous scene and the inhomogeneous scenes are as in the previous section 4.3.3.6.2.

Figure 4-51 shows that inhomogeneous scenes can introduce XCO_2 biases of several tenths of a ppm (up to 0.4 ppm), which roughly correlates with an increased χ^2 of the spectral fit. The values for χ^2 of the spectral fit become larger if spectral shift and stretch/squeeze is not included in the retrieval. Including spectral shift and stretch/squeeze in the retrieval significantly improves the spectral fit but it does not necessarily improve the XCO_2 biases.

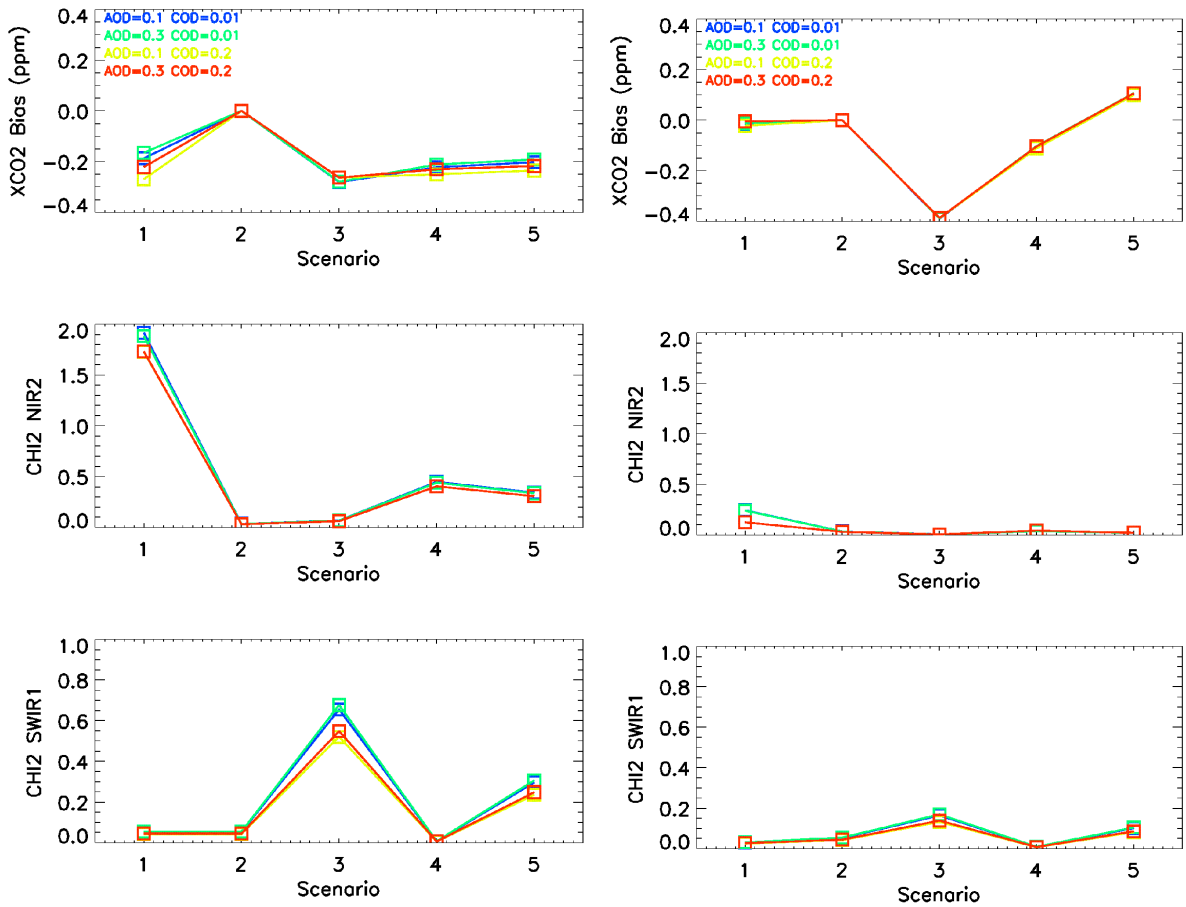

Figure 4-51: XCO_2 bias for 5 spatially inhomogeneous scenes for 4 geophysical scenarios (upper panel). The middle and lower panels give the χ^2 of the spectral fit in the NIR2 and SWIR1 band respectively. The left and right panels are for retrieval without and with fitting spectral shift and stretch/squeeze, respectively.

4.3.3.7. Sensitivity to calibration uncertainties

ULe has studied potential XCO_2 biases introduced in the XCO_2 retrievals by uncertainties in the instrument calibration of several key parameters: FWHM of the ILS, additives zero level offset and multiplicative gain. The calculations have been carried out for all scenes with a vegetation surface and SZA of 50°. The errors have been calculated using the same state vector and *a priori* covariance matrices as for the end-to-end retrieval discussed in section 4.3.1.2. The XCO_2 bias for the instrument calibration have been inferred using linear error [RD49] analysis instead of end-to-end retrievals which should give realistic XCO_2 errors as long as the errors do not become large.

The XCO_2 error estimates have been inferred assuming an uncertainty of 1% of the FWHM of the ILS in the NIR-2 or the SWIR-1 band, a 1% uncertainty of the continuum for an additive offset for each band and a 1% uncertainty of a multiplicative gain for each band. As illustrated by Figure 4-52, **for the NIR-2 band, it is found a small sensitivity to uncertainties in the calibration of the ILS with errors of a few tenth ppm. For the SWIR-1, the errors related to the ILS calibration exceed 1 ppm** which might be due to the higher spectral resolution in SWIR-1.

Furthermore, it is demonstrated that the XCO_2 retrieval is very sensitivity to additive, uncorrected offsets and an uncertainty of 1% of the continuum will introduce XCO_2 errors of several ppm (up to 8 ppm). XCO_2 errors due to uncertainties in gain show a relatively large variation with values ranging from 1-2 tenth of a ppm to 1 ppm. The complete set of the linear error analysis is summarized in Figure 4-52 and Figure 4-53.

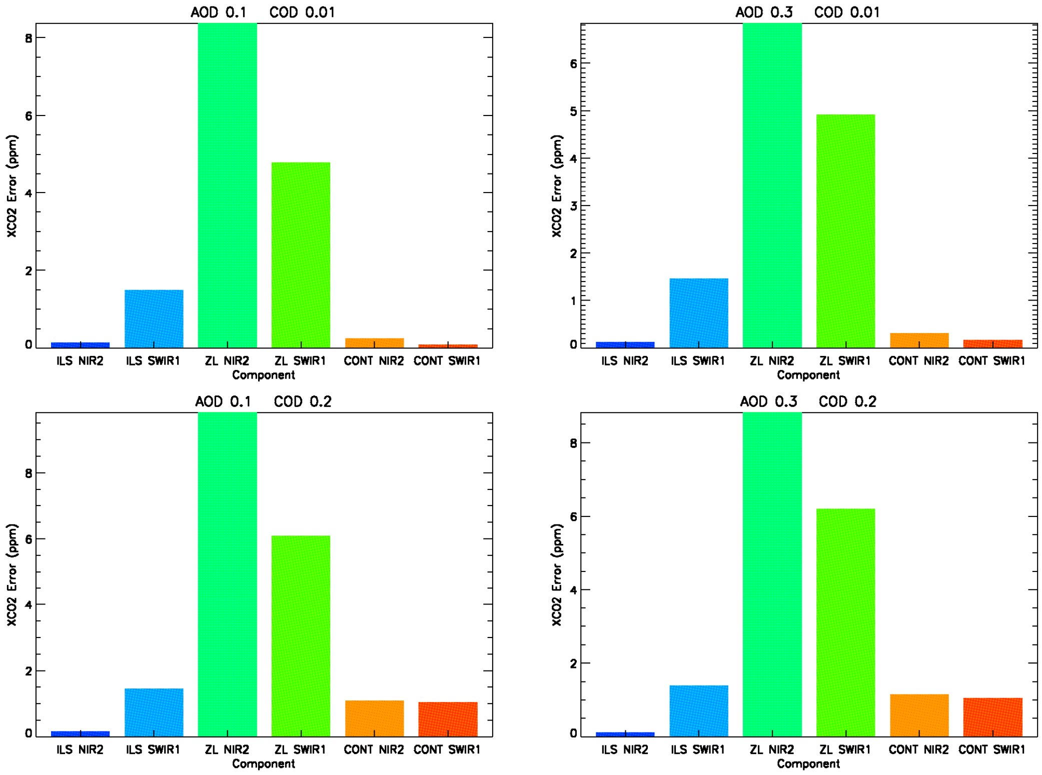

Figure 4-52: **XCO_2 bias due uncertainties in instrument calibration for vegetation surface and SZA of 50° for AOD of 0.1 (left) and AOD of 0.3 (right) without (top) and with cirrus (bottom). The assumed uncertainties in instrument calibration are 1% of FWHM of the ILS, 1% (additive) zero level offset of the continuum value and 1% of the (multiplicative) gain (continuum).**

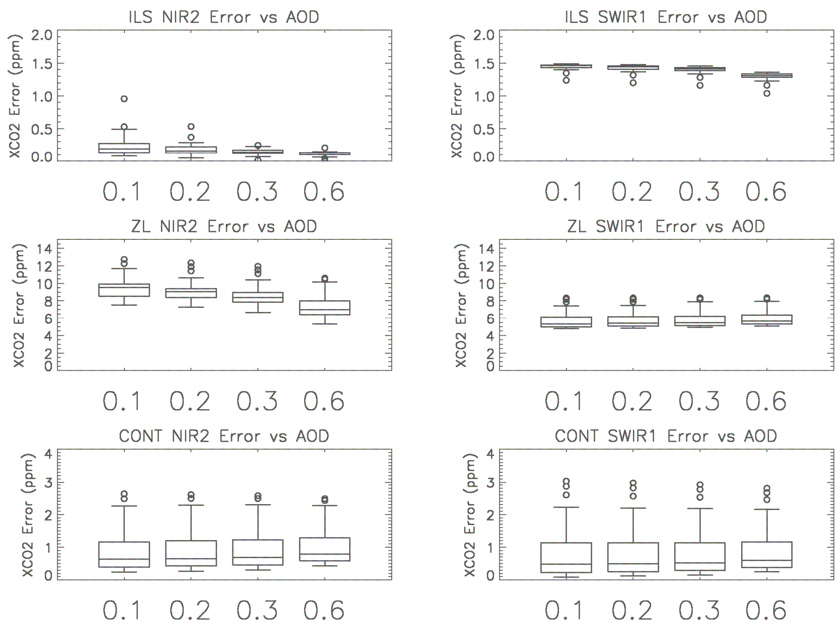

Figure 4-53: XCO_2 bias due uncertainties in instrument calibration for all scenes with vegetation surface and SZA of 50° as a function of AOD. The assumed uncertainties are as given above.

4.4. Analysis of the XCO_2 single-sounding errors: Sentinel-5-UVNS combined with other instruments

4.4.1. Limited KNMI results intended for comparison with the results of ULe and IUP-UB

KNMI considered Henyey-Greenstein based phase functions because the single scattering albedo, the Angstrom coefficient, the phase function, and the aerosol optical thickness can be varied independently, which makes it a very flexible model. Harmonization of the aerosol optical thickness with the aerosol optical thickness used by IUP-UB in SWIR-1 and NIR band is possible by using the aerosol optical thickness given by IUB and calculating the corresponding Angstrom coefficient. The spectral variation of the aerosol optical thickness is given by:

$$\tau(\lambda) = \tau(\lambda_0)\,(\lambda / \lambda_0)^{-\alpha} \quad \textbf{Equation 4-5}$$

Where:

- α is the angstrom coefficient;
- τ is the aerosol optical thickness;
- λ is the wavelength;
- and τ (λ_0) is the reference aerosol optical thickness, known at the wavelength λ_0.

By demanding that the aerosol optical thickness is the same at IUP-UB and KNMI at 760 and 1600 nm the angstrom coefficient is calculated (*cf.* Table 4-6). Once the Angstrom coefficient is known, one can calculate the nominal aerosol optical thickness at 550 nm that is used by KNMI (*cf.* Table 4-7).

Table 4-6: Aerosol optical thickness copied from IUP-UB and the corresponding Angstrom coefficient.

Aerosol model	Optical thickness at 760 nm	Optical thickness at 1600 nm	Angstrom coefficient
CC	0.39	0.09	1.970
CP	0.40	0.10	1.862
DE	0.60	0.50	0.245

Table 4-7: Nominal aerosol optical thickness at 550 nm and the values used by KNMI.

Aerosol model	Nominal aerosol optical thickness at 550 nm	Optical thickness at 550 nm used by KNMI
CC	0.60, 0.3, 0.2, 0.1	0.737, 0.368, 0.246, 0.123
CP	0.60, 0.3, 0.2, 0.1	0.730, 0.365, 0.243, 0.121
DE	0.60, 0.3, 0.2, 0.1	0.649, 0.324, 0.216, 0.108

In the remainder of this document KNMI uses the nominal aerosol optical thickness at 550 nm to label results. After harmonizing the optical thickness there remains a difference due to the single scattering albedo and the phase function.

The Henyey-Greenstein phase function is defined as:

$$P(\Theta) = \frac{1 - g^2}{(1 + g^2 - 2g\cos\Theta)^{3/2}}$$

Equation 4-6

In equation 4-6, the asymmetry parameter **g** is a measure for the amount of forward scattering.

A limited number of calculations have been performed in order to make it possible to compare results with those of the other groups. In all cases the asymmetry parameter **g** is 0.70, except when explicitly mentioned otherwise, and the single scattering albedo is 0.95 for aerosol and 1.0 for the cirrus cloud. A positive bias means that the retrieved XCO_2 is larger than the true value of XCO_2.

Table 4-8: Results for SZA = 25°, a cirrus optical thickness (COT) of 0.01, and a cirrus altitude (CAL) of 8 km. The cirrus optical thickness and the cirrus altitude are not fitted. Fit parameters are: surface albedo at 760 nm, surface albedo at 1600 nm, aerosol Angstrom coefficient, aerosol optical thickness at 550 nm, and the columns of CO_2 and H_2O.

Simulation					Retrieval (*a priori* values)					Results for XCO_2	
ALB	**AOT**	**ATY**	**COT**	**CAL**	**ALB**	**AOT**	**ATY**	**COT**	**CAL**	**Bias (ppm)**	**Precision in percent**
VEG	0.1	CC	0.01	8	SAS	0.2	CP	0.01	8	-0.04	0.26
VEG	0.1	DE	0.01	8	SAS	0.2	CP	0.01	8	1.41	0.28
VEG	0.6	CC	0.01	8	SAS	0.2	CP	0.01	8	-0.12	0.37
VEG	0.6	DE	0.01	8	SAS	0.2	CP	0.01	8	1.69	0.38

Table 4-9: Same as Table 4-8, but for a solar zenith angle of 75°.

Simulation					Retrieval (*a priori* values)					Results for XCO_2	
ALB	**AOT**	**ATY**	**COT**	**CAL**	**ALB**	**AOT**	**ATY**	**COT**	**CAL**	**Bias (ppm)**	**Precision in percent**
VEG	0.1	CC	0.01	8	SAS	0.2	CP	0.01	8	0.02	0.33
VEG	0.1	DE	0.01	8	SAS	0.2	CP	0.01	8	-0.59	1.02
VEG	0.6	CC	0.01	8	SAS	0.2	CP	0.01	8	0.04	0.69
VEG	0.6	DE	0.01	8	SAS	0.2	CP	0.01	8	1.01	0.81

The results shown in Table 4-8 and Table 4-9 show a precision usually better than 1% and a bias mostly less than 1 ppm. Here it is assumed that the phase function of the aerosol is known and is the same for the simulation and the retrieval. When the asymmetry parameter **g** changes from 0.70 to 0.60 for the retrieval, while it remains 0.70 for the simulation, the results for the fourth case in Table 4-9 change from 1.01 to 1.51 ppm for the bias and from 0.81 to 0.70 for the precision. Hence uncertainty in the phase function has some effect but the effect is not very large.

Table 4-10: Results for SZA = 25°, an aerosol optical thickness of 0.1 and a fixed aerosol type (CP). The aerosol optical thickness and the aerosol Angstrom coefficient are not fitted. Fit parameters are: surface albedo at 760 nm, surface albedo at 1600 nm, cirrus optical thickness, cirrus altitude, and the columns of CO_2 and H_2O.

Simulation					Retrieval (*a priori* values)					Results for XCO_2	
ALB	**AOT**	**ATY**	**COT**	**CAL**	**ALB**	**AOT**	**ATY**	**COT**	**CAL**	**Bias (ppm)**	**Precision in percent**
VEG	0.1	CP	0.05	6	SAS	0.1	CP	0.1	10	0.00	0.35
VEG	0.1	CP	0.05	14	SAS	0.1	CP	0.1	10	0.00	0.35
VEG	0.1	CP	0.4	6	SAS	0.1	CP	0.2 [1)]	8 [1)]	0.00	0.37
VEG	0.1	CP	0.4	14	SAS	0.1	CP	0.1	10	0.00	0.51

[1)] Changed *a priori* values to obtain convergence.

Table 4-11: Same as Table 4-10, but the aerosol optical thickness is 0.2 in the simulation and 0.1 in the retrieval. As the aerosol optical thickness is not fitted this introduces a bias.

Simulation					Retrieval (*a priori* values)					Results for XCO_2	
ALB	**AOT**	**ATY**	**COT**	**CAL**	**ALB**	**AOT**	**ATY**	**COT**	**CAL**	**Bias (ppm)**	**Precision in percent**
VEG	0.2	CP	0.05	6	SAS	0.1	CP	0.1	10	5.08	0.36
VEG	0.2	CP	0.05	14	SAS	0.1	CP	0.1	10	4.94	0.35
VEG	0.2	CP	0.4	6	SAS	0.1	CP	0.2 [1)]	8 [1)]	1.75	0.37
VEG	0.2	CP	0.4	14	SAS	0.1	CP	0.1	10	2.63	0.50

[1)] Changed *a priori* values to obtain convergence.

Table 4-10 shows that the altitude and the optical thickness of the cirrus cloud can be fitted accurately, and no bias occurs for XCO_2 because the model for simulation is identical to the model for retrieval after the fit. If, however, the true aerosol optical thickness is 0.2 instead of 0.1 a bias is introduced as shown in Table 4-11. The bias occurs because the aerosol opticalthickness is not fitted. This bias can vary between 1.75 ppm and 5.08 ppm. It is larger for an optically thin cirrus cloud. To compensate for the larger aerosol optical thickness the fit procedure increases the surface albedo from 0.100 to 0.103 at 1600 nm, which leads to the bias of 2.63 ppm in XCO_2 in the fourth line of Table 4-11.

KNMI results (Table 4-10 and Table 4-11) show that an error in the assumed aerosol optical thickness of 0.1 at 550 nm may give rise to errors in the retrieved XCO_2 of 2 – 5 ppm. This error might reduce somewhat when both the aerosol optical thickness and the cirrus optical thickness are fitted. The DISAMAR software has to be extended to test this.

For the 16 cases listed in Table 4-8, Table 4-9, Table 4-10 and Table 4-11, the Mean Random Error (MRE) and the Root Mean Square Systematic Error (RMSSE) were calculated yielding MRE = 1.6 ppm and RMSSE = 2.0 ppm. In comparison, results obtained from IUP-UB and ULe taken from Table 4-5 provide MRE = 1.0 – 2.0 ppm and RMSSE = 0.06 – 3.39 ppm. Hence, the KNMI results and the IUP-UB / ULE results are in excellent agreement.

Moreover, considering the approach used by KNMI in the next sub-sections, robust conclusions can be delivered and interpreted in common agreement for the expected XCO_2 performances through the synergy of S-5-UVNS with VII or 3MI, in terms of error reduction from a S-5-UVNS sounder stand alone.

4.4.2. Combination of Sentinel-5-UVNS-VII

4.4.2.1. Introduction

The VII mission is a cross-purpose medium resolution, multi-spectral optical imaging serving operational meteorology, oceanography and climate applications as derived in terms of user needs by application experts. The main users of the VII mission will be the WMO real time users, *i.e.* NWP centres of National Meteorological Services and ECMWF in addition to operational nowcasting services of National Meteorological Services [RD37]. The VII mission is also relevant to non real-time users. Then, the primary objectives of the Post-EPS VII mission are to provide high quality imagery data for global and regional NWP, NWC and climate monitoring. They can be ensure through the provision of, for example, high horizontal resolution cloud products including microphysical analysis, aerosol products, atmospheric water-vapour gross profiles at high horizontal resolution, polar atmospheric motion vectors, sea and ice surface temperature and sea ice coverage. The instrument will be a passive satellite radiometer capable of measuring thermal radiance emitted by the Earth and solar backscattered radiation, in specified spectral bands in the UV, visible and infra-red parts of the the electromagnetic spectrum [RD37]. Specifc instrument specifications of VII, directly related to the simulations achived in the next sections are given in Table 4-13, page 156.

In this section, the use of VII is considered in order to characterise optical properties of the atmosphere in order to improve the retrieval of XCO_2. Specifically, it is assumed that an unspecified retrieval algorithm can deliver the aerosol optical thickness at 550 nm based on VII observations and consider how that information will improve the accuracy of the retrieved XCO_2.

The approach used here differs from the approach used in previous sections. Here we do not consider an ensemble of explicit scenarios, but use the *a priori* information in the retrieval algorithm to define the possible states of the atmosphere. A consequence is that XCO_2 systematic and random errors cannot be easily separated as all errors are assumed here to be random. Let us take as example the aerosol optical thickness. The *a priori* value is set for the aerosol optical thickness equal to the true value (value used in the simulation). When the *a priori* error of the aerosol optical thickness is equal to 0.1, the system considers that ensemble of aerosol optical thicknesses taken into account is normally distributed around the *a priori* value with a one sigma width of 0.1. The retrieval takes one iteration step because the true value is the *a priori* value. When the *a posteriori* error for the aerosol optical thickness, calculated in the retrieval, is nearly 0.1 it means that the measurement contains no significant information on the aerosol optical thickness. If, however, the a *posteriori* error (one sigma) is 0.01, the measurement reduces the uncertainty in the aerosol optical thickness with a factor of 10.

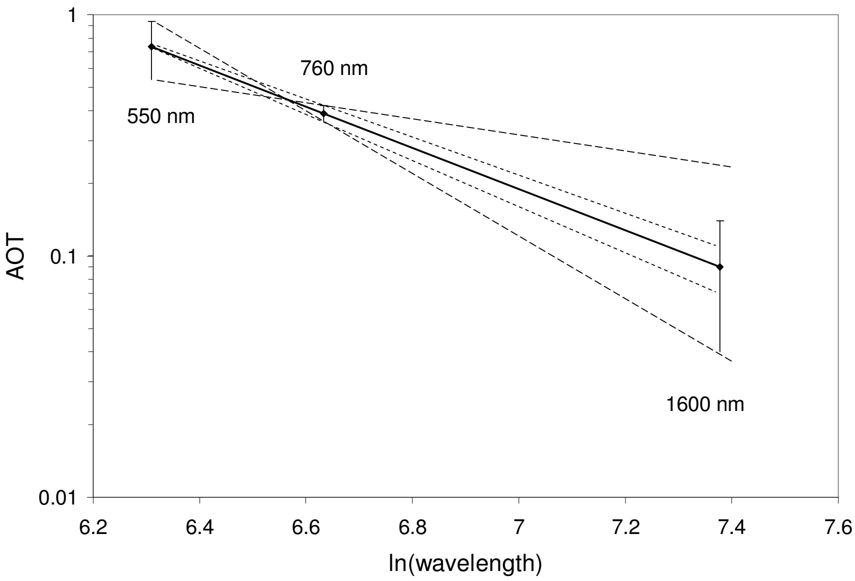

Figure 4-54: Illustration of the constraint on the aerosol optical thickness at 1600 nm due to external information on the optical thickness at 550 nm. The aerosol model is CC. If the aerosol optical thickness at 550 nm is accurately known (lines indicated by short dashes) the error in the optical thickness at 1600 nm is reduced. If the aerosol optical thickness has an error of 0.2 at 550 nm (lines indicated by long dashes) and error in the optical thickness at 1600 nm is not constrained by our knowledge at 550 nm but is determined by the error due to the fit in the CO_2 window. Note that the error at 1600 nm depends strongly on the error at 760 nm. Here it is assumed that the error in the aerosol optical thickness at 760 nm is 0.03 and the error at 1600 nm is 0.06.

This mechanism is used in Optimal Estimation to investigate the effect of external information on the error in the retrieved XCO_2. Figure 4-54 is an illustration of the manner in which the constraint works. If the aerosol optical thicknesses at 550 nm and 760 nm are accurately known the retrieved error for the aerosol optical thickness at 1600 nm is relatively small, because the error is determined by the errors at 550 and 760 nm (lines indicated by short dashes). If the error at 550 nm is relatively large (*e.g.* 0.2 when the optical thickness is 0.737) the error at 1600 nm is determined by the error obtained during the CO_2 fit in the 1600 nm band (lines indicated by long dashes). It is also important to note that the error in the retrieved aerosol optical thickness at 760 nm depends on the altitude of the aerosol layer. If the aerosol is close to the surface the error is larger than for high aerosol layers (e.g. at 3 km altitude).

In this section the results are given in terms of the relative error in percent. To obtain errors in ppm, the error in percent must be multiplied with 3.9.

4.4.2.2. Sensitivity to solar zenith angle, surface albedo, and aerosol type

Based on validation studies for MODIS [RD66] it is expected that the aerosol optical thickness at 550 nm can be determined with an accuracy between 0.05 and 0.10 over land. Figure 4-55 shows some results when external knowledge of the aerosol optical thickness, *e.g.* from VII, is available. The retrieved error for XCO_2 is shown for three solar zenith angles, two aerosol models and three assumptions for the precision of the aerosol optical thickness for the external source, namely 1.0 (no significant information on the aerosol optical thickness), 0.1, and 0.05. The results show that for the dust model (DE) information on the aerosol optical thickness does not reduce the error in XCO_2 in a significant manner. However, for the Continental Clean aerosol model (CC) the error in XCO_2 reduces when the aerosol optical thickness is known from external sources, but only for solar zenith angles of 25° and 75°.

For the CC model external knowledge helps because the aerosol optical thickness is small at 1600 nm, about 0.09. Such a small aerosol optical thickness can not accurately be fitted and the fitted Angstrom coefficient is inaccurate. By adding knowledge of the aerosol optical thickness at 550 nm the Angstrom coefficient is determined more accurately and the error in XCO_2 reduces. In contrast, the dust model has an aerosol optical thickness of 0.23 at 1600 nm and the fit in the O_2 A band and the CO_2 band are so accurate that the additional information from the imager has no effect of the error in XCO_2. It has not been investigated why the external information has no effect at a solar zenith angle of 50° for the CC aerosol model. Perhaps the reason is that the error is already small for this geometry.

In Figure 4-56, vegetation is replaced by soil and sand and similar results are obtained, but the pattern of the error is different. It is interesting to note that the precision of XCO_2 for the sand/soil case is about the same for the CC and DE models, except for a SZA of 75°.

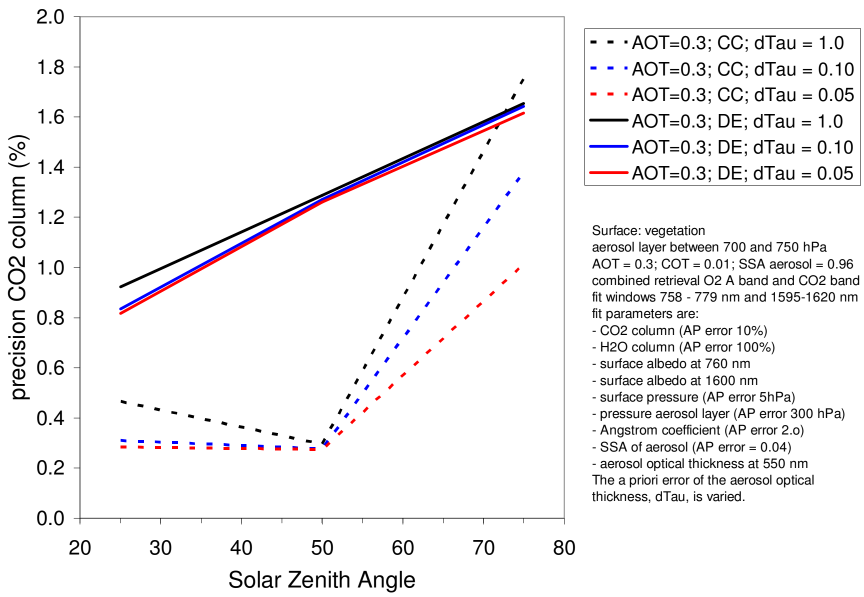

Figure 4-55: Error in the retrieved XCO_2 for three values of the solar zenith angle and 2 aerosol models (CC and DE). The aerosol optical thickness is 0.3. The *a priori* error on the aerosol optical thickness, dTau, at 550 nm varied and results are given for dTau = 1.0, 0.1, and 0.05.

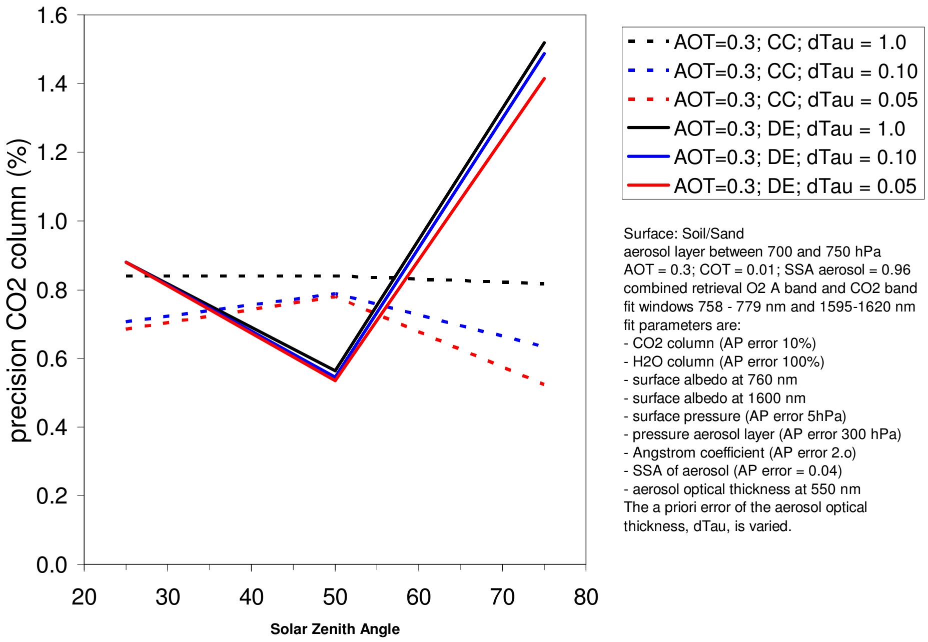

Figure 4-56: Same as Figure 4-55, but for sand/soil instead of vegetation

4.4.2.3. Sensitivity to aerosol optical thickness

In Figure 4-57, results are shown for a fixed SZA and four values of the aerosol optical thickness. Again some improvements are observed for the CC model and no improvement for the DE model when the aerosol optical thickness at 550 nm is known. It is interesting to note that the error of XCO_2 increases with optical thickness for the clean continental (CC) case, as expected, but decreases with optical thickness for the dust (DE) case, which is unexpected. The calculations show that when the durst aerosol optical thickness increases, the error in the retrieved aerosol optical thickness and the error in the retrieved altitude of the aerosol layer decreases. This decrease leads to the reduction of the error in the retrieved CO_2 column. In the present section, the aerosol is located between 700 and 750 hPa. Additional calculations show that the error is nearly independent on the dust aerosol optical thickness when the dust aerosol is located in the boundary layer. In contrast, for the CC aerosol model, the error in the retrieved aerosol optical thickness increases with the aerosol optical thickness, leading to the expected increase in the error for the CO_2 column. This shows that the present problem deals with a complicated system and it is difficult to predict what will happen if one of the 9 fit parameters changes.

An initially unexpected result is that for dust (DE) aerosol the error in the retrieved CO_2 column decreases with the aerosol optical thickness, while for continental clean (CC) aerosol the error increases with the aerosol optical thickness. It is important here to note that we deal with an elevated aerosol layer located between 700 and 750 hPa. Calculations for dust aerosol located in the boundary layer give an error in the retrieved CO_2 column that is nearly independent on the aerosol optical thickness. Table 4-12 lists the *a posteriori* precision for all the fit parameters. Considering the CC aerosol model, it is found that with increasing aerosol optical thickness the surface pressure, the aerosol single scattering albedo, and the top pressure of the aerosol layer become more accurate wheras the other parameters become less accurate. For the DE aerosol model similar effects occur, except that the surface pressure becomes less accurate and the aerosol optical thickness becomes more accurate. As we are dealing with 9 fit parameters and some of the retrieved parameters become more accurate and others less accurate when the aerosol optical thickness increases, it is difficult to predict what will happen in a particular case. In this case it is mainly the reduction of the error in the aerosol optical thickness and top pressure of the aerosol layer that leads to the decrease of the error in the CO_2 column for the dust model.

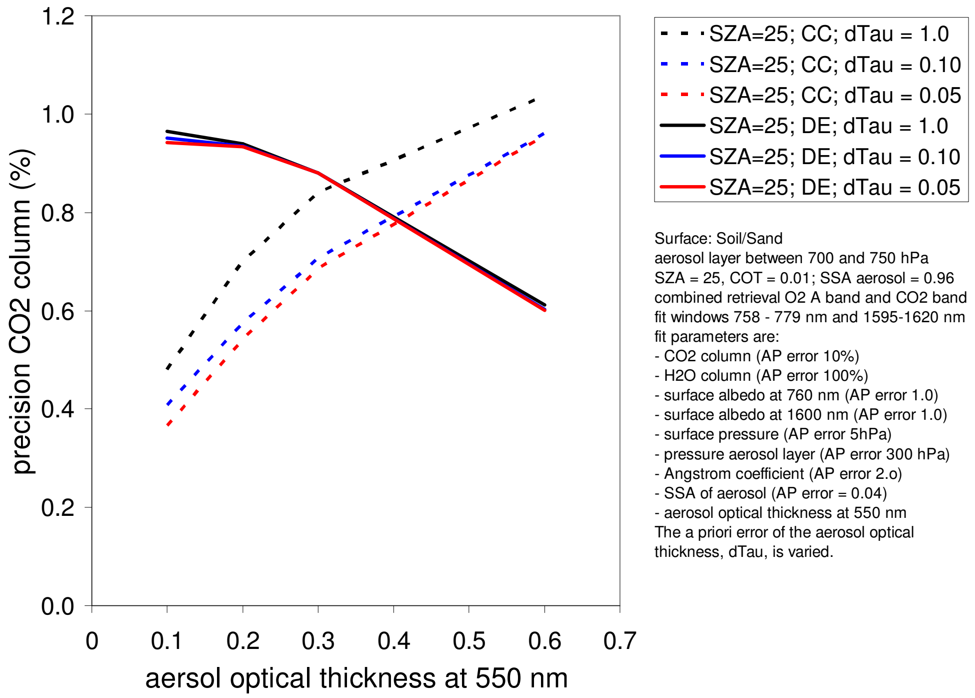

Figure 4-57: Same as Figure 4-56, but for a fixed SZA of 25° and three values of the aerosol optical thickness.

Table 4-12: Precision of the retrieved parameters for the results present in Figure 4-57 for two values of the aerosol optical thickness, 0.3 and 0.6 and two aerosol models, CC and DE. Here the *a priori* error of the aerosol optical thickness, dtau is 1.0.

Parameter	Error CC for AOT = 0.3 – 0.6	Error DE for AOT = 0.3 – 0.6
CO_2 column (%)	0.81 – 0.99	0.80 – 0.58
H_2O column (%)	1.9 – 2.1	1.4 – 1.0
Surface pressure (hPa)	2.6- 0.5	1.0 – 2.0
Surface albedo NIR-2	0.0018 - 0.0023	0.0047 - 0.0075
Surface albedo SWIR-1	0.00079 - 0.00084	0.0058 - 0.0089
AOT (550 nm)	0.17 - 0.34	0.15 - 0.13
Aerosol SSA	0.022 - 0.012	0.033 - 0.024
Aerosol angstrom coefficient	0.27 - 0.36	0.21 - 0.25
Top pressure aerosol layer (hPa)	97 - 67	66 - 22

4.4.2.4. Sensitivity to aerosol altitude

Figure 4-58 illustrates the effect of changing the pressure level of an aerosol layer. The error in XCO_2 tends to increase with the altitude of the aerosol layer. However, for the aerosol model CC and an uncertainty of 0.05 in the aerosol optical thickness, a reduction in the error takes place when the pressure becomes less than 700 hPa (red dotted line). The effects of knowing the aerosol optical thickness is similar as before.

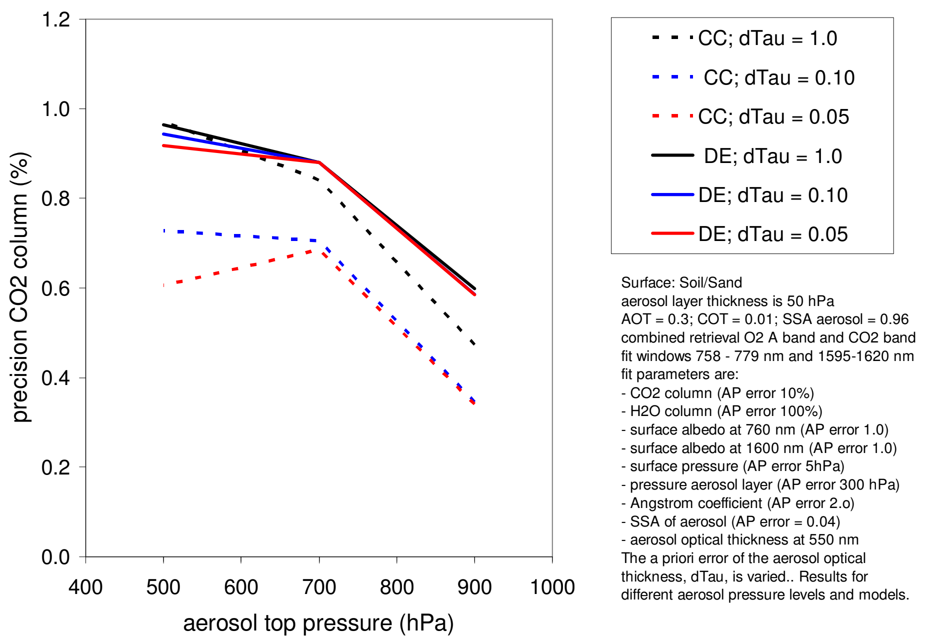

Figure 4-58: Precision in the retrieved XCO_2 for three values of the pressure at the top of an aerosol layer (900, 700, and 500 hPa) and 2 aerosol models (CC and DE). The aerosol optical thickness is 0.3 and the solar zenith angle is 25°. The *a priori* error on the aerosol optical thickness, dTau, at 550 nm varied and results are given for dTau = 1.0, 0.1, and 0.05.

4.4.2.5. Sensitivity to cirrus optical thickness and cirrus altitude

In this section, the CC aerosol model is considered and it is assumes that the aerosol is located in the boundary layer 0 – 2 km. We further assume an aerosol optical thickness of 0.1 and vary the altitude of the cirrus layer. Results are given for a cirrus optical thickness of 0.01, 0.1, and 0.4 while the altitude of the cirrus layer is 6, 10, or 14 km. The solar zenith angle is 25° or 75°, the viewing direction is nadir and the surface is vegetation.

The Angstrom coefficient for cirrus is small, and is set to 0.0 with an *a priori* variance of 0.1. The single scattering albedo for cirrus is 1.0. The fit parameters used are:

- Column CO_2 (*a priori* error 10%);
- Column H_2O (*a priori* error 100%);
- Surface albedo at 760 nm (*a priori* error 1.0);
- Surface albedo at 1600 nm (*a priori* error 1.0);
- Surface pressure (*a priori* error 5 hPa);
- Cirrus optical thickness at 550 nm (*a priori* error 1.0, 0.1, 0.05);
- Cirrus Angstrom coefficient (*a priori* error 0.1);
- Cirrus altitude / pressure (*a priori* error 500 hPa).

Figure 4-59 shows the error in XCO_2 as a function of altitude of the cirrus cloud. The error becomes large, up to 4% for a solar zenith angle of 75° and a large optical thickness of 0.6. In this case the error is dominated by the *a priori* error in the Angstrom coefficient. If this error is set to zero the error reduces from 2.1% to 0.43% for an altitude of 6 km. Because the Angstrom coefficient itself is set to zero there is no wavelength dependence of the cirrus optical thickness in the model. Using external information on the cirrus optical thickness has no effect unless it is more accurate than the cirrus optical thickness that is retrieved from the O_2 A band. A typical value of the accuracy of the optical thickness retrieved from the O_2 A band is 0.01 and imagers are not able to reach this precision. These results indicate that it is necessary to know the wavelength dependence of the cirrus optical thickness accurately, with an uncertainty in the Angstrom coefficient much less than 0.1, to get an uncertainty in the retrieved XCO_2 of about 0.5%, at least for large solar zenith angles. It is difficult to estimate the uncertainty in the wavelength dependence of cirrus clouds as the wavelength dependence is a function of the size distribution of the ice particles which can vary significantly.

In Figure 4-59, it is assumed that the aerosol is perfectly known. In practise the errors will therefore be larger due to the uncertainty of the optical properties of the aerosol. The software package DISAMAR used for these simulations cannot fit aerosol and cirrus properties simultaneously when they occur in different parts of the atmosphere. Figure 4-59 shows that the altitude of an aerosol layer has some influence on the accuracy of the results but the effect is less than a factor of 2. In order to get some information on the effect of uncertain aerosol properties in combination with uncertain cirrus properties, aerosol and cirrus are placed in a layer at 6 km altitude and fit the properties of both aerosol and cirrus.

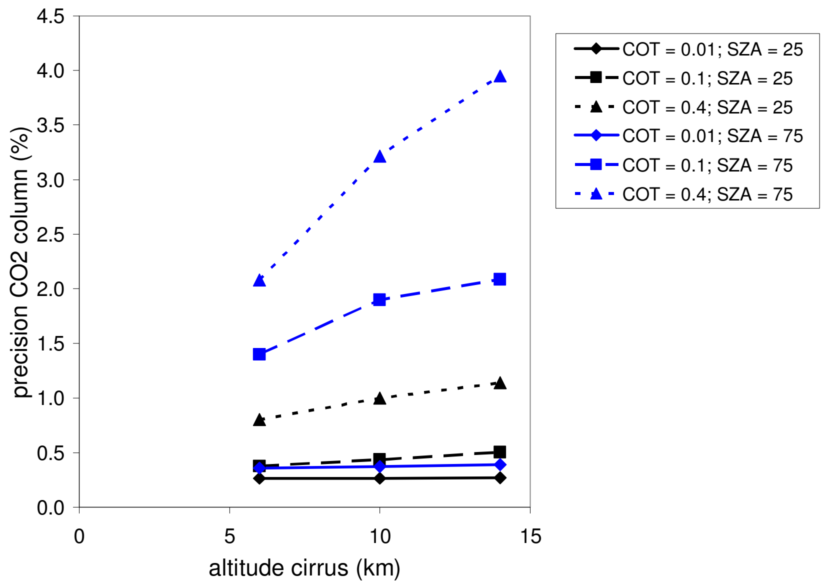

Figure 4-59: Precision in the retrieved XCO_2 in percent plotted as function of the altitude of a cirrus cloud for two values of the solar zenith angle (SZA), 25° (black) and 75° (blue), and three values of the cirrus cloud optical thickness (COT), 0.01 (solid), 0.1 (dashed), and 0.4 (dotted). The CC aerosol model is used and the aerosol optical thickness is 0.1. The aerosol is located in the boundary layer (0 – 2 km).

The solid line corresponds to the line indicated by the long dashes in Figure 4-59, showing that the movement of the aerosol from the boundary layer to 6 km has not much impact on the results. Figure 4-60 shows that uncertainty in the aerosol parameters causes the increase of the error of the retrieved XCO_2, in particular for large solar zenith angles.

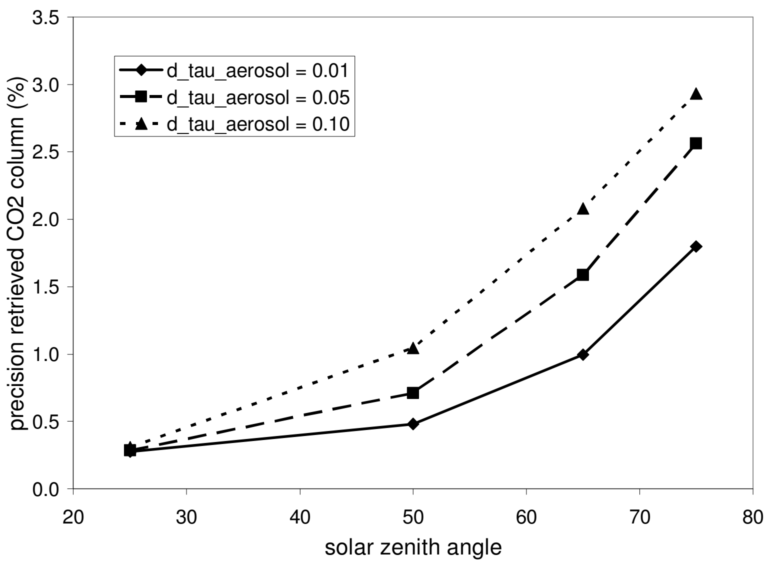

Figure 4-60: Precision in the retrieved XCO_2 in percent plotted as function of the solar zenith angle when cirrus cloud and aerosol is present at 6 km altitude. The parameters for the simulation are the same as those Figure 4-59 with COT = 0.1 (long dashes), except that the aerosol is located at 6 km and that the aerosol optical thickness, aerosol single scattering albedo, and the aerosol angstrom coefficient are also fitted. The *a priori* errors for the aerosol parameters are 0.04 for the single scattering albedo, 2.0 for the angstrom coefficient and 0.01, 0.05, or 0.10 for the aerosol optical thickness (d_tau_aerosol).

4.4.2.6. Using radiances from Sentinel-5-UVNS-VII

In the previous sections, it is assumed that the aerosol optical thickness at 550 nm, obtained from VII using an unspecified algorithm, can be used to constrain the error in the retrieved XCO_2. Here we briefly discuss another approach, namely using radiances from spectral band number VII-24 which has a central wavelength of 1630 nm and a FWHM of 20 nm. Information on aerosol can be obtained from the measured radiance if the surface albedo is known. Some simulations have been performed to determine how accurate the surface albedo has to be known in order to reduce the error in the retrieved XCO_2. The signal to noise ratio is specified as 300 for a typical scene [RD37]. However, we take a much larger value because VII pixels can be added to cover the footprint of the Sentinel-5-UVNS spectrometer. Therefore we will use a SNR of 2700 instead of 300. Its precise value is not really important for our purposes. The fit interval used is 1626 nm – 1634 nm. The fit interval is divided into 5 spectral pixels each having a width of 2 nm, a FWHM of 4 nm, and an individual SNR of 1200. These differences with the true band 24 of VII will not affect these results and are introduced for convenience and to save calculation time. All the instrumental parameters used here are summarized in Table 4-13.

Table 4-13: VII instrument parameters used as input for this study.

VII	Band
Parameter	VII-24
Spectral range [nm]	Central wavelength at 1630 nm Fit Interval used: 1626 nm – 1634 nm
Spectral resolution FWHM [nm]	Effective FWHM of about 9 nm 5 spectral pixels in the fit interval, each having a width of 2 nm and a FWMH of 4 nm.
Signal-to-noise ratio (SNR) [-]	2700 (instead of the specification of 300 in [RD37]) on the global spectral range. 1200 for each individual spectral pixel.

In the calculations, spectral band at 1630 nm is added and instead of changing the *a priori* error of the aerosol optical thickness, the *a priori* error in the surface albedo is changed at 1630 nm. The *a priori* error of the surface albedo at 760 nm and 1600 nm is the same as before, namely 1.0. The *a priori* error of the aerosol optical thickness is kept constant at 1.0.

Figure 4-61 shows results for a solar zenith angle of 25°, two aerosol models, and two values of the aerosol optical thickness at 550 nm. Figure 4-62 is the same as Figure 4-61, except that the solar zenith angle is 75° instead of 25°.

Inspection of Figure 4-61 and Figure 4-62 shows that the use of band 24 of VII can help to reduce the error in the retrieved value of XCO_2 in most cases (not for CC and an aerosol optical thickness of 0.1) but only if the surface albedo is known with and accuracy of about 0.001. Current surface albedo databases, *e.g.* the one for OMI created by [RD50], have an accuracy of about 0.02 – 0.03. It is very unlikely that surface albedo at 1630 nm can be known with the required precision. **Therefore, conclusion is that the use of the VII band 24 as described above can, in practise, not improve the accuracy of the retrieved value of XCO_2.**

Calculations were performed to test the influence of the signal to noise ratio (SNR) for band 24 of VII. The results are shown in Figure 4-63. From the figure it is clear that the precision of XCO_2 is due to the uncertainty in the atmosphere / surface parameters and that a change of a factor of 2 in the SNR has little effect.

In these simulations, it is assumed that the phase function of the aerosol is known and that wavelength dependence of the aerosol optical thickness is given by the Angstrom law. In reality that will not be true although a pre-selection of aerosol models might be used, based on 3MI observations. Hence, the errors will be somewhat larger than presented here. It remains to be investigated how much larger those error will be.

XCO_2 systematic errors would occur if there are significant model errors, such as a wavelength dependence of the aerosol optical thickness that cannot be described by the Angstrom law for the wavelength region considered (550 – 1620 nm), aerosol that occurs in different layers but is treated as occurring in one layer, errors in the absorption cross section of CO_2, and inaccuracies in the radiative transfer calculations. It is beyond the scope of this project to investigate such model errors.

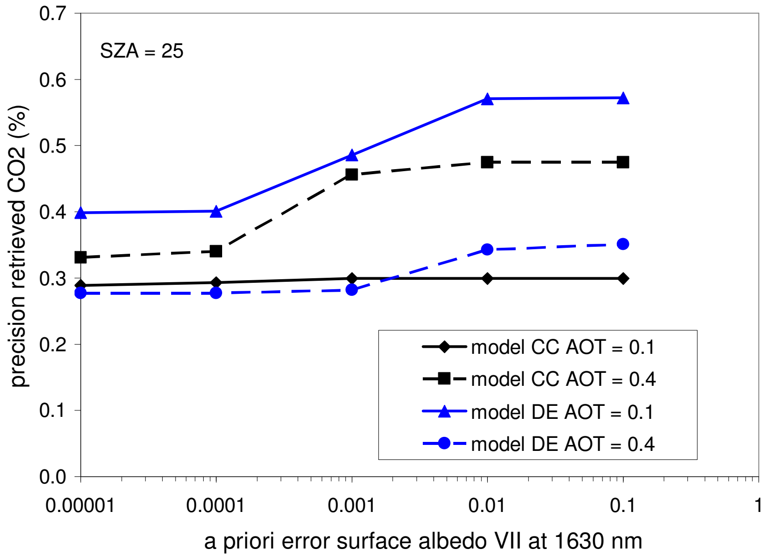

Figure 4-61: Precision in the retrieved XCO_2 in percent plotted as function of the *a priori* precision of the surface albedo in band 24 of VII. Results are given for two aerosol models and two optical thicknesses. The aerosol is located in the boundary layer (0-2 km) and the cirrus optical thickness is 0.01. Cirrus properties are not fitted. The parameters values are the same as in Figure 4-55 with an *a priori* error for the aerosol optical thickness of 1.0. Solar zenith angle is set to 25°.

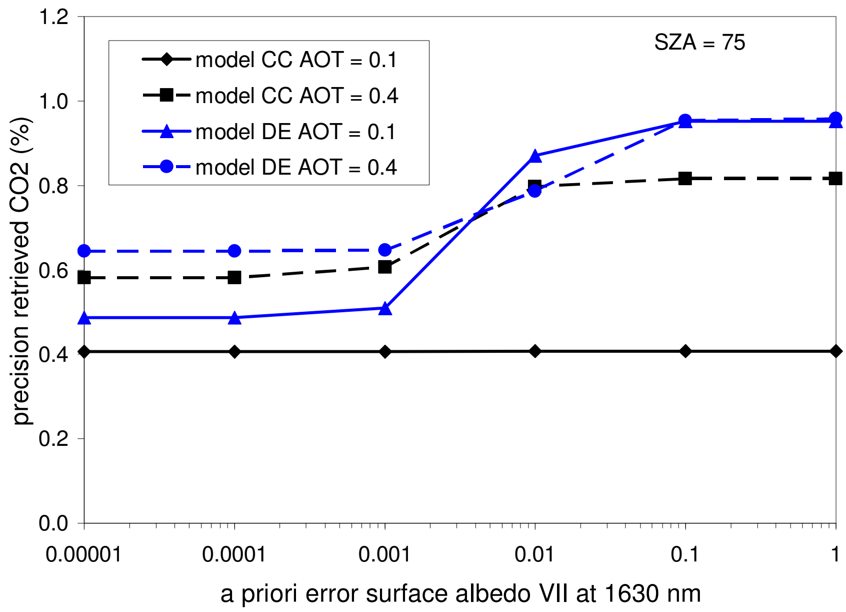

Figure 4-62: Same as Figure 4-61 but for a solar zenith angle of 75°.

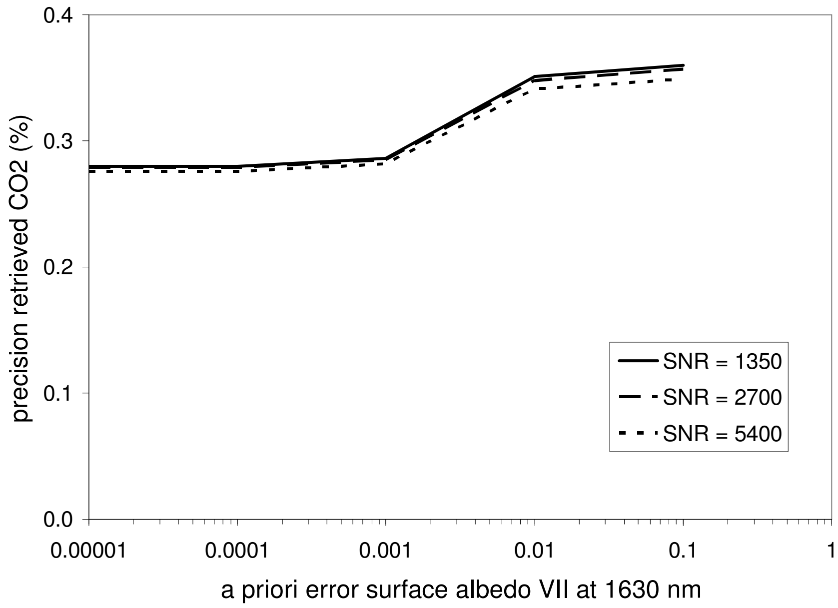

Figure 4-63: Same as Figure 4-61, but only for the DE aerosol model and an aerosol optical thickness of 0.4. Results are given for three values of the overall signal to noise ratio.

4.4.3. Combination of Sentinel-5-UVNS-3MI

The Multi-Viewing Multi-Channel Multi-Polarisation Imaging Mission (3MI) is a high performance radiometer aimed at providing aerosol characterization for climate monitoring, atmospheric chemistry and more specifically air quality. The 3MI also contributes to artefact correction on other sensors (*e.g.* the IRS, the VII and the UVNS), present on the same platform, and addresses those measurements that require multi-viewing capability due to anisotropy of scattering, and multi-polarisation because of aerosol and cirrus cloud's particle shape anf orientation variety [RD37].

The main objectives of the 3MI mission is tro provide high quality imagery of aerosols parameters for climate records (such as an angstrom coefficient for aerosol and identification of aerosol type), surface albedo, cloud characterization (in particular, the extension, optical depth and particle size related to cirrus clouds) and products related to the ocean colour thematic [RD37].

The 3MI instrument has as heritage the POLDER instrument currently flown on PARASOL, the MISR flown on EOS-Terra and the APS instrument studied for NPOESS. The instrument will be a passive satellite radiometer capable of measuring polarised radiances reflected by the Earth under viewing geometries in specified spectral bands from the UV to the shortwave infra-red parts of the electromagnetic spectrum. Paloraization and radiance wille be measured in 12 spectral bands and 10 (threshold) or 14 (goal) directions. The Spatial Sampling Distance (SSD) is better or about the same as for the Sentinel-5-UVNS (1 – 6 km depending on channel and whether the goal or threshold is achieved) [RD37]. This information can be used, in principle, to preselect aerosol models used in the retrieval of XCO_2. 3MI has a spectral band at 1650 nm with a FWHM of 40 nm. Measurements could be used in that band similar as discussed before for band 24 of VII.

However, 3MI observes the atmosphere and the surface. As shown is section 4.4.2.6, very accurate information on the surface is required in order to reduce the error in the retrieved XCO_2. Similar conclusions are expected using 3MI. The multi-angle observation and the measured polarization can constrain the aerosol properties but accurate knowledge of the bidirectional and polarization properties of the surface are needed. For optically thick aerosol layers, knowledge of the surface properties is less of an issue as most light is coming from the aerosol layer. However, users are interested retrieving XCO_2 in scenes with in optically thin aerosol close to the surface because that this will give the most accurate results (see *e.g.* Figure 4-58). In those situations it is not expected that 3MI is able to contribute significantly in reducing the error in XCO_2.

5. Summary of the Sentinel-5 baseline CO_2 performance and recommendation for enhancements

5.1. Short discussion on the nature of XCO_2 systematic errors

The purpose of this chapter 5 is a first confrontation of the user requirements expressed in Table 2-7, page 70, related to the present study with the current XCO_2 performances derived from the S-5-UVNS synthetic measurements. This confrontation allows providing recommendations for enhancing the current Sentinel-5-UVNS instrumental specifications.

There are actually 3 types of XCO_2 systematic errors:

- The **XCO_2 systematic errors caused by geophysical effects**: they are related directly to the observed scene but are also determined by the instrument, as the magnitude of these errors depends on the instrument capabilities and performances (*e.g.* spectral coverage and resolution). However, these errors should not be included in the CO_2 instrumental budget (such as calibration related errors). The errors are mainly dominated by scattering related errors (*i.e.* sun zenith angle, albedo, aerosol type, AOT, COT and cirrus altitude) but also meteorological errors (*e.g.* temperature) and other errors related to the atmospheric composition (*e.g.* H_2O) play a role. Under the chapter 4, the bias values are clearly dominated by the scattering related effects (SSE values close to 2 ppm).
- The **instrumental XCO_2 systematic errors**: they can be related to the radiometric calibration, spectral calibration, co-registration artefacts and calibration of the ILSF.
- The **coupled (between specific geophysical conditions and missing information in the instrument characterization) XCO_2 systematic errors**: *i.e.* problems of spatial inhomogeneity which could not be taken into account during the XCO_2 retrieval due to missing information (*e.g.* on the actual ILS); errors associated with the retrievals (assumptions made in the forward model, through the radiative transfer model, for aerosols, clouds and for the homogeneity of the observed scene). Some of these errors have been considered here but a real complete assessment of this type of XCO_2 systematic errors is outside the scope of this activity.

It can therefore be concluded that the estimates of the XCO_2 systematic errors given here are likely an underestimation of the expected total systematic errors. However, more studies are necessary to verify this statement.

5.2. Summary and discussion of the current XCO_2 Sentinel-5-UVNS performances

Analyses related to the XCO_2 performances of S-5-UVNS stand alone show that:

- **The XCO_2 random errors computed by both of the expert groups (IUP-UB and ULe) present significant dependence with respect to SZA and albedo values. The values are of the same order or even smaller (better) than the XCO_2 requirements:** average values vary between 1 ppm (ULe) and 1.68 ppm (IUP-UB) with SRE between 0.12 ppm and 0.57 ppm for all the scattering scenarios. Differences may be explained by the different state vector elements and the different *a priori* values. Note that only the random error (*i.e.* SNR related) has been established. This provides a lower limit of the achievable precision as other factors are also expected to effectively contribute to "noise", such as "geophysical noise", *e.g.* caused by variability of atmospheric parameters such as aerosols and (undetected) clouds. Nevertheless, it is believed that the single observation threshold precision requirement can be met at least for **application 1**.
- **The scattering effects are clearly the main contributors of the high values obtained for the XCO_2 systematic errors (RMSE of ~2 ppm for IUP-UB for all aerosol and cirrus scenario). This is confirmed by the ULe results with SSE = 1.86 ppm.** Note that reliably estimating the achievable accuracy by providing a single number to be compared with the requirement is very difficult and not without problems. The value of ~2 ppm is the best estimate for this quantity as obtained during this study using two different retrieval methods. **It is very encouraging that both groups, IUP-UB and ULe, come to similar conclusions.** However there are also clear limitations. For example aerosols and clouds not only generate biases but also contribute to "geophysical noise", as seen above. In fact it cannot be ruled out that part of this error contributes effectively to precision (random noise) rather than to accuracy (bias). However, in this study it is assumed that aerosols and clouds only contribute to the bias. This means that the effective systematic error may be smaller in reality. The real impact on the inferred surface fluxes of aerosols and clouds can only been assessed when both the random and the systematic error of the individual retrievals are reliably established for single observations and if this information is used within an inverse modelling framework to determine the impact on the inferred surface fluxes. Nevertheless, we demonstrated with our results that scattering related XCO_2 errors will at least meet the threshold requirement of 2 ppm in its current specification is a robust finding.
- **Impact of meteorological parameters (such as temperature) and horizontally inhomogeneous scenes is rather small (SSE = 0.1-0.2 ppm – IUP-UB-ULe).** However, only a part of the impact of inhomogeneous scenes was studied as each group used inhomogeneous scenes in the radiative transfer models.
- **CO_2 profile uncertainties can impact the accuracy of the XCO_2 product up to 0.2 ppm.**
- **Instrumental calibration uncertainties can have a strong impact on the XCO_2 product, depending on the spectral band considered.** Whereas uncertainties in the calibration of the ILS in the NIR-2 spectral domain presents a very small impact on the XCO_2 accuracy (errors of a few tenth ppm), **ILS calibration errors in SWIR-1 can generate associated XCO_2 errors higher than 1 ppm. Furthermore, XCO_2 retrieval is very sensitivity to additive, uncorrected offsets and an uncertainty of 1% of the continuum will introduce XCO_2 errors of several ppm (up to 8 ppm).** XCO_2 errors due to uncertainties in gain (multiplicative offsets) show a relatively large variation with values ranging from a 1-2 tenth of a ppm to 1 ppm.
- **By comparing the SSE values of the XCO_2 systematic errors related to all the scattering scenarios, a very good agreement is obtained with 1.98 ppm (IUP-UB) and 1.86 ppm (ULe).** This is a very good result, although some differences can be observed when looking in detail at few specific scenarios.

In a second step, the synergy of the S-5-UVNS sounder with VII (and with 3MI qualitatively) has been addressed by KNMI, for reducing the error in XCO_2. This synergy has been analysed in 2 ways:

- Using the aerosol optical thickness (AOT) derived from VII measurements at 550 nm (derived from an unspecified retrieval algorithm);
- Or using directly the radiances measured in band 244 of VII centred at 1630 nm.

Although previous studies focused on MODIS products allow expecting a precision value close to 0.05 for the AOT, very few improvements are observed on the XCO_2 product when using this external product. However, if an algorithm could be developed to derive the aerosol optical thickness with an accuracy of 0.01, either using VII, 3MI or a combination of both, that would help for large solar zenith angles (see Figure 4-60). But, by using the AOT derived from VII or 3MI (or both of them) will not help to meet the XCO_2 user requirements as errors are expected to vary from 0.25 % up to 2% (1 – 8 ppm).

The use of radiances in band 24 of VII centred at 1630 nm is briefly explored to reduce the error in XCO_2. A significant reduction of the error is obtained when the surface albedo in band 24 is known with a precision of about 0.001, depending at little on the aerosol models used. However, it is estimated that surface albedo databases, developed using OMI data and representative for visible wavelengths are accurate to 0.02 – 0.03. Obtaining a surface albedo database with the required accuracy of 0.001 is not possible. **Hence, radiances in band 24 of VII cannot be used to improve the retrieved XCO_2 in any significant manner.**

The same conclusions are obtained concerning a potential synergy between 3MI and S-5-UVNS. If users wish, in the future, to use 3MI and S-5-UVNS for simultaneous XCO_2 retrievals, strong improvements in the current algorithms should be necessary. **The fundamental issue for VII and 3MI is that the knowledge of surface properties (bidirectional surface albedo and for 3MI polarization properties) is requested.** The surface properties are usually known with a limited accuracy which leads to a limited accuracy of the aerosol properties. It is the power of strong absorption bands that due to line absorption one can distinguish between surface and aerosol properties. This advantage is not available for the imagers. Therefore the main contribution of the imagers will be to select the homogeneous pixels.

5.3. Preliminary discussions on the comparison of Sentinel-5 mission with specifc satellite missions dedicated to CO_2 monitoring

Table 5-1 summarizes specifications of existing and future planned space-borne missions, in terms of horizontal resolution and XCO_2 precisions (*i.e.*, random errors). These missions are dedicated to the CO_2 total column observations. The requirements for a single XCO_2 observation may be summarized as follows:

- OCO and GOSAT seem well suited for monitoring CO_2 total net fluxes at the global / regional scales (between 500 and 1000 km);
- OCO present high performances (in terms of XCO_2 uncertainty);
- CarbonSat, with a wide swath of 500 km and a spatial resolution and sampling of 2 km should be very relevant for local anthropogenic emissions (such as cities and power plants).
- Some hopes are related to GOSAT, concerning the CO_2 anthropogenic emissions, as it presents a swath width of 800 km, with a horizontal resolution of ~10 km. However, since the TANSO-FTS instrument is not sampling continuously across and along the swath, the global coverage is low, which means that substantial spatial/temporal averaging of the data is necessary.

In comparison with the space-borne missions mentioned above, Sentinel-5 will have a much higher spatial coverage, with a swath width of 2500 km (5 times larger than CarbonSat), and a spatial sampling and resolution between 5 km (1.6 times better than GOSAT at nadir) and 10 km. Thus, the number of observations will be much denser over a given area and this is a clear advantage for all 3 applications considered here.

Moreover, all CO_2 dedicated missions (such as OCO, GOSAT and CarbonSat) have a local time overpass in the early afternoon (typically 13:00, *cf.* Table 5-1). This is because it is preferable that the satellite acquires data along the sunlight part of the orbit, with an equatorial crossing time close to noon, in order to increase the solar flux, and therefore the signal to noise ratio [RD45] [RD69]. **The orbit for Sentinel-5 is a low-earth orbit with local time overpass in the morning (9:30).** The long-term agreement between the European and US operational agencies is that Europe provides the mid-morning and evening operational observations (typically 9:30; 21:30) while the early afternoon (+ night) is traditionally covered by the NOAA operational agency. An early morning overpass time of Sentinel-5 is not well suitable for CO_2 observations. The variability in boundary layer development at European latitudes is much higher in mid-morning than in early-afternoon which could lead to additional uncertainties. Also the boundary extent is on average significantly smaller in the mid-morning than in the early-afternoon, which is less desirable in cases of reduced sensitivity close to the Earth surface [RD65]. On the other hand, in the morning, fewer clouds are present (in general) and on average the wind speed is lower than in the early afternoon when the planetary boundary layer is well developed due to the peak in daytime convection. **The exact impact of a mid-morning overpass time would have to be examined in more details.**

In terms of CO_2 precision, it seems that Sentinel-5 could present reasonable values of XCO_2 random errors when comparing with the OCO, GOSAT and CarbonSat missions. Comparisons of XCO_2 systematic erros is not accessible for now, as studies are still progress for characterising the performances of GOSAT, OCO, and CarbonSat in terms of biases.

Finally, the optimal extent of the swath has to be determined by the characterisation of the off-nadir increase in the total error budget along the swath. A practical trade-off could be to limit the pixels along the swath usable for CO_2 retrieval to those for which the expected total error will not exceed the peak-to-peak amplitude of the targeted CO_2 variations. For example, the capability to sound the lower atmosphere would be increased by maximising the observations in sun-glint geometry over ocean. This could be achieved by pointing the instrument backwards of forwards along-track (whilst retaining the across track swath).

Table 5-1: Some specifications of space-borne instruments capable of measuring CO_2 [RD28] and [RD75]

Specifications	OCO	GOSAT	SCIAMACHY	CarbonSat
Tropospheric gases measured	CO_2, O_2	CO_2, CH_4, O_2, O_3, H_2O	O_3, NO_2, CH_4, CO, CO_2, H_2O, SO_2, HCHO, etc…	CO_2, CH_4
CO_2 sensitivity	Total column including near surface	Total column including near surface	Total column including near surface	Total column including near surface
Spatial resolution (km)/	1.29x2.25/5.2	10.5/80-790	30x60/960	2x2/500
CO_2 precision (random error) (ppm)	1-2	4	4	1-3
Local time	13:30	13:00	10:00	13:30
Revisit time (days)	16	3	6	6
Lifetime (years)	2	5	5 (as specified) 12 now envisaged	5(3)
Viewing modes	Nadir, glint, target	Nadir, glint, target	Limb, nadir	Nadir, sun-glint tracking, sun over diffuser

5.4. First confrontation of the current XCO_2 Sentinel-5-UVNS capabilities with the XCO_2 user requirements

5.4.1. XCO_2 Sentinel-5-UVNS spatial scales

S-5-UVNS observations will present spatial scales (resolution and sampling) between 5 and 10 km. For large observation viewing angles, the horizontal scales will be up to 30 km in the current configuration. By comparing the user requirements given in Table 2-7, only the **applications 1** and **application 2** are accessible in terms of spatial scales. **Applications 2** and **3** cannot be met by the Sentinel-5 mission due to a too coarse horizontal resolution along the whole (for **application 3**) or parts of the (**application 2**) across-track swath. However, this last statement is mostly true for the **application 3** and partially true for the **application 2** (a few remote observations may present acceptable spatial resolution in a given area according to this application).

5.4.2. XCO_2 Sentinel-5-UVNS errors

The following first analyses can be made:

- The overall values for the XCO_2 random errors derived from the individual S-5-UVNS measurements as specified currently meet the XCO_2 **precision** as required by the users for individual S-5-UVNS observation. Statistically, whatever the simulated cases, the average value is even lower than the goal required for application 1 (2 ppm) and is lower than the threshold of the 2 other applications. For some specific simulations, some values are even less than 1 ppm, which is the required goal for the application 2 and application 3. Then, **current instrumental specifications of the Sentinel-5-UVNS sounder should meet the required XCO_2 precision on individual XCO_2 product.**
- The overall values of XCO_2 **systematic errors** derived from the S-5-UVNS measurements as specified currently meet the threshold XCO_2 accuracy required in Table 2-7, but not the breakthrough and the goal values. It is reminded that the threshold XCO_2 systematic error is based on an important assumption, that very numerous and exploitable XCO_2 observations are available over a given area, depending on the size of the region observed, the associated application and the spatio-temporal structure of the XCO_2 systematic errors.

Thus, the fact that Sentinel-5 only meets the threshold value required of XCO_2 systematic error, and not the breakthrough, is an important limit is a key result related to the current S-5-UVNS instrumental specifications in view of CO_2 monitoring. Characterization and mitigation of the XCO_2 systematic errors is one of the important aspects of inverse modelling techniques for retrieving CO_2 surface fluxes. XCO_2 random and systematic errors are used in order to weight the contribution of individual XCO_2 measurements and *a priori* CO_2 fluxes, accounting for transport model errors. Depending on the application considered by the user and the data used in the inversion process, XCO_2 systematic errors must be carefully considered as their impact on the assimilation of XCO_2 products in an inverse model (for retrieving CO_2 surface fluxes) cannot be completely assessed without more extensive studies. Indeed, the estimation of the CO_2 surface fluxes is clearly dependent on several parameters that are not only related to measured XCO_2 random and/or systematic errors:

- Model transports errors which may be linked to the so-called representation error (*i.e.* mismatch between the time and space that is represented by measured samples and that of corresponding samples of the atmospheric transport model);
- Uncertainty of *a priori* CO_2 surface fluxes (depending of this uncertainty, measured XCO_2 systematic errors could have a high impact on the estimation or, on the contrary, a rather low impact);
- *a priori* knowledge meteorological parameters considered in the transport model (*e.g.* local wind conditions, PBL height).

5.5. Recommendations for enhancing the XCO_2 systematic errors derived from Sentinel-5-UVNS measurements

The recommendations stated in this section are based on the main conclusions mentioned above: *i.e.* there is a clear need to reduce the XCO_2 systematic errors related to the major scattering effects contributing to the spectral measurements with S-5-UVNS. Some of these errors cannot be fully reduced by the retrieval algorithms.

Instrumental XCO_2 systematic errors can be reduced by carefully controlling the processing of the spectral measurements (careful calibration, etc.) collected by the S-5-UVNS sounder (*i.e.* the so-called L1 measurements). However, controlling and characterising additive offsets to values as low as, say, 0.1% might be challenging. Then fitting a stray light contribution might be needed to reduce the error on XCO_2 L2 inversion.

Mitigation of the XCO_2 systematic errors can be achieved through several different approaches, depending on their sources. **Geophysical XCO_2 systematic errors** depend on how exactly the inverse problem has been formulated for retrieving the column averaged mixing ratio.

- Some geophysical parameters can be introduced in the state vector and can be retrieved simultaneously with CO_2 itself. What is then needed for these contributing parameters is a good *a priori* knowledge (contained in the vector $\mathbf{x_a}$), a small *a priori* error (contained in the matrix $\mathbf{S_a}$) and a reliable forward/inverse model for their contribution to the spectrum, which is also containing the information on CO_2.
- In other cases, some intervening geophysical parameters are not retrieved as such (because the information content of the spectrum covering the useful CO_2 spectral signatures is incomplete) and are then to be included in the **b** vector (which has to be known as precisely as possible from other sources) with a well controlled $\mathbf{S_b}$ matrix (small diagonal elements). The **b** vector and the $\mathbf{S_b}$ matrix are related to the model background, needed as input for the XCO_2 retrieval. The specification of the $\mathbf{S_b}$ matrix allows characterising the errors associated with the parameterisation as input of the forward modelling. But again, the forward model describing the impact of these additional geophysical parameters on the spectra used to derive CO_2 must be well characterized.

However, geophysical XCO_2 systematic errors can be decreased by focusing on the 2 following main recommendations, which are based on improvements of the current instrumental specifications associated with the S-5-UVNS sounder itself. The following recommendations are considered as high priority:

- To investigate how to use efficiently the information on CO_2, aerosol/cloud optical thickness, and surface albedo for the individual SWIR-1 and/or SWIR-2 bands. The objective is to further mitigate the impact of the scattering effects on the XCO_2 retrieval. The SWIR-2 band is a spectral region which presents strong absorption lines of CO_2. This band is used for OCO, GOSAT and CarbonSat in order to further reduce CO_2 retrieval errors caused by clouds and aerosols. Moreover, another objective which will be investigated is to reduce the effects of not knowing the aerosol / cloud properties, in particular the wavelength dependence of these properties.
- To investigate the additional value of using an improved spectral resolution in O_2 A (NIR-2) band (mainly for the surface pressure and altitude of aerosol). Thus the combination of an improved NIR-2 band with the SWIR-2 could be a good way for reducing the XCO_2 scattering errors. However, this last statement has to be verified quantitatively (*i.e.* does an enhanced spectral resolution in the NIR-2 band help very much for a XCO_2 retrieval or just a little?).

These recommendations are the main strong recommendations for mitigating the impacts of not precise scattering simulations when retrieving a CO_2 total column. Other improvements could be planned, as follows, but they are considered as a lower priority and could not be studied under the present study:

- **Potential capabilities by improving spectral resolutions in the SWIR-1 and SWIR-2 spectral domains:** in particular, the advantages of increasing the resolution of the SWIR-1 channel versus obtaining and using better spectroscopy knowledge in the SWIR-1 band for the retrieval cannot be clearly given in the present study: An improved spectroscopy versus relaxed SWIR-1 resolution needs to be de-coupled for many reasons. It is not clear how good spectroscopy will be in the future. A detailed study on how good the spectroscopy needs to be (*i.e.* on the spectroscopic requirements for this application) is out of scope of this study. Even the impact of studying spectroscopic errors on XCO_2 has not been studied here as this is out of scope. For this study, it is assumed that all spectroscopic parameters are perfect. Finally, the sensitivity of the retrieval to spectroscopic errors will depend on the spectral resolution and thus it is worthwhile to study this question.

- **Potential capabilities by improving SNR in the NIR-2, SWIR-1 and SWIR-2 spectral domains.**
- Potential sensitivity in the NIR-2 on the XCO_2 product.

Furthermore, the dependdance of the accuracy of the CO2 column as a function of viewing angle has to be studied in detail in another framework. It is however expected that XCO_2 errors get quite large at the "end of the swath" because the light path / airmass factor increases which increases the sensitivity to aerosols and clouds (see for example the SZA dependence of XCO_2 errors) and because the ground pixel size increases as well as the probability for cloud contamination. A guess is that probably only 50% of the swath width can be used, *i.e.* ± 500 km instead of the full ± 1000 km.

In a last part, analyses focused on potential capabilities by using VII (and 3MI) in synergy with enhanced S-5-UVNS measurements are further under chapter 6 by considering the two following issues:

- Can we use efficiently VII and/or 3MI measurements for filtering inhomogeneous / contaminated (by aerosol and/or cirrus) S-5-UVNS observations, since these would not provide sufficiently precise XCO_2 column information? This last question would imply to address the definition of thresholds related to the content of aerosol and cirrus (for instance) in the observation pixels (*i.e.* beyond this or these threshold(s), the S-5-UVNS measurement is considered as not exploitable for a CO_2 total column retrieval).

6. First analyses of the suggestions for improvements of the current S-5-UVNS instrumental specifications

6.1. Simulations of the enhanced L1B S-5-UVNS products

In order to improve the performance of the Sentinel-5-UVNS sounder alone, the approach studied here is to move towards the specification of a "CO_2 dedicated satellite mission" such as OCO, GOSAT and CarbonSat.

The current OCO, GOSAT and CarbonSat XCO_2 "baseline retrieval approach" is (or is planned to be) based on a 3-band retrieval approach: *i.e.* XCO_2 retrieval using simultaneously three bands:

- the O_2 A-band spectral region (around 0.76 µm, in the following referred to as NIR-2);
- the 1.6 µm week CO_2 band spectral region (SWIR-1 or SW1);
- and the 2.05 µm strong CO_2 band spectral region (SWIR-2 or SW2).

Indeed, the relatively transparent and interference free SWIR-1 spectral region is considered to be the primary source of information to obtain CO_2 columns with high near-surface sensitivity. There are also other reasons why this band is important for accurate CO_2 column retrieval: *e.g.* very little interference with the absorption features of other gases such as H_2O.

Using only this spectral region would however result in too large scattering related errors: *i.e.* errors due to variability of aerosols and undetected (thin or sub-pixel) clouds. Furthermore, surface pressure is also needed in order to convert the CO_2 column into the requested dry-air column averaged mixing ratio XCO_2. To obtain additional information on atmospheric scattering parameters (*i.e.* on the light path) and on surface pressure, the NIR-2 band can be used. Due to the large spectral distance between the NIR-2 and the SWIR-1 bands, the NIR-2 band alone is however not sufficient as it does not permit to reliably transfer the values of the scattering (or light path) parameters to the spectrally distant 1.6 µm spectral region, where this information is required. Therefore at least one additional band "on the other side" is needed located at wavelengths larger than 1.6 µm. For this purpose the SWIR-2 spectral band has to be added.

There may be however also other options such as using only the SWIR-2 band.

Based on simulations, this has been studied and proposed by [RD40], using a limited number of simulations. The author of [RD40] (*i.e.* Butz *et al.*) also tried real GOSAT data but so far this has not resulted in a peer-reviewed publication.

Therefore, there is at present not sufficient evidence that this method is superior to the 3-band approach. As a result, the current baseline for XCO_2 retrievals is still the "3 band retrieval" approach. However, a 3-band approach requires channel co-registration which leads to a technically more challenging instrument to build. The channel co-registration is not studied in the present study.

6.1.1. Instrument parameters

The S-5-UVNS instrument parameters listed in Table 6-2 have been used in this chapter. As explained above, these S-5-UVNS enhanced instrument specifications are based on the OCO, GOSAT and CarbonSat specifications which are given in Table 6-1. The specifications for NIR-2 and SWIR-1 are identical as used in chapter 4. But, in addition, the effects of an improved NIR-2 spectral resolution using the listed goal (G) specification of 0.06 nm have been considered. The used specification for SWIR-2 is also shown in Table 6-2. The present SWIR-2 is extratected from [RD9] specification is used as a starting point for this study. It is an "initial best guess" starting point and not the expected "optimum" (so far no studies have been undertaken to determine this optimum).

Table 6-1: Extracts of OCO, GOSAT and CarbonSat instrument specifications as depicted in [RD24] [RD46].

		Band		
Space-borne missions	**Parameter**	**NIR-2**	**SWIR-1**	**SWIR-2**
OCO	**Spectral range [nm]**	758 - 772	1594 - 1619	2045 - 2081
	Spectral resolution FWHM [nm]	~0.045	~0.08	~0.1
GOSAT	**Spectral range [nm]**	758 - 775	1560 - 1720	1920 - 2080
	Spectral resolution FWHM [nm]	0.015	0.08	0.1
CarbonSat	**Spectral range [nm]**	757 - 775	1559 - 1675	2043 - 2095
	Spectral resolution FWHM [nm]	0.045 (T) 0.03 (G)	0.35 (T) 0.15 (G)	0.125 (T) 0.1 (G)

Table 6-2: Sentinel-5-UVNS instrument parameters used as input for the present chapter. The SSR is the number of spectral resolution elements (detector pixel) per spectral resolution Full Width at Half Maximum (FWHM). The SNR is the Signal-to-Noise Ratio per detector (not per FWHM). For the NIR-2 spectral band, two values of the resolution can be used denoted by goal (G) and threshold (T).

Enhanced S-5-UVNS	Band		
Parameter	**NIR-2**	**SWIR-1**	**SWIR-2 [RD9]**
Spectral range [nm]	750 - 775	1590 - 1675	2043 - 2085
Spectral resolution FWHM [nm]	0.4 (T) 0.06 (G)	0.25	0.125
Spectral sampling ratio (SSR) [-]	3	3	3
Spectral sampling interval (nm)	0.1333 (T) 0.02 (G)	0.0833	0.04
Signal-to-noise-ratio (SNR) [-]	500 @ 755 nm See [RD7] Radiance dependence square root According to [RD8], additional tests only in section 6.2.3, page 181, were performed by degrading the SNR when improving the spectral resolution (ULe work).	See [RD7] Radiance dependence approximately square root	100 * $\sqrt{(RAD/5x10^{11})}$ with RADiance in [phot./s/nm/cm^2/sr]

6.2. Analysis of the XCO_2 single-sounding retrieval error: enhanced Sentinel-5-UVNS stand alone focused on a 3-band retrieval approach and an improved NIR-2 spectral domain

The present section presents results focused on enhancements of the Sentinel-5-UVNS sounder by considering two main improvements, with respect to the main results given in section 4.3 and the main recommendations provided in section 5.5:

- Firstly, in addition of the existing NIR-2 and SWIR-1 spectral domains, to consider the use of the SWIR-2 spectral band;
- And then to improve the spectral resolution of the NIR-2 spectral domain.

Thus, the analyses in the following sub-sections are focused on the expected contributions when considering both of these issues (individually and together).

6.2.1. Set up of the instrument configurations

The following instrument configurations associated with Table 6-2 have been studied here:

- **"T-SW2"**: NIR-2 threshold spectral resolution (*i.e.* 0.4 nm FWHM), no SWIR-2, *i.e.* the same configuration as also used under chapter 4. This configuration has been included mainly for reference purposes for comparison with the improved instrument configurations described below: IUP-UB and ULe.
- **"G-SW2"**: NIR-2 goal spectral resolution (*i.e.* 0.06 nm FWHM; no other changes, *i.e.* same SNR (upper limit, unrealistic as SNR likely will be lower for higher resolution)), no SWIR-2: IUP-UB and ULe.
- **"G-SW2*"**: NIR-2 goal spectral resolution (*i.e.* 0.06 nm FWHM; with a degradation of the SNR according to [RD8], no SWIR-2: ULe only.
- **"T+SW2"**: NIR-2 threshold spectral resolution (*i.e.* 0.4 nm FWHM), with SWIR-2: IUP-UB and ULe.
- **"G+SW2"**: NIR-2 goal spectral resolution (*i.e.* 0.06 nm FWHM; no other changes, *i.e.* same SNR (upper limit, unrealistic as SNR likely will be lower for higher resolution)), with SWIR-2: IUP-UB and ULe.
- **"G+SW2*"**: NIR-2 goal spectral resolution (*i.e.* 0.06 nm FWHM; with a degradation of the SNR according to [RD8], with SWIR-2: ULe only.

6.2.2. IUP-UB results

6.2.2.1. First step: True XCO_2 equal to the *a priori* XCO_2

The starting point for the IUP-UB activities is the chapter 4 results. They are summarized in Figure 6-2, showing the quality filtered results (XCO_2 bias) for the 8 spatial regions also used and analyzed in chapter 4 based on the 1800 analyzed scenes. The results are shown in terms of histograms of the XCO_2 bias (systematic error) caused by aerosols and clouds. In summary, the GLO (global) region (top left) present biases as follows:

- The absolute value of the systematic error is less than 0.5 ppm for 79% of all scenarios). This means that 79% of the scenes have biases in the range -0.5 ppm to +0.5 ppm.
- The absolute values of the bias are less than 1 ppm for 82% of all scenarios (*i.e.* is in the range -1 ppm to +1 ppm).
- The mean random error is 1.6 ppm. All the simulations present random error values between 0.7 and 3.4 ppm.

Figure 6-1 shows examples of the generation of simulated S-5-UVNS spectral radiances and their (random) errors (in terms of inverse SNR).

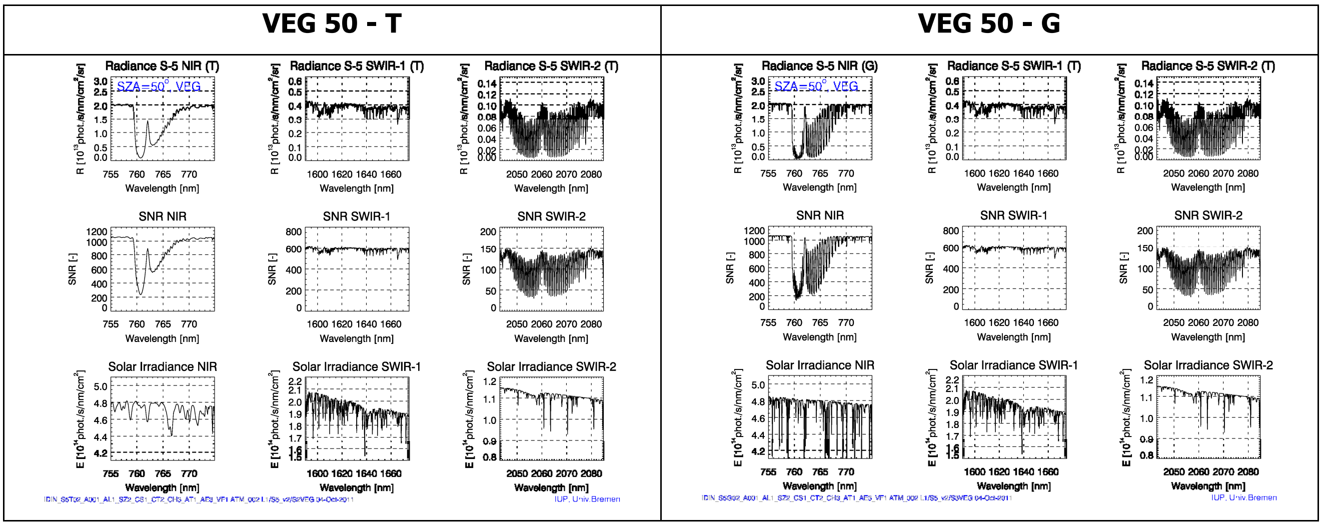

Figure 6-1: S-5-UVNS radiances, SNR and solar irradiance for all 3 bands. Scenario: Vegetation albedo, SZA 50° (*i.e.* "VEG50"). Left: for threshold (T) NIR-2 spectral resolution requirement. Right: for goal (G) NIR-2 spectral resolution requirement.

Similar plots have been generated also for the 3 other configurations "G-SW2", "T+SW2" and "G+SW2". They are illustrated in Figure 6-3, Figure 6-4 and Figure 6-5. As can be observed, the bias is not systematically reduced while instrument specification is improved. This observation is clearly confirmed in Figure 6-6, where the results for all the configurations are combined by showing cumulative bias distributions as well as mean random errors.

The following conclusions can be derived from the Figure 6-6 :

- Whatever XCO_2 random error, *i.e.* the single observation "precision", or XCO_2 systematic error considered, it is expected to get better values (*i.e.* the value as small as possible in absolute) when improving the instrument specification.
- The XCO_2 random error values computed confirm the assumption above: *i.e.* for the worst case "G-SW2", the precision is approx. 1.8 ppm whereas for the best case "G+SW2"the, precision is about 1.1 ppm.
- The XCO_2 systematic error does not always confirm this assumption. Indeed, in the present section, the bias often gets worse when the instrument is enhanced. The explanation for this apparent paradox is the following: the retrieval algorithm is based on the Optimal Estimation Method (OEM) and under chapter 4, the true XCO_2 (for the observed atmosphere) is equal to the *a priori* XCO_2 (the atmosphere assumed for the retrieval). For the OEM, the retrieved XCO_2 is equal to or at least close to the *a priori* XCO_2 if the observation does not provide any information, *e.g.* in case of a very low SNR. If the *a priori* XCO_2 is equal to the true XCO_2 (as the case for atmosphere ATM01 is used in chapter 4 to avoid complications due to additional smoothing errors), then the XCO_2 bias is essentially zero if the observations have a low SNR as under these conditions the retrieval essentially ignores the observations and returns the *a priori* XCO_2 value as retrieved XCO_2 value.

  If now the observations get a stronger weight, *e.g.* by reducing the measurement error (higher SNR) or by adding an additional channel, the bias gets larger as in this case typically the retrieved XCO_2 differs from the *a priori* XCO_2 (the difference between these two values is the bias as the *a priori* XCO_2 equals the true XCO_2 for ATM01).

  In summary, if the *a priori* XCO_2 is equal to the truth, it is better to ignore the (erroneous) observations because considering them may enhance the systematic error of the retrieved XCO_2.

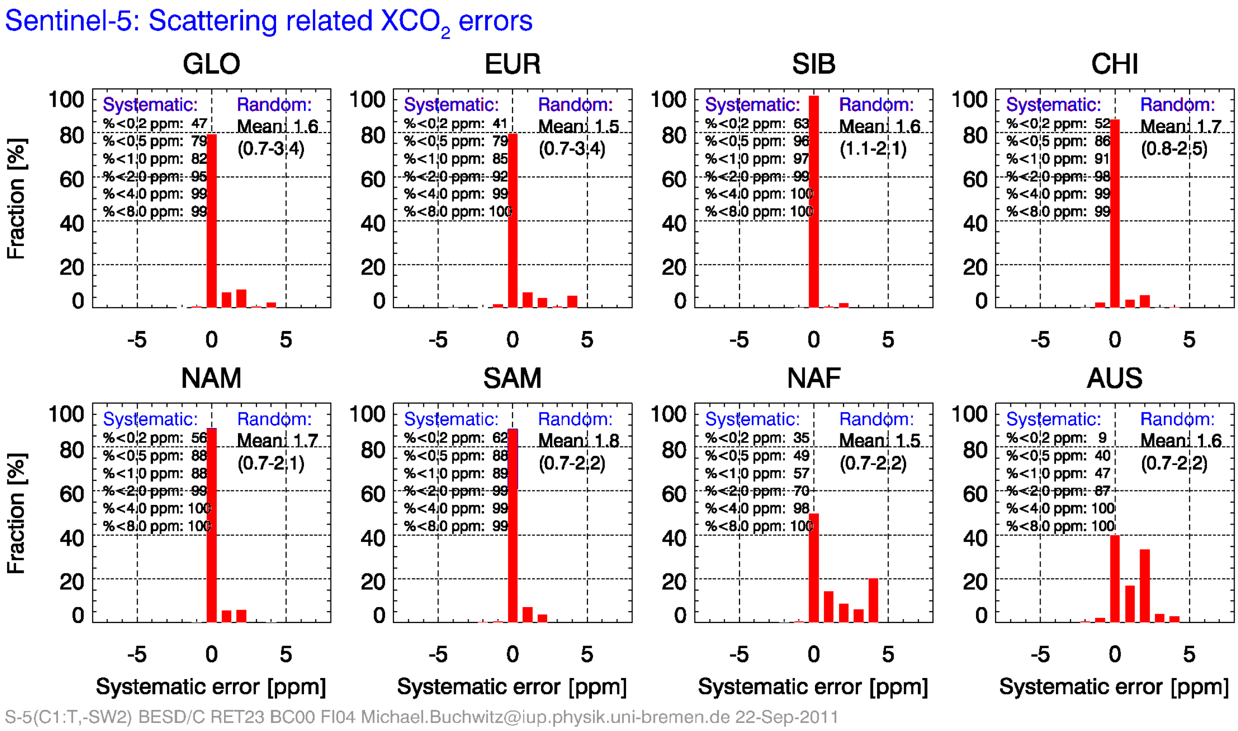

Figure 6-2: Histograms of the XCO_2 bias for 8 regions plus additional information for instrument configuration C1 (and atmosphere ATM01 where XCO_2 true = XCO_2 *a priori*). The width of each histogram bar is 1 ppm (*i.e.* -0.5 – +0.5 ppm, +0.5 – +1.5 ppm, etc.). Moreover, the following elements are listed: (i) the fractions of the scenarios with a bias less that a given bias (*e.g.* the percentage of the scenes with a bias < 0.2 ppm), (ii) the XCO_2 random error ("precision"; listed is the mean value (in ppm) and in brackets the min/max values (in ppm)).

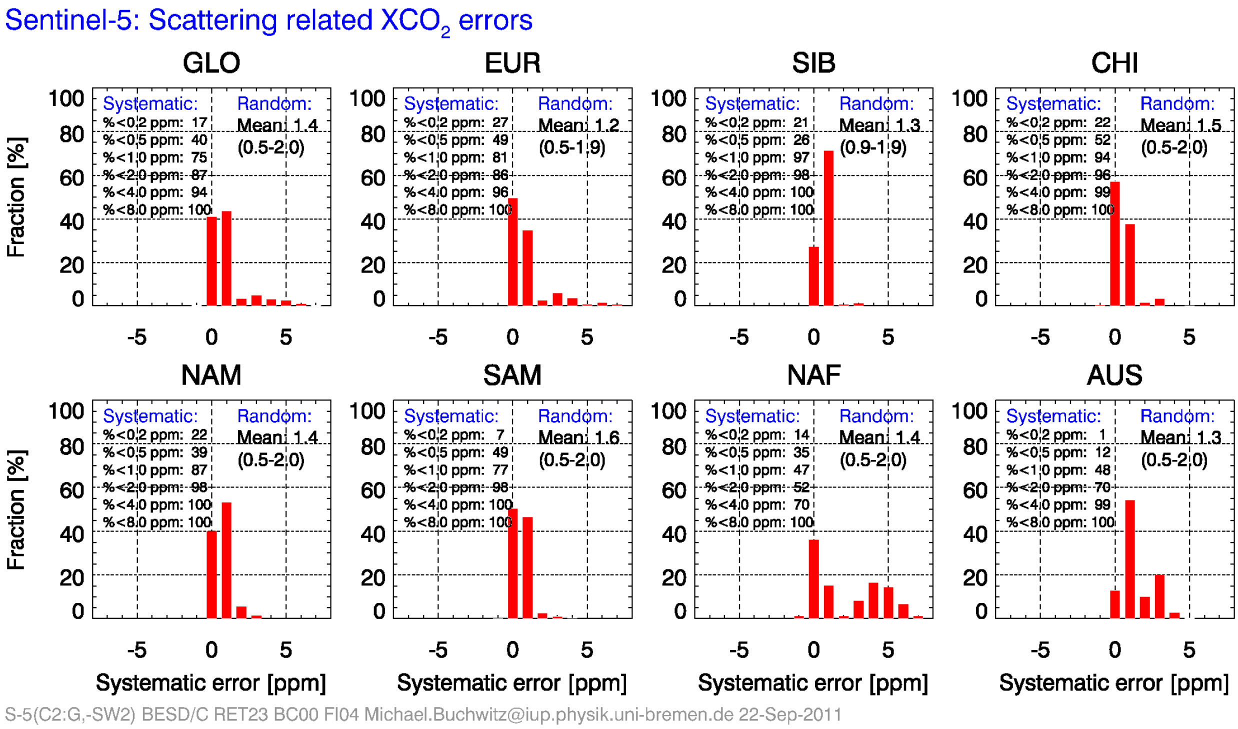

Figure 6-3: As Figure 6-2 but for configuration C2.

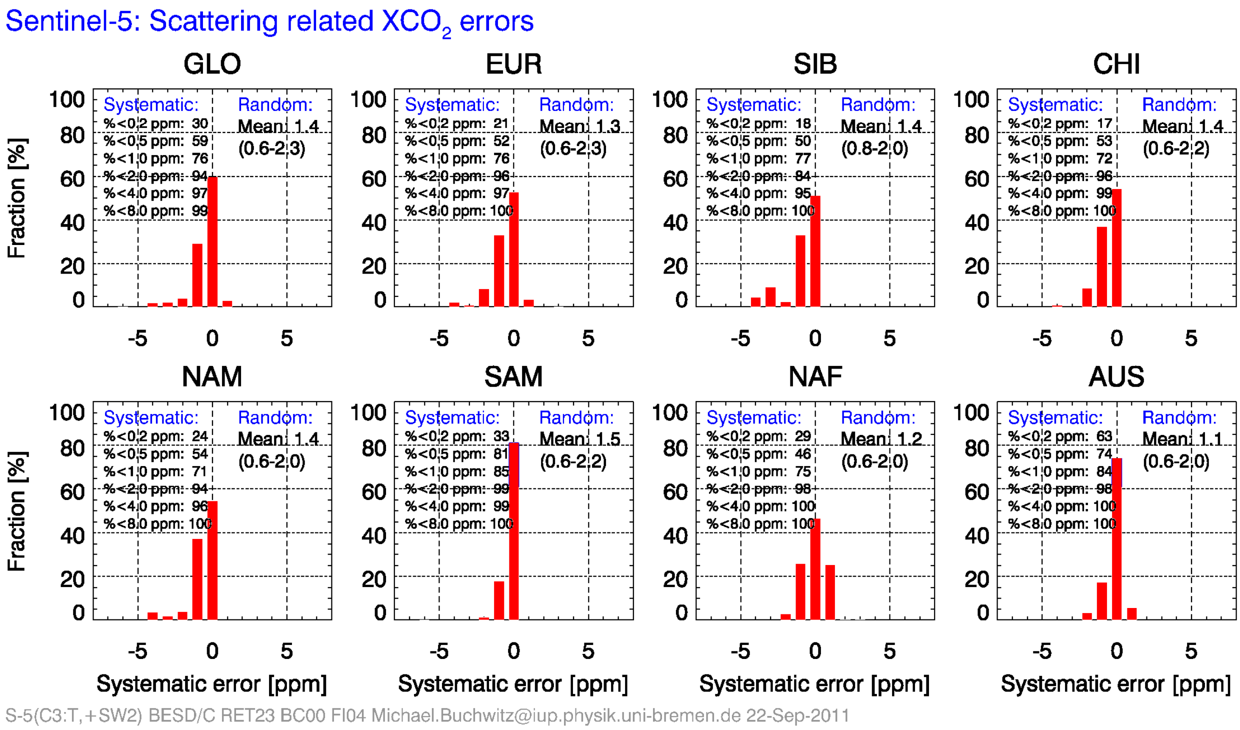

Figure 6-4: As Figure 6-2 but for configuration C3.

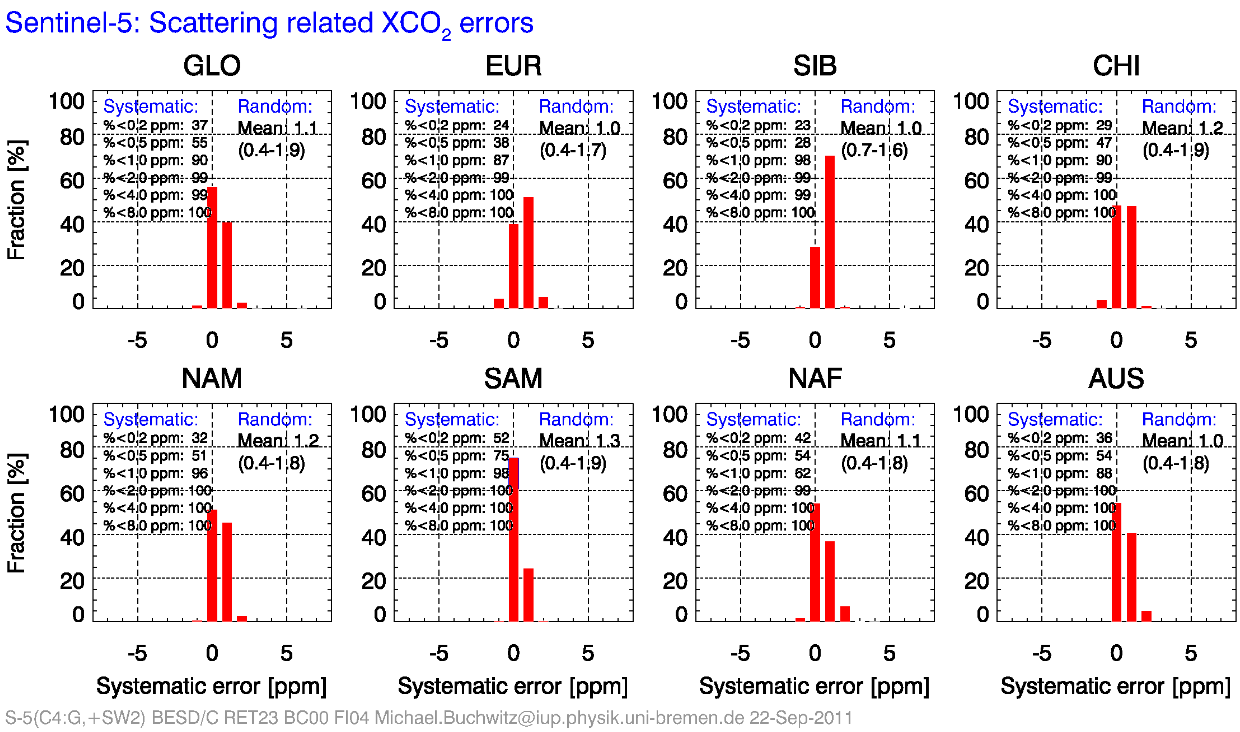

Figure 6-5: As Figure 6-2 but for configuration C4.

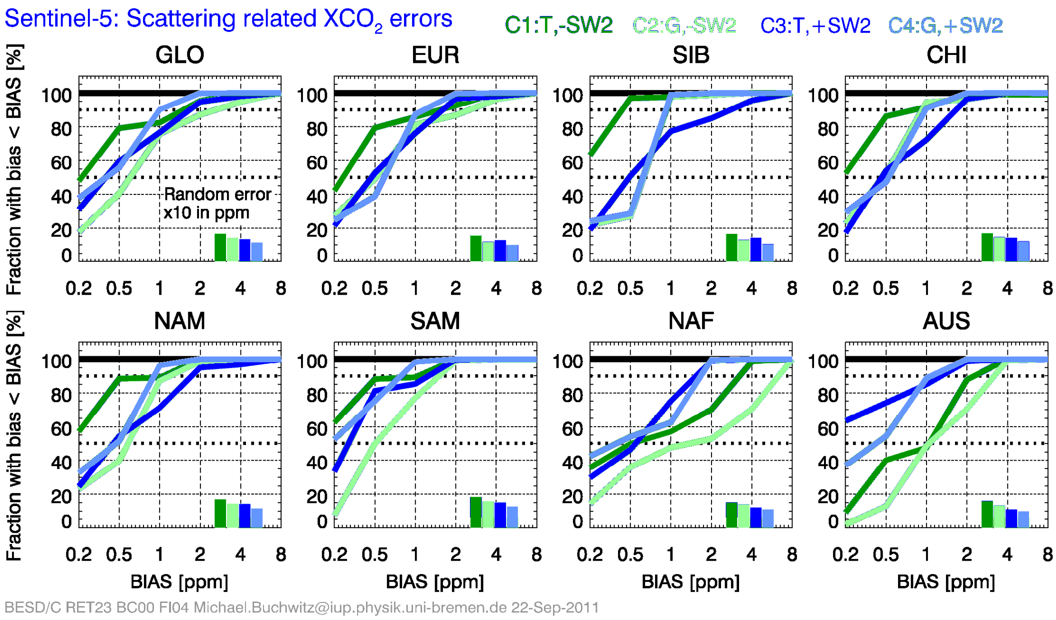

Figure 6-6: Cumulative bias distributions for configurations C1-C4 for all eight regions (atmosphere ATM01). Also shown are the mean random errors as vertical bars (note that the y-value of each bar has to be divided by 10 to get the precision in ppm, i.e., a height of 20 ppm corresponds to a precision of 2 ppm (1-sigma)).

6.2.2.2. Second step: True XCO_2 differs from the *a priori* XCO_2

Thus, approach under chapter 4, used to quantify systematic errors, needs to be modified if the goal is to estimate to what extent systematic errors can be reduced by using a better instrument.

The most obvious next step to achieve this is to use another atmosphere ("ATM02") where the true XCO_2 differs from the *a priori* XCO_2. For this purpose a CO_2 vertical profile has been used for the simulated observations, which significantly differs from the *a priori* profile used for the retrieval. For this purpose a typical northern hemisphere mid-latitude summer CO_2 profile has been used, which is identical with the one also used in [RD23]. This profile is shown in Figure 6-7.

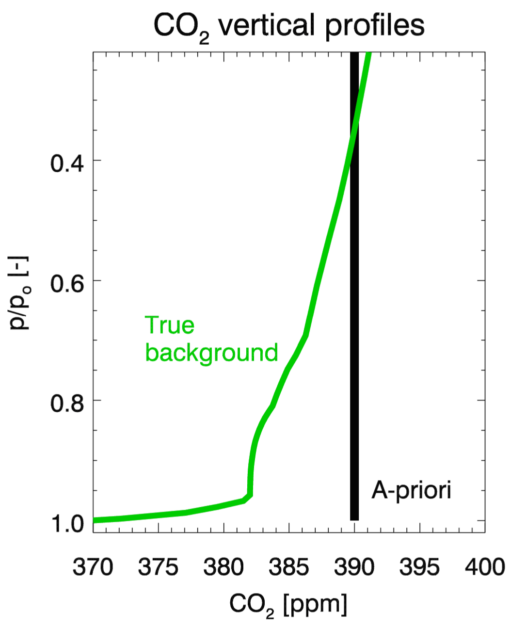

Figure 6-7: The "new" true (= "observed") CO_2 vertical profile of ATM02 is shown on the left in green (XCO_2 = 387 ppm). The *a priori* CO_2 profile used for the retrieval is shown in black (ATM01 with XCO_2 = 390 ppm) [RD23]

All S-5-UVNS observations for all the 1800 scenarios have been recomputed by considering the "perturbed" CO_2 profile (ATM02) shown in Figure 6-7, which significantly differs from the *a priori* profile (ATM01). These simulated observations have been used for XCO_2 retrieval using the same BESD algorithm with identical input parameters and using the same post-processing filtering criteria as also used chapter 4. Also the same analysis method has been used to obtain statistical information on the XCO_2 systematic and random errors. The results are shown in Figure 6-8 (unfiltered XCO_2 results for all VEG50 scenarios all four configurations), Figure 6-9, Figure 6-10, Figure 6-11 and Figure 6-12 (bias histograms for "T-SW2", "G-SW2", "T+SW2" and "G+SW2") and summarized in Figure 6-13 (over plotted cumulative bias distributions and precision values (vertical bars) for all the four configurations).

As can be seen from Figure 6-8, BESD succeeds for many scenarios to identify that the XCO_2 of the observed scene is about 3 ppm lower than the XCO_2 of the model *a priori* atmosphere (dotted green line) assumed for the retrieval. This shows that BESD is doing what it is supposed to do, at least qualitatively. As can also be seen, the retrieved XCO_2 can deviate significantly from the true XCO_2 (solid green line) for many scenarios (mostly for the desert dust aerosol scenes with high AOT as already found in chapter 4). Post-processing filtering therefore remains to be essential.

As can be deduced from Figure 6-13, the bias may or may not be reduced if a better instrument is used. This can be more clearly observed in Table 6-3, where key numerical results are listed.

As shown in Table 6-3, the XCO_2 random error ("precision") clearly improves when the instrument is improved (*e.g.* for ATM02, from 1.7 ppm for "T-SW2" to 1.3 ppm for "G-SW2" and to 1.1 ppm for "G+SW2").

Concerning the systematic errors, this mitigation is however not always observed. As can be seen (for ATM02), the fraction of scenarios with a bias less than 0.2 ppm increases while the instrument is considered as improved: from 10% of all scenes for "T-SW2" to 15% for "T+SW2" to 20% for "G+SW2". For the 0.5 ppm error limit, this is however not the case: 42% of the scenes have a bias less than 0.5 ppm for "T-SW2" but only 41% for "T+SW2" and only 39% for "G+SW2".

Clearly, this is in contradiction to the expectation that a better instrument should result in smaller biases.

This result points at a fundamental problem of the analysis method. It appears that the BESD retrieval algorithm, which is under development at IUP-UB, is not yet under all conditions able to make use of the additional information provided by a better instrument. Therefore no strong conclusions with respect to instrument improvements can be drawn at this stage using BESD. Significant improvements of BESD are required before this application can be addressed.

Therefore, the focus of the future IUP-UB activities in this context has to be on improving BESD (*e.g.* full implementation of an iterative retrieval scheme, full coupling to on-line RTM simulations, etc.).

Retrieved XCO_2 – ATM02 – ALL VEG50 scenarios - no post-processing filter	
"T-SW2"	**"G-SW2"**
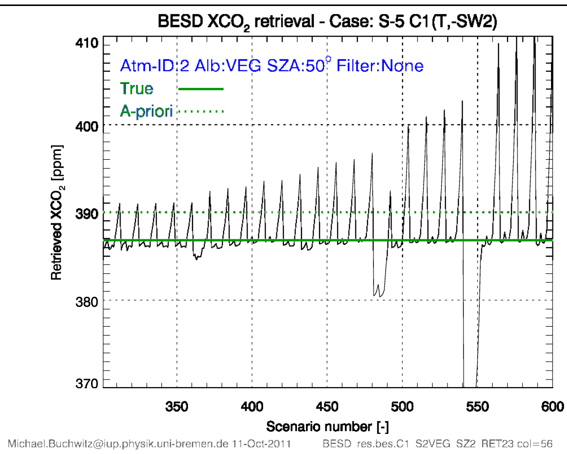	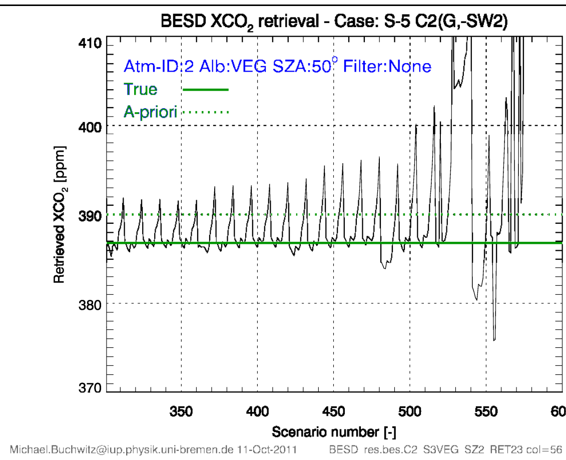
"T+SW2"	**"G+SW2"**
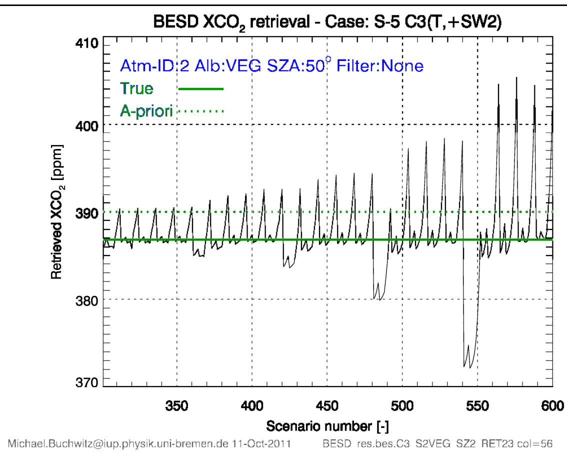	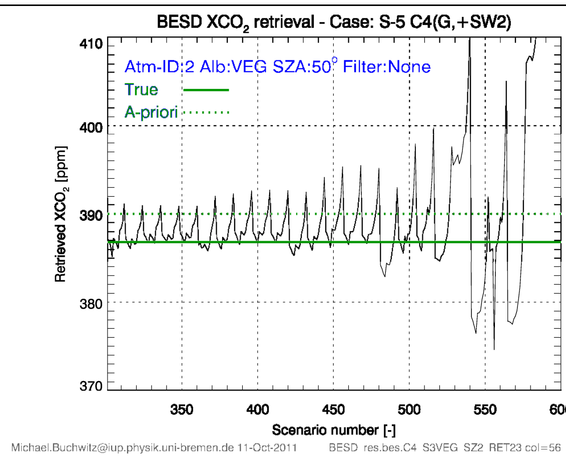

Figure 6-8: Retrieved XCO_2 for all VEG50 scenarios for atmosphere ATM02 for all four configurations: *i.e.* "T-SW2", "G-SW2", "T+SW2" and "G+SW2" configurations.

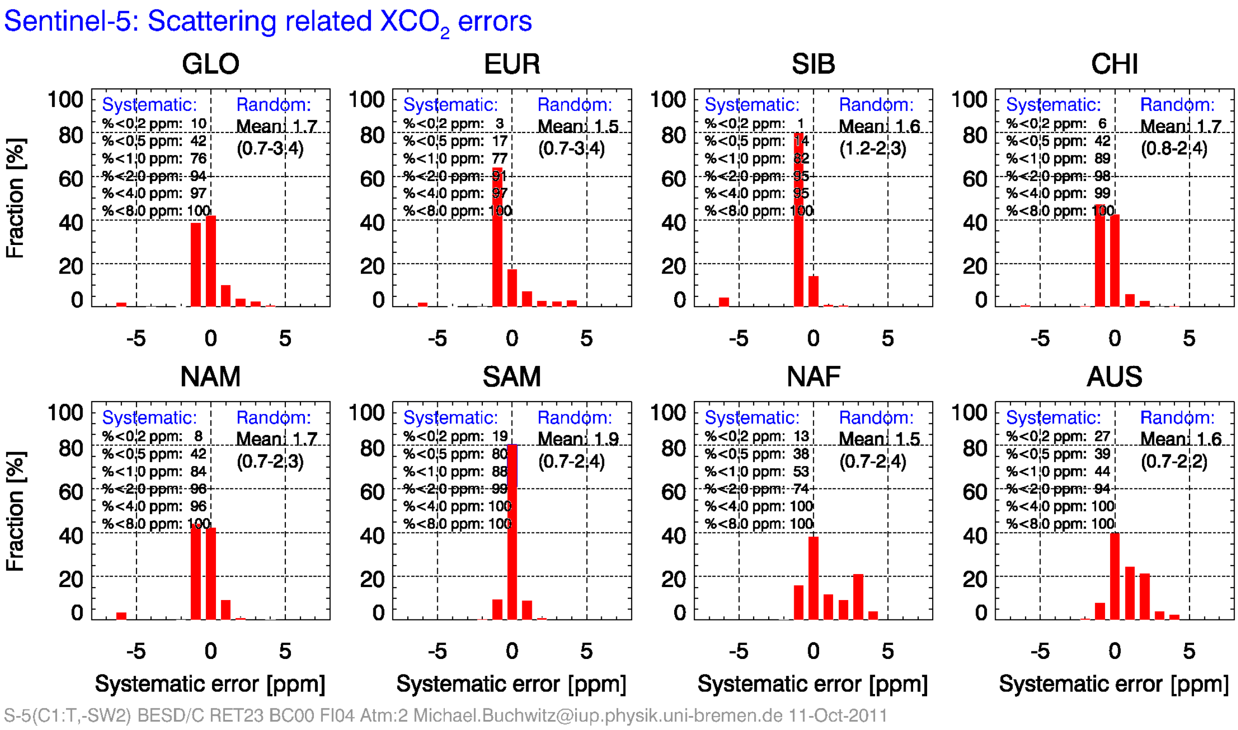

Figure 6-9: As Figure 6-2 but for ATM02.

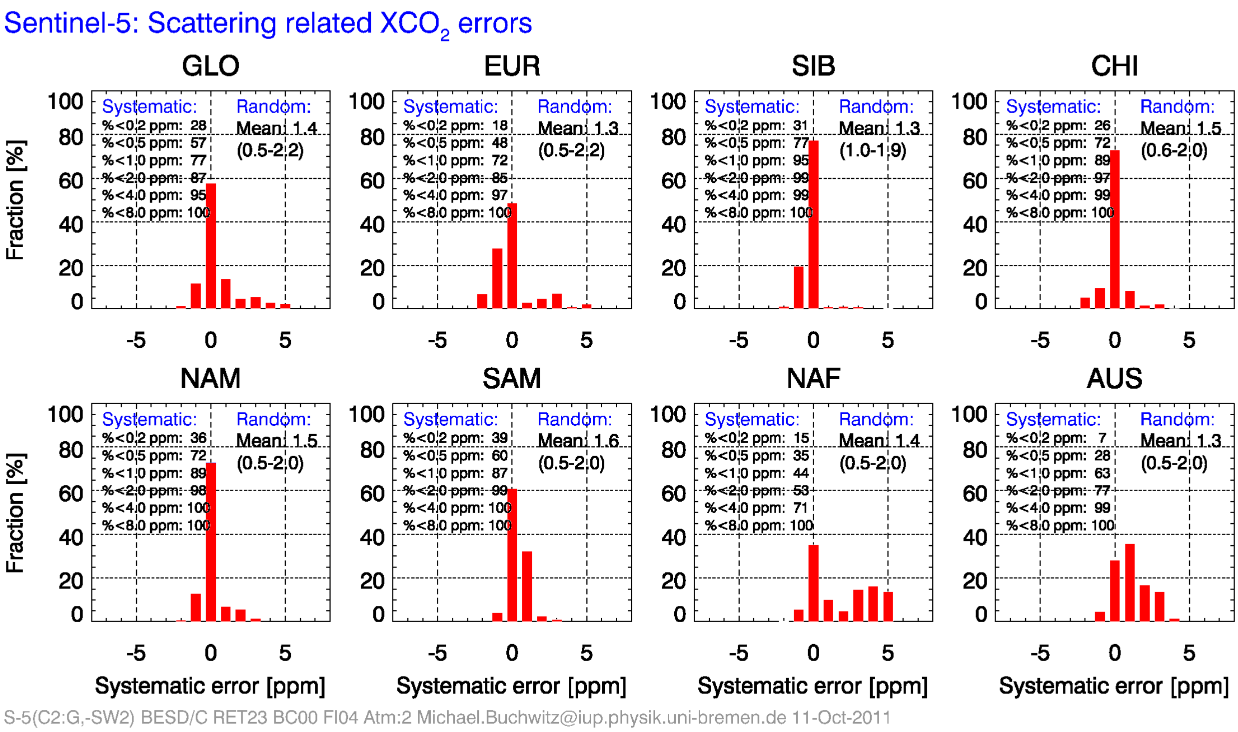

Figure 6-10: As Figure 6-3 but for ATM02.

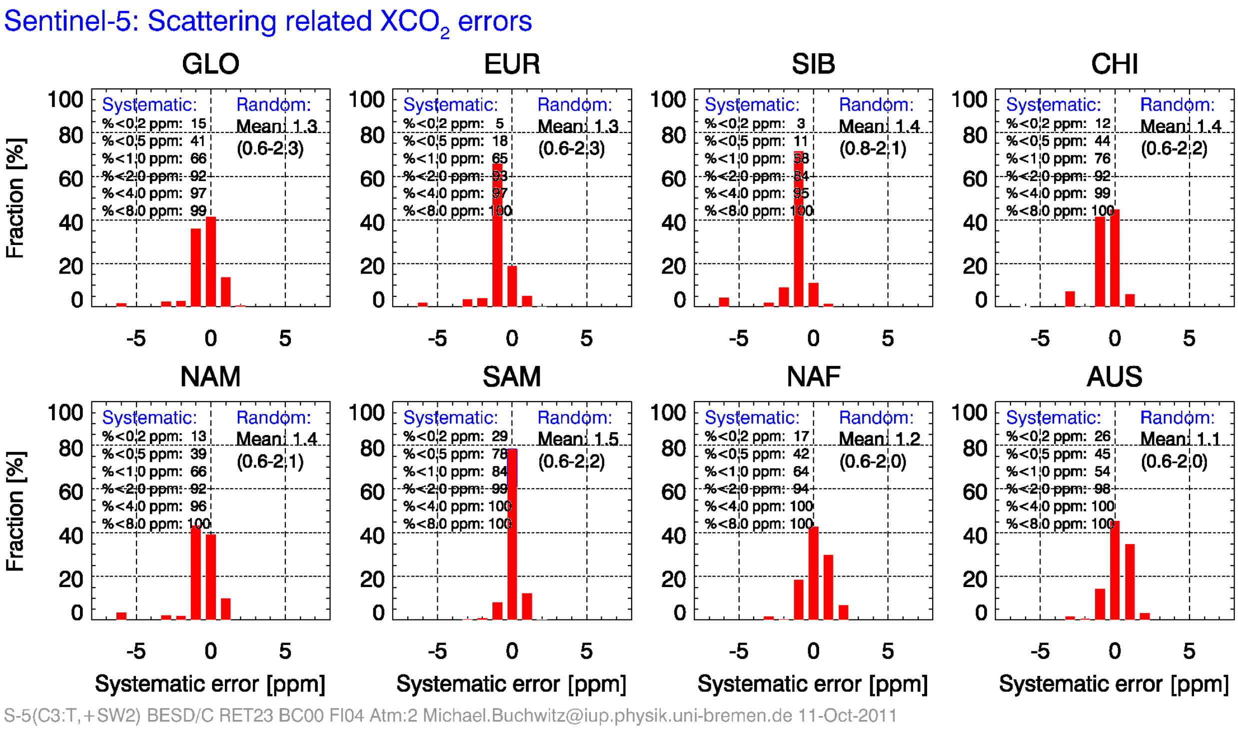

Figure 6-11: As Figure 6-4 but for ATM02.

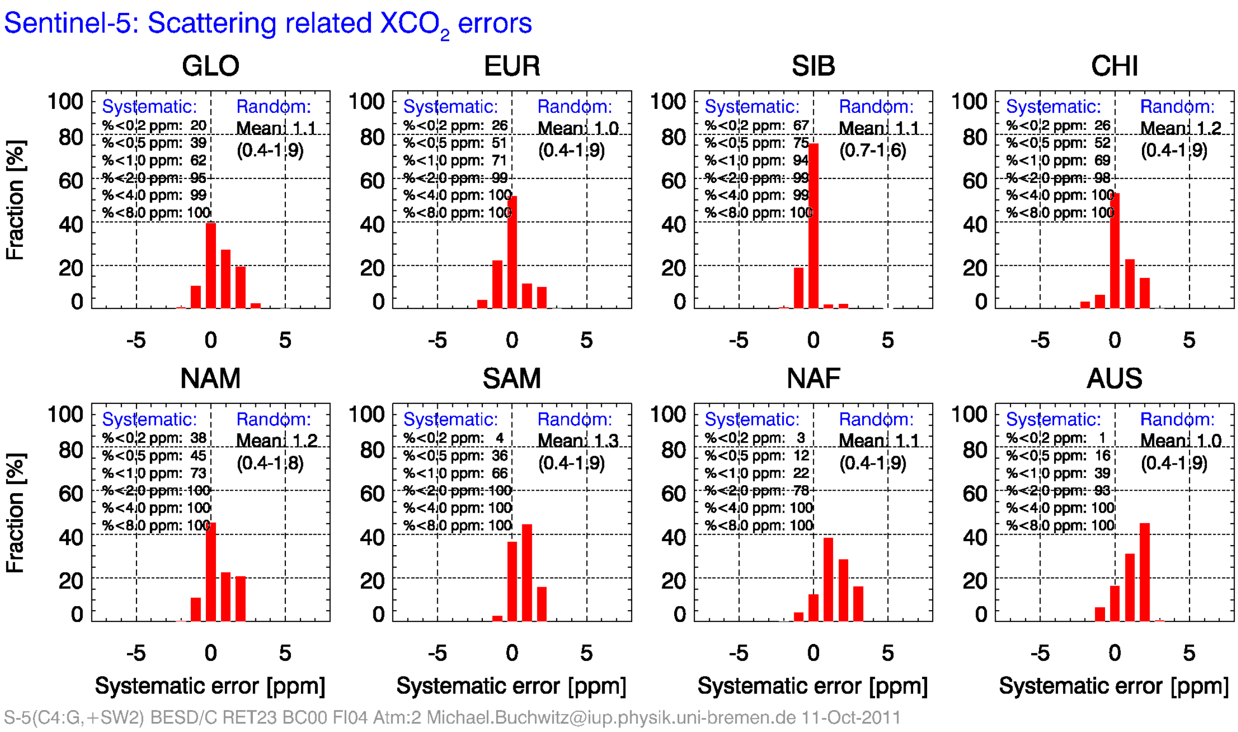

Figure 6-12: As Figure 6-5 but for ATM02.

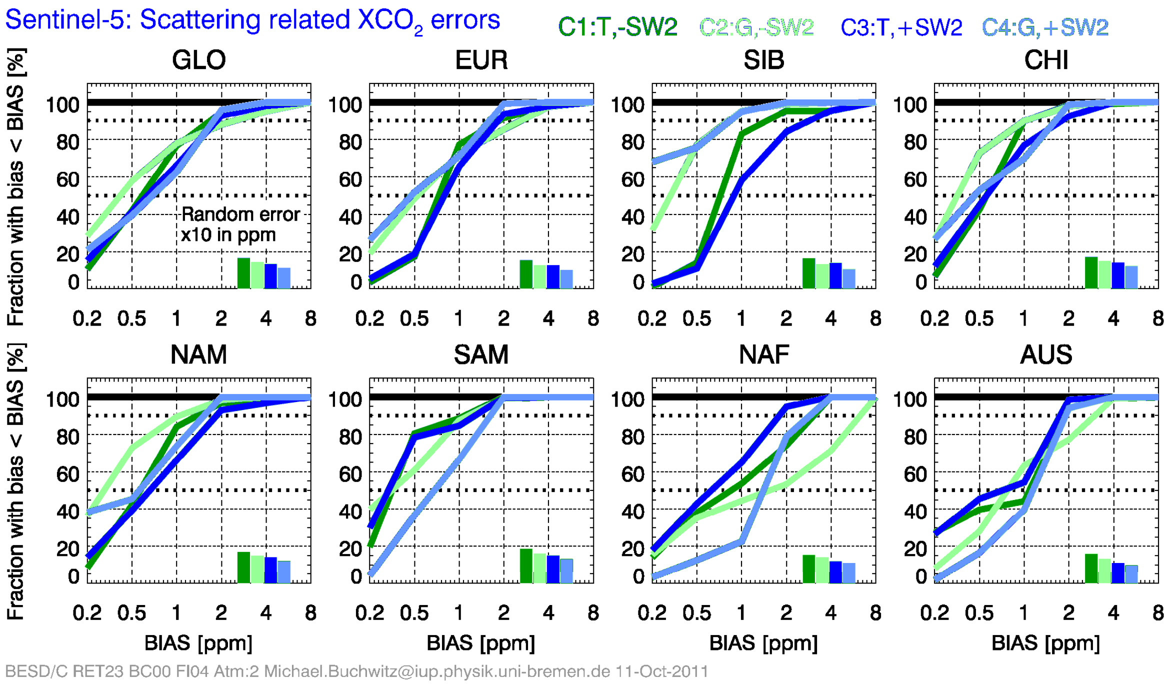

Figure 6-13: As Figure 6-6 but for ATM02.

Table 6-3: Systematic and random XCO_2 errors for all four configurations C1-C4 for the two atmospheres ATM01 (left) and ATM02 (right)

	Systematic Error Fraction of scenarios with systematic error < X ppm In % of scenes (after quality filtering)							
X [ppm]	ATM01				ATM02			
	T-SW2	G-SW2	T+SW2	G+SW2	T-SW2	G-SW2	T+SW2	G+SW2
0.2	47	17	30	37	10	28	15	20
0.5	79	40	59	55	42	57	41	39
1.0	82	75	76	90	76	77	66	62
2.0	95	87	94	99	94	87	92	95
4.0	99	94	97	99	97	95	97	95
8.0	99	100	99	100	100	100	99	100
Random error [ppm] (mean value and range)	1.6 (0.7-3.4)	1.4 (0.5-2.0)	1.4 (0.6-2.3)	1.1 (0.4-1.9)	1.7 (0.7-3.4)	1.4 (0.5-2.2)	1.3 (0.6-2.3)	1.1 (0.4-1.9)
	No need to consider averaging kernels as no smoothing error as true CO_2 = *a priori* CO_2				Additional contribution from smoothing error as averaging kernels not considered			

6.2.2.3. Summary and discussions

The purpose under the present section was to investigate to what extent systematic XCO_2 retrieval errors derived from S-5-UVNS sounder stand alone, mainly due to clouds and aerosols, can be reduced by moving towards a CO_2 dedicated instrument such as OCO.

The proposed approach here is similar to the approach employed under chapter 4. The difference is the study, in addition to the current baseline S-5 instrument configuration (so-called "T-SW2" configuration: NIR-2 band with threshold spectral resolution of 0.4 nm per FWHM, SWIR-1 band and no SWIR-2) three configurations for an improved instrument: "G-SW2" with an improved NIR-2 band), "T+SW2" with the SWIR-2 spectral region added and "G+SW2" which considered as well the addition of the SWIR-2 spectral band and the improved spectral resolution in the NIR-2.

Simulated S-5-UVNS observations have been generated for 14400 cases (*i.e.* 1800 scenes x 4 instrument configurations x 2 model atmospheres with different CO_2 profiles). The OEM-based BESD retrieval algorithm has been applied to all simulated observation to quantify random and systematic XCO_2 retrieval errors.

The main conclusions in the present section may be summarised as follows:

- **Random XCO_2 errors:** It has been shown that the XCO_2 random error, *i.e.* the single measurement XCO_2 precision, can be significantly improved using an improved instrument configuration. In average, the single observation precision is typically 1.7 ppm for "T-SW2", 1.4 ppm for "G-SW2", 1.4 ppm for "T+SW2", and 1.1 ppm for "G+SW2". The range of precision values in terms of extreme (*i.e.* min/max) values reduces from 0.7-3.4 ppm for "T-SW2" to 0.4-1.9 ppm for "G+SW2", *i.e.* roughly improves by a factor of two.
- **Systematic XCO_2 errors caused by aerosols and clouds:** The results related to such a systematic error are much more complex and less clear compared to the random error. A better instrument did not result systematically in smaller systematic errors. This is most likely due to shortcomings of the BESD retrieval algorithm, which is under development at IUP-UB, and has not yet been applied to such an application. It appears that BESD is not yet able to reliably extract the additional information available in the radiance spectra of an improved instrument. These results points at a fundamental issue of the analysis method used for this chapter by IUP-UB. Therefore, no strong conclusions can be drawn from the IUP-UB analysis at this stage. A focus of future work at IUP-UB will be to investigate such results with the goal to further improve the BESD retrieval algorithm. This likely requires the full implementation of an iterative retrieval scheme with full coupling of BESD to (unfortunately very time consuming) on-line radiative transfer simulations. Within this study the tight schedule only permitted to perform first steps in this direction. In fact the underlying assumption of this study was that appropriate tools exist to reliably address all the aspects of this study. This was obviously not the case for all tools which have been used in this study.

6.2.3. ULe results

ULe has studied the following 4 instrument configurations: T-SW2, G-SW2*, T+SW2, G+SW2*. However, for the improved NIR-2 spectral resolution simulations (G), the SNR has been modified according to [RD8]. Thus, the '*' symbol have been added to the name of the instrument scenario to distinguish them from the simulations mentioned in section 6.2.1. Simulations named G+SW2 have been carried out also in addition with an unchanged SNR.

The summary of the XCO_2 retrieval results for the 4 instrument configuration studied in the present chapter and the instrument configuration from the chapter 4 are summarized in Table 6-4. In this table, the results are provided for all converged retrievals ('All') and for the retrievals filtered according to the filter used in chapter 4 ('Filter'). However, this filter had been established for the results for the "T-SW2" configuration and thus some adjustments are necessary for the other configurations. Therefore, results for a filter adjusted for the specific instrument configuration ('Filter 2') are also given. Values in brackets for 'Filter 2' give the results when snow surfaces are also omitted.

6.2.3.1. Focus on XCO_2 2-Band retrieval with improvement of the spectral resolution in the NIR-2

The method of 2-band retrieval (*i.e.* NIR-2 + SWIR-1 spectral domains) of XCO_2 was carried out with increased spectral resolution in NIR-2. This has been compared to the 2-band retrieval achieved under chapter 4. As can be seen from Figure 6-14 and Figure 6-15, the degrees of freedom (DOF) associated with the ensemble of retrieved parameters are increased by approximately 1. In particular, the degrees of freedom of CO_2 increase a little (a few tenths). As a consequence of this higher information content provided by the G-SW2* configuration, a higher number of simulations which are inversed tend to pass the filter (434 instead of 346) which results in an increase of the standard deviation of the XCO_2 bias from 1.86 ppm to 2.68 ppm. As can be seen from Figure 6-16 and Figure 6-17, large scatter error values, associated with the XCO_2 bias for G-SW2*, are observed close to the filter threshold of 1.2 ppm and for the smallest values of degrees of freedom for CO_2. To take into account this effect, an additional filter criterion has been included, based on the degrees of freedom for CO_2 with a threshold of 1.1 (so-called 'Filter 2a'). This additional criterion reduces the number of retrievals from 434 to 384 and the standard deviation of the XCO_2 bias to 1.86 ppm which is equivalent to the filtered results for T-SW2. Moreover, the precision or XCO_2 random error is almost identical between the configurations "T-SW2" and "G-SW2*" for the filtered results.

The only apparent advantage in the results of these simulations of improving the spectral resolution in NIR-2 seems to be an increase in the number of retrievals that pass the filter.

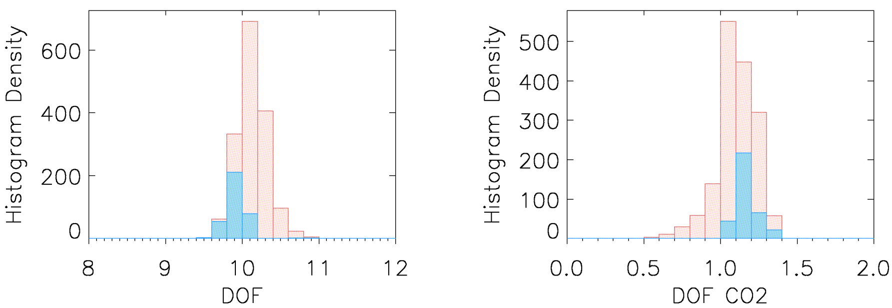

Figure 6-14: Degrees of freedom (left) for the 2-band retrieval from chapter 4 (T-SW2) and degrees of freedom for CO_2 (right). Red columns are all retrievals and blue columns are the filtered retrievals.

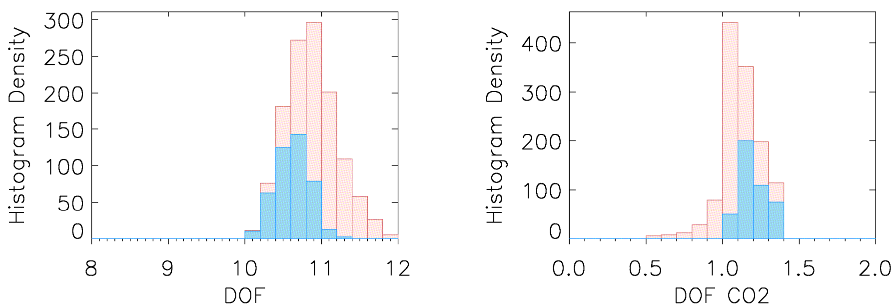

Figure 6-15: Degrees of freedom (left) for the 2-band retrieval with increased NIR-2 spectral resolution (G-SW2*) and degrees of freedom for CO_2 (right). Red columns are all retrievals and blue columns are the filtered retrievals.

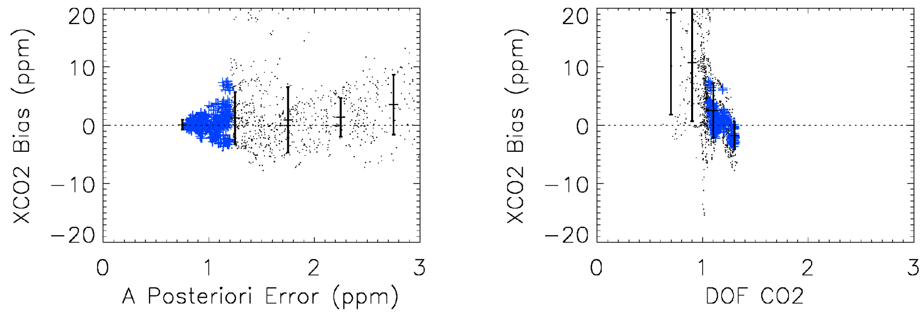

Figure 6-16: XCO_2 bias as a function of *a posteriori* error (left) and degrees of freedom of CO_2 (right) for G-SW2*. The black dots are all retrievals and the blue crosses are the filtered retrievals. Also given is the mean value and StdDev for all scenes and for a number of bins.

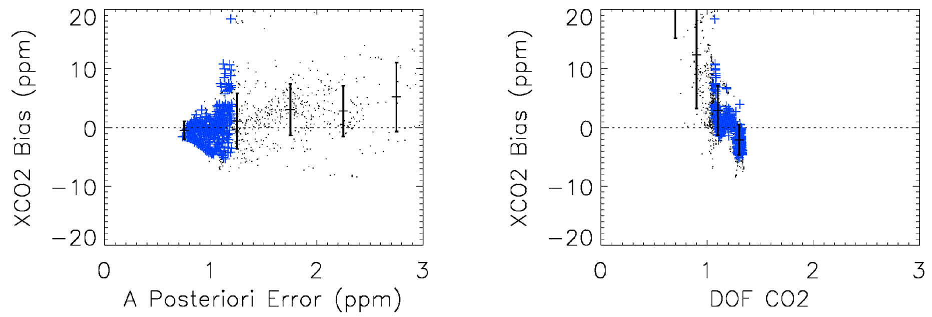

Figure 6-17: As Figure 6-16 but for the configuration G-SW2*

The details of the filtered retrieval results for the configurations "T-SW2" (Filter) and "G-SW2*" (Filter 2a) are shown in Figure 6-18. The spread of the XCO_2 systematic error is mostly larger for "G-SW2*". However, the configuration "G-SW2*" results in a clearly smaller range of XCO_2 systematic error values for retrievals with SZA=75° or cirrus height of 14 km.

The main difference between "T-SW2" and "G-SW2*" is the improvement of the spectral resolution in the O_2 A band with a degradation of the signal to noise ratio. Thus, the largest differences between both instrument configurations in the retrieval of aerosol and cirrus optical depths are expected to be observed.

Figure 6-19 and Figure 6-20 provide correlation plots of retrieved and true aerosol, cirrus and total optical depth together with the correlation coefficient and parameters of a linear fit. Indeed, it is found that the higher resolution of "G-SW2*" results in a slope close to unity between true and retrieved total optical depth. However, the correlation coefficients are unchanged between "G-SW2*" and "T-SW2" and also the retrieval of aerosol and cirrus optical depth themselves are not improved. This is not surprising as the 2-band retrieval will only optimize the light path associated with the O_2 A band region and thus a clear separation between cirrus and aerosol is difficult. It should also be pointed out that the setup of the aerosol profile in the simulation with a significant fraction of free tropospheric aerosol will result is some overlapping of aerosols and cirrus cloud which will be difficult (or impossible) to untangle for the retrieval.

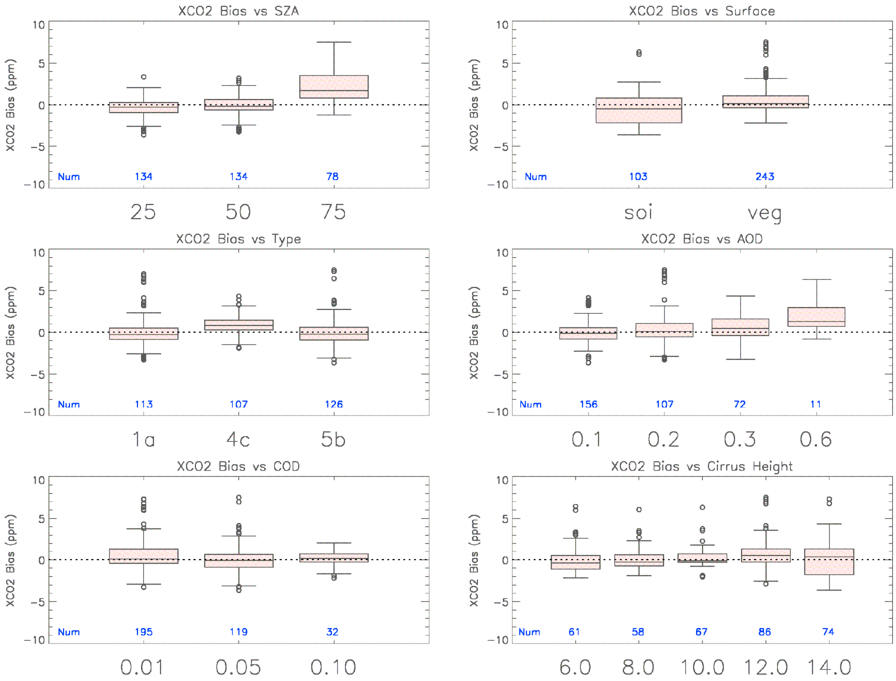

"T-SW2" configuration

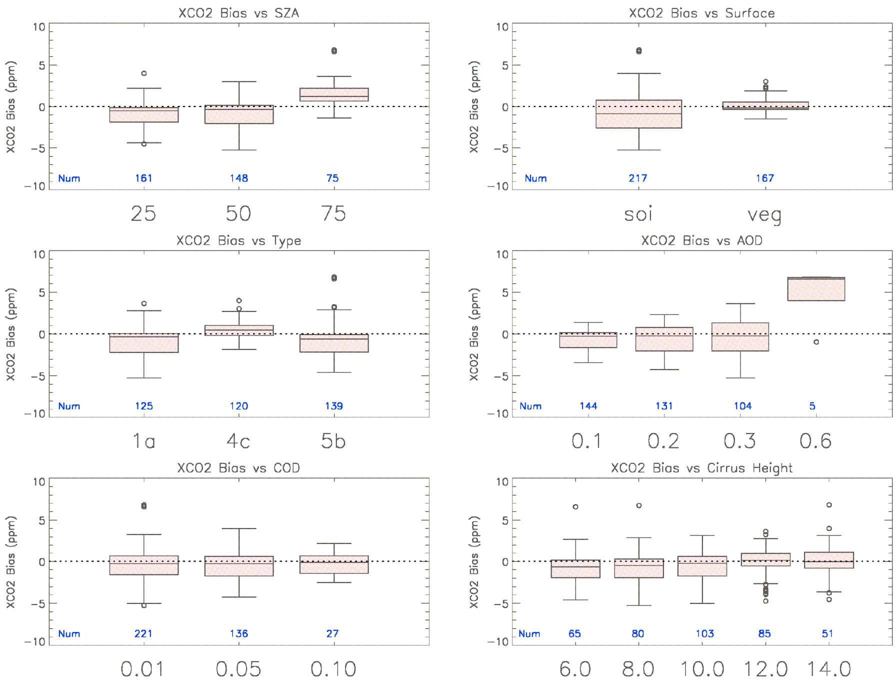

"G-SW2" configuration*

Figure 6-18: XCO_2 for different SZA, surfaces, aerosol types, aerosol optical depth, cirrus optical depth and cirrus height – Configuration "T-SW2" (top) and "G-SW2" bottom). The filter is applied for "T-SW2" and Filter2a for "G-SW2*"

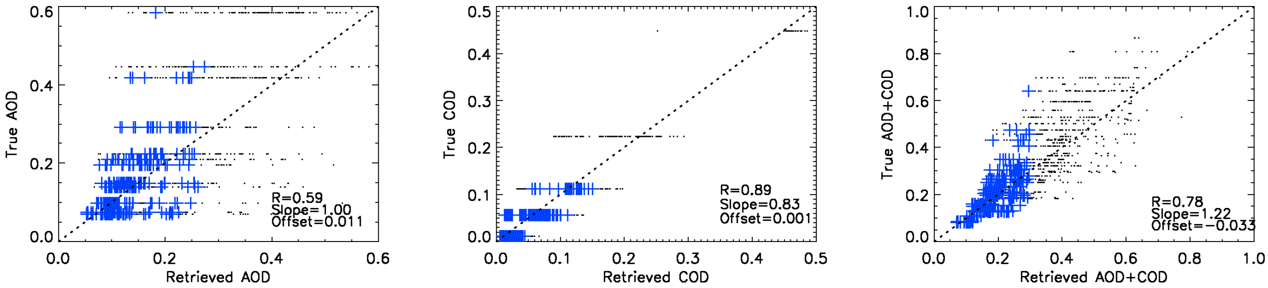

Figure 6-19: Correlation plots between true and retrieved aerosol optical depth (left), cirrus optical depth (middle) and total optical depth (right) for the configuration T-SW2. Black dots give all retrievals while blue crosses give the filtered retrievals.

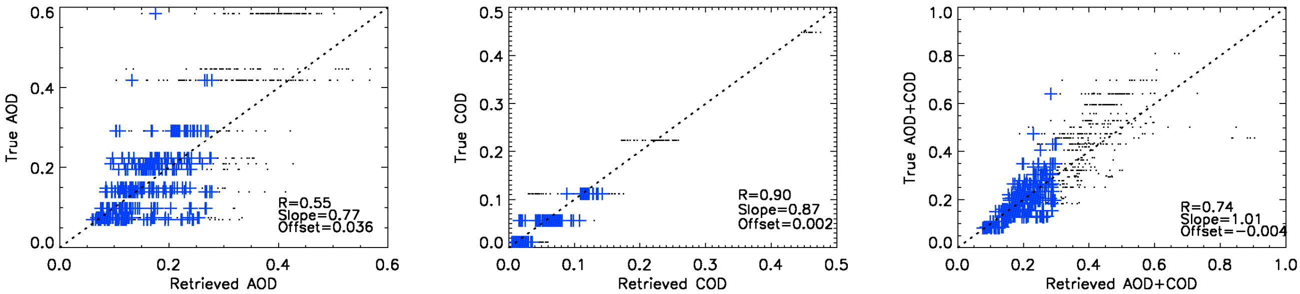

Figure 6-20: Correlation plots between true and retrieved aerosol optical depth (left), cirrus optical depth (middle) and total optical depth (right) for G-SW2*. Black dots give all retrievals and blue crosses give the filtered (*i.e.* Filter2a) retrievals.

6.2.3.2. Focus on XCO_2 3-Band retrieval

This section provides comparisons between the XCO_2 2-band and 3-band retrievals using the threshold spectral resolution of the NIR-2 spectral domain ("T-SW2" and "T+SW2"). The first result is that a higher number of retrievals fail to converge for the configuration "T+SW2". Nevertheless, a higher number of retrievals pass the filter for "T+SW2" compared to "T-SW2". Thus it can be assumed that the failed retrievals primarily represent cases that would not have passed the filter.

As shown by the top panel of Figure 6-21, adding the SWIR-2 spectral band (*cf.* configuration T+SW2) leads to an increase of the values of degrees of freedom by about 4 compared to T-SW2. Furthermore, values of degrees of freedom for CO_2 increase clearly (of approximately 0.5) with two distinct regimes that correspond to the 2 types of surface: vegetation and soil (retrievals related to ice surfaces are removed through the filter).

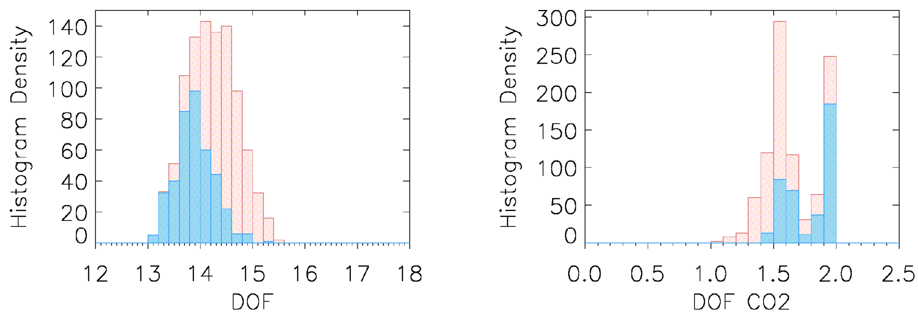

"T+SW2" configuration

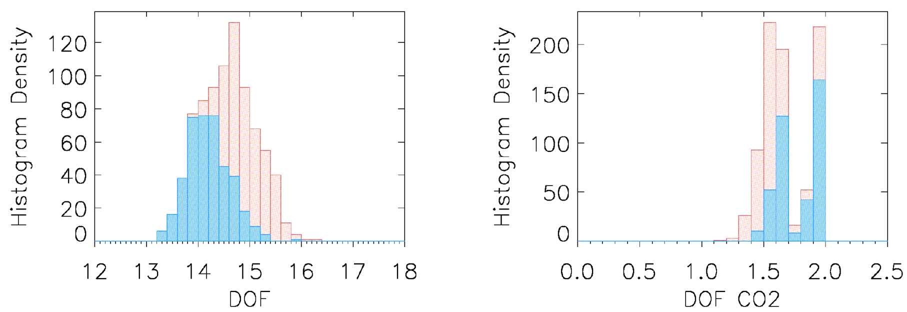

"G+SW2" configuration*

Figure 6-21: Degree of freedom (left) and degrees of freedom for CO_2 (right) for different configurations: T+SW2 (top) and G+SW2* (top). Red columns are all retrievals whereas blue columns are the filtered retrievals.

Due to the higher information content of the configuration "T+SW2", a higher number of retrievals meet the filter criteria compared to the configuration "T-SW2" (399 instead of 346). A clear improvement in the standard deviation of the XCO_2 bias, which is reduced to 1.43 ppm, is also observed. However, the number of simulations presenting non-converging steps (>2) in the retrieval procedure increases significantly. Such retrievals show a clear increased tendency to be biased and it is thus necessary to tighten the threshold for filtering the number of retrievals of non-converging steps (currently set to <4).

For all the 3-band retrievals, an addition filter (named Filter 2b) using the following criterion is defined:

- Number of diverging step < 2;
- AOT+COT < 0.4;
- DOF (CO_2) >1.5;
- CHI^2 < 1;
- P_{surf} bias < 10 hPa;
- XCO_2 *a posteriori* error < 1.3 ppm.

Note that the thresholds for the second and last criteria are larger than for the standard filter used so far and the thresholds for criteria 3, 4 and 5 are unchanged. Adopting this filter allows reducing the number of retrievals to 342 (which is very similar to the number of retrievals for the configuration "T-SW2" with filter) and further improves the standard deviation of the XCO_2 bias to 0.88 ppm. A few tens of retrievals over snow are selected by this filter. However, one might want to remove them as well, and thus the standard deviation reduces to 0.79 ppm. The spread of the XCO_2 biases obtained for "T+SW2" (top panel of Figure 6-22) is much smaller compared to "T-SW2" (bottom panel of Figure 6-22) and the median values show very little variation with the different geophysical parameters.

Figure 6-23 shows the correlations between retrieved and true aerosol, cirrus and total optical depth for the configuration "T+SW2". The correlation coefficients are closer to unity for all 3 cases (aerosol, cirrus and total) with slopes close to one. In particular, the retrieval of aerosol optical depth is largely improved compared to "T-SW2" which is likely the main driver for the improvements in XCO_2 bias.

Increasing the NIR-2 spectral resolution for the 3-band retrieval (*i.e.* G+SW2* configuration) leads to relatively small increase in degrees of freedom and degrees of freedom for CO_2 (bottom panel of Figure 6-21). Thus, the degradation of the signal-to-noise ratio mostly compensates the increased information content from the higher spectral resolution. Very similar retrieval results between "T+SW2" and "G+SW2*" have also been found when using the standard filter (see Table 6-4) and when using 'Filter 2b' the results seem to be a little improved. Details on the XCO_2 biases are shown in Figure 6-22 between configurations "T+SW2" and "G+SW2*". In particular, Figure 6-24 illustrates that "G+SW2*" configuration leads only to small improvements in the retrieval of aerosol, cirrus and total optical depth compared to "T+SW2*".

Simulations of S-5-UVNS spectra for the "G+SW2" configuration have been performed without degrading the signal to noise ratio. In this case, the number of retrievals selecting by the standard filter is increased by 100 compared to the "G+SW2*" configuration (*cf.* Table 6-4). The standard deviation of the bias increases also to 1.8 ppm. When adopting Filter 2b, the standard deviation becomes smaller with respect to "G+SW2*" and comparable to "T+SW2". When removing in addition snow scenes, a very clear improvement of the standard deviation of the XCO_2 bias is found with a value of 0.66 ppm which is smaller than for any other configuration. However, at the same time, the number of scenes is substantially reduced so that a comparison to the other configurations is somewhat problematic.

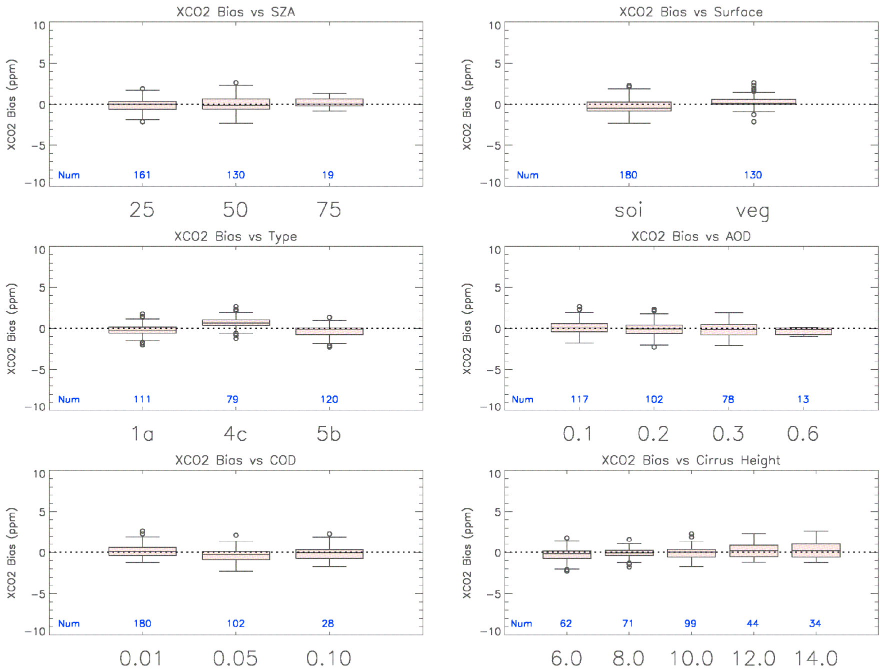

"T+SW2" configuration

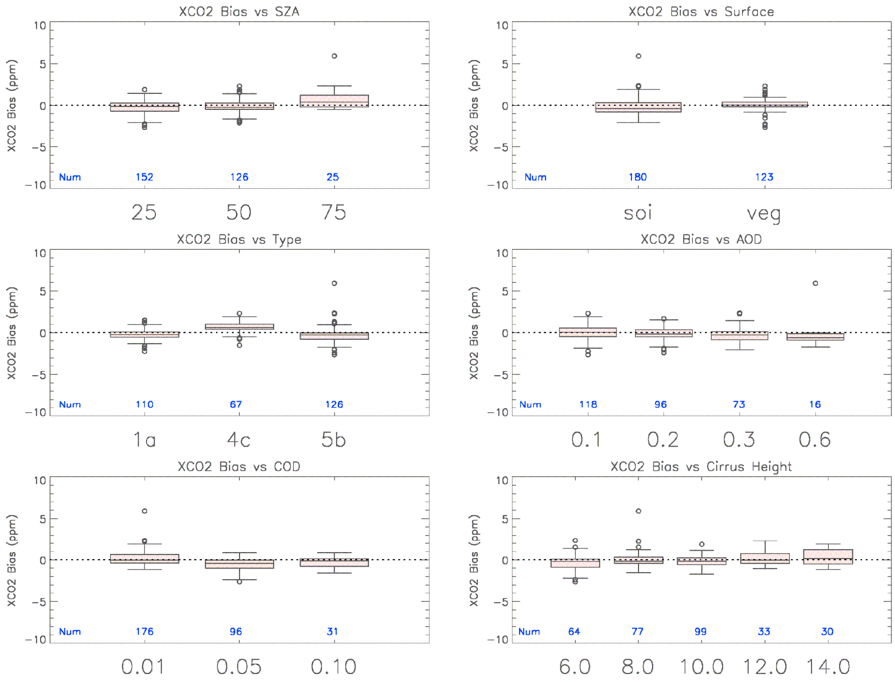

"G+SW2" configuration*

Figure 6-22: XCO_2 for different SZA, surfaces, aerosol types, aerosol optical depth, cirrus optical depth and cirrus height "T+SW2" (top) and "G+SW2*" (bottom). In both of these cases, Filter2b + snow filtering is applied.

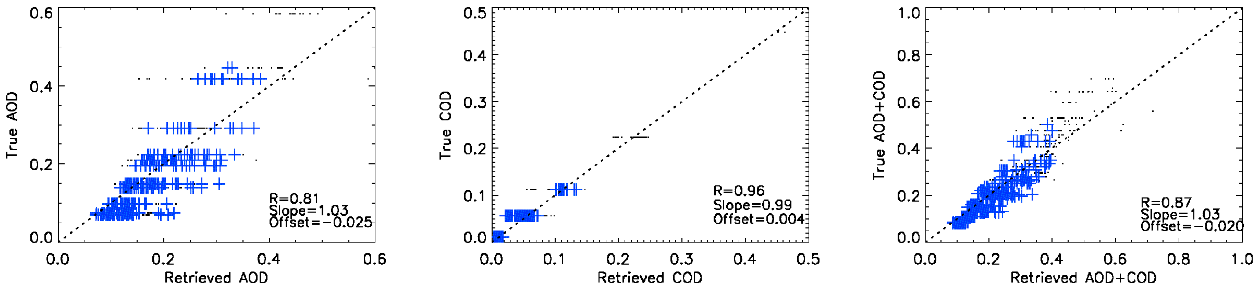

Figure 6-23: Correlation plots between true and retrieved aerosol optical depth (left), cirrus optical depth (middle) and total optical depth (right) for "T+SW2". Black dots give all retrievals and blue crosses give the filtered retrievals.

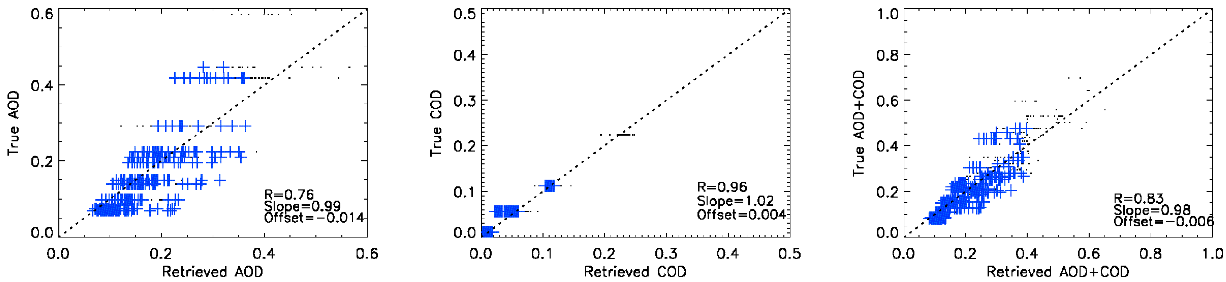

Figure 6-24: Correlation plots between true and retrieved aerosol optical depth (left), cirrus optical depth (middle) and total optical depth (right) for "G+SW2*". Black dots give all retrievals and blue crosses give the filtered retrievals.

Table 6-4: Summary of the retrieval results for the 4 instrument configuration studied in chapter 6 and the instrument configuration from chapter 4. Results are given for all converged retrievals ('All'), for the retrievals filtered according to the filter used in chapter 4 ('Filter') and for a filter adjusted for the specific instrument configuration ('Filter 2a' and ('Filter 2b'). Values in brackets for 'Filter 2b' give the results when also snow surfaces are omitted.

	T-SW2		*G-SW2**			*T+SW2*			*G+SW2**			*G+SW2*		
	All	**Filter**	**All**	**Filter**	**Filter2a**	**All**	**Filter**	**Filter2b**	**All**	**Filter**	**Filter2b**	**All**	**Filter**	**Filter2b**
Number of converged scenes	**1614**	**346**	**1235**	**434**	**384**	**957**	**399**	**342 (310)**	**826**	**403**	**365 (303)**	**718**	**506**	**352 (249)**
Mean XCO_2 systematic error (ppm)	**2.99**	**0.31**	**2.99**	**0.18**	**-0.43**	**1.28**	**0.28**	**0.09 (-0.03)**	**1.30**	**0.46**	**0.15 (-0.08)**	**1.06**	**0.59**	**0.26 (-0.08)**
StdDev XCO_2 systematic error (ppm)	**7.37**	**1.86**	**7.13**	**2.68**	**1.86**	**3.17**	**1.43**	**0.88 (0.79)**	**2.76**	**1.41**	**1.07 (0.88)**	**2.63**	**1.80**	**0.91 (0.66)**
Mean XCO_2 random Error (ppm)	**2.28**	**1.00**	**1.87**	**0.99**	**0.97**	**1.29**	**0.84**	**0.87 (0.83)**	**1.18**	**0.85**	**0.87 (0.80)**	**0.99**	**0.83**	**0.81 (0.73)**
StdDev XCO_2 random Error (ppm)	**1.74**	**0.12**	**1.61**	**0.12**	**0.12**	**0.68**	**0.14**	**0.17 (0.13)**	**0.57**	**0.16**	**0.18 (0.13)**	**0.46**	**0.16**	**0.17 (0.10)**

6.2.3.3. Summary and discussions

In the present exercise, ULe investigated how the XCO_2 retrieval performance changes when increasing the spectral resolution of the NIR-2 spectral domain and/or when including the SWIR-2 spectral region in order to achieve XCO_2 retrievals using simultaneously 3 spectral bands. The focus was on the XCO_2 systematic errors or "biases" introduced by aerosols and cirrus clouds which have been investigated with simulations for the same 2700 geophysical scenarios as in chapter 4.

Increasing the spectral resolution in the NIR-2 spectral domain when a XCO_2 2-band retrieval is considered (*i.e.* the G-SW2* configuration) increases the overall degrees of freedom of the retrieval, but the effect on the *a posteriori* error of XCO_2 is small. It clearly improves the quality of the retrieval of the total (aerosol + cirrus) optical depth but it does not lead to an improvement in the (standard deviation) XCO_2 biases.

Adding SWIR-2 (*i.e.* use a strategy of XCO_2 3-band retrieval) increases the overall degrees of freedom and the degrees of freedom for CO_2. Thus, as it can be expected, the *a posteriori* error decreases by 0.1-0.2 ppm for the mean XCO_2 random error for the filtered results.

A 3-band retrieval methodology shows a much improved retrieval performance in terms of XCO_2 biases compared to the 2-band retrieval methodology and the standard-deviation of the XCO_2 biases is less than 1 ppm when adopting a relatively strict filter. The 3-band retrieval also shows a much improved retrieval of the aerosol and cirrus optical depth. The performances of the XCO_2 retrievals show a very high improvement when considering a strategy of XCO_2 3-band retrieval. However, to increase the NIR-2 spectral resolution when considering only 2 spectral bands (*i.e.* NIR-2 + SWIR-1), the enhancements in terms of performances of the XCO_2 retrievals seem to be very small in comparison.

The fact that an improved retrieval performance with increased spectral resolution of NIR-2 is not observed is somewhat surprising and it would require a more detailed study to help better understand this behaviour. An important question is to which extent the results of this retrieval study depends on the systematic setup of the simulations. The aerosol profiles used in the simulations are very broad and there is no variation in the vertical distribution of the aerosol profiles and thus increased information content on the vertical aerosol distribution might have a small impact on the standard deviation of the XCO_2 biases. Variations in the cirrus profile are included in the simulations, but cirrus is already reasonably well retrieved when considering the threshold spectral resolution in the O_2 A band (specifically for the 3-band retrieval). Also, certain features of the retrieval such as retrieving logarithm of aerosol and cirrus extinction might limit the ability of the XCO_2 retrieval to take full advantage of the gain of information on the vertical distribution of aerosols and cirrus.

6.3. Analysis of the XCO_2 single-sounding retrieval error: enhanced Sentinel-5-UVNS stand alone focused on the ways to mitigate the impact of scattering effects

6.3.1. Introduction and background

6.3.1.1. Introduction

The software tool used in the present section 6.3, DISAMAR, has limitations. It can currently not fit the phase function; therefore it is kept as fixed and the same phase function is used for the simulated measurement and the retrieval. Similarly, it cannot fit simultaneously a cirrus cloud optical thickness and an aerosol optical thickness; therefore we focus here on pixels that contain aerosol but no cirrus cloud, and assume that a cirrus cloud has similar effects as a high altitude aerosol layer.

Results are compared for the following four cases:

- Use all three bands;
- Use O_2 A band and the 1600 nm CO_2 band (as in the chapter 4);
- Use O_2 A band and the 2050 nm CO_2 band;
- Use only the 2050 nm CO_2 band.

The specifications considered for the spectral bands are given in Table 6-2.

The standard algorithm for retrieving XCO_2 involves the use of different spectral bands:

- the 760 nm band for O_2;
- the weak 1600 nm band for CO_2;
- and the strong 2050 nm band for CO_2.

Such an algorithm will be used for the OCO-2 instrument and is already exploiting GOSAT observations. The argument given for using three bands is that the 760 nm band and the 2050 nm can be used to obtain information on the mean optical path of photons that are reflected back to the sensor. The mean optical path for the weak absorption band at 1600 nm is then obtained by interpolation.

However, by exploiting simulations, [RD40] found that using only the strong CO_2 band around 2050 nm is more accurate than the use of the three bands. In order to make suggestions for improvement of XCO_2 retrieval from the Sentinel-5-UVNS instrument, *e.g.* by adding the strong CO_2 band at 2050 nm, it seems necessary to investigate first what the best configuration would be.

If [RD40] assumption is correct, it would be better to ignore the 1600 nm band for CO_2 retrieval,. Further, simulations based only on the SWIR-2 spectral band would be sufficient when assuming that the surface pressure is known from NWP model calculations. Otherwise, the surface pressure has to be determined from the NIR-2 spectral band. However, a combined retrieval using simultaneously NIR-2 and SWIR-2 spectral domains is then not required; separate retrievals could be performed and then potential problems with co-registration and errors due to uncertainties in the wavelength dependence of the aerosol optical thickness could be mitigated.

6.3.2. Background

For example, for an atmosphere with a scattering layer (aerosol or cirrus) at some altitude in the atmosphere, it can be assumed that the temperature profile, the profiles of absorbing gases, and the absorption cross sections of the absorbing gases are known precisely. For obtaining a good XCO_2 retrieval by using only one spectral band, the following parameters have to be known:

- Surface pressure;
- Surface albedo;
- Altitude of the scattering layer;
- Optical thickness of the scattering layer;
- Single scattering albedo of the particles in the scattering layer;
- Phase function of the particles in that scattering layer.

Here, it is assumed that the wavelength range considered is small enough so that one can deal with spectrally averaged values. Furthermore, it is assumed that homogeneous pixels are considered for the XCO_2 retrievals, *i.e.* it is assumed that the optical properties do not vary over the pixel. Errors due to inhomogeneous pixels are discussed later. Generally, the parameters are not precisely known and they have to be derived from the measured spectrum or they have to be estimated using climatological information.

If more than one spectral band is used, the retrieval algorithm has to derive the parameters for each spectral band separately, unless the wavelength dependence of these parameters is known. For example, the weak absorption band at 1600 nm is not suited to derive the aerosol optical thickness and the altitude of the scattering layer. This is mainly due to the associated absorption which is weak in this spectral domain. The altitude of the scattering layer does not depend on the wavelength and it can be retrieved from other spectral bands. However, the optical thickness of the scattering layer does vary with wavelength. The optical thickness at 760 nm and the optical thickness at 2050 nm can be retrieved with some precision, provided the wavelength dependence of the optical thickness, for estimating the aerosol optical thickness at 1600 nm, is known. If this assumed wavelength dependence is incorrect, the atmospheric model used for the retrieval is inconsistent with the true atmosphere.

[RD40] used for their retrieval a least squares fit which becomes unstable when too many parameters are fitted. As a result, a simple parameterization for the aerosol properties is considered, assuming a power law for the size distribution of the particles. If the true atmosphere contains different aerosol components with different size distributions, the assumed model for the retrieval is inconsistent with respect to the aerosol models used when generating the simulated measured spectra. This inconsistency is a source of error that is not present when one spectral band is used. This might be the reason that they get better results using only the strong absorption band at 2050 nm.

In the present simulations, two aerosol components are used, *i.e.* dust particles and continental polluted particles, for simulation and retrieval. More parameters can be fit by considering the optimal estimation method than by using least squares fits. Moreover, some parameters will not be fit accurately as there is not enough information. In this manner, inconsistencies are avoided between the model used for the simulated reflectance spectrum and the model used in the retrieval.

6.3.3. Sentinel-5-UVNS stand alone

6.3.3.1. Investigations on the combinations of several spectral domains

Figure 6-25 shows the error in the retrieved CO_2 column for different combinations of spectral bands. It shows that the goal for the random error of 1 ppm (0.25%) is met for the following combinations:

- NIR-2 + SWIR–1 + SWIR–2;
- NIR-2 + SWIR–2;
- SWIR–2 with a SNR that is a factor of 2 larger than the reference case.

This goal is nearly met when using the SWIR–2 spectral domain with SNR for the reference case. Finally, it is not met for the configuration using simultaneously NIR-2 and SWIR–1 spectral regions.

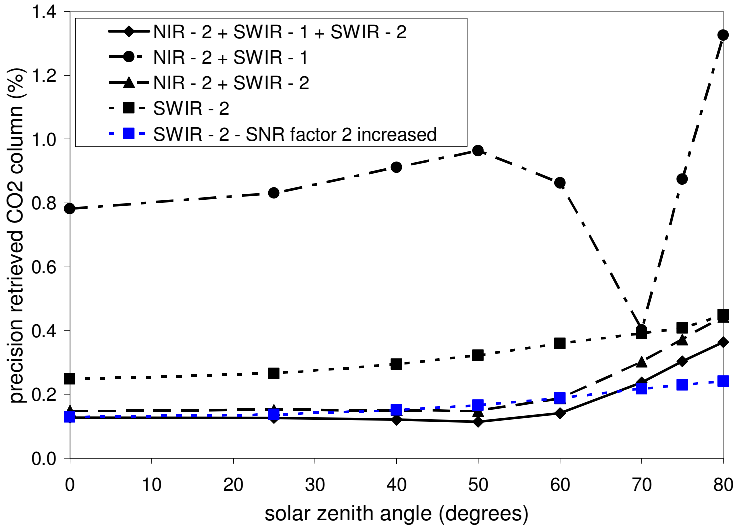

Figure 6-25: Precision of retrieved CO_2 column in percent plotted as function of the solar zenith angle for different combinations of spectral bands. For the NIR-2 spectral domain, the threshold setting was used.

The reduction of the XCO_2 error with solar zenith angle close to 70° when using simultaneously NIR-2 SWIR–1 has not been investigated because the requirement is not met for this combination of spectral bands. Note that the XCO_2 uncertainty here is larger than the random error discussed in chapter 4 because part of the XCO_2 systematic error of chapter 4 is here labelled as random error. Uncertainties in the aerosol model are assumed to be part of the random error and not part of a systematic error.

It is interesting to note that use of only the SWIR–2 band gives errors on the retrieved total column of CO_2 between the goal (0.25%; 1 ppm) and the threshold (0.50%; 2 ppm). That goal can be obtained if the signal to noise ratio in this band is increased with a factor of 1.5 - 2.

6.3.3.2. Focus on the averaging kernels

Figure 6-26 shows the averaging kernel for the column of CO_2 derived from the combination of SWIR-1 and SWIR-2 on one hand, and for each spectral band separately on the other hand when aerosol and cloud are absent in the atmosphere.

Figure 6-26 shows that the sensitivity for CO_2 at high altitudes is reduced if the SWIR-1 spectral region is used instead of the SWIR-2, which may be due to the weak absorption by CO_2 in SWIR-1. The altitude dependence (minimum at 12 km and maximum at 50 km) of the averaging kernel derived from SWIR-2 is probably largely due to the temperature and pressure dependence of the CO_2 absorption cross section. This last aspect has not been investigated. The sensitivity in the free troposphere is similar for all bands. Close to the surface, the sensitivity is larger when using SWIR-1 than using SWIR-2 spectral region. However, the differences in sensitivity are rather small and, as mentioned before, it is not advised to use only the SWIR-1 spectral band. Based on the averaging kernel, there is no preference for using both SWIR-1 and SWIR-2 spectral bands, compared to using only the SWIR-2 band.

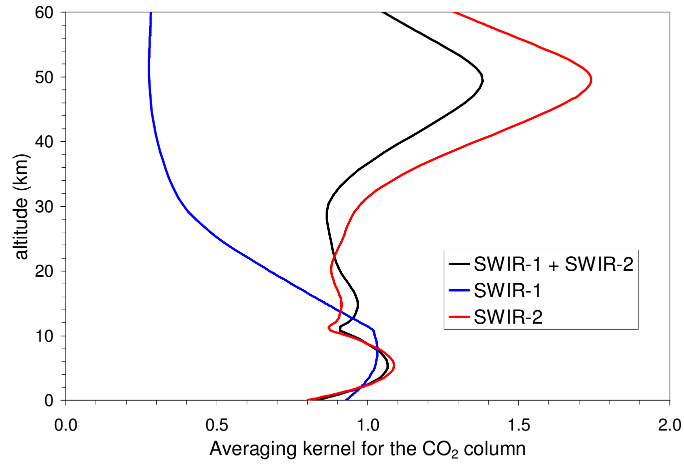

Figure 6-26: Averaging kernel for the CO_2 column plotted as function of altitude for the different spectral bands. The surface reflectance model is vegetation and the atmosphere contains no cloud or aerosol. The solar zenith angle is 25° and the viewing direction is nadir.

6.3.3.3. Changing the SNR for the different spectral bands

Numerical experiments were performed using the combination of the 3 spectral bands, *i.e.* NIR-2, SWIR–1 and SWIR–2 where the SNR of one of the spectral bands was multiplied by 0.5 or 2.0.

Figure 6-27 shows that changing SNR for the SWIR-2 spectral band has the most important impact (dotted lines). Increasing or decreasing the SNR of the NIR-2 or SWIR-1 spectral band has a lower influence on the uncertainty of the retrieved CO_2 column. This confirms that SWIR-2 spectral region is the main source of information for the retrieved CO_2 column. When increasing the SNR for SWIR-1 by a factor of 2, a reduction of the XCO_2 error from 0.30% to 0.27% is obtained. This result shows that SWIR-1 spectral region is able to give some additional information on the CO_2 column. If co-registration problems and uncertainties in the wavelength dependence would not occur, then the 3-band retrieval strategy is the most accurate. However, it is assumed here that the wavelength dependence of the aerosol components follow an angstrom law. If the actual wavelength dependence deviates from the angstrom law, the 3-band retrieval strategy might give larger errors. Deviations from the angstrom law have not been investigated.

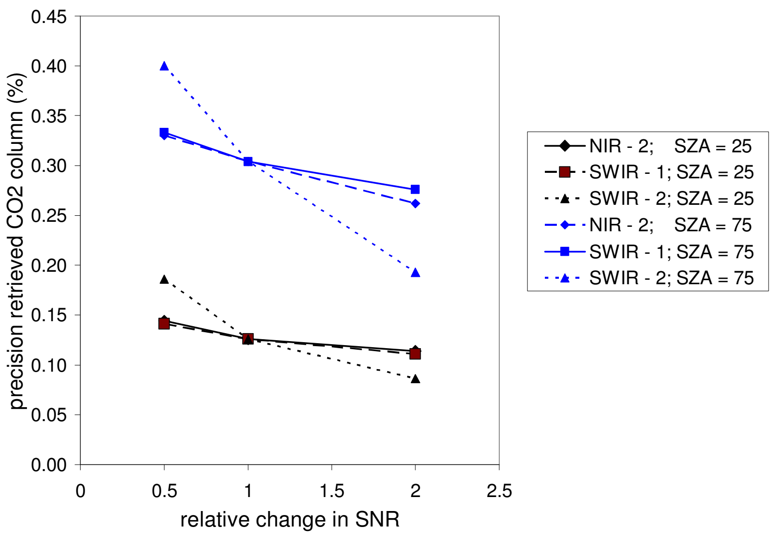

Figure 6-27: Effect of changing SNR in one of the three spectral bands plotted for two values of the solar zenith angle (25° and 75°).

6.3.3.4. Changing the *a priori* precision of the angstrom coefficient

Figure 6-28 shows the effect of changing the *a priori* error of the aerosol models on the quality of the retrieved CO_2 column. When *a priori* error in the angstrom coefficient increases, it means that the uncertainty of the size distribution of the aerosol components increases. However, Figure 6-25 shows that this has little effect on the error associated with the retrieved CO_2 column. The interpolated value of the aerosol optical thickness at 1600 nm using the retrieved aerosol optical thickness at 760 and 2050 nm is more accurate if the *a priori* error in the angstrom coefficient is smaller. Apparently, the interpolation error is not important here because the error in the CO_2 column increases only a little when the *a priori* error in the angstrom coefficient increases. Calculations indicate that addition of the SWIR-2 spectral band at 2050 nm leads to a more accurate retrieval of the CO_2 column by itself (see Figure 6-25) and not indirectly through a better estimate of the aerosol optical thickness at 1600 nm. This is also supported by the fact that XCO_2 retrieval using the combination of NIR-2 and SWIR-2 spectral bands is nearly as accurate as using all the three bands (see Figure 6-25).

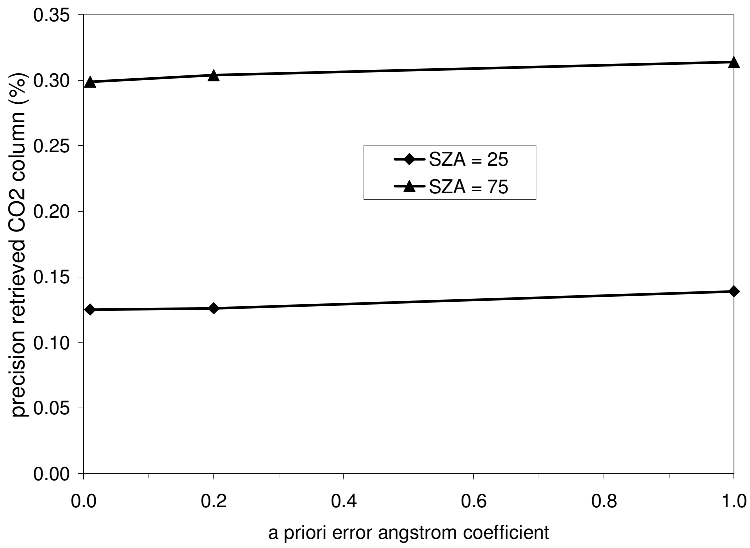

Figure 6-28: Effect of changing the *a priori* error of the angstrom coefficient for the two aerosol components plotted for two values of the solar zenith angle (25 and 75 °).

6.3.3.5. Surface pressure derived from S-5-UVNS measurements in NIR-2 spectral band

Unless the surface pressure can be obtained from a NWP model, it is necessary to retrieve the surface pressure from the oxygen A band. It is expected that a NWP model yields accurate mean value for the surface pressure but in some specific regions, biases of 2 – 10 hPa might occur. This would yield biases in the retrieved XCO_2 from 0.8 – 4.0 ppm. Therefore, it is useful to investigate the accuracy of the surface pressure derived from the O_2 A band.

For the simulations, only the oxygen A band is considered as absorbing gas, and only the dust aerosol model is used. No cirrus is present. The surface albedo is 0.20 (sand/soil or vegetation). Two values of the SZA (25° and 75°) and two values of the FWHM in the NIR-2 spectral band (0.06 nm and 0.40 nm) are considered. The SNR (500 at 758 nm for FWHM = 0.40 nm) is scaled using shot noise such that overall the same amount of photons is detected for both spectral resolutions. Furthermore, the *a priori* error of the surface pressure is changed from 5 hPa to 10 hPa. The other parameters to be fitted are the aerosol optical thickness, the surface albedo and the top pressure of the aerosol layer (Figure 6-29 only). The aerosol is located in the boundary layer (0-2 km). As before, all errors are assumed to be random errors and the precision of the retrieved surface pressure is plotted in Figure 6-29 and Figure 6-30.

Figure 6-29 shows the precision of the retrieved surface pressure as a function of the aerosol optical thickness for the two values of the SZA and the two values of the FWHM. The error in the retrieved surface pressure is rather large even for small aerosol optical thicknesses. An increase in spectral resolution from FWHM = 0.40 nm (dashed lines) to FWHM = 0.06 nm (solid lines) reduces the error with about one third, except for a large aerosol optical thickness and a SZA of 75°. Assuming an average error of 4 hPa, this means that the average error in XCO_2 is 1.6 ppm. The analysis of the correlation between the various errors shows that the error in the top pressure of the aerosol layer (*e.g.* the extension of the boundary layer) is strongly correlated with the error in the surface pressure. When repeating the calculations, but without fitting the top pressure of the aerosol layer, the associated results are shown in Figure 6-30. Therefore, the XCO_2 error is small for a SZA of 25° but becomes large for a SZA of 75° and an aerosol optical thickness larger than 0.1.

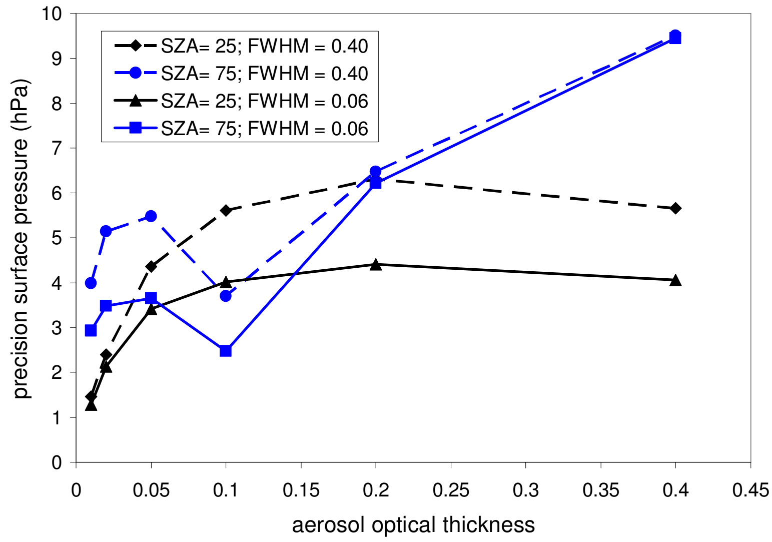

Figure 6-29: Precision of the retrieved surface pressure obtained from the NIR-2 band plotted as function of the aerosol optical thickness at 550 nm for two values of the solar zenith angle and two spectral resolutions.

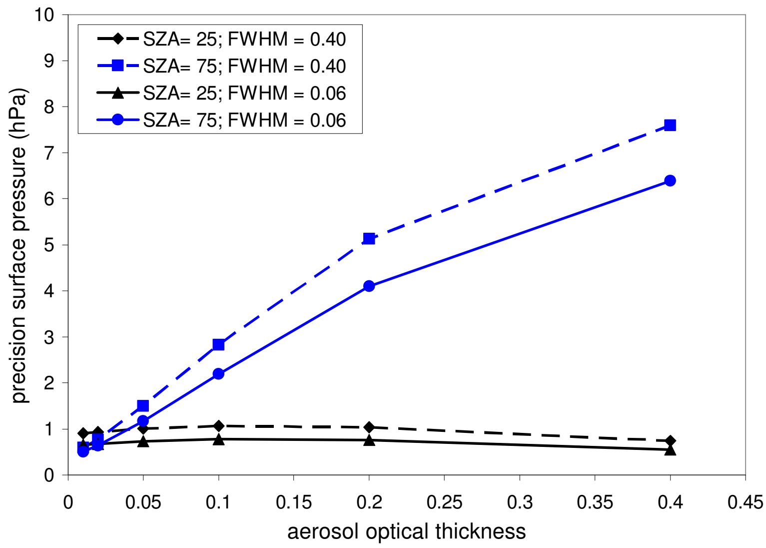

Figure 6-30: Same as Figure 6-29, but the top pressure of the aerosol layer is now not fitted.

Because the error is large if the top pressure of the aerosol layer is fitted, the option of not fitting the top pressure of the aerosol layer is further explored. The bias in the retrieved surface pressure is computed when the assumed top pressure differs from the retrieved pressure. By assuming that the actual top pressure is 900 hPa, XCO_2 retrievals are performed using top pressure values of 950 hPa and 850 hPa. That assumption is true for an extension of the boundary layer about 1 km. Then, XCO_2 retrievals assumed about 0.5 km and 1.5 km for the extension of the boundary layer. The bias in the retrieved surface pressure is given by Figure 6-31 for two values of the solar zenith angle. Figure 6-32 shows the retrieved aerosol optical thickness for the same cases as those in Figure 6-31.

Figure 6-31 shows that the retrieved surface pressure has a bias of less than 2 hPa as long as the aerosol optical thickness is less than 0.1. This means that fitting the top pressure of the aerosol layer is not required to derive the surface pressure from the NIR-2 spectral band. Figure 6-32 shows that the retrieved aerosol optical thickness differs substantially from the true aerosol optical thickness, showing that an effective aerosol optical thickness is derived. If we have an incorrect assumption of the extent of the boundary layer in the retrieval the aerosol optical thickness is adjusted in such a manner that about the same shielding of oxygen absorption occurs as in the simulated spectrum. This mechanism reduces the error in the retrieved surface pressure but also leads to an effective aerosol optical thickness that differs from the true value. In fact, this effective aerosol optical thickness varies with the surface albedo as illustrated in Figure 6-33.

Figure 6-33 shows that the effective optical thickness varies with the surface albedo For SZA value of 25° and an assumed top pressure of 950 hPa the effective aerosol optical thickness changes from 0.060 to 0.021 when the surface albedo changes from 0.10 to 0.30. This demonstrates that the shielding of oxygen absorption also depends on the surface albedo.

It is expected that similar shielding of absorption, but now by CO_2, will occur for the SWIR-1 and SWIR-2 spectral bands. However, unless the extension of the boundary layer is known, the retrieved effective optical thickness will differ from the true optical thickness for each of the three bands (for SWIR-1 this is not important as it contains little aerosol information) and the difference will depend on the surface albedo in the three bands. Hence, even if the true aerosol optical thickness is known precisely in all the three spectral bands, they can not be directly used without knowledge on the extension of the boundary layer.

This makes it difficult to use information from external sources (VII and / 3MI) in the retrieval algorithm. Many of these difficulties can be eliminated or, at least, mitigated if XCO_2 retrievals derived from the combination of different wavelength bands are not considered. The NIR-2 spectral band can be exploited for deriving the surface pressure and the SWIR-2 spectral band for estimating the CO_2 total column. When both of these spectral domains are used simultaneously, they provide the quantification of the XCO_2.

A practical approach might be to use two retrievals from the NIR-2 band. In the first retrieval the altitude of a scattering layer is fit contrary to the surface pressure. If the altitude is less than approximately 2 km, and the retrieved aerosol optical thickness is less than ~0.1, the pixel can be considered as exploitable for a second retrieval. In the second retrieval, the top of the boundary layer is fixed to a climatological average value and the surface pressure is fit. This will yield a fairly accurate value for the surface pressure.

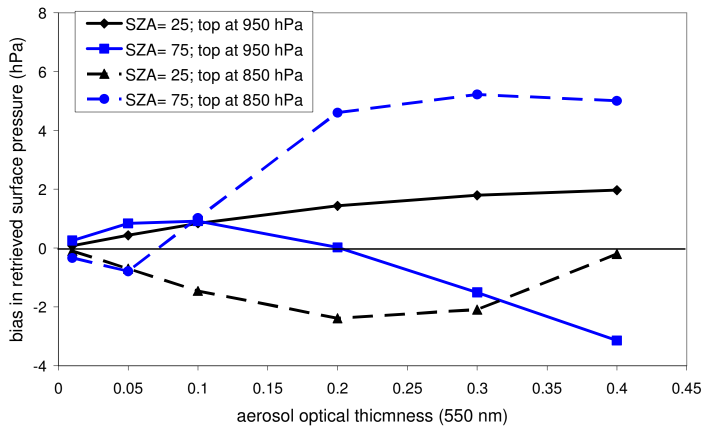

Figure 6-31: Bias in the retrieved surface pressure plotted as function of the aerosol optical thickness when the top of the boundary used in the simulation (900 hPa) differs from the top used in the retrieval (850 hPa or 950 hPa). The dust aerosol model is used and the surface albedo is 0.20. The fit parameters are the surface albedo, the aerosol optical thickness and the single scattering albedo of the aerosol particles. Results are given for two values of the solar zenith angle (SZA).

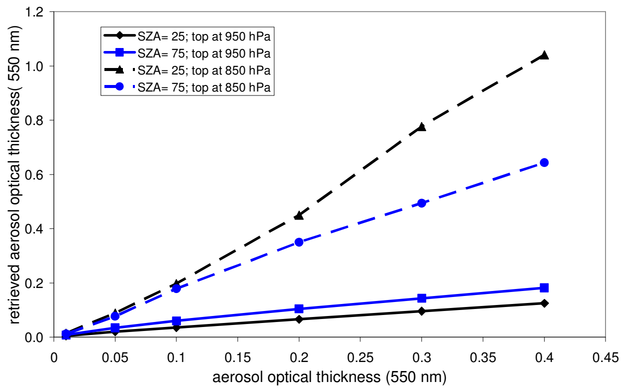

Figure 6-32: Retrieved aerosol optical thickness for the cases considered in Figure 6-31.

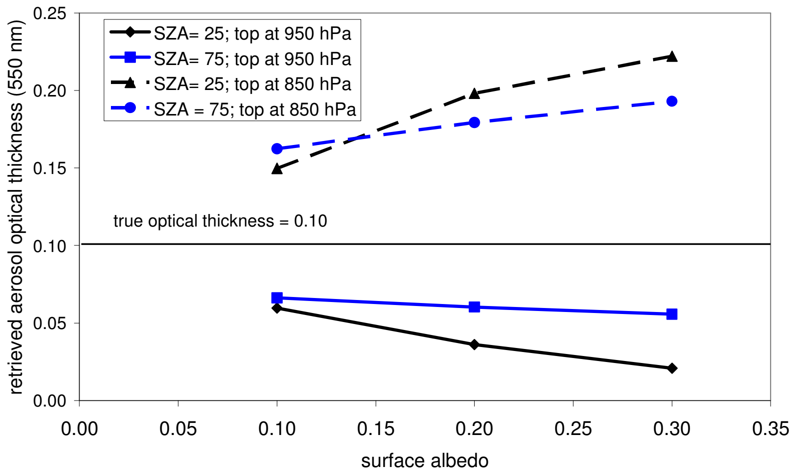

Figure 6-33: Retrieved (effective) aerosol optical thickness as in Figure 6-32, but only for a true optical thicknessof 0.10, and for different values of the surface albedo. The top of the aerosol layer used in the simulation is located at 900 hPa.

6.3.3.6. Co-alignment error

When more than one spectral band is used for XCO_2 retrieval, the same atmosphere is observed but the pixel in one band is shifted with respect to the other. It is expected that the overlap between the pixels in the spectral bands ranges from 75% to 95%. When a simultaneous XCO_2 retrieval is used for the spectral bands and a shifted pixel contains a cloud while the others do not contain it, severe convergence problems or a poor fit can be expected. By applying a filter of the retrievals, based on χ^2 and the number of iterations, very large errors in the retrieved XCO_2 can be eliminated.

A numerical experiment was performed where a background DE aerosol load was present for the entire pixel with an optical thickness of 0.1. In addition, a part of the pixel contained CP aerosol with an optical thickness of 0.3. The fraction covered with CP aerosol was 0.2 for NIR-2, 0.3 for SWIR-1, and 0.4 for SWIR-2. In the retrieval, the aerosol optical thickness was assumed to be the same for each part of the pixel and the angstrom coefficient, the aerosol optical thickness, and the surface albedo (in each spectral band) was fitted, apart from the CO_2 and H_2O columns. The surface model considered is vegetation and the solar zenith angle is 25 degrees. In this case, the error in the retrieved CO_2 column is small, 0.03%. This illustrates that sometimes co-alignment errors do not result is large errors in XCO_2. As calculations for a single retrieval are very time consuming, only a few examples were calculated. From these results it is expected that the XCO_2 errors are similar as those for inhomogeneous pixels discussed in 6.3.4. A full investigation of co-alignment errors would take 300 – 2000 retrieval experiments which is beyond the scope of this project.

It remains prudent to try to eliminate effects of co-alignment errors as much as possible by using individual retrievals for separate spectral bands whenever that is possible.

6.3.4. Potentialities to use VII or 3MI in addition of S-5-UVNS in the case of inhomogeneous scenes

In the previous sections, the optical properties are assumed to not vary within a pixel. However, the aerosol optical thickness, the presence of clouds and the surface may present some variations within a pixel. This leads to several effects:

1) Inhomogeneous illumination of the instrument slit leads to changes in the instrument line shape (slit function) resulting in pseudo noise. This was investigated in chapter 4 (using the combination of NIR-2 and SWIR-1 spectral domains) where it was found that errors in XCO_2 of several tenths ppm can be expected (up to 0.5 ppm or 0.12%).
2) An average value of the aerosol optical thickness and other aerosol parameters will be retrieved, leading to errors in the retrieved XCO_2 when the actual aerosol optical thickness varies over the pixel.
3) An average surface albedo is retrieved for each spectral band, which may result in errors in the retrieved the retrieved XCO_2.

The present section 6.3.4 tries to provide an (initial) estimate of effects 2 and 3 (mentioned above) using the independent pixel approximation. For that purpose, XCO_2 retrievals using only the SWIR-2 spectral band and the aerosol dust model are considered in the following sections.

6.3.4.1. Inhomogeneous aerosol load

In order to estimate the effect of an inhomogeneous aerosol load, the simulated S-5-UVNS reflectance spectrum was calculated assuming that half of the pixel is covered with dust aerosol and the other half is aerosol free. There is no cloud. Calculations were performed for a surface albedo of 0.05, two solar zenith angles (25° and 75°), two values of the altitude of the aerosol layer (1 km and 6 km), and several values of the aerosol optical thickness. During the retrieval, it is assumed that the aerosol covers the entire pixel.

As the model used for simulation differs from the model used for retrieval, iterations are needed to find a correct solution. Generally, the retrieved aerosol optical thickness is about half of the actual optical thickness because half of the pixel is covered with aerosol. The difference between the simulation and the retrieval leads to a bias in the retrieved XCO_2. Figure 6-34 shows the bias plotted as a function of the aerosol optical thickness.

Figure 6-34 shows that the bias increases with the aerosol optical thickness, solar zenith angle and altitude of the aerosol layer. The calculations are for an extreme case in which half of the pixel is aerosol free and the other half contains all the aerosols present in the observed scene. Regularly, a less extreme contrast will occur. For this extreme case a XCO_2 bias up to 4 ppm occurs for the elevated aerosol layer, a solar zenith angle of 75° and a large aerosol optical thickness. Therefore, it would be prudent to use a threshold for the retrieved optical thickness of ~0.1, and the retrieved altitude of the aerosol layer, say 2 km, and discard all pixels that do not meet these thresholds.

Although no calculations were performed for cirrus clouds, we can assume that similar XCO_2 errors as those for aerosol at 6 km altitude would occur for inhomogeneous cirrus clouds. If a threshold is used for the retrieved altitude of aerosol, most of the effects of substantial cirrus clouds will be eliminated.

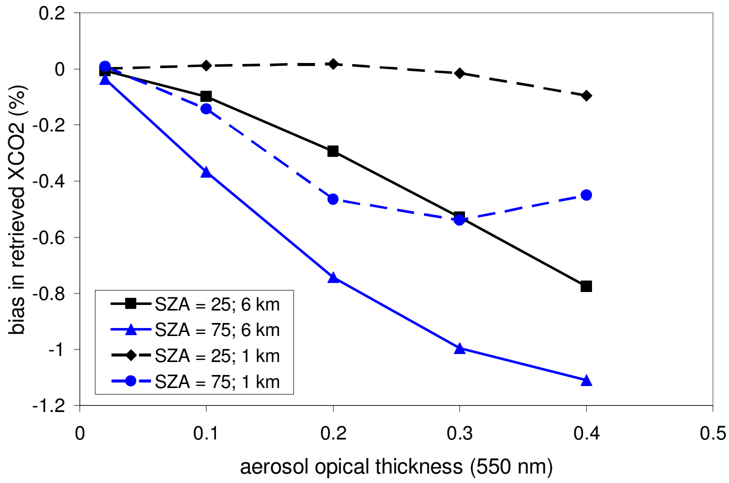

Figure 6-34: Error in the retrieved CO_2 column in percent when the aerosol covers half the pixel for the simulation and covers the full pixel for the retrieval, plotted as function of the true aerosol optical thickness. Here dust aerosol model was used and the SWIR-2 spectral band. Results are given for two altitudes of the aerosol layer and two solar zenith angles. The viewing direction is nadir.

6.3.4.2. Inhomogeneous surface albedo

For an initial estimate of the effects of an inhomogeneous surface albedo, half of the pixel is assumed to be covered by vegetation (albedo 0.05 in SWIR-2 spectral region) and half covered by sand/soil (albedo 0.30). The aerosol optical thickness is the same for each part of the pixel. The simulated S-5-UVNS reflectance spectrum was obtained by averaging the radiances for vegetation and sand/soil. Next retrieval was performed assuming a surface albedo that is the same for each part of the pixel. Typically, the retrieved surface albedo is 0.175. Calculations were performed for three values of the aerosol optical thickness, 2 altitudes of the aerosol layer and two values of the solar zenith angle. The bias in the retrieved CO_2 column due to an assumed constant surface albedo is shown in Figure 6-35. It clearly shows that for aerosol in the boundary layer the XCO_2 bias value is small. However, it becomes significant for elevated aerosol layers (and cirrus clouds) when they have a significant optical thickness. If one rejects pixels with a significant altitude (say > 2 km) for the scattering layer, the bias in XCO_2 can be kept small.

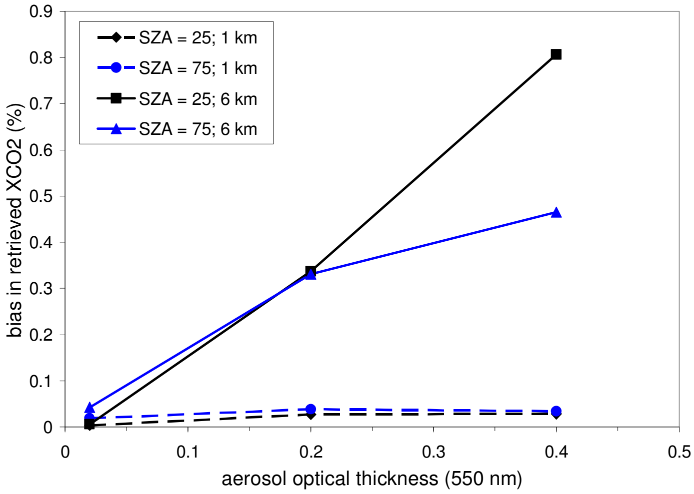

Figure 6-35: Error in the retrieved CO_2 column in percent when the half of the pixel is covered by vegetation and the other half by sand/soil, plotted as function of the aerosol optical thickness. The aerosol load is the same for each part of the pixel. Here the dust aerosol model was used and the SWIR-2 band. Results are given for two altitudes of the aerosol layer, two solar zenith angles, and three values of the aerosol optical thickness. The viewing direction is nadir. The bias is the result of assuming one surface albedo for all parts of the pixel in the retrieval.

6.3.4.3. Detecting inhomogeneous pixels

Inhomogeneous pixels where the surface albedo varies strongly can be detected using the imager VII which has a small pixel size. However, detecting pixels with an inhomogeneous aerosol load or inhomogeneous cirrus clouds will be difficult using an imager like VII. It will be difficult to distinguish between variations in the surface albedo and relatively small variations in radiance due to cirrus or aerosol.

The OMI instrument has so-called small pixels at two wavelengths. As they are not co-added, they have a higher spatial resolution. The small pixels are used to detect clouds as clouds make the pixel inhomogeneous and to correct for wavelength shifts due to inhomogeneous illumination of the slit. It remains to be investigated whether the use of small pixels would be feasible for the SWIR-2 spectral band. That might replace the need for imager data for detecting inhomogeneous surface albedo values. The use of imager data would complicate the retrieval algorithm substantially.

Inhomogeneous scenes will tend to increase the χ^2 parameter associated with the fit. Hence by filtering on χ^2 values, one might eliminate some or most of the inhomogeneous pixels. This last aspect remains to be investigated.

6.3.5. Summary and discussions

In chapter 4, it was found that the current configuration for the Sentinel-5-UVNS instrument is not suitable to retrieve XCO_2 with high quality. Hence a better XCO_2 retrieval algorithm and/or more spectral measurements (*i.e.* use more than NIR-2 and SWIR-1 spectral bands) are needed.

Adding the strong absorption band at 2050 nm helps to get considerably smaller errors. If great care is taken in the retrieval algorithm to avoid inconsistencies, this approach might yield the best results. To avoid inconsistencies two or more aerosol components with different size distributions have to be included in the retrieval. However, if the SNR of the strong absorption band is increased with a factor of 1.5 – 2, then preference is given to using only the strong absorption band for the retrieval of the CO_2 column. The main reasons are that inconsistencies with regard to the wavelength dependence of the aerosol properties are fully excluded and that possible problems with inter-band co-alignment issues are avoided.

From the point of view of the sensitivity for CO_2 as a function of altitude, as illustrated by the column averaging kernel, there is no reason to include the weak absorption band at 1600 nm, because the combined SWIR-1 and SWIR-2 spectral bands have nearly the same sensitivity.

The NIR-2 spectral band is used to obtain aerosol information as well as the surface pressure as it is expected that the surface pressure provided by NWP models will not be sufficiently accurate. In order to fit the surface pressure, a two-step retrieval is proposed, where the surface pressure is only fitted in the second step and the extension of the boundary layer is fixed to a climatological mean value.

Moreover, use of external information on the aerosol optical thickness, *e.g.* obtained from VII or 3MI, will not be practical for XCO_2 retrieval unless the extension of the boundary layer is well known. The main reason is that it is required to know the effective aerosol optical thickness, not the true optical thickness if the extent of the boundary layer is not known.

Finally, VII or 3MI could be used for filtering out Sentinel-5 observations, before performing XCO_2 retrievals. Typically, large XCO_2 errors are expected when observation pixels contain aerosol (or cirrus) at high altitude. Therefore, pixels with aerosol close to the surface have to be selected. The XCO_2 errors also tend to increase with the aerosol optical thickness and only pixels the retrieved aerosol optical thickness of which is small enough are then selected. In order to minimize such errors, a threshold can be used to select only those pixels where the altitude of the retrieved scattering layer is less than ~ 2 km and where the optical thickness of the scattering layer is less than 0.1 – 0.2.

Alternatively, spatial information might be used to identify inhomogeneous pixels. Then less constrained threshold values might be used. When exploiting inhomogeneous pixels where the aerosol load differs within the pixel considerable XCO_2 errors can occur. Large errors can also occur when the surface albedo varies with a pixel and there is a substantial amount of aerosol / cirrus at high altitudes.

This selection can be done using the SWIR-2 band, because the optical thickness in the CO_2 band is of interest. If only SWIR-1 is available, the NIR-2 band can be used as SWIR-1 is too weak to determine the aerosol optical thickness with sufficient precision. In addition, there are options to select only pixels :

- That converges after 3 or 4 iteration steps;
- That has a chi-squared that is sufficiently small.

If these selection procedures are not sufficient one might use VII to detect inhomogeneous pixels, based on the standard deviation of the radiances measured by VII. The standard deviation is calculated for all VII-pixels within the Sentinel-5 pixel considered.

If not enough pixels pass the test then one might consider corrections for inhomogeneous pixels, using the radiances measured by VII, assuming that the differences in radiances are due to differences in surface albedo. It is then assumed that the aerosol load is (nearly) homogeneous for the pixel. This will be approximately correct for background aerosol and photochemical smog, but probably not for aerosol plumes. A pattern recognition system might be necessary to detect aerosol plumes. Using calculations for 2 – 4 different values for the surface albedo can then reduce the error in XCO_2, even for elevated aerosol layers, thereby increasing the number of pixels where the retrieved XCO_2 is sufficiently accurate.

All the items highlighted above consist of our suggestions for filtering the Sentinel-5 observations and are of great interest to filter the "bad" retrievals. However, more work on this topic is required to determine precisely how to deal with inhomogeneous scenes.

7. First evaluation of the capabilities of the Sentinel-5 mission for monitoring the total CO_2 surface fluxes (natural and anthropogenic) at the global to regional scale

7.1. Introduction

7.1.1. Context and Objectives

In chapter 2 requirements in terms of CO_2 level 2 space-borne products have been addressed for specific CO_2 applications, with respect to the user needs and the challenging requirements currently addressed in the scientific community for obtaining accurate estimations of the CO_2 surface fluxes. The transfer of the so-called L4 requirements (*i.e.* requirements on the estimations of the surface fluxes) into CO_2 L2 requirements (*i.e.* the total column of CO_2) is in reality a difficult exercise. Indeed, the L4 requirements are not unique as they are directly related to specific characteristics: *e.g.* spatial scales, temporal scale and accuracy. Then depending on the exact objectives of each application, the requirements in terms of density of the remote sensing observations available over a given geographical area, the associated uncertainties, and the sensitivity to the surface can vary significantly from one application to another.

Moreover, as explained in section 2.5, page 54, transport inversion models are "typically" used for the estimations of the surface fluxes for exploiting the measurements of atmospheric CO_2 concentrations. Thus, the accessible requirements for the estimation of the CO_2 surface fluxes are also dependent on the errors that can be introduced by the atmospheric transport model. Typical errors induced by the model may be dependent on the following parameters:

- the methods of aggregation of the surface fluxes uncertainties over large areas (spatial correlations);
- the representation by the model of the diurnal and seasonal variations of the surface fluxes and the boundary layer height;
- the representation errors (difference between a point measurement and the averaged value over the model grid cell);
- the characterization (or not) of the correlations between space-borne observations;
- an accurate *a priori* knowledge of meteorological parameters.

Of course, the list above can be extended. As already explained in chapter 2, the requirements are mainly derived from a rigorous and critical review performed during the present project and all the expertise available in the consortium. However, such an exercise, with clear distinction between specific applications, is somewhat innovative and should be consolidated in the future. Indeed, the difficulties stated here show that very accurate requirements on the L2 products, in order to state if typical XCO_2 observations are really useful / exploitable (or not), can be derived in a comprehensive way by using a transport inversion model.

In particular XCO_2 requirements in section 2.5.5.1, page 59, are given for the following application "monitoring **total net CO_2 surface fluxes** (natural and anthropogenic) at the **global to regional scale (~500-1000 km)**". Such an application is directly related to the need to answer to the 2 following main topics:

- The feedback **of vegetation on climate change during the 21st century** (threshold);
- The **modelling of land-vegetation dynamics** (goal).

The XCO_2 requirements for this application (see explanations in section 2.5.5.1, page 59, and Table 2-7, page 70) are mainly derived from an exercise [RD30] using the "Mission CO_2 Simulator" jointly developed by LSCE and NOVELTIS (see sections 7.1.2 and 7.2.1). However, as the present application is related to very large scales, it is explained that these requirements must not be considered as definite requirements. Indeed, users shall not consider requirements on each parameter (*e.g.* spatial resolution, precision, systematic error etc…) alone but rather the combination of these requirements together.

Therefore, the main objective of the present chapter is to analyse the capabilities of the Sentinel-5-UVNS sounder to provide valuable information (*i.e.* estimations of CO_2 surface fluxes associated with suitable uncertainties) for this specific application, based on the current instrument specifications and so, the associated expected XCO_2 performances, as quantified in chapter 4. The attention of the reader is drawn on the fact that this exercise is preliminary (*i.e.* some consolidations could be imagined in the future) and is valid only for the application mentioned here, not for the applications related to smaller scales (*i.e.* city scale or local point sources).

7.1.2. Description of the proposed approach

The "Mission CO_2 Simulator" jointly developed by LSCE and NOVELTIS aims at linking the precision of atmospheric CO_2 concentration observations to a precision in terms of CO_2 fluxes emitted by the surface (land and ocean) at a regional or global scale, and for one or several observation networks (space-borne missions, network of ground stations, or a combination of them) [RD30]. By determining analytically the theoretical error reduction on the CO_2 surface fluxes that an observation network allows achieving, this simulator thus offers a very convenient solution to evaluate the relative potentials and compare the theoretical performances between several space borne mission concepts (defined by orbitography, observation geometry, spatial resolution, measurement uncertainty, etc.) in terms of error reduction on the CO_2 fluxes emitted by the surface.

The approach described in this chapter is summarized in Figure 7-1. Based on precise orbitography elements and observation configuration provided in [RD8] and [RD14], on the XCO_2 capabilities (*i.e.* random errors and systematic errors) quantified from the current instrument specifications (see Table 4-5, page 118), the "Mission CO_2 Simulator" is used with respect to application 1 for:

- Quantifying the Sentinel-5 capabilities in terms of theoretical error reductions on the CO_2 surface fluxes;
- Comparing the theoretical Sentinel-5 capabilities for L4 products with those of OCO;
- Quantifying the theoretical Sentinel-5 capabilities in terms of total *a posteriori* L4 error.

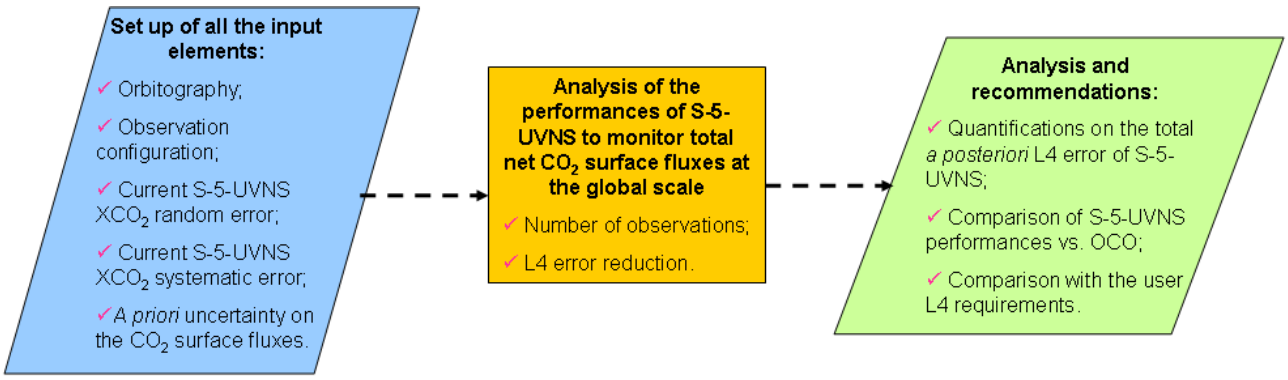

Figure 7-1: Description of the proposed approach under chapter 7.

7.2. Set up of the simulations

7.2.1. Methodology

The simulator is based on a Bayesian approach with a matrix implementation to solve the inverse problem and to compute the posterior error statistics of the CO_2 surface fluxes, given

- the sensitivity of the atmospheric CO_2 concentrations to the CO_2 surface fluxes (using an atmospheric transport model);
- and the *a priori* error statistics on observations and on the CO_2 surface fluxes.

The following notations are employed: **x** is the state vector corresponding to the spatio-temporal CO_2 fluxes emitted by the surface, $\mathbf{x_b}$ is an *a priori* estimation of these fluxes, and $\mathbf{P_b}$ is the *a priori* variance covariance matrix of the uncertainty on $\mathbf{x_b}$.

Given a set of observations of atmospheric CO_2 concentration **y**, and their associated error covariance matrix, **R**, the optimal state vector of the CO_2 surface fluxes **x** corresponds to the minimum of the following misfit function, under the assumption of Gaussian error distribution (**R** and $\mathbf{P_b}$):

$$J(x)= (x-x_b)P_b^{-1} (x-x_b)^T + (H(x)-y)R^{-1} (H(x)-y)^T \quad \textbf{Equation 7-1}$$

H is the observation operator that quantifies the sensitivity of the atmospheric CO_2 concentrations to the CO_2 surface fluxes. The simulator computes the *a posteriori* error covariance matrix that is associated to the solution CO_2 surface fluxes:

$$P_b' = (H^TR^{-1}H+ P_b^{-1})^{-1} \textbf{Equation 7-2}$$

The matrix **H** is determined by the LMDz atmospheric transport model [RD61] [RD80], and for the spatio-temporal coordinates of the observations **y**. The atmospheric CO_2 concentrations at the model resolution (3.75° in longitude, 2.5° in latitude, and 19 atmospheric levels) are convoluted vertically to derive column-integrated CO_2 concentrations. The surface fluxes to be optimized are aggregated into an ensemble of small size regions (296 "big" regions corresponding to thematically homogeneous areas with respect to land surface or to administrative/geopolitical regions - Figure 7-2, as well as 97 individual pixels over Europe).

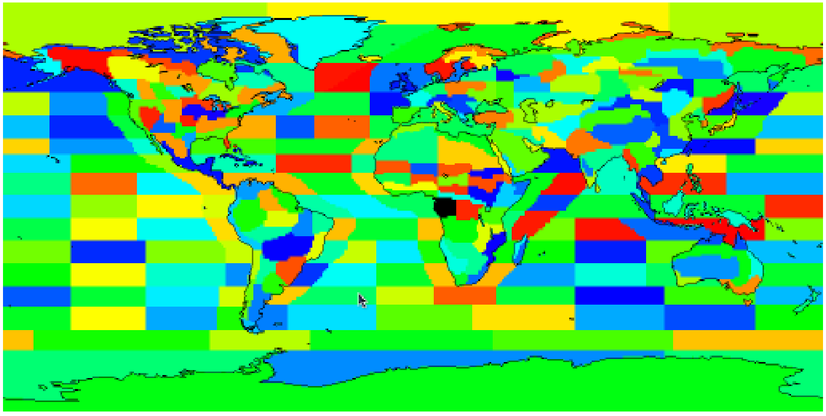

Figure 7-2: Map of the 296 regions.

The analysis of the *a posteriori* error covariance matrix $\mathbf{P_b'}$ with respect to the *a priori* error statistics on the surface CO_2 fluxes (matrix $\mathbf{P_b}$), allows computing the error reduction on the weekly and seasonal CO_2 fluxes for the ensemble of regions considered. The comparison of the error reduction achieved for different mission concepts allows evaluating their relative relevance with respect to the gain of information on the surface fluxes.

7.2.2. Matrix elements of the simulator

The simulator relies on the determination of three different matrices:

1) the error on the land surface fluxes (**P_b**);
2) the error on the observations (**R**);
3) the transport operator **H** that allows mapping the CO_2 fluxes to the observed CO_2 concentrations.

The approaches used to define these matrices, and the underlying assumption/simplifications, are detailed in the following sub-sections. These assumptions may have a large effect on the results (posterior error covariance matrix on the surface fluxes **P_b'**). Nevertheless, as these assumptions are the same for the several scenario studied, it is expected that they have little effect on the relative performances of the instruments considered and on the comparative exercise.

7.2.2.1. Transport operator

For a given instrument, the **H** matrix quantifies the sensitivity of the observations to the surface fluxes. It can be considered as the Jacobian matrix of the LMDz transport model for an ensemble of observations distributed in space and time, which is controlled by the geometric and orbital characteristics of each instrument considered.

In detail, the matrix **H** associated to each instrument corresponds to a sub-sample of the global response function of the model (independent on the observation configurations associated with the measurements). The latter are determined by the LMDz model for 296 predefined "big" regions (+ 97 pixels for Europe) (see Figure 7-2), on a 3.75° (longitude) x2.5° (latitude) grid, and for 19 vertical levels. The vertical dimension is then further reduced by computing the column averaged concentration XCO_2 accounting for the vertical weighting function (see section 2.5.2, page 58). Then, for a given instrument, the elements of the matrix **H** are related to the terms of the global response function associated to the observations (defined with the ensemble of triplets latitude, longitude, date).

The simulations (atmospheric CO_2 concentration in each grid cell) are performed assuming that the CO_2 tracers are emitted with a unitary flux uniformly distributed over each region and each 8 days period. The transport of the CO_2 tracer is done until the end of the year.

Offline simulations use advection terms which are derived from the LMDz model forced by the meteorological fields of 2005 provided by ECMWF.

7.2.2.2. *A priori* error on the land surface fluxes

The prior uncertainty on the surface fluxes (averaged over the year) is indicated in Figure 7-3. The matrix **P_b** contains the information on the uncertainties of the CO_2 fluxes emitted by the surface, as well as the spatio-temporal correlations on these uncertainties.

Over the oceans, the uncertainties on the CO_2 surface fluxes are smaller than those over land and are set to a constant value of 0.2 g C m^{-2} day^{-1}. Over land, the error is a function of the activity of vegetation (null fluxes and uncertainties over desert or ice surfaces, low uncertainties during the winter) and increases during the growing season; it is defined from the net respiration of land ecosystems simulated by the ORCHIDEE global vegetation model [RD64]. The value of the error over land varies typically between 1 and 5 g C m² day^{-1}.

The definition of the *a priori* variance covariance matrix on the surface fluxes accounts for the spatial and temporal correlation of the errors:

- Several studies have demonstrated the existence of a strong auto-correlation of the error associated with the weekly fluxes simulated by the ORCHIDEE model and with the observations when compared to few site specific flux data; the typical correlation length computed is of one month. Consequently, the temporal correlations are computed following an exponentially decreasing error correlation with a decay time of one month (4 weeks).

- Spatial correlations between errors associated with different "big" regions are defined using a exponentially decreasing law depending of the mean distance between the regions:

Correlation = exp(-distance/correlation_length) Equation 7-3

- The value of the correlation length is set to 500 km for land, and 1000 km for ocean.

The total global annual uncertainty is of the order of 3-4 g C m^{-2} day^{-1} over land, and less than 1 g C m^{-2} day^{-1} over ocean. The Figure 7-3, accounting for the spatial and temporal error correlation, shows a strong difference between land regions in the tropics and at high latitudes.

The *a priori* covariance matrix $\mathbf{P_b}$ defined in this manner should be considered as a crude approximation, as it neglects some characteristics of the carbon cycle. In particular, the error correlation terms are only partially determined: for instance the use of the exponential decay for the correlations in time implies that these are always positive whereas, in reality, negative correlations can occur (*e.g.* between the flux errors in summer and winter as an excess of carbon uptake during the growing season is likely to enhance the ecosystem respiration in the following months).

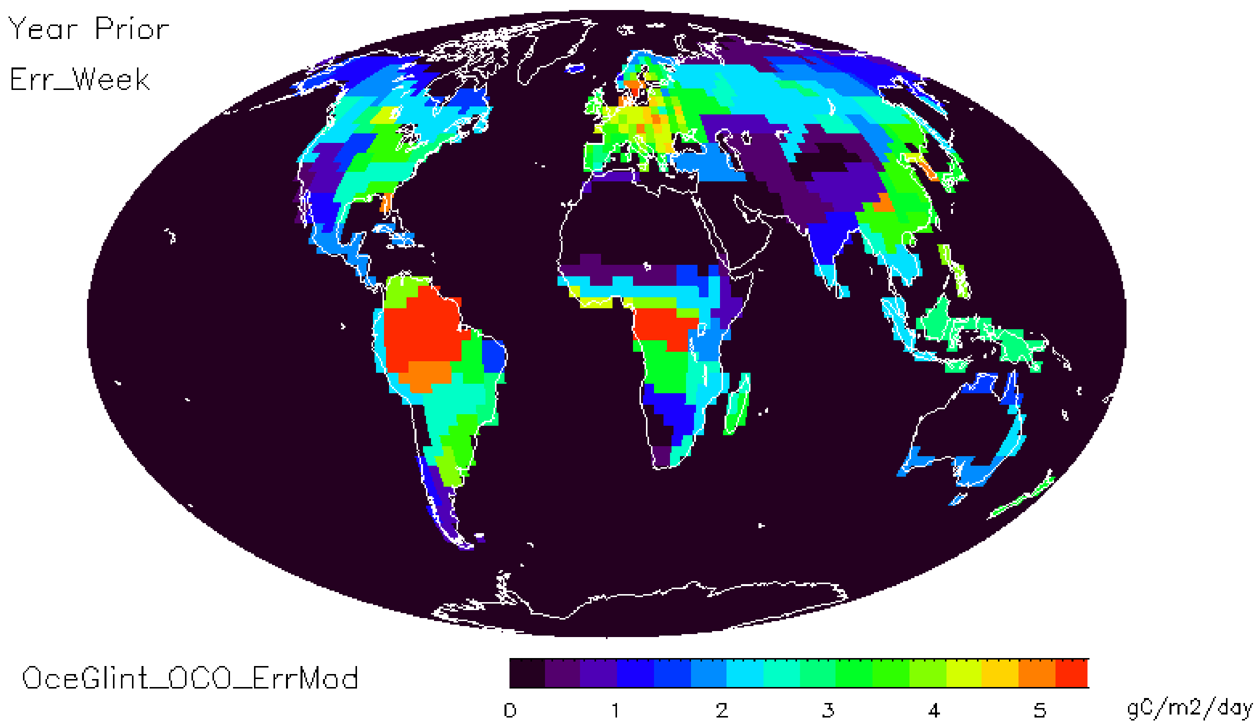

Figure 7-3: Annual *a priori* error (in g C m^{-2} day^{-1}) associated to each LMDz grid point (3.75°x2.5°).

7.2.2.3. XCO_2 Observation errors

Observation uncertainty, or observation error, is also a critical parameter to assess the potential impact of an observing system. The observation uncertainty concerns the difference between simulated and observed quantities and thus includes errors associated with atmospheric transport and also observation errors related to the retrieval processing. Note that the quadratic random error is discussed here. It is necessarily positive. The observation error for an individual observation may take positive or negative values. The observation error of individual measurements for a given location and time of observation is assumed to follow a Gaussian distribution with a "quadratic mean" that is discussed below.

The **R** matrix contains the error on the atmospheric CO_2 concentration products (vertically integrated over the atmospheric layers for the space-borne measurements) associated with each instrument. In the present study, these errors are considered as uncorrelated (**R** is therefore a diagonal matrix). The validity of this assumption is (partially) ensured by the aggregation of the observations (after aggregation, the observations are "far" apart: *i.e.* their distance is rather large, of 200 km).

For a selected observation, i.e. an observation that will be used in the optimisation scheme corresponding to several aggregated satellite observations (see section 7.2.3.1), the XCO_2 observation error depends on three components:

- a "random" error **Er** that decreases with the number of clear space-borne observations available in the considered model grid box;
- a "systematic" error **Es**;
- a "model" error **Em** that quantifies the uncertainty of the transport modelling.

The total error **Et** (expressed in ppm) is the quadratic sum of these three components:

$$Et^2 = Er^2 + Es^2 + Em^2 \quad \textbf{Equation 7-4}$$

It has to be noticed that several assumptions are considered for each source of error. These assumptions are clearly a limit of the present exercise: *i.e.* if these assumptions are changed in a near future, then all the results presented here may be not valid and a new study should be achieved. More details are given in the next sub-sections. These assumptions are highlighted with the summary of the results in the section 7.4 of the present chapter.

7.2.2.3.1 XCO_2 random observation error

The XCO_2 random error is here assumed to be associated with the radiometric noise of the spectral measurement. Thus, 2 measurements, which are spatially close, are expected to present independent radiometric noise independently: *i.e.* they are not correlated.

The "random" component of the error decreases as an inverse function of the number of observations as following:

$$Ea = Eperf / Nobs^k \qquad \textbf{Equation 7-5}$$

Where:

- **Eperf** is the level 2 performances in terms of XCO_2: *i.e.* the random error associated with each individual observation of the instrument considered
- **k** is a parameter that determines the decay law with the number of observations **Nobs**. In the case of completely uncorrelated errors, **k=0.5**.

Different assumptions are made for the OCO and Sentinel-5 instruments. They are detailed in section 7.2.3.

7.2.2.3.2 XCO_2 systematic observation error

By definition, contrary to the random error, the XCO_2 systematic error, for a given super observation, is not dependent on the number of observations. It is typically induced by an incorrect knowledge of aerosol information or an uncertainty of the temperature profile (for example). In that case, 2 close measurements (in space and time) may present identical or similar XCO_2 errors. However, the day-to-day variation, in a given box of the model, can be expected uncorrelated. Thus, the bias is here assumed systematic in the sense that for a same geophysical condition of the observation, the same XCO_2 error value is expected. But, as aerosol, temperature, and other geophysical parameters vary within each box, the XCO_2 error is not systematic from one day to another day. For example, the XCO_2 bias value may be positive one day, and negative another day. The same reasoning can be performed for the spatial distributions.

Therefore, it is assumed in this exercise that the XCO_2 systematic errors do not present a typical spatial/temporal structure (*i.e.* the systematic characteristics of the error only apply within a model grid box on a given day). The spatial distribution of the systematic error (between model grid boxes) is fully random, without any spatial structure and follows a Gaussian distribution.

Note that solving the inverse problem according to Equation 7-1 and Equation 7-2 is based on the assumption that the observation errors are Gaussian. Therefore, the term "systematic" only indicates that it is an observation that does not decrease by averaging within the model grid box.

The XCO_2 systematic error is difficult to determine before real data become available and past experience have shown that the actual products do not always have the expected level of accuracy. Typically, in other studies using the "Mission CO_2 Simulator" (*e.g.* in [RD30]), a very large number of radiative transfer simulations are performed in order to analyse the impact of geophysical parameters. For satellite missions using the differential absorption technique, it is found that surface reflectance, airmass (characterized by the solar and viewing angles) and aerosol optical thickness are key parameters. For instruments such as OCO, GOSAT, and SCIAMACHY, empirical formula taking into account the variation of the XCO_2 uncertainties, mostly the random errors, as a function of these key parameters have been developed [RD30].

In the present study, the simulations performed for the current Sentinel-5-UVNS in chapter 4 show that the systematic error does not present a specific variation with respect to the geophysical parameters (after filtering). As a consequence, the XCO_2 systematic errors are considered as a constant (*i.e.* one and unique number, and not an empirical formulae as explained above) although it would have been preferable to consider an empirical formula taking into account geophysical variations (*e.g.* SZA or aerosol). This choice was made because the radiative transfer simulations presented above do not show any clear tendency, in terms of error, with the various geophysical parameters (after the filtering proposed by ULe and IUP-UB). The description of such constant is given in section 7.2.3.2.2, depending on the observing system considered.

In addition, it is assumed that the XCO_2 error, although considered as systematic, is not a regional bias. The constant value that is defined in 7.2.3.2.2 is the "quadratic mean" of the error defined in equation 7-4. Individual errors can take positive or negative values, and have no spatial and temporal patterns. Potential regional biases on the XCO_2 retrievals are not considered here. Such regional biases, depending on their spatio-temporal structure, would have large (disastrous) impacts on the results. These impacts cannot be quantified further without knowledge on the spatio-temporal structure of the systematic error.

The choice of such a constant systematic uncertainty is clearly one major limitation of this study and this has to be kept in mind when analysing the following results.

7.2.2.3.3 XCO_2 transport model error

Most studies take a constant value to account for the modelling error. Here, it is proposed to go one step further and it is assumed that the modelling error increases with the CO_2 concentration variability. Indeed, past studies based on LMDz atmospheric transport model have illustrated this effect. This is mainly due to the (relatively coarse) spatial resolution (*i.e.* size of the grid cell) which limits the potential to simulate high variability of the CO_2 concentrations. On the contrary, if the CO_2 concentrations are homogeneous over a given area, the model resolution would be a smaller limitant factor to be able to reproduce these concentrations. Then, the modelling error is estimated per month and per grid box. The model error is defined (for each LMDz box and each month) as the monthly average of the standard deviation values on the column-integrated CO_2 concentrations over temporal windows of 5 days (**Em0**) (see Figure 7-4). Then, this variable **Em0** is scaled by the following relationship:

$$Em = 0.8 \times Em0 + 0.2 \quad \textbf{Equation 7-6}$$

Such a design of the error allows representing the major characteristics of the model uncertainty (related to the temporal variability of the concentrations, smaller over oceans). Similar assumptions related to the XCO_2 systematic errors are considered for the XCO_2 transport error: *i.e.* within a given box, the error values are assumed to be correlated but there is no temporal correlation from one day to another.

The histogram of the scaled model error over a year is presented in Figure 7-5 for two regions (Tropical Africa and Siberia). This figure considers all the values associated with all the pixels comprised in the area considered, over one year. The range of variation of the model error is comprised between the theoretical bounds (0.2 ppm and 3.5 ppm depending on the area and the month of the year).

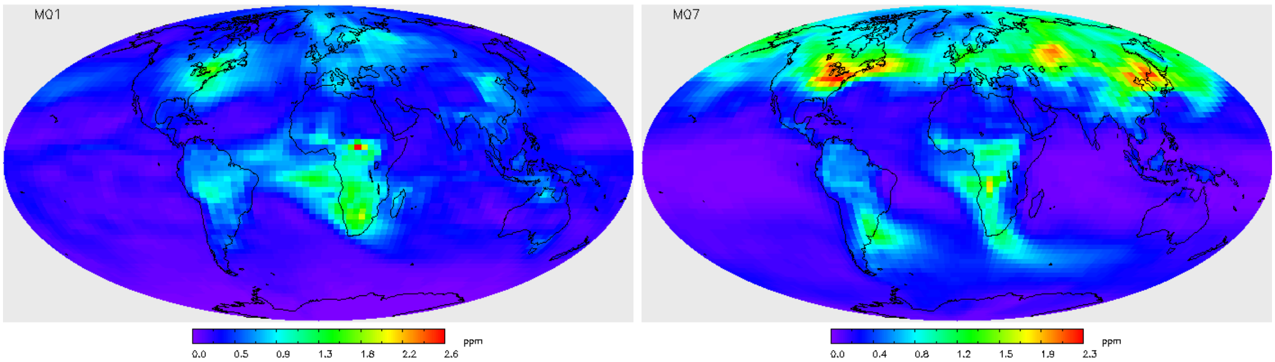

Figure 7-4: Maps of the monthly averaged standard deviation (*i.e.* Em0), for 2 months (January and July) computed for 5 days temporal windows for each grid point.

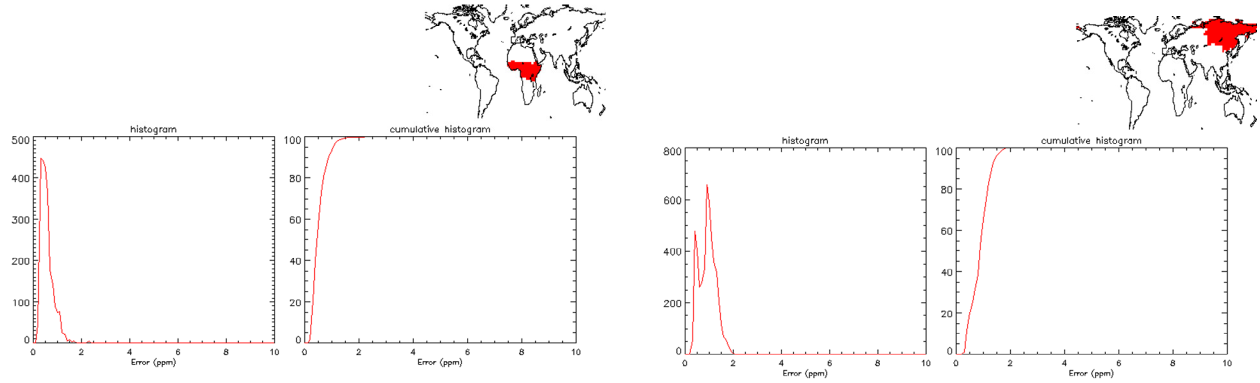

Figure 7-5: Histogram and cumulative histogram of the transport model error over the year for Tropical Africa (left) and Siberia (right).

7.2.3. Observing systems considered

In the present exercise, the capabilities in terms of error reduction over land surface, on the estimation of the surface CO_2 fluxes, are compared between the following observation systems:

- 2 OCO instruments with a unique spatial resolution and sampling common for both of these instruments, but with 2 types of XCO_2 systematic errors (see section 7.2.3.2.2 for more explanations):
  - 0 ppm, named "OCO";
  - 0.5 ppm named OCO_Es05.
- 2 Sentinel-5-UVNS instruments with a unique XCO_2 systematic error (see section 7.2.3.2.2) common for both of these instruments, but with 2 different spatial resolution values (mentioned as goal and threshold in [RD8]):
  - 5 km, named Sentinel-5 – 5 km;
  - 10 km, named Sentinel-5 – 10 km.

7.2.3.1. Impact of the observation geometry

The spatio-temporal sampling of the observations depends on various configuration parameters of the instruments considered: orbit, spatial resolution (footprint of a pixel on the surface), observation geometry (FOV along- and across- track, etc.)

The sampling of the Earth surface by the OCO instrument is performed assuming a FOV of 3 km and considering a distance of 7 km between two consecutive FOVs along-track as well as 12 FOVs across-track plus. Besides, the observation geometry changes depending on the type of surface beneath the satellite: nadir over land and the direction of glint over ocean.

The Sentinel-5-UVNS instrument has ± 45° (~2500 km) across-track scanning capabilities. Two spatial resolutions are considered for Sentinel-5-UVNS according to [RD8]: 5 km and 10 km. These resolutions are for nadir viewing and the IFOV of the instrument increases with the off-nadir angle.

In order to describe realistically the impact of cloud coverage on the amount of available satellite observations, the MODIS cloud mask product at 1 km is used. Whenever a cloud is present in the Sentinel-5 IFOV, the corresponding observation is not declared valid for a good CO_2 retrieval. Although, we do use the MODIS Aqua orbit to account for the cloud cover, the Sentinel-5 local time of observation is used to compute the sun and view angles (see Table 7-1).

The clear observations are then aggregated at the resolution of the LMDz transport model. For these aggregated observations, also referred as "super-observations", the barycentre of all clear observations is chosen in order to determine the time, coordinates of the locations (latitude, longitude), the observation geometry (solar and viewing zenith angles), as well as the number of clear observations **Nobs**. It is important to note this value of **Nobs** associated to each super-observation is used for the computation of the random term of the observation error (section 7.2.3.2.1) at each super-observation scale.

Therefore, the spatial scales of the observations and across track swath have two distinct effects on the matrix components of the simulator:

- Firstly, they determine the number of observations **Nobs** associated with each of the super-observations, and hence impact the “magnitude” of the decrease of the random error associated with the super-observations.
- Secondly, they impact the number of super-observations which thus impacts the size of the **R** and **H** matrices.

Table 7-1: Observation configuration of the OCO and Sentinel 5 instruments

	OCO	OCO_Es05	Sentinel-5 – 5 km	Sentinel-5 – 10 km
Spatial resolution (km)	3	3	5	10
Spatio-temporal sampling	+ 7 km distance between 2 consecutive FOV observed along track + 12 FOVs observed across-track + Nadir over land / Glint over ocean		Imaging of the surface accounting for a FOV across-track of ± 45° (~2500 km)	
Equator crossing local solar time	13h30		9h30	

7.2.3.2. Observation error

7.2.3.2.1 Random error term

The determination of the random error term is derived from the XCO_2 performances associated which single satellite observations (*i.e.* **Eperf**) and at the scale of the so-called "super-observation". The XCO_2 random errors of single observations are considered as follows:

- OCO: the variable **Eperf** depends on the surface albedo in the three bands of the instrument (NIR, SWIR-1 and SWIR-2) and on the solar zenith angle. A look-up table depending on these parameters has been derived by CNES. It is used to compute the value of **Eperf** corresponding to the actual observation configurations following a linear interpolation procedure. Thus, the distribution of these values provided in the look-up table indicates the minimum and maximum **Eperf** magnitudes, as illustrated in Figure 7-6.

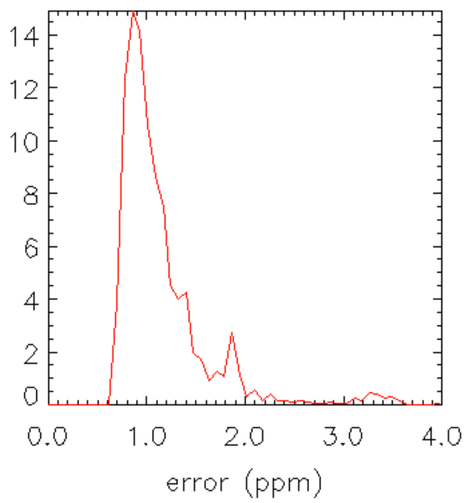

Figure 7-6: Distribution of the level 2 performance error (quadratic mean) for the OCO instrument.

- Sentinel-5: the level 2 performance error is taken from the Mean Random error given in Table 4-5. **Eperf** is set to the value of 1 ppm computed by ULe over all scattering filtered scenarios (*i.e.* all aerosol and cirrus).

As explained in section 7.2.2.3.1, the random error term is derived from the XCO_2 performances associated which single satellite observations. It is reduced over large regions (*i.e.* super-observations), through the parameter **k**, which represents the decay law with respect to the number of observations **Nobs**. The value **k** is not identical between the two observing systems:

- OCO: the value of **k** has been set to 0.25 which corresponds to a compromise between the case where the errors are fully uncorrelated (**k**=0.5) and the case where the errors are correlated over very short distances.
- Sentinel-5: as currently there is no knowledge on potential correlations between each of the Sentinel-5 observations, **k** has been set arbitrarily to the value of 0.5. The number of Sentinel-5 observations within a given model grid box is so large that this error becomes negligible.

7.2.3.2.2 Systematic error term

As explained in section 7.2.2.3.2, simulations performed in chapter 4 based on current instrument specifications of Sentinel-5-UVNS do not allow to establish a clear relationship between the XCO_2 systematic errors (when applying the filter of the retrievals) and key geophysical parameters. Then, it is proposed in this exercise to consider the XCO_2 systematic error, associated with single space-borne observations), as a constant (*i.e.* no empirical formula can be derived).

Values of this constant are defined as follows:

- Sentinel-5: the value is derived from the Standard Deviation Systematic error, over the filtered scattering analysed cases, computed by ULe: *i.e.* **Es** = 1.86 ppm.
- OCO: here two cases are considered. The first value, set to 0 ppm, is derived from current CNES activities in progress by LSCE and NOVELTIS (where no systematic error is considered for now for OCO observations). A specific simulation has been performed in addition for the present exercise by considering **Es** = 0.5ppm. This value was selected with respect to the expected OCO XCO_2 performances [RD3] [RD30] but also because of the breakthrough requirement proposed and given in Table 2-7, page 70, but that value has still to be considered carefully.

The Table 7-2 summarizes the differences between the considered instruments in terms of observation error definition.

Table 7-2: Differences between OCO and Sentinel-5 observing systems, considered in the present exercise, related to the XCO_2 observation error definition.

	OCO	OCO_Es05	Sentinel-5 – 5 km	Sentinel-5 – 10 km
Random error associated with a single observation (ppm)	Function of the surface reflectance and solar zenith angle		1	
Random error decrease law with respect to the number of observations	$Nobs^{0.25}$		$Nobs^{0.5}$	
Transport model error (yes / no)	Yes (see section 7.2.2.3.3)	Yes (see section 7.2.2.3.3)	Yes (see section 7.2.2.3.3)	Yes (see section 7.2.2.3.3)
Systematic error associated with a single observation (ppm)	0	0.5	1.86	1.86

7.3. Results

Simulations using the mission CO_2 simulator have been performed based on all the parameters described in the previous sections. The results are analysed and compared in the following sections with a focus on a few major characteristics of the *a posteriori* error covariance matrix:

- the number of observations delivered by each observing instrument;
- the associated error reduction (with respect to the *a priori* information on the fluxes);
- the total *a posteriori* errors associated with the estimates of CO_2 surface fluxes.

The results presented here cannot be fully compared to the works performed in [RD30] as the assumptions which were considered are not equivalent here (*e.g.* formulation of the XCO_2 random errors, formulation of the XCO_2 systematic errors, etc…).

7.3.1. Number of cloud free observations

The comparison of the number of cloud free observations obtained from each instrument allows a first assessment of their respective constraint onto the surface CO_2 fluxes. The spatial patterns of the total number of super-observations in each grid cell of the LMDz model associated with each instrument are presented for summer (*cf.* Figure 7-7) and winter (*cf.* Figure 7-8) seasons, and for the all year (*cf.* Figure 7-9).

Clearly, the density of the clear observations provided by the two Sentinel-5 observing systems is much higher than the density of OCO observations: this is mainly due to the large across-track swath of Sentinel-5. Depending on the place and time, the number of observations available for Sentinel-5 can be from about 3 up to about 10 times larger than for OCO. The total number of super-observations obtained for OCO over the year is of 177984; it is of 708146 for Sentinel-5 at 10 km, and 923573 for Sentinel-5 at 5 km. On average there are about 5.2 times more measurements available from Sentinel-5 than from OCO to constrain the surface CO_2 fluxes; and 1.3 times more for the 5 km spatial resolution of Sentinel-5 as compared to the 10 km case. The impact of the reduction of the Sentinel-5 spatial resolution (when going from 5 km to 10 km) particularly affects the mid-latitudes regions over ocean as well as the tropical forests (South America, South Africa and Indonesia). This is due to the frequent occurrence of broken cloudiness in this region.

Some regions of the globe are seldom (if not never) covered by OCO because of cloud contamination (tropics and Southern polar ocean). For these regions of interest for understanding the carbon cycle, the Sentinel-5 mission offers a unique opportunity to gain knowledge on the CO_2 surface fluxes, because of its large across-track swath.

Note the number of "super-observations" accounted for in the inversion is tightly linked to the choice of the value of the distance of spatial aggregation, here set to 200 km. A larger distance (for instance 300 km) would decrease the number of independent super-observations for Sentinel-5.

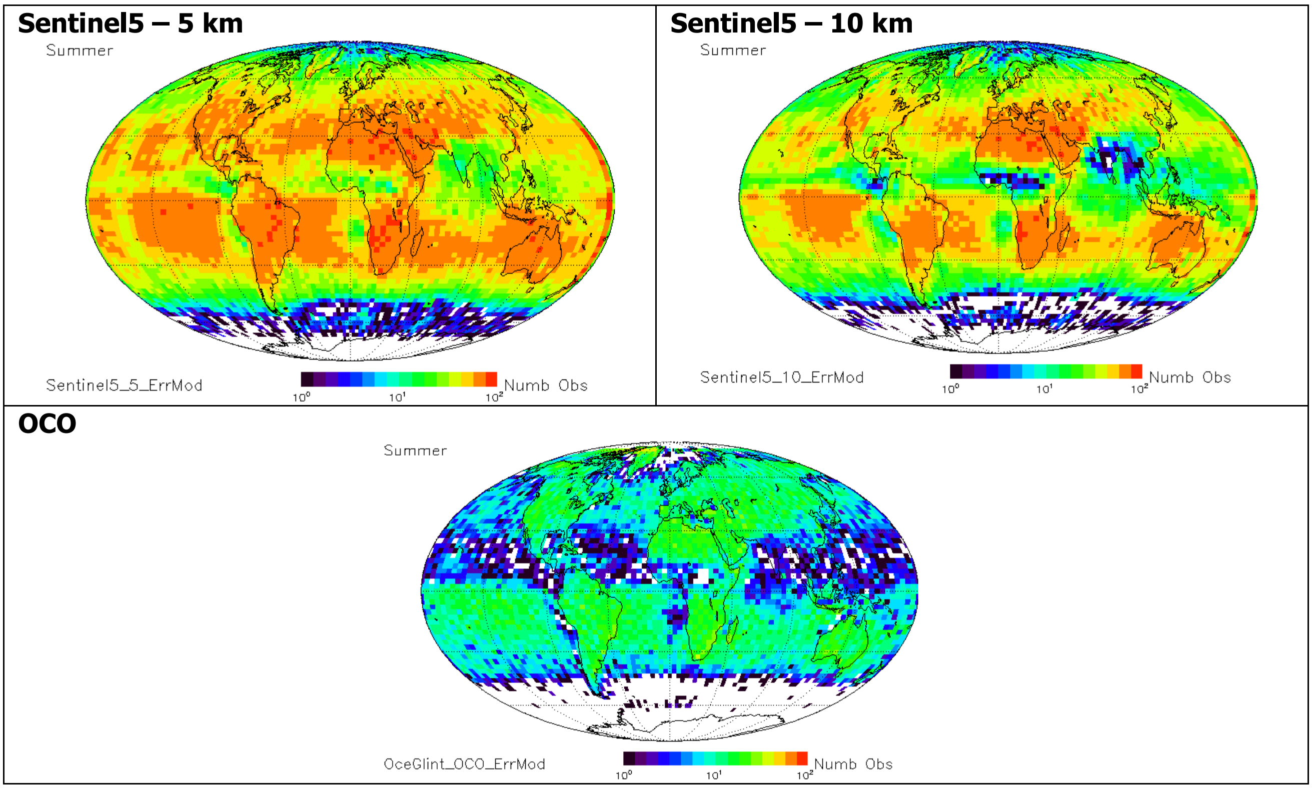

Figure 7-7: Total number of super-observations over the summer season per grid cell of the LMDz model for Sentinel-5 at 5 and 10 km spatial resolutions, and for OCO.

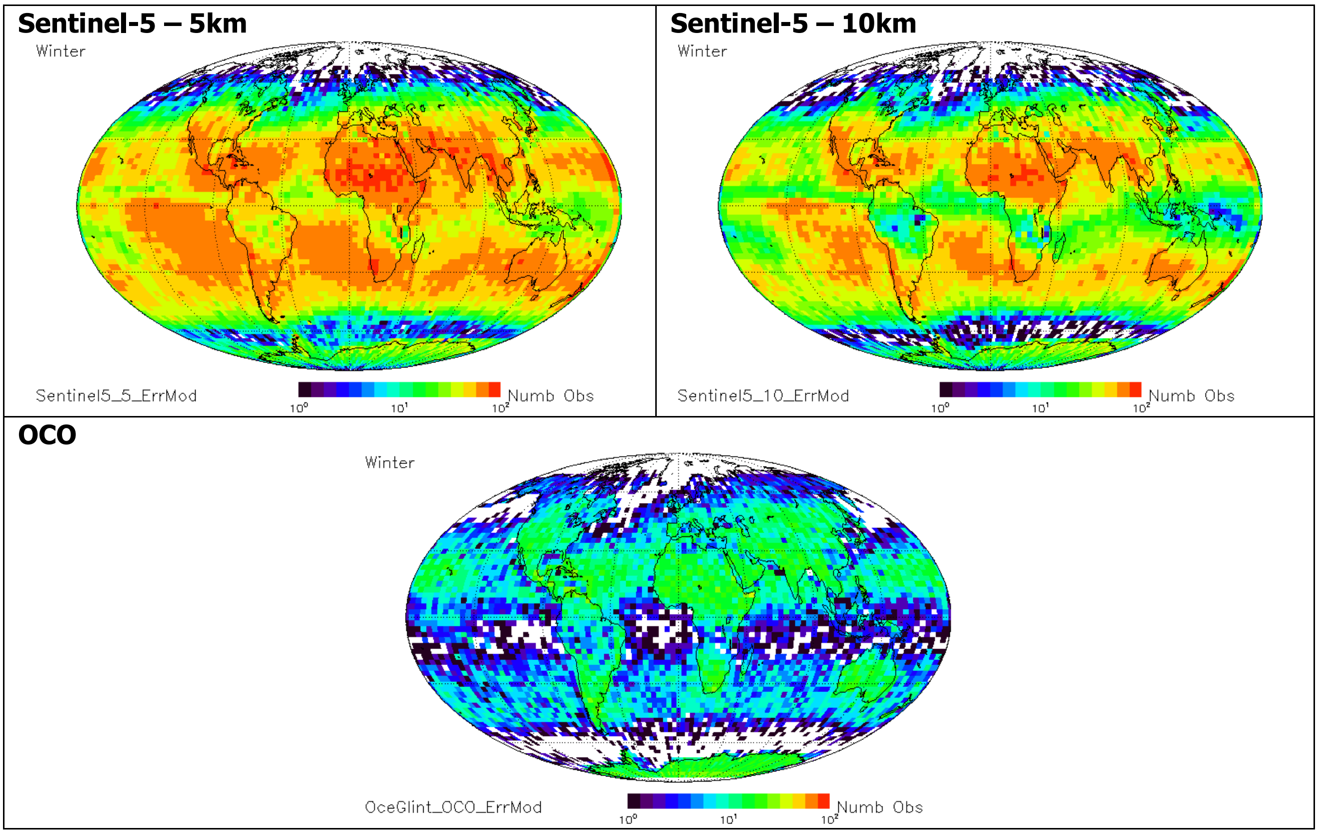

Figure 7-8: Total number of super-observations over the winter season per grid cell of the LMDz model for Sentinel-5 at 5 and 10 km spatial resolutions, and for OCO.

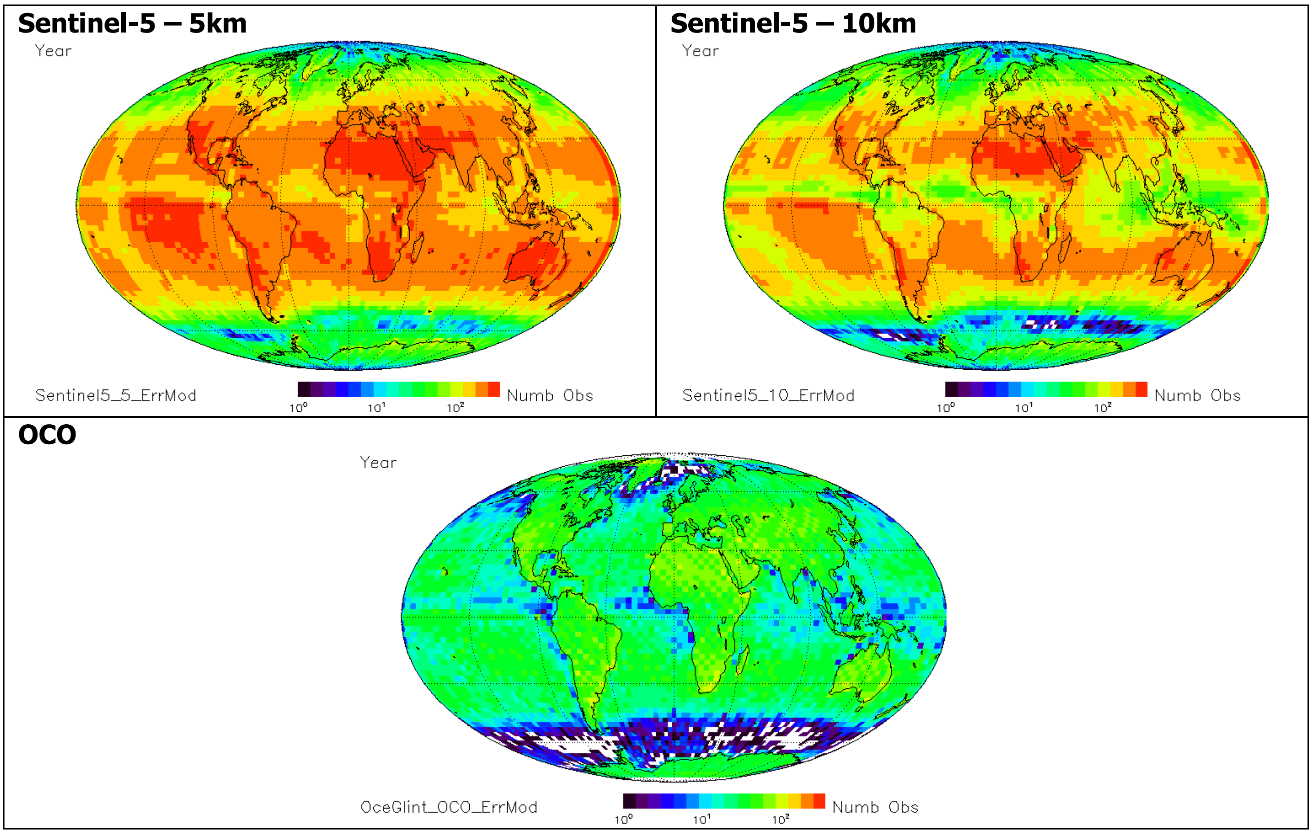

Figure 7-9: Total number of super-observations over all the year per grid cell of the LMDz model for Sentinel5 a 5 and 10 km spatial resolutions, and for OCO.

7.3.2. Total observation errors

The Figure 7-10 illustrates how the different geometric and geophysical hypotheses associated with each of the four observing systems impact the total observation error. The analysis is focused on four geographical regions of interest, their choice being guided by their specificity in terms of carbon cycle and their potential vulnerability to climate change. The analytical method makes it possible to combine the statistical results for areas that aggregate several of the pre-defined regions.

The Figure 7-10 presents the distribution of the total observation XCO_2 errors (combining the random, systematic, and model terms), considering all the super-observations available in the region considered, over one year. The number of all observation pixels available is also indicated and as it was analysed previously (see section 7.3.1), this number is higher for the Sentinel-5 observing systems and lower for OCO systems.

The spread of the distribution of the model error is mainly controlled by the random and model error terms. Compared to the distribution of the sole model error (*cf.* Figure 7-5), the results show a very similar spread around the median value. This indicates that the random error has a very small impact on the total observation error due to the high number of observations available from the OCO and Sentinel-5 instruments. This is particularly well illustrated when comparing the two Sentinel-5 instruments, which only differ by the spatial resolution of the pixel footprint and hence by the number of observations **Nobs** used to compute the random error. The associated histograms are almost identical, indicating that it is crucial to properly assess the values of the systematic term.

The minimal value of the observation errors is given by the "systematic" error term, which explains the smaller errors of the OCO instruments. Thus, as the XCO_2 systematic errors, associated with single observations, are larger for the Sentinel-5 observations (1.86 ppm) and lower for OCO (between 0 ppm and 0.5 ppm, depending on the observing system considered). The resulting total observation error is higher values for the Sentinel-5 instruments, whatever the geographical region considered. For Sentinel-5, the median value is ~2 ppm while it is ~between 0.8 and ~1 ppm for OCO.

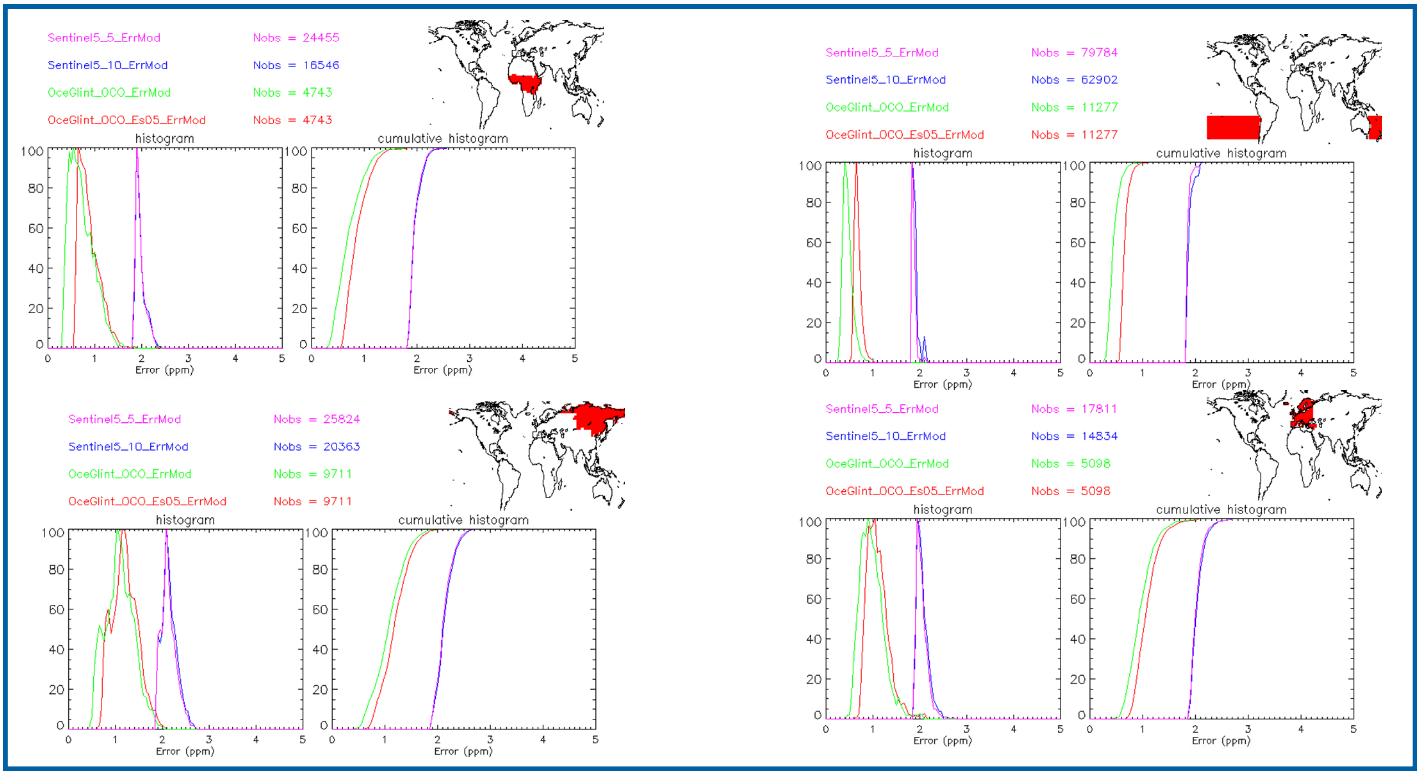

Figure 7-10: Histogram and cumulative histogram of the total observation error over the year for Tropical Africa, Siberia, South Pacific Ocean and Europe. The total number of observations available in each region for the year is also provided.

7.3.3. Error reduction on the CO_2 surface fluxes

Considering the weekly error for the *a priori* and *a posteriori* CO_2 surface fluxes for a given region, the error reduction on the weekly fluxes is determined as follows:

$$ER_{week} = 1 - \frac{\sigma_{week}^{post}}{\sigma_{week}^{prior}} \quad \textbf{Equation 7-7}$$

Where:

- ER_{week} is the weekly error reduction;
- σ_{week}^{post} is the *a posteriori* uncertainty associated with the CO_2 surface flux estimate for each week and region over one year;
- σ_{week}^{prior} is the *a priori* uncertainty associated with the CO_2 surface flux estimate for each week and region over one year.

The analytical flux inversion yields the posterior uncertainty for each week and region over one year together with the correlation terms. Since, there is no reason to focus on one particular week, the (*a priori* or *a posteriori*) uncertainties mentioned in Equation 7-7 are obtained through the quadratic-mean weekly error de fined as:

$$\sigma_{week} = \sqrt{\frac{1}{N}\sum_i \sigma_i^2} \quad \textbf{Equation 7-8}$$

In this equation:

- σ_{week} is the quadratic-mean weekly (*a priori* or *a posteriori*) error;
- N is the number of periods (*i.e.* 48);
- σ_i is the uncertainty for each week and region.

The error reduction ranges from 0 to 1, high values indicating improved knowledge of the CO_2 surface fluxes.

The comparison of the maps of the error reduction on the weekly fluxes, averaged over the year, obtained for the four instruments, is presented in Figure 7-11. The spatial patterns obtained for the four instruments are similar, and follow that of the map of *a priori* error on the surface fluxes (see Figure 7-3).

For OCO, when increasing the observation error by addition of a 0.5 ppm "systematic" error, the impact seems to be low except for a few regions (South-East and East of China, Siberia) where the error reduction slightly decreases (of ~5%).

For the Sentinel-5 instruments, the impact of the degradation of the spatial resolution of the observations (5 km to 10 km) is manifest in the inter-tropical region, especially over land in the Southern part. Considering the very small difference of the observation errors between the two Sentinel-5 configurations, such an impact is mainly explained by the changes induced on the number of constraints accounted for in the transport operator **H**, which dimensionality is determined by the number of super-observations. A **H** matrix with higher dimension (*i.e.* higher number of elements related to the number of the super-observations and considered as independent in the inversion) induces a stronger constraint on the CO_2 surface fluxes.

The comparison of the performances of the Sentinel-5 and OCO instruments reveals only slight differences. The main differences appear over land for the inter-tropical region where Sentinel-5 provides a denser spatio-temporal monitoring (see Figure 7-7, Figure 7-8 and Figure 7-9) and then may provide better performances despite the lesser quality of the observations. Over ocean, the performances of the OCO scenario that does not account for a systematic error term remain usually higher than those of the two Sentinel-5 scenarios. However, this better performance of OCO over ocean vanishes as soon as the systematic term reaches 0.5 ppm.

Figure 7-12 highlights the temporal variation of the differences obtained between the two OCO instruments and the two Sentinel-5 observing systems for the four regions previously defined (*cf.* Figure 7-10). For the extra-tropical regions over land, the small seasonal cycle reflects the same cycle of the *a priori* errors on the surface CO_2 fluxes (smaller in winter at mid and high latitudes). Note that the values of the error reduction are very high given that the *a priori* error is relatively large.

These results allow clarifying the previous analyses regarding the relative performances of the OCO and Sentinel-5 configurations. Over tropical Africa for instance, the higher number of measurements available for Sentinel-5 counter-balance their high biases (as compared to OCO): the error reduction achieved by the Sentinel-5 instruments match that of OCO, which provides lower number of observations over the surface mainly because of the cloud coverage and the swath width.

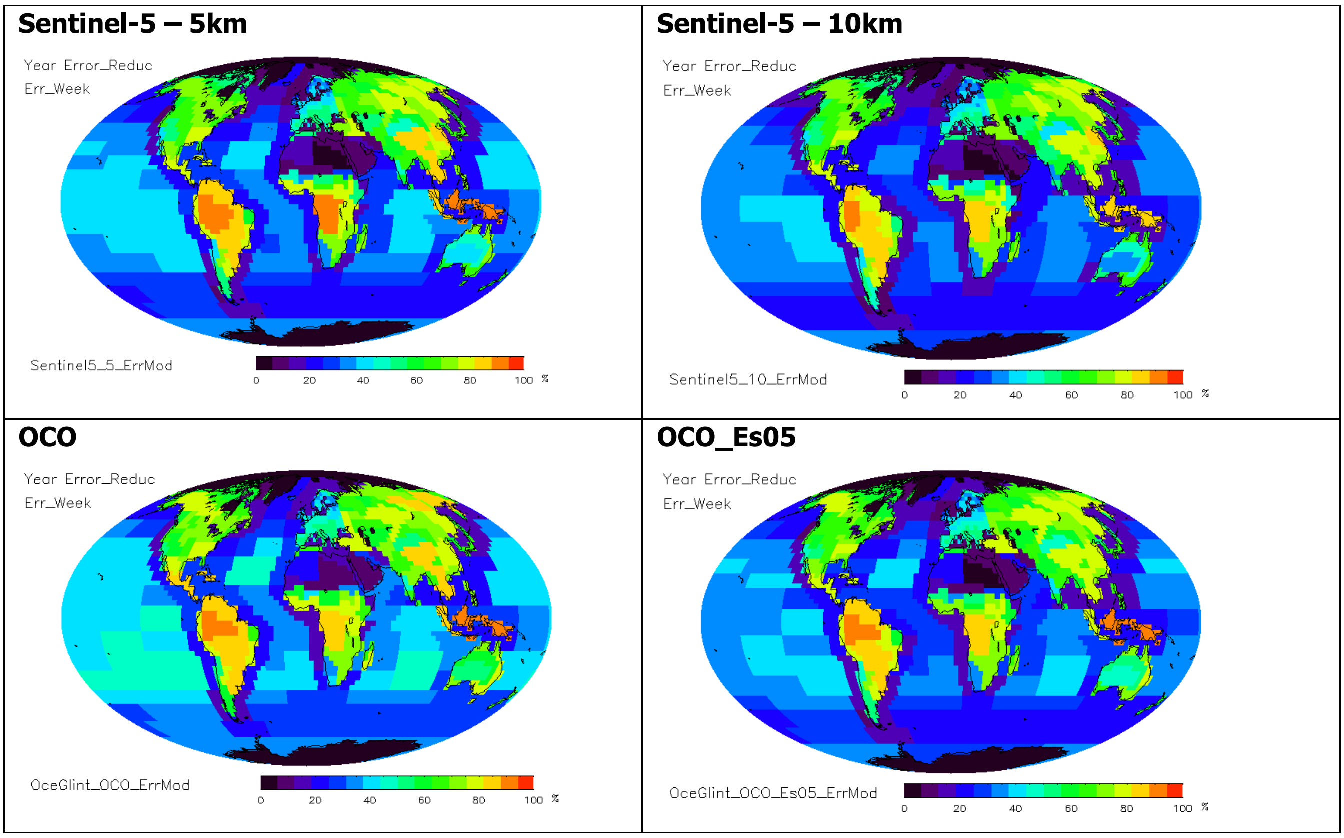

Figure 7-11: Maps of the error reduction on the weekly fluxes, over one year, for the two OCO and the two Sentinel-5 observing systems.

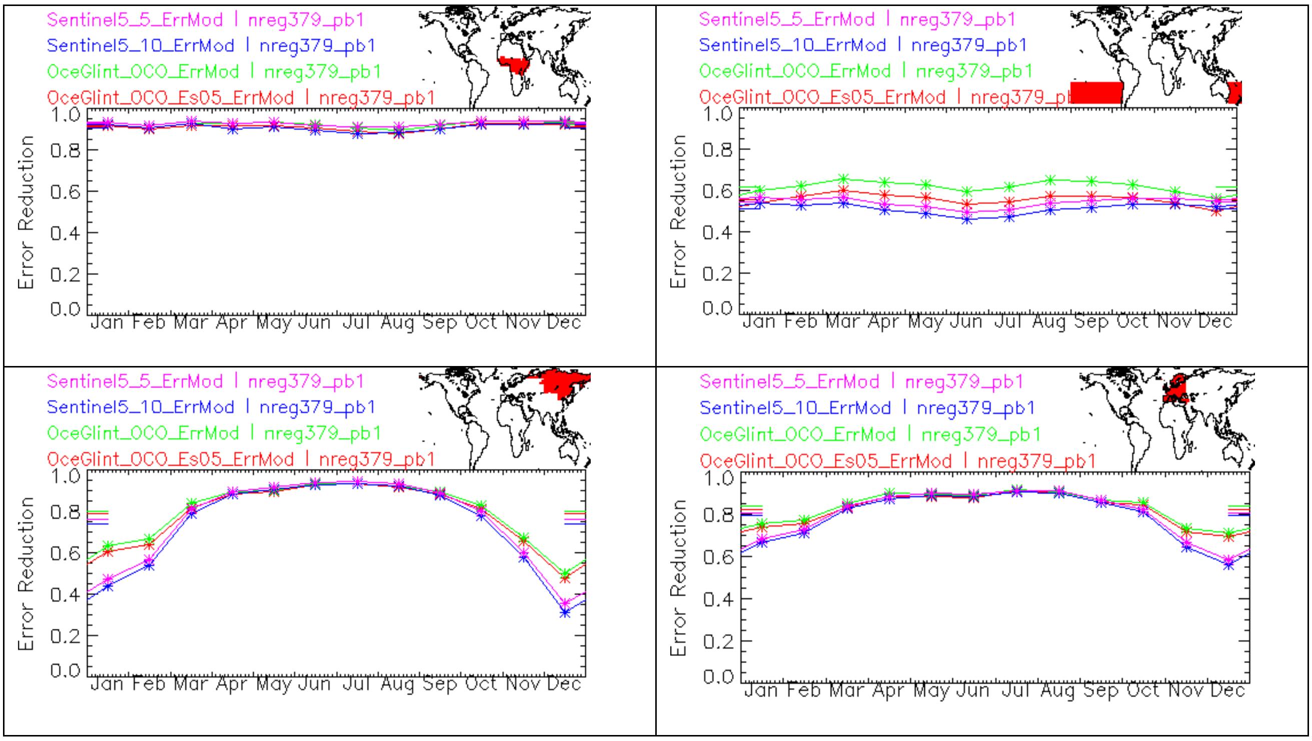

Figure 7-12: Temporal variation of the error reduction on the weekly fluxes obtained for the two OCO instruments and the two Sentinel5 configurations, over Tropical Africa, Southern Pacific Ocean, Siberia and Europe.

7.3.4. Total *a posteriori* error on the surface CO_2 fluxes

The statistical results associated with the theoretical total *a posteriori* errors, computed through the present analytical approach, are presented for the LMDz regions (Tropical Africa, Siberia, South Pacific ocean and Europe), and for the all year in Figure 7-13.

It is necessary to stress that, as the error reduction, they depend on many hypotheses, in particular regarding the *a priori* flux uncertainties, their spatial and temporal covariances, and the choice of the aggregated "eco-regions" that are assumed homogeneous in terms of CO_2 flux errors. Hence, considering these various assumptions for the simulator, there is more confidence on the relative performances of each observation than on absolute values.

Figure 7-13 shows higher posterior error values over Europe with respect to the other bigger regions. This is explained by the fact that for these "big" regions, the *a priori* errors on the surface CO_2 fluxes over the corresponding pixels are very well correlated (*i.e.* correlation length ~1), whereas over Europe, the related pixels are considered individually in the inversion. The associated errors vary as a function of the distance between the neighbouring pixels (eq. 7-3). Therefore, one observation over a "big" region constrains strongly all the pixels in the surrounding of this given region whereas an observation over Europe constraints very slightly the neighbouring pixels. Nevertheless, despite these different assumptions for Europe and the rest of the globe, the figures allow interpreting the relative differences between the instruments.

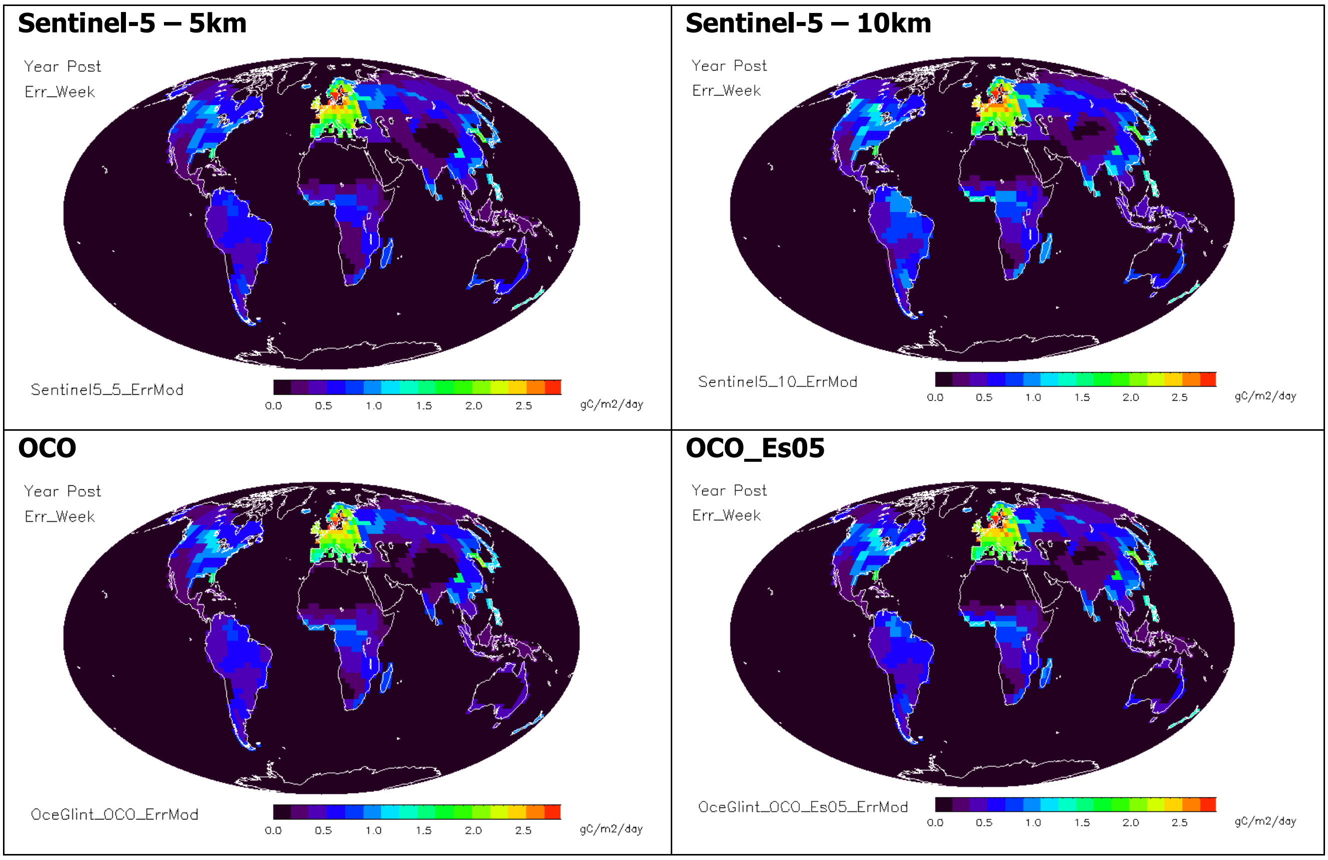

Figure 7-13: Maps of the total *a posteriori* error associated with the surface CO_2 fluxes, over one year, for the two OCO and the two Sentinel-5 observing systems

7.4. Summary and discussion

The analytical approach employed in the present chapter allowed for the first time to perform an assessment of the performances of the Sentinel-5 mission with respect to the application 1 in chapter 2: *i.e.* monitoring total net CO_2 surface fluxes (natural and anthropogenic) at the global to regional scale. The analyses are derived from the "Mission CO_2" simulator jointly developed by NOVELTIS and LSCE. It has to be noted that these results shall not to be transferred to more local CO_2 applications, which would require further studies. Moreover, many assumptions are considered here (*e.g.* constant systematic error for each configuration, *a priori* covariances on the surface CO_2 fluxes, etc...). Thus, the absolute values related to the performances of Sentinel-5 and OCO have to be carefully considered.

The present approach is based on precise characteristics of the orbitography and geometry of OCO and Sentinel-5, and the computed Sentinel-5 XCO_2 systematic error (*cf.* chapter 4) derived from the current S-5-UVNS instrument specifications. The constant value of 0.5 ppm, assumed to be the XCO_2 systematic error of OCO, as for now derived from several studies [RD3] [RD30].

The results deduced in this present study are only valid within the major assumptions that have been made. Therefore, the results obtained in the present chapter are firstly summarised below in section 7.4.1. And then, the limitations associated with these results are clearly mentioned in the section 7.4.2. Because of these limitations, these results have to be considered carefully in the future.

7.4.1. Summary of the present results

The main results which are obtained from this specific exercise are:

- The large across-swath width of the Sentinel-5 instrument combined to a relatively high spatial resolution of the observations (comparable to that of OCO) results in a very dense monitoring of the Earth surface that might counter-balance a disadvantageous systematic observation error (1.86 ppm) as compared to OCO (0 ppm and 0.5 ppm) as shown by the similar performances (in terms of error reduction) between the different instruments.
- Because of the assumptions stated in section 7.4.2, it is assumed that a relatively large systematic error term on XCO_2 products, derived from Sentinel-5 instrument as specified currently, should not affect the potential gain of this mission for the application 1 as large and dense measurements would be provide. This result suggests however that it is critical to carefully address a better analysis and estimate of systematic errors when assessing Sentinel-5 performances in a view of CO_2 monitoring.
- Although Sentinel-5 should deliver very numerous observations over a given area, one needs to look at global statistics of the abundance of good quality CO_2 measurements (e.g. using cloud and aerosol statistics) to study how many useful measurements will actually be available from the Sentinel-5 mission. This specific point has not been considered in the present study where only academic cases have been investigated.
- The systematic errors should depend on various geophysical parameters (*e.g.* albedo, aerosol optical depth, airmass etc…) as it was done for OCO in [RD30]. However, the current performances of Sentinel-5 may be overestimated as the present exercise assumed that all the single "clear" measurements delivered by the sounder are exploitable. As explained in the previous chapters, a filtering of the "bad" XCO_2 retrievals was necessary to deduce the single bias of 1.86 ppm and seems necessary in presence of contaminated scenes (because of residual aerosol or clouds) or over scenes with strong heterogeneities.
- Nonetheless, compared to OCO, it is still expected that much higher number of measurements will be provided. Therefore, the performances of the Sentinel-5 mission, in terms of error reduction on the estimates of surface CO_2 fluxes, would be interesting. Furthermore, as Sentinel-5 will have a very long lifetime (operational mission), it could provide interesting measurements to monitor the mid to long term carbon cycle response to climate change. The main scientific and challenging question is: will it be possible in the future years to have a system able to deal with this requested

very high number of XCO_2 measurements? For now, most of the scientists, because of the current tools available for retrieving estimates of the total column of CO_2 and for inverse modelling inverse when computing the surface fluxes, prefer to have a reasonable number of exploitable observations with a very small bias (such as promised by OCO) rather the contrary. This is because of the unlikely assumption that large errors decrease through averaging as the square root of the number of observations. For the natural CO_2 flux monitoring, it may be better to reduce the number of observations ingested in the inverse model if a better individual SNR can be obtained.

- The constraints on the accuracy with respect to the estimates of surface CO_2 fluxes allowed by a space-borne observing system seem to be a compromise between the accuracy of the observations and the quantity of available observations. Therefore, the user requirements on the XCO_2 systematic errors should not be discussed as a single value, but should be defined with clearly stated assumptions on the capacity to have (or not) a high number of single measurements exploitable in a given area. Thus, provided that an observing system can deliver very numerous XCO_2 measurements (as Sentinel-5), a threshold of 2 ppm related to a single XCO_2 product can be accepted. However, if the considered observing system would provide much fewer exploitable measurements over the Earth surface (*i.e.* limited swath width, or a large swath with a high fraction of invalid measurements) then the requirements would be for an XCO_2 error on the order of 0.5 ppm or less.

7.4.2. Discussion on the major assumptions

The major assumption considered in the present exercise is that biases in the XCO_2 measurements have no spatial or temporal pattern. For example, a day-to-day variation (of the XCO_2 bias) within a given box model is considered uncorrelated. It is clear that actually, a global (and moreover constant) bias has a very small impact for estimating the surface CO_2 fluxes. Thus, the main issue for the next OSSE studies is to be able to well characterise the spatial and temporal structure of the XCO_2 bias values.

If a demonstration is made with OCO or GOSAT that XCO_2 systematic errors present spatial and/or temporal structure at a regional scale, then the impact on the fluxes estimations will be major. The filtered results obtained under chapter 4 do not allow deducing, at least for now, that such structure exists in the remote sensing measurements. If, for example, XCO_2 systematic errors are positive over land, and negative over sea, the inversion system will generate a strong CO_2 source over continental surfaces with no connection to reality. As another example, if the presence of aerosol in an observation scene generates a positive bias in the XCO_2 retrieval, then the flux estimate will be positively biased over aerosol source regions.

Finally, the real problem of a space-borne mission dedicated to CO_2 monitoring is not the XCO_2 systematic error value itself but, actually, its spatio-temporal structure. Thus, a precise chaterization of this structure is needed to characterise the L4 performances for the Sentinel-5 mission. Some develoments of the "Mission CO_2 Simulator" are currently in progress in order to be able to take into account the spatio-temporal structure of the XCO_2 bias. Indeed, this exercise has been done with the current version of this software, by transferring directly the theoretical L2 errors into L4 errors. Then, the future version of the "Mission CO_2 Simulator" shoud allow to characterise more precisely the L4 performances of Sentinel-5. However, this exercice requires the definition of the spatio-temporal structure of the systematic errors. As it was out of scope to the present short study, in the future, spatio-temporal structures in the systematic errors need to be more systematically investigated.

As a consequence, the results presented in the previous section are actually rather optimistic (both for Sentinel-5 and for OCO). But, they represent the state-of-the art of the scientific knowledge on the Sentinel-5 XCO_2 bias values, their structure and their theoretical impact on the L4 estimates. If Sentinel-5 observations were available today, this is the typical way in which they would be used.

8. Conclusions and recommendations

8.1. Conclusion on the current performances of the Sentinel-5 mission for CO_2 monitoring with respect to the associated user requirements

8.1.1. User requirements on the CO_2 space-borne products

A literature review of user requirements for CO_2 monitoring and flux determination by Sentinel-5 mission has been performed, with a strong support of the scientist expertise. This activity has considered various aspects such as climate protocol monitoring, surface emission estimation, source attributions (anthropogenic versus natural) on the relevant spatial and temporal scales.

The global needs to better monitor CO_2 are supported by the fact that CO_2 concentrations are at the highest level in the past 56 million years in the atmosphere [RD15] [RD43]. Current mixing ratios of CO_2 have increased by nearly 40% from 280 ppm, in pre-industrial times, to more than 386 ppm today. They are still rising at about 2 ppm per year [RD27]. For the period 2000-2008, an average of about 28.5 Gt CO_2 yr^{-1} was released into the atmosphere by burning fossil fuels. It is estimated that an average of 5.6-9.3 Gt CO_2 yr^{-1} was emitted due to deforestation and land-use change during the same interval. One of the major uncertainties is related to the location of the sinks, their response in the near-future under the pressure of climate change and the detection, quantification and monitoring of large/local anthropogenic sources.

Three specific applications have been identified in order to describe the user needs and transfer them into requirements for CO_2 L4 flux and L2 remote sensing products:

- Application 1: Monitoring **total net CO_2 surface fluxes** (natural and anthropogenic) at the **global scale (~500-1000 km)**;
- Application 2: Monitoring **anthropogenic city CO_2** surface emissions at **city scale (~20 – 50 km)**;
- Application 3: Monitoring **large anthropogenic power plant CO_2** surface emissions at **local/point scale (~1 km)**.

Application 1 allows addressing **global total net fluxes** at the resolution scale of a few hundred kilometres. This application is based on the fact that remote sensing measurements are not able to differentiate natural and anthropogenic surface fluxes of CO_2. As natural CO_2 fluxes are clearly more diffuse and more uncertain than anthropogenic ones, application 1 is driving the requirements for total net CO_2 surface fluxes, mostly related to natural fluxes at this spatial scale.

Monitoring natural fluxes at global scale is crucial for two questions:

- The **feedback of vegetation induced by the rate of climate change during the 21st century**: this objective is considered as a threshold objective in this case. Indeed, vegetation has been taking up a significant fraction of anthropogenic carbon dioxide and some simulations of the 21st century indicate that vegetation may respond negatively to climate change and become a net source of carbon to the atmosphere after ~2050.
- The **modelling of land-vegetation dynamics**: this objective is considered as a goal in this case. Models of the scientific community for vegetation and soil dynamics allow calculating the exchange of carbon with the atmosphere. Their development is very helpful to understand the functioning of ecosystems and to predict their future behaviour including their response to climate change.

Application 2 is focused on **major cities** and **application 3** is matching the scale of **power plants**. Both represent the main part of the CO_2 anthropogenic emissions generated by countries. Moreover, the only way to detect and quantify CO_2 anthropogenic emissions from remote sensing measurements is to focus on localised sources for which the flux magnitudes are stronger and more local than for biosphere (more diffuse). The remaining emission sources (*e.g.*: transport ...) are too diffuse to be clearly distinguished from natural fluxes from space based CO_2 measurements.

The requirements on the remote sensing products, associated with the 3 applications are synthesised in the previous sections (see Table 2-3, page 53 and Table 2-7, page 70). Specific requirements for applications 2 and 3 (*i.e.* CO_2 anthropogenic emissions) can be also summarized as follows on the CO_2 **L2 products**:

- **Spatial scales (resolution and sampling):** single column observation should present a spatial sampling and horizontal resolution between 1 km (local emissions) and 10 km (city scale, typically between 20 x 20 km² and 50 x 50 km²). More particularly, for monitoring CO_2 emissions associated with the power plants, the L2 spatial scale must not exceed 2 km.
- **Revisit time:** whatever the application 2 or the application 3 considered, a single column observation must be revisited at least every 6 days for estimating yearly fluxes. This requirement is based on the assumption that CO_2 anthropogenic emissions do not change significantly from month to month. However, it can be interesting to have 3-monthly (cities) or monthly (power plants) fluxes able to capture seasonal cycle related to seasonal consumption of energy over European areas. Thus, goals of 1 day (power plants) and 3 days (cities) are required for the CO_2 L2 products. These differences are explained by the fact that time averaged emissions may be washed out because of the variations of synoptic conditions.
- **Random errors:** for a single column observation, the random errors required are 2 ppm as threshold and 1 ppm as goal.
- **Systematic overall errors:** 2 ppm (threshold), 0.5 ppm (breakthrough) and 0.2 ppm (goal).
    - It is assumed that these values are obtained after a bias correction has been applied: *i.e.* they can be considered as persistent systematic overall errors values which remain, even though biases are corrected considering aerosol, clouds or other ancillary information, instrumental calibration or regional biases. Large scale biases can usually be removed by validation and very small scale biases appear almost random. Thus, the spatial scale associated with each application may be considered as the scale of the ensemble used for deriving the accuracy requirement.
    - **Threshold value can be accepted if the observing system considered is able to deliver very numerous and exploitable XCO_2 products over a given area, and if XCO_2 systematic errors do not present a regional structure.** If the considered observing system can provide only few such products and/or if characterization of the biases show clearly a regional pattern, then the breakthrough value has to be required, and not the threshold.
- **Stability errors:** as systematic overall error but per year.

The requirements associated with application 3 are derived from an OSSE study as described in [RD23].

The requirements associated with application 1 (total net CO_2 fluxes at the global scale) are derived from an OSSE study based mostly on OCO, A-SCOPE and GOSAT space-borne missions [RD30] (see sections 2.4.2 and 2.5.5.1). Furthermore, these specific requirements are not “cast in iron” requirements and they can be slightly modified (even relaxed regarding their precision) considering the spatial and temporal coverage ensured by the Sentinel-5 mission.

An assessment using an OSSE has been conducted under chapter 7 by taking into account all the precise elements of the mission (orbitography, spatial resolution, spatial sampling, swath width etc…). One of the main results of this exercise is to show that constraints on the accuracy with respect to the estimates of surface CO_2 fluxes allowed by a space-borne observing system might be a compromise between the accuracy of the observations and the quantity of available observations. Then, it demonstrates that the user requirements on the XCO_2 systematic errors should not be discussed as a single value, but should be defined with clear assumptions on the capacity to have (or not) a high number of single measurements exploitable in a given area. **Thus, provided that an observing system can deliver very numerous XCO_2 measurements (as Sentinel-5) and that XCO_2 systematic errors do not present specific regional patterns as discussed in chapter 7, a threshold of 2 ppm related to a single XCO_2 product may be accepted.** However, **if the considered observing system would provide a few exploitable measurements over the Earth surface** (*i.e.* limited swath width, or high swat width but too many products not exploitable because of strong heterogeneities in the scene for example) **or the biases patterns present a structure at a regional scale, then a XCO_2 bias of the order of 0.5 ppm** (as a maximum) will be necessary. This exercise justifies fully when the threshold value on the XCO_2 systematic may be tolerated and when the breakthrough value is strongly required.

8.1.1. Quantification of the current XCO_2 Sentinel-5 performances

An important volume of simulations has been performed under the present study by 3 groups of scientific experts in order to assess the capabilities of the Sentinel-5-UVNS sounder to monitor CO_2. These performances are obtained from existing XCO_2 retrieval algorithms. As shown in the document, the results obtained by the 3 groups are very consistent which gives confidence with respect to the joint conclusions. Preliminary instrumental specifications, as made available to the consortium by ESA, of the S-5-UVNS have been considered in order to assess the current XCO_2 Sentinel-5 performances.

Relevant efforts have been done for harmonizing the 3 analysis methods with common data sets: specific geophysical scenarios have been defined by varying many parameters (scattering effects, various SZA, aerosol, cirrus, temperature, H_2O, CO_2), common instrument parameters (based on the ESA specifications in [RD14] and [RD8]). The definition of the 2700 geophysical scenarios has been agreed by the entire consortium and has been accepted by ESA. Each of the scientific experts used its own retrieval methodology. All algorithms are based on the methodology called OEM [RD74].

Comparisons of the results from IUP-UB, ULe and KNMI showed good agreement. Indeed differences are small, allowing consistent conclusions. IUP-UB and ULe have focused on the XCO_2 performances associated with S-5-UVNS stand alone. Analyses are based on the computations of the random XCO_2 errors (*i.e.* how the SNR impacts the XCO_2 uncertainty) and the systematic XCO_2 error (*i.e.* related to the bias induced by geophysical atmospheric conditions but uncertainties linked to instrumental artefacts such calibration or others…). KNMI has focused on the synergy of the S-5-UVNS with VII and 3MI, with methodology that differs from IUP-UB and ULe, by characterising the total XCO_2 error (*i.e.* the *a posteriori* error as formulated by the Optimal Estimation Methodology).

Very detailed discussion focused on the evaluation of the XCO_2 performances derived from Sentinel-5-UVNS measurements as the instrument is specified for now are given in chapter 5, page 159. The conclusion below synthesized this discussion.

The main conclusions of the current capacities of the Sentinel-5 mission for CO_2 monitoring are:

- **Current XCO_2 random error derived from the S-5-UVNS measurements meet the XCO_2 precision as required by the users.** Statistically, independently from the cases simulated, the average value is even lower than the goal requirement of application 1 (2 ppm) and is lower than the threshold requirement (2 ppm) of the 2 other applications. For some specific simulations, some values are even less than 1 ppm, which is the required goal for the applications 2 and 3.
- **Current XCO_2 systematic errors derived from the S-5-UVNS measurements are** estimated to be on the order of 2 ppm when applying the retrieval algorithms used for this study. It is expected that this error can be further reduced using optimized retrieval algorithms but to what extent cannot be said without further study. Depending on the scenarios studied a large fraction of the scenes may have errors below 0.5 ppm (breakthrough requirement) but there are also cases where the error is larger than 2 ppm. This indicates that from a systematic error point of view, Sentinel-5 seems to be able to meet the 2 ppm threshold requirement or is at least at the edge of meeting this requirement..However, this specifc requirement is associated with major assumptions: *i.e.* one can tolerate such bias value only if the considered observing system is able to deliver very numerous and exploitable XCO_2 observations over a given area and if the structure of the systematic errors do not present regional patterns.

Synergy of the S-5-UVNS sounder with VII (and with 3MI qualitatively) have been addressed by KNMI in order to mitigate the error on XCO_2 when performing a XCO_2 retrieval. When using aerosol information (*i.e.* aerosol L2 product) as input of the retrieval, very few improvements are observed on the XCO_2 product although previous studies focused on MODIS product allow expecting to value up 0.05 for the AOT. Same conclusions are deduced when considering radiances in band 24 of VII or radiances of 3MI (*i.e.* the L1 products). Indeed, to improve the retrieved XCO_2 in any significant manner by using such radiances, the fundamental issue for VII and 3MI is that knowledge of surface properties (bidirectional surface albedo and for 3MI polarization properties) are requested. But, distinction between surface and aerosol properties which are possible for high spectral resolution observations in line absorptions bands, are not possible when VII and 3MI radiances are used.

The scattering effects are clearly the main contributors of the high values obtained for the XCO_2 systematic errors. This last point is the key result of this study related to the current S-5-UVNS instrumental specifications in a view of CO_2 monitoring. However, XCO_2 systematic errors should be carefully considered here as the impact on the assimilation of XCO_2 products in an inverse model (for retrieving CO_2 surface fluxes) cannot be accurately assessed without more extensive studies. Indeed, the quality of assimilation of XCO_2 space-borne products is clearly dependent on several parameters which do not include XCO_2 random and systematic errors: *e.g.* model transports errors which may be linked to the so-called representation errors, uncertainty of *a priori* CO_2 surface fluxes, *a priori* knowledge meteorological parameters considered in the transport model etc...

Finally, an assessment of the performances of the Sentinel-5 mission has been achieved by NOVELTIS and LSCE with respect to the so-called application 1 in chapter 0: *i.e.* monitoring total net CO_2 surface fluxes (natural and anthropogenic) at the global to regional scale. The analyses are derived from the "Mission CO_2" simulator jointly developed by NOVELTIS and LSCE. The present approach is based on precise characteristics of the orbitography and geometry of OCO and Sentinel-5, and the current performances of the Sentinel-5 mission in a view of CO_2 monitoring (*cf.* chapter 4) derived from the current S-5-UVNS instrument specifications.

The major assumption considered in this specifc exercise is that XCO_2 bias does not present a typical regional structure but that they are distributed globally. Moreover, this distribution is assumed to be statiscal (Gaussian). Associated with this assumption, two main and important results presented here allow deducing:

- The large across-swath width of the Sentinel-5 instrument combined to a relatively high spatial resolution of the observations (comparable to that of OCO) results in a very dense monitoring of the Earth surface that seems to counter-balance a disadvantageous systematic observation error (1.86 ppm) as compared to OCO (0 ppm and 0.5 ppm) as shown by the similar performances (in terms of error reduction) between the different instruments. **Again, this message is valuable only if XCO_2 systematic errors (derived from OCO and Sentinel-5) do not present a spatio-temporal pattern at the regional scale.**
- Therefore, the performances of the Sentinel-5 mission, in terms or error reduction on the estimates of surface CO_2 fluxes, has potential to monitor CO_2 monitoring for surface fluxes at a large scale, **provided that XCO_2 biases do present only global structures.**

However, such results assumed that a large part of the XCO_2 S-5-UVNS observations would be exploitable. This may an overestimation as, for now, because of the existing tools, many scientists prefer to have a low number of XCO_2 observations with very individual associated biases.

These conclusions may be modified if, in the future, a clear and complete description of the spatial-temporal structure of the bias is available and if, in addition, this structure presents particular regional aspects. But, these results may be considered, for now, as the ways Sentinel-5 observationswould be used currently.

8.2. Recommendations of improvements for CO_2 monitoring by the Sentinel-5 mission

The recommendations which are provided through all the works achived during the present study may be structured as follows, by order of priority:

1) **Firstly, further development of the XCO_2 retrieval algorithms is actually necessary in order to fully exploit a strategy of 3-band XCO_2 retrieval: *i.e.* a simultaneous combination of the so-called NIR-2, SWIR-1 and SWIR-2 spectral domains.**

The topic 1) is mainly justified by the difficulties to have solid quantitative results under chapter 6, in the present study. Indeed, some investigations were performed in order to analyse to which extent XCO_2 systematic errors, derived from S-5-UVNS sounder stand alone, mainly due to clouds and aerosols, can be reduced by considering the aspects mentioned above. Although more than 15000 simulations (including associated results in the previous section) have been performed, some conclusions remain here not sufficiently clear in terms of quantified improvements. However, the algorithms have achieved successful XCO_2 retrievals for very dense simulations in chapter 4, by considering the current instrument specifications for S-5-UVNS. Then, two main recommendations are deduced with respect to the above points 2) and 3). Both of the recommendations are based on the necessity to reduce as much as possible the scattering related XCO_2 systematic errors.

2) **Secondly, despite of the point 1), common results delivered allow recommending strongly to add a 2 micron spectral band to the Sentinel-5 mission baseline.**

Whatever the algorithms employed, it is confirmed that to open the SWIR-2 spectral band, *i.e.* to add a 2 micron spectral band to the Sentinel-5 mission baseline, (*cf.* topic 2)) on the Sentinel-5-UVNS instrument would help to improve highly the quality of the XCO_2 retrieval. The SWIR-2 band is a spectral region which presents strong absorption lines of CO_2 A band. This band is used for OCO, GOSAT and CarbonSat in order to further reduce CO_2 retrievals errors induced by clouds and aerosols. For example, if a 3-band retrieval strategy is considered, the impact may be characterized by higher containt information with respect to the CO_2, an improved retrieval of the aerosol and cirrus optical depth and a potential of decreasing the XCO_2 systematic errors. As a magnitude of order, depending on the strategy of filtering the data which is selected after the XCO_2 retrievals, an improvement of ~0.8 ppm may be expected (in comparison of a strategy of 2-band retrieval) when considering the SWIR-2 instrument specifications (see Table 6-2, page 170, and [RD9]).

However, as highlighted by the first results of KNMI, great care has to be taken in the retrieval algorithm to avoid inconsistencies. It is suggested having two or more aerosol components with different size distributions included in the retrieval as in the study of ULe. Moreover, if the SNR of the strong absorption band is increased with a factor of 1.5 – 2, then it should be preferable to use only the SWIR-2 spectral band for the retrieval of the CO_2 column. The main reasons are that inconsistencies with regard to the wavelength dependence of the aerosol properties are fully excluded and that possible problems with inter-band co-alignment issues are avoided.

3) **In a case of the strategy of 2-band retrieval (*i.e.* NIR-2 + SWIR-1), it is suggested to improve the spectral resolution in the O_2 A band, *i.e.* the NIR-2 spectral region, mainly for potentially providing more accurate information on the surface pressure and aerosol/cirrus (*e.g.* altitude).**

The improvement of the spectral resolution in the O_2 A band (*cf.* topic 3)), *i.e.* the NIR-2 spectral region from 0.4 nm to 0.06 nm (ideally or at least to 0.12 nm), is mainly recommended for providing more accurate information on the surface pressure and aerosol/cirrus (*e.g.* altitude). To what extent a less stringent improvement, *e.g.* 0.12 nm, would be sufficient has not yet been investigated but should be studied as a very high spectral resolution is supposed to present a high benefit. Would a SWIR-2 spectral band not be available (*cf.* topic 2), this recommendation is especially important.

This issue has been briefly quantified:

- The increase of the spectral resolution (from 0.4 nm to 0.06 nm) in the NIR-2 spectral domain, when a XCO_2 2-band retrieval is considered, induces an increase of the overall degrees of freedom of the retrieval. The quantification of the impact on the XCO_2 precision and the XCO_2 systematic error is clearly dependent on the methodology used during the XCO_2 retrieval but also, on the methodology employed for filtering the "bad" retrievals.
- NIR-2 spectral band is mainly necessary for obtaining scattering information and to get (better) information on the surface pressure. It is expected that the surface pressure provided by NWP models will not be sufficiently accurate under all conditions as a very high (*e.g.* 1 hPa) NWP accuracy is likely not available under all conditions. In order to fit the surface pressure, a two-step retrieval is proposed (by one of the partners), where the surface pressure is only fitted in the second step and the extension of the boundary layer is fixed to a climatological mean value. However more studies are needed to confirm this.

4) **Finally, a comprehensive study is necessary in order to well characterise all the numerous observations delivered by the Sentinel-5-UVNS sounder, especially w.r.t. temporal and spatial variations in XCO_2 systematic errors. Then, the goal would be to establish a methodology for filtering the data and ensure an exploitation of an ensemble of "good" XCO_2 datasets for the inverse modelling (when estimating the CO_2 surface fluxes).**

As it was already suggested under chapter 4, Sentinel-5 mission will provide very dense and numerous observations through it very large swath width (~2500 km). Thus, in order to ensure an exploitation of an ensemble of "good" XCO_2 datasets for the inverse modelling (when estimating the CO_2 surface fluxes), a processing of filtering the observations may be necessary (*cf.* topic 4)). The filtering of the results is implicitely already highlighted by the results in chapter 4. Indeed, for example, IUP-UB simulations show that almost 80% of the results a bias value less or equal 0.5 ppm (which is the breakthrough requirement). Thus, if a clear and relevant methodology is available for filtering the 20% "bad" XCO_2 retrievals, then inverse modelling would be sure to exploit only the accurate S-5-UVNS XCO_2 products. Of course, the filtering methodology depends on the XCO_2 retrieval algorithm and is therefore closely related to the (to be optimized) algorithm itself.

The main point is that inhomogeneous aerosol (cirrus) loads and inhomogeneous surface albedo values lead to significant errors for elevated aerosol (cirrus) layers. Therefore, pixels with aerosol close to the surface have to be selected. The errors also tend to increase with the aerosol optical thickness and only pixels whose retrieved aerosol optical thickness is small enough should be selected. This selection may be achieved:

- By using the SWIR-2 spectral band as some information related to the optical thickness in the CO_2 band might be exploitable. Then, this iformation can help to detect the scenes with aerosol close to the surface and extreme cases such as desert dust aerosol as identified by the UVNS Absorbing Aerosol Index (AAI) data product.

- If only the SWIR-1 is available, the NIR-2 band is requested to determine the aerosol optical thickness with sufficient precision (lines absorption in the SWIR-1 spectral region are too weak for such goal). Then, again, scenes may be filtered with respect to their content in terms of aerosol.
- Selection of the scenes with successful XCO_2 retrievals may be performed after the XCO_2 retrieval, by focusing on some criteria based on the results of the XCO_2 retrievals (*e.g.* analyses of the retrieved aerosol optical thickness and cirrus optical thickness, statistical analyses of the differences between the simulated and the observed S-5-UVNS spectra, filtering of the scenes related to high solar zenith angle values, analyses of the number of iteration steps or selection of the retrievals presenting a chi-squared sufficiently small…);
- If the selection procedures mentioned above are not sufficient, then before the XCO_2 retrievals, external information (mainly from VII and 3MI instruments) may be considered either on the aerosol optical thickness of the heterogeneity present in the S-5-UVNS pixels, which can generate important XCO_2 errors:
    - However, AOT derived from VII or 3MI instruments can be useful only if the extent of the boundary layer is well known. The main reason is that it is required to know the effective optical thickness, not the true optical thickness if the extent of the boundary layer is not known.
    - Analyses of the degree of the heterogeneity of the scenes should be based on how the aerosol load differs within the pixel or the variation of the surface albedo. Therefore, it is proposed to consider thresholds for selecting only the pixels where the altitude of the retrieved scattering layer is less than ~ 2 km and where the optical thickness of the scattering layer is less than 0.1 – 0.2.

8.3. Summary of Sentinel-5-UVNS instrument specifications for complying with applications 1 and 2 requirements

The present study showed that XCO_2 requirements associated with **application 1** are met by the Sentinel-5-UVNS sounder specifications considered here. Moreover, the Sentinel-5 mission has potential with respect to the **application 2**.

This study allows to provide the following strong recommendations about the Sentinel-5-UVNS instrument for complying with **applications 1** and **2** requirements:

- **Application 1** will be possible for the Sentinel-5 mission if the following minimum XCO_2 requirements are met:
    - The **NIR-2 spectral resolution** could be between **0.4 nm** (threshold) and **0.06 nm** (goal) (currently 0.12 nm);
    - **Pixel size** must be equal or smaller than **10 km**;
    - **XCO_2 random error** within current performances (about an **average of 1.6 ppm** over all simulated cases under this study);
    - **XCO_2 systematic error** better than **2 ppm**:
        - Instrumental XCO_2 systematic errors shall represent only a small fraction of this 2 ppm requirement;
        - Spatio-temporal structures associated with the geophysical XCO_2 systematic errors shall be further analysed.
- **Application 2** could be accessible (assuming that **application 1** requirements are met) but development of expertise on L2-L4 OSSE and inversion approaches at city scales are needed.

8.4. Perspectives

All the recommendations presented in the previous section are based on the conclusions of the chapter 4, where the results may be considered very relevant and solid, but the quantifications of the expected improvements have to be consolidated in order to provide ESA with very detailed recommendations on the enhancements to carry out on the L1B instrument specifications. Indeed, the underlying assumption of this study was that appropriate tools exist to reliably address all the aspects of this study, without any modification or improvement, only small adjustments. Numerous simulations performed in this study (chapter 4 and chapter 6) show that further adjustments / developments of the current software are required for filling this goal. However, such developments are not possible in the framework of this present study.

Thus, the present section recommends future works, considered as necessary by the consortium, for improving in detail the current recommendations, related to the enhancement of the Sentinel-5 mission, delivered in the present report to ESA.

The main recommendations are structured as follows. They are all considered with high priorities, at the same level:

a) Consolidation of the user requirements by performing comprehensive OSSE studies;

All the user requirements addressed in the present study are mainly based on a comprehensive literature view. These requirements are deduced for 3 specifc applications. However, the major requirements in the literature addresse general objectives of CO_2 monitoring and only few and very recent studies make a distinction between large scales and local scale (cities down to point sources). Thus, some of these requirements are also derived from the expertise available in the consortium. However, transferring the L4 requirements (*i.e.* the estimates of surface CO_2 fluxes) into XCO_2 requirements is a very difficult exercise, in theory. Such transfer needs clearly to be consolidated through an inverse modelling exercise, using an atmospheric transport. Indeed, some unknowns remain today on the way that the combination of all the quantitative requirements stated in Table 2-7, in addition of other parameters related to the transport model, would impact (or not) estimations of the surface fluxes. As an example, the preliminary OSSE study achieved under chapter 7 illustrates that the requirements on the XCO_2 systematic error may be actually dependent on the number of observations allowed by the observing system. Moreover, the crucial point to be considered is not the XCO_2 systematic error value itself, but rather the spatial and temporal distribution of the XCO_2 bias. Complete studies are thus necessary in order to be able to characterise the distribution of this variable (on synthetic data or on existing data such as GOSAT). Moreover, the OSSE studies should evaluate the impact of regional structures for the so-called applications 1 and 2 separately.

b) Further develop and validate algorithms dedicated to Sentinel-5 XCO_2 retrieval in order to be able to better exploit remote sensing observations for retreving XCO_2 products from a 2-band and a 3-band strategy;

As shown in the exercices presented in chapter 6, the algorithms of XCO_2 retrievals have still limitations and are still improving, specifically for 3-band retrievals. The main remaining difficulty is to properly treat the the wavelength dependance of the spectral signature related to the aerosols and clouds. Indeed, when considering SWIR-2 spectral region, the transfer of aerosol information related to the NIR-2 spectral domain into the SWIR-2 remains a difficult exercise, as mentioned by KNMI. Furthermore, the ways to better consider aerosol information as input of the software is not sufficiently known today. Some studies are necessary to better characterise this problem, and to establish a clear methodology for consolidating the existing algorithms.

c) Establishment of a clear and consistent methodology for filtering the very numerous Sentinel-5 observations;

As mentioned in all the previous sections, the strong benefit from the Sentinel-5 mission is the number of observations and the wide spatial coverage. However, it will be necessary to filter the observations to select the good XCO_2 retrievals only when estimating the surface CO_2 fluxes. Several methodologies are recomendned in the present study. But, a comprehensive work is necessary in order to well quantify the contribution of each proposed methodlogy.

Thus, various complete works are recommended in order to:

- Establish a comprehensive statistics over the globe, and for example over a 1-year observation, for characterising the correct and the bad XCO_2 retrievals. Furthermore, such a characterization would allow deducing if such statistcs distribution is Gaussian;
- Investigate how well and if products which are simultaneously observed from a same platform (especially VII and possibly 3MI) can be used through the filtering methodology;
- Assess the relevance of each filtering methodology by analysing the impact on the accuracy of the CO_2 surface fluxes estimates.

d) Characterization of spatial and temporal variations in XCO_2 systematic errors;

The OSSE studies presented in chapter 7 have several limits. In particular, the performances of the Sentinel-5 missions are evauluated by transferring the L2 errors into L4 errors assuming a random and Gaussian statistics distribution of the L2 errors. It is assumed that there are no significant spatial or temporal structures in the XCO_2 systematic errors. Biases that are fully constant (in space and time), or that have very small spatial and temporal scales, have no significant impact on the surface CO_2 fluxes. On the other hand, those with regional (≈1000 km) to continental scales, or a monthly to seasonal structure, might have a severe impact on the results. Then, in order to be able to characterise precisely the real impact of the estimates of the fluxes:

- Accurate information on spatial and temporal structure of the XCO_2 systematic error or bias must be characterized (such an exercise could be performed with synthetic or existing real space-borne data, such as GOSAT).
- Such a typical structure should be considered in a new OSSE study. This study cannot perform a transfer of L2 uncertainties into L4 uncertainties (as the assumptions related to the methodlogy would be wrong now). The impact has to be assessed by directly estimating a CO_2 surface flux over a given area, and by comparing with a referent value.

e) Improvement of current OSSE software in order to make a full assessment of the current/improved CO_2 performances of Sentinel-5 mission.

A development of the "Mission CO_2 simulator" achieving the second point is planned and could be then used for such studies. It could be also employed for comparing L4 performances with different configurations of observing systems, as follows:

- CO_2 observations derived from all space-borne measurements except Sentinel-5. It has to be noticed that spatial and temporal variations of systematic errors of all sensors used are then necessary;
- CO_2 observations derived from *in situ* measurements only;
- CO_2 observations derived from specific ground based measurements, such as TCCON network;
- CO_2 observations derived from only Sentinel-5;
- CO_2 observations derived from *in situ* and/or space-borne measurements and Sentinel-5.